SILVA FENNICA

Vol. 46(5B), 2012

Minna Pulkkinen

On Non-Circularity of Tree Stem Cross-Sections: Effect of Diameter Selection on Cross-Section Area Estimation, Bitterlich Sampling and Stem Volume Estimation in Scots Pine

The Finnish Society of Forest Science
The Finnish Forest Research Institute

Abstract

Pulkkinen, M. 2012. On non-circularity of tree stem cross-sections: Effect of diameter selection on cross-section area estimation, Bitterlich sampling and stem volume estimation in Scots pine. Silva Fennica 46(5B): 747–986.

In the common methods of forest mensuration, including stem volume models and Bitterlich sampling, stem cross-sections are assumed to be circular. In nature this assumption is never exactly fulfilled. Errors due to non-circularity have been presumed to be small and unimportant but studied little: theoretical and empirical studies exist on cross-section area estimation, but errors in stem volume estimation have not been investigated at all, and errors in Bitterlich sampling are theoretically known only for stand basal area estimation. In the theoretical part of this study, we developed methods for quantifying the systematic and sampling errors that 22 common ways of selecting diameter within non-circular cross-sections induce (i) in area estimates by the circle area formula, (ii) in stand total estimates by Bitterlich sampling, and (iii) in stem volume estimates by a volume equation, by a cubic-spline-interpolated stem curve, and by a generalised volume estimator. In the empirical part, based on the digital images of 709 discs taken at 6–10 heights in 81 Scots pine stems from different parts of Finland, we investigated the variation in cross-section shape, and demonstrated the magnitude of the errors presented in the theoretical part. We found that non-circularity causes systematic overestimation of area and volume, and inflicts potentially systematic error on stand total estimates by Bitterlich sampling. In our data these effects were small, but the finding is not generalisable due the skewed size distribution and poor geographical representativeness of the data. We recommend using diameter derived from girth for both tree and stand level estimation, as it involves no sampling error and produces clearly the most stable systematic errors.

Keywords forest mensuration, cross-section, non-circularity, basal area, stem volume, Bitterlich sampling, Scots pine
E-mail minna.pulkkinen@iki.fi
Received 21 September 2012 **Accepted** 12 December 2012
Available at http://www.metla.fi/silvafennica/full/sf46/sf465747.pdf

Cover photo by Metla/Erkki Oksanen

Contents

Acknowledgements

Many people gave invaluable help in this study. The topic was suggested to me by Juha Lappi, who first became a supervisor and then a friend. I wish to thank him warmly and sincerely for his pertinent advice and lucid comments, particularly in the earlier phase of the work, for his alert action in the final publication phase of the work, and for the many profound discussions that we have had throughout the years.

The work began as a MSc project at the then Faculty of Forestry of the University of Joensuu (nowadays the School of Forest Sciences of the University of Eastern Finland). The disc data were generously provided by the VAPU project of the Finnish Forest Research Institute led by Kari T. Korhonen at the Joensuu Research Station. The discs were photographed by Matti Hälinen, using the rack system constructed by the staff in the Imaging Centre of the University; these staff also printed the photographs. With the vectorisation of the raster images of the scanned photographs, Janne Soimasuo and Ari Turkia lent a crucially helping hand. I am indebted to all these persons for their indispensable contribution.

All along the way, Bertil Matérn inspired the work with his excellent early (1956) paper. He was also kind enough to elucidate, in an exchange of letters, the issues in the paper that I was not able to fathom out myself. Further, he generously placed at my disposal some older literature that is hard to get hold of. I wish I could have completed the work before his demise, so that he could have appraised the extension of his original ideas, particularly those about the effect of non-circularity on Bitterlich sampling.

The ideas on Bitterlich sampling started to germinate during my working in the spatial statistics group led by Antti Penttinen at the Department of Statistics of the University of Jyväskylä, and during my half-year visit to the spatial statistics group at the Department of Mathematical Sciences of Aalborg University. I am grateful to these two statistics communities for sowing the seeds of the ideas in my mind, as well as for setting good examples of rigorous statistical thinking and presentation.

I carried out almost all the computation work after the MSc thesis, as well as a considerable part of writing, at the Vantaa Research Centre of the Finnish Forest Research Institute. The group of forest yield and growth study, and later also the group of forest technology, became my hearth and home there. My thanks are due to the researchers and other staff for their approving and encouraging attitude, and to the Institute for very good working facilities. Particularly, I am indebted to Carl-Gustaf Snellman for his assistance in computational problems, and to Jari Hynynen for arranging additional funding after the grant awarded for the work ran out. I also gratefully acknowledge Sointu Virkkala for drawing Figure 22. At that time, Timothy Gregoire was kind to send me the copies of some highly relevant works, especially those by G. R. Grosenbaugh that would have been difficult to obtain otherwise, for which I express my gratitude.

Outside the research institutions, Harri Hypén played an important role. I am especially obliged to him for one significant brainstorm, during a car drive to Eastern Finland, in which we sketched the algorithm for computing the inclusion regions of trees in Bitterlich sampling from the vector images of the cross-section contours. I also gratefully acknowledge him for drawing the original version of Figure 25.

I resumed writing, after a considerable break, while working at the Departments of Forest Ecology and Forest Resource Management (nowadays merged into one, the Department of Forest Sciences) of the University of Helsinki. I wish to give my heartfelt thanks to Annikki Mäkelä and Pauline Stenberg, my superiors, for their encouragement and support, which they gave also in the concrete form of arranging funding. My thanks are also due to the colleagues in the forest ecology modelling group, from whom I learnt much of doing research work, particularly the necessity of always asking what one's results really

mean and imply, which then benefitted the writing of the thesis. Pertti Hari deserves special thanks for initiating and persisting with regular mentoring discussions, as a result of which the focus of the work was changed from empirical to theoretical findings. Finally, I wish to give recognition to all the people at the Department for making it such a lively and versatile community, to which it was a pleasure to belong, also outside the working hours.

In the finalisation phase, Christophe Godin's help and support was indispensable. I am much obliged to him for the discussions that helped shape the introductory and summary chapters, as well as for the pivotal technical solutions for converting the manuscript into the format required by the publisher.

Juha Heikkinen and Göran Ståhl, the official pre-examiners, gave a substantial amount of their time for reviewing the thesis. I wish to thank them sincerely for their work. Matti Maltamo, the professor of forest mensuration formally responsible for the defence process, deserves thanks for his upholding attitude and prompt aid in all the technicalities related to the process.

Numerous institutions funded the study: the COMAS Graduate School of the University of Jyväskylä, the Academy of Finland, the Faculty of Forestry of the University of Joensuu / the School of Forest Sciences of the University of Eastern Finland, and the Foundation for Research of Natural Resources in Finland (grants number 1552/99, 1578/00, 1603/01) are hereby gratefully acknowledged.

Throughout the years, my near and dear, close and far, have tried to make me see, understand and remember the beauty of life, in its myriad aspects. I wish to give them my deepest thanks for this. As Mephistopheles puts it in his well-known words in J. W. von Goethe's play Faust: "Grau, theurer Freund, ist alle Theorie, und grün des Lebens goldner Baum [My friend, all theory is grey, and green the golden tree of life]."

List of Symbols

Cross-Section

A	area of a cross-section
A_C	area of the convex closure of a cross-section
$\hat{A}_j$	estimator of cross-section area based on the circle area formula and diameter selection method j
$\hat{A}_{Gj}$	generalisation of estimator $\hat{A}_j$ for n similarly selected diameters
$(A_C–A)/A_C$	relative convex deficit of a cross-section
$(\hat{A}_0–A_C)/A_C$	relative isoperimetric deficit of a cross-section
$B(\theta)$	breadth of a cross-section in direction θ, with respect to the centre of gravity; $B:[0, \pi)\rightarrow(0, \infty)$
$B_C(\theta)$	breadth of the convex closure of a cross-section in direction θ, with respect to the centre of gravity; $B_C:[0, \pi)\rightarrow(0, \infty)$
b_e/a_e	girth-area ellipse ratio of a cross-section; axis ratio of the ellipse that has the same perimeter and area as the convex closure of a cross-section
C	girth of a cross-section; perimeter of the convex closure of a cross-section
C_p	perimeter of a cross-section
CV_D	coefficient of variation of diameter in a cross-section; $CV_D=\sigma_D/\mu_D$
$D(\theta)$	diameter of a cross-section in direction θ; $D:[0, \pi)\rightarrow(0, \infty)$
D_A	true area diameter of a cross-section; diameter that produces the area of a cross-section when substituted in the circle area formula; $D_A=2[A/\pi]^{1/2}$
D_{Ac}	convex area diameter of a cross-section; diameter that produces the area of the convex closure of a cross-section when substituted in the circle area formula; $D_{Ac}=2[A_C/\pi]^{1/2}$
D_{max}	maximum diameter of a cross-section
D_{min}	minimum diameter of a cross-section
$F_\xi(\xi; \alpha)$	cumulative distribution function of diameter direction ξ parallel to plot radius in Bitterlich sampling with viewing angle α
$f_\xi(\xi; \alpha)$	probability density function of diameter direction ξ parallel to plot radius in Bitterlich sampling with viewing angle α
$p(\theta)$	support function of the convex closure of a cross-section; $p:[0, 2\pi)\rightarrow(0, \infty)$
$R(\theta)$	radius of a cross-section in direction θ from the centre of gravity; $R:[0, 2\pi)\rightarrow(0, \infty)$
$R_C(\theta)$	radius of the convex closure of a cross-section in direction θ from the centre of gravity; $R_C:[0, 2\pi)\rightarrow(0, \infty)$
R_{max}	maximum radius of a cross-section
$\overline{R}_q$	quadratic mean of the observed radii in a cross-section
$\mathbf{R}$	landmark configuration of a cross-section; collection of the observed radii in a cross-section; $\mathbf{R}=(R(j\cdot 1°))_{j=0, 1, ..., 359}$
$\mathbf{R}^*$	centred pre-shape of a landmark configuration of a cross-section; $\mathbf{R}^*=(R^*(j\cdot 1°))_{j=0, 1, ..., 359}=(R(j\cdot 1°)/\overline{R}_q)_{j=0, 1, ..., 359}$
θ	general symbol of direction; diameter direction with uniform distribution in $[0, \pi)$
θ_{Dmax}	direction of D_{max}
θ_{Dmin}	direction of D_{min}
θ_{Rmax}	direction of R_{max}
τ	plot radius direction in Bitterlich sampling
ξ	diameter direction parallel to plot radius in Bitterlich sampling; $\xi\sim F_\xi(\xi; \alpha)$ with viewing angle α

μ_D	girth diameter of a cross-section; within-cross-section expectation of diameter over the uniform direction distribution in $[0, \pi)$; $\mu_D=C/\pi$
$\mu_{D(\xi)}$	mean Bitterlich diameter, parallel to plot radius, in a cross-section; within-cross-section expectation of diameter over the distribution of the diameter direction ξ parallel to plot radius in Bitterlich sampling
$\mu_{D(\xi+\pi/2)}$	mean Bitterlich diameter, perpendicular to plot radius, in a cross-section; within-cross-section expectation of diameter over the distribution of the diameter direction $\xi+\pi/2$ perpendicular to plot radius in Bitterlich sampling
σ_D^2	diameter variance in a cross-section; within-cross-section variance of diameter over the uniform direction distribution in $[0, \pi)$
$\sigma_{D(\xi)}^2$	variance of Bitterlich diameters, parallel to plot radius, in a cross-section; within-cross-section variance of diameter over the distribution of the diameter direction ξ parallel to plot radius in Bitterlich sampling
$\sigma_{D(\xi+\pi/2)}^2$	variance of Bitterlich diameters, perpendicular to plot radius, in a cross-section; within-cross-section variance of diameter over the distribution of the diameter direction $\xi+\pi/2$ perpendicular to plot radius in Bitterlich sampling
$\gamma_D(\varphi)$	within-cross-section covariance of the diameters intersecting at angle φ over the uniform direction distribution in $[0, \pi)$; diameter autocovariance function in a cross-section; $\gamma_D:[0, \pi/2)\rightarrow[0, \infty)$
$\rho_D(\varphi)$	within-cross-section correlation of the diameters intersecting at angle φ over the uniform direction distribution in $[0, \pi)$; diameter autocorrelation function in a cross-section; $\rho_D:[0, \pi/2]\rightarrow[-1, 1]$
$\rho_D(\pi/2)$	within-cross-section correlation of perpendicular diameters over the uniform direction distribution in $[0, \pi)$
$\rho_{D(\xi)}(\pi/2)$	within-cross-section correlation of the diameters parallel and perpendicular to plot radius in Bitterlich sampling
Stem	
$A(h)$	area of the cross-section of a stem at height h; cross-section area function; $A:[0, H]\rightarrow[0, \infty)$
$\hat{A}_j(h)$	estimator of the area of the cross-section of a stem at height h based on the circle area formula and diameter selection method j; area estimation function; $\hat{A}_j:[0, H]\rightarrow[0, \infty)$
$D(\theta, h)$	diameter in direction θ at height h, $\theta\in[0, \pi)$
$D_j(h)$	diameter selected with method j at height h
$D_A(h)$	true area diameter D_A at height h; true stem curve; $D_A:[0, H]\rightarrow[0, \infty)$
$D_{Ac}(h)$	convex area diameter D_{Ac} at height h
$\mathbf{D}_j$	vector of diameters selected with method j at the observation heights **H** in a stem
$\mathbf{D}_A$	vector of true area diameters at the observation heights **H** in a stem
$\mathbf{D}_{Ac}$	vector of convex area diameters at the observation heights **H** in a stem
H	length of a stem; height of a tree determined from the ground level
H	vector of the observation heights in a stem
V	true volume of a stem
$\tilde{V}$	estimated true volume of a stem; $\tilde{V}=\tilde{V}_S$
V_C	convex volume of a stem (approximately the volume of the convex hull of a stem)
$\tilde{V}_C$	estimated convex volume of a stem; $\tilde{V}_C=\tilde{V}_{CS}$

$\tilde{V}_L$	best estimate of the volume of a stem by the re-estimated Laasasenaho three-variable volume equation involving true area diameters
$\tilde{V}_{CL}$	best estimate of the convex volume of a stem by the re-estimated Laasasenaho three-variable volume equation involving convex area diameters
$\hat{V}_{Lj}$	estimator of stem volume based on the re-estimated Laasasenaho three-variable volume equation, involving true area diameters, and on diameters selected with method j
$\hat{V}_{CLj}$	estimator of convex stem volume based on the re-estimated Laasasenaho three-variable volume equation, involving convex area diameters, and on diameters selected with method j
$\tilde{V}_S$	best estimate of the volume of a stem by cubic-spline-interpolated stem curve obtained from true area diameters
$\tilde{V}_{CS}$	best estimate of the convex volume of a stem by cubic-spline-interpolated stem curve obtained from convex area diameters
$\hat{V}_{Sj}$	estimator of stem volume by cubic-spline-interpolated stem curve obtained from diameters selected with method j
$\hat{V}_{Gj}$	estimator of stem volume by general stem volume estimator involving diameters selected with method j
$\mu_{\hat{A}j}(h)$	mean function of area estimation process $\{\hat{A}_j(h), h\in[0, H]\}$ in a stem; $\mu_{\hat{A}j}:[0, H]\rightarrow[0, \infty)$, $\mu_{\hat{A}j}(h)=E[\hat{A}_j(h)]$
$\mu_{\Delta\hat{A}j}(h)$	mean function of area estimation error process $\{\hat{A}_j(h)–A(h), h\in[0, H]\}$ in a stem; $\mu_{\Delta\hat{A}j}:[0, H]\rightarrow\mathbb{R}$, $\mu_{\Delta\hat{A}j}(h)=E[\hat{A}_j(h)–A(h)]$
$\sigma_{\hat{A}j}^2(h)$	variance function of area estimation process $\{\hat{A}_j(h), h\in[0, H]\}$ in a stem; $\sigma_{\hat{A}j}^2:[0, H]\rightarrow[0, \infty)$, $\sigma_{\hat{A}j}^2(h)=Var[\hat{A}_j(h)]$
$\gamma_{\hat{A}j}(h, k)$	covariance function of area estimation process $\{\hat{A}_j(h), h\in[0, H]\}$ in a stem; $\gamma_{\hat{A}j}:[0, H]\times[0, H]\rightarrow\mathbb{R}$, $\gamma_{\hat{A}j}(h, k)=Cov[\hat{A}_j(h), \hat{A}_j(k)]$
$\rho_{\hat{A}j}(h, k)$	correlation function of area estimation process $\{\hat{A}_j(h), h\in[0, H]\}$ in a stem; $\rho_{\hat{A}j}:[0, H]\times[0, H]\rightarrow[–1, 1]$, $\rho_{\hat{A}j}(h, k)=\gamma_{\hat{A}j}(h, k)/[\sigma_{\hat{A}j}(h)\sigma_{\hat{A}j}(k)]$
Stand	
A_{Ci}	area of the convex closure of the breast height cross-section of tree i
$\hat{A}_{ji}$	estimator of the area of the breast heigh cross-section of tree i based on the circle area formula and diameter selected with method j
D_i	breast height diameter of tree i with circular breast height cross-section
G	relative basal area of a tree stand; $G=\Sigma_{i\in\mathbf{I}}A_{Ci}/\lvert\mathbf{L}\rvert$ in stand **I** in region **L**
$\hat{G}_{HT}$	Horvitz-Thompson estimator of G, based on a sample taken from the tree stand
I	tree stand in **L**; set of the trees growing in **L** and reaching above breast height
L	region of interest in Bitterlich sampling
$\lvert\mathbf{L}\rvert$	area of **L**
$\mathbf{M}_i(\alpha)$	inclusion region of tree i in Bitterlich sampling with viewing angle α
$\mathbf{M}_i(\alpha)_a^b$	sector of $\mathbf{M}_i(\alpha)$ edged by the rays emanating in directions a and b from the centre of gravity of the breast height cross-section of tree i
$\lvert\mathbf{M}_i(\alpha)\rvert$	area of $\mathbf{M}_i(\alpha)$
$r_i(\alpha)$	radius of the inclusion region of tree i with circular breast height cross-section in Bitterlich sampling with viewing angle α
$\mathbf{s}_Q(\alpha)$	sample of trees selected with Bitterlich sampling with viewing angle α at a uniformly randomly located point Q

Y	total amount of a characteristic of interest in a tree stand; $Y=\Sigma_{i\in \mathbf{I}}Y_i$ in stand **I** in region **L**
$\hat{Y}_{HT}$	Horvitz-Thompson estimator of Y, based on a sample taken from the tree stand
α	viewing angle in Bitterlich sampling, relascope angle
$\kappa_i(\alpha)$	basal area factor of tree i in Bitterlich sampling with viewing angle α; $\kappa_i:(0, \pi)\rightarrow(0, 1)$, $\kappa_i(\alpha)=A_{Ci}/\lvert\mathbf{M}_i(\alpha)\rvert$
$\pi_i(\alpha)$	inclusion probability of tree i growing in **L** in Bitterlich sampling with viewing angle α; $\pi_i(\alpha)=\lvert\mathbf{M}_i(\alpha)\rvert/\lvert\mathbf{L}\rvert$

General

$Pr\{A\}$	probability of event A
$S_3(a; \mathbf{A}, \mathbf{B})$	interpolating cubic spline based on the vector **B** of values observed at the vector **A** of one-dimensional locations
$\delta_i(\mathbf{A})$	random indicator variable; $\delta_i(\mathbf{A})=1$, if $i\in \mathbf{A}$, and $\delta_i(\mathbf{A})=0$, if $i\notin \mathbf{A}$

Diameter Selection Methods within Cross-Section

0	girth diameter; mean diameter $\mu_D=C/\pi$ of over the uniform direction distribution in $[0, \pi)$
1	"random" diameter; diameter taken in a uniformly distributed direction in $[0, \pi)$
2	arithmetic mean of the diameter in 1 and the diameter perpendicular to it
3	geometric mean of the diameters in 2
4	arithmetic mean of two "random diameters"; arithmetic mean of two diameters taken independently in uniformly distributed directions in $[0, \pi)$
5	geometric mean of the diameters in 4
6	arithmetic mean of the minimum diameter and the maximum diameter
7	geometric mean of the diameters in 6
8	arithmetic mean of the minimum diameter and the diameter perpendicular to it
9	geometric mean of the diameters in 8
10	arithmetic mean of the maximum diameter and the diameter perpendicular to it
11	geometric mean of the diameters in 10
1ξ	diameter taken parallel to plot radius in Bitterlich sampling
2ξ	arithmetic mean of the diameters in taken parallel and perpendicular to plot radius in Bitterlich sampling
3ξ	geometric mean of the diameters in 2ξ
4ξ	arithmetic mean of the diameter taken parallel to plot radius in Bitterlich sampling and a diameter taken independently in a uniformly distributed direction in $[0, \pi)$
5ξ	geometric mean of the diameters in 4ξ
$1\xi 90$	diameter taken perpendicular to plot radius in Bitterlich sampling
$4\xi 90$	arithmetic mean of the diameter taken perpendicular to plot radius in Bitterlich sampling and a diameter taken independently in a uniformly distributed direction in $[0, \pi)$
$5\xi 90$	geometric mean of the diameters in $4\xi 90$
min	minimum diameter
max	maximum diameter

1 Introduction

In the common methods of forest mensuration, the cross-sections of tree stems are assumed to be circular: The area of a stem cross-section is usually estimated with the circle area formula. The volume of a stem is typically estimated as the solid of revolution of a stem curve, or with a volume equation constructed with a combination of circle-base geometric solids (cones, paraboloids, neiloids) as the starting point. Trees to be measured in forest inventories are often selected with Bitterlich sampling (relascope sampling), where the inclusion probabilities, required in the estimator of the stand total of any characteristic of interest, are estimated by assuming that the breast height cross-sections of the selected trees are circular. The basal area of a stand is estimated either as the sum of the treewise estimates of cross-section area given by the circle area formula, or, as is most often the case in practical forestry, by multiplying the number of trees selected in Bitterlich sampling with the so called basal area factor; the latter is a special case of the stand total estimation in Bitterlich sampling and thus assumes circularity on the breast height cross-sections of the trees.

In nature, however, the cross-sections of tree stems are hardly ever exactly circular. Non-circularity occurs due to defects and deformations inflicted by pathogens or mechanical damages, but also without them, in entirely healthy and undamaged trees. Asymmetric growing space affecting the access of a tree to light has been suggested to be one potential cause of non-circularity: with uneven spatial distribution of light, the crown would develop asymmetrically, and the stem should then compensate the resulting mass imbalance by increased wood formation in the direction of the torsional moment. Observations have been reported both for (e.g. Isomäki 1986, Robertson 1991) and against (e.g. Bucht 1981, Bouillet and Houllier 1994) this idea. Wind is another factor proposed to induce non-circularity (Banks 1973, Grace 1977). The mechanism would essentially be similar to the one suggested above: winds blowing continuously from the same direction would cause a torsional moment, which the stem should then counteract by forming more wood in the direction of the wind. Observations supporting this idea have been reported, for example, by Müller (1958a) and Robertson (1986, 1990, 1991). Through the same mechanism, growing in a steep slope or in a leaning position could also result in non-circular stems (Pawsey 1966, Loetsch et al. 1973). Regular heavy snow loads, in turn, could encourage trees to develop straight stems with circular cross-sections to resist the bending forces of the load (Professor emeritus Pertti Hari, personal communication). In general, eccentric radial growth has often been found to be associated with reaction wood formation (e.g. Burdon 1975, Harris 1977, Robertson 1991). The factors listed above could explain the age-related variation in non-circularity: old trees tend to have more irregular cross-sections than young ones, simply because they have been exposed to inflicting growing conditions for a longer time. However, even if growing in similar conditions, some species appear to be more non-circular than others: according to Kärkkäinen (2003), broad-leaved species in Finland are in general more non-circular than coniferous ones; Loetsch et al. (1973), in turn, mention *Tectona grandis*, *Carpinus betulus* and *Robinia pseudacacia* as the species with very irregular cross-sections.

Following from the circularity assumption, the key characteristic of a stem cross-section is its diameter. Yet in a non-circular cross-section there is no single diameter value but diameter varies with direction. In practice, diameter is typically measured with a caliper, which gives the distance between two parallel tangents (that are perpendicular to the direction in which the diameter is being measured), or with a girth tape, by dividing the perimeter measurement by π, which gives the mean of the calipered diameter over all directions (as we will see in Chapter 2). It is important to differentiate between diameter variation due to non-circular shape and diameter variation caused by measurement errors (arising from faulty

handling of instruments, adverse measurement conditions, psychological factors etc.); in literature this distinction has not always been made, but genuine measurement errors have erroneously been ascribed to non-circularity (Matérn 1990).

Variation in diameter within a cross-section of a tree causes variation in the output of such a cross-section area or volume estimator where the diameter is used as an input variable: the estimate of area or volume depends on the selection of diameter. This selection involves the choice of the measurement direction, the number of diameters to be measured and the type of mean (geometric, arithmetic, quadratic) to be applied to the measured diameters. Volume models often involve diameters at more than one height in the stem; the more heights are involved the more complex variation non-circularity potentially induces in the volume estimates. The within-tree variation in estimator output can be characterised by bias and variance. Bias is a measure of the systematic error due to non-circularity: it is the deviation of the mean of all possible estimates, obtained with all possible outcomes of the diameter selection, from the true value, or in other words, the mean error expected over all possible outcomes of the diameter selection. Variance of all possible estimates around their mean, in turn, quantifies the sampling error related to non-circularity; from it we can derive the likely range of the error in the estimate associated with one outcome of the diameter selection.

In Bitterlich sampling, variation in diameter within the breast height cross-section causes variation in the estimate of the inclusion probability of a tree, since the estimator of the probability, based on the circularity assumption, involves the breast height diameter as its input variable. In addition (as we will see in Chapter 4; not shown before), non-circularity inflicts another separable error component in the inclusion probability estimate, dependent only of the cross-section shape and independent of diameter selection. The combination of these errors then decides how the tree contributes, due to its non-circularity, to the bias of the stand total estimator of any characteristic of interest.

In his path-breaking study, Matérn (1956) derived, without postulating anything about the shape of a cross-section, the bias and the approximative variance for the area estimators based on the circle area formula and some common diameter selection methods (diameter derived from perimeter, diameter calipered in a random direction, mean of this diameter and its perpendicular, or mean of two diameters calipered in random directions). On the basis of the bias formulae, he could show that these area estimators systematically overestimate true cross-section area. Furthermore, he developed theory on the effect of non-circularity on basal area estimation with Bitterlich sampling and was able to establish that the overestimating bias induced by non-circularity is practically (with the commonly used small viewing angles) the same as we would get by calipering every stem in one randomly chosen direction. In a later work (1990), he then applied this theory in data that consisted of contour drawings made on over one hundred discs sawn on a about forty Scots pine and Norway spruce stems. Besides Matérn's work, no other theoretical developments concerning the effect of within-cross-section diameter variation on area estimation are to be found in literature. Likewise, the effect of non-circularity on stem volume estimation or on estimation of other stand totals than basal area in Bitterlich sampling appear hitherto theoretically unexplored.

Many empirical studies addressing non-circularity have focused on the shape of cross-sections, investigating with simple shape indices to what extent cross-sections deviate from a circle and how this deviation is related to position of the cross-section in the stem, tree species, silvicultural treatments, growing conditions etc. (e.g. Renvall 1923, Solbraa 1939, Williamson 1975, Kellogg and Barber 1981, Okstad 1983, Mäkinen 1998). Another large set of empirical studies have concerned cross-section area estimation with the circle area formula and different diameter selection methods, reporting differences in area estimates between the diameter selection methods and, more recently with the emergence of less

laborious area measurement methods, also the errors with respect to true area (e.g. Kennel 1959, Chacko 1961, Kärkkäinen 1975a, Biging and Wensel 1988, Gregoire et al. 1990). In many of these studies, in particular earlier ones, data consist of field measurements with a caliper or a girth tape and are thus very likely to contain measurement errors. A clearly distinct branch of studies, making use of ample data of cross-section radii provided by scanners employed in sawmills, have tested different models of cross-section shape with the aim of adapting sawing patterns to maximise the sawing yield (e.g. Skatter and Høibø 1998, Saint-André and Leban 2000). Practically no empirical studies seem to exist concerning the effect of within-cross-section diameter variation on volume estimation nor concerning the effect of non-circularity on Bitterlich sampling.

Nonetheless, the effects of non-circularity are worth investigating, even though other sources of error (sampling errors, measurement errors, model misspecification errors, estimation errors in model parameters, model residual errors) probably induce much more uncertainty in the results of forest inventories: on the basis of Matérn's theoretical results, it is realistic to anticipate that non-circularity might inflict systematic errors also in volume estimates and stand total estimates by Bitterlich sampling, and that these, although presumably small in magnitude, can then cumulate into considerable errors in large area inventories. Further, in research purposes where one often strives for eliminating confounding factors, taking non-circularity effect into account may clarify and consolidate the results of analyses; particularly, when estimating growth with the difference between diameters, cross-section areas or stem volumes at two time points, the potentially asymmetric growth in non-circular cross-sections need be heeded.

This study concerns the effects of non-circularity on (i) cross-section area estimation with the circle area formula, (ii) stand total estimation in Bitterlich sampling with the circularity assumption, and (iii) stem volume estimation by a standard three-variable volume equation, by a non-parametric stem curve often applied in research purposes, and by a theoretical general volume estimator based on a cross-section area estimation function. The estimators considered are commonly used for standing trees or felled sample trees and involve dimensions of stems that can be measured from outside with the usual measurement equipment (calipered diameters, perimeters given by a tape, height obtained with a hypsometer or a tape). The diameter selection methods included in the examination are such that they exist in literature and are used, or could in principle be used, in practice. The first aim of the study was to develop further the existing theory: to derive the missing statistical properties of the area estimators under within-cross-section diameter variation, to devise methods for estimating similar statistical properties for the volume estimators, and to unravel theoretically how non-circularity affects Bitterlich sampling, without postulating anything about cross-section shape. The second aim of the study was to investigate with reasonable data how cross-section shape varies in Scots pine and of what magnitude the above-mentioned theoretically established effects of non-circularity can be in practice.

In the theoretical part of the work, we (i) derived the within-cross-section bias, approximative variance and true variance for the area estimators based on the circle area formula and five common diameter selection methods (involving diameters calipered in randomly chosen directions and their perpendiculars; methods already addressed by Matérn), as well as their generalisations up to n diameters, (ii) described how non-circularity of breast height cross-sections influences inclusion probabilities of trees and hence stand total estimation in Bitterlich sampling, (iii) derived the non-uniform direction distributions for the diameters measured parallel or perpendicular to plot radius in Bitterlich sampling, and presented the within-cross-section bias, approximative variance and true variance for the area estimators based on the circle area formula and eight diameter selection methods involving these diameters, and (iv) presented methods for estimating the within-tree bias and variance of

the three types of volume estimators (volume equation, non-parametric stem curve, theoretical general volume estimator based on a cross-section area estimation function) with the diameter selection methods considered in (i) and (iii).

The empirical part of the work relied on the data of 709 discs taken at 6–10 heights in 81 healthy Scots pine stems in different parts of Finland; to eliminate measurement errors, the characteristics of the cross-sections were computed from digital images. With these data, we (i) investigated the variation in cross-section shape in different parts of the stems by means of some scalar and functional indices, (ii) estimated the within-cross-section biases and variances of the area estimators based on the circle area formula and 22 diameter selection methods (including those considered in the theoretical part), (iii) estimated the within-tree biases and variances of the three types of volume estimators with the same 22 diameter selection methods, and (iv) estimated, still with the same 22 diameter selection methods, the tree-specific errors caused by non-circularity in the inclusion probabilities in Bitterlich sampling, imparting the contribution of each tree in the bias of a stand total estimate. Owing to some defects in the data (non-probabilistic sampling of trees with uneven spatial distribution over Finland, skewed size distribution with small trees highly over-represented, debarking of discs before imaging), the empirical results cannot be generalised to any defined population (such as the Scots pine trees in Finland) or do not compare with the usual characteristics (that include bark) but should rather be taken as illustrations.

As a final remark, non-circularity was here studied as a static geometric phenomenon: the biological processes forming cross-section shape and the factors influencing these processes (site conditions, competition, management history of the stand etc.) were beyond the scope of this study.

2 Geometrical and Statistical Concepts

In this chapter, we introduce the notions of convex closure and support function, the latter of which we then use to define the key concept of diameter. Then we describe diameter selection within a cross-section of a tree stem as a random experiment involving sampling from diameter direction distribution and present some characteristics to summarise the diameter distribution within a cross-section. Further, we illustrate with artificial examples how these characteristics relate to the shape of the convex closure of a cross-section. Finally, we define radius and breadth, two other dimensions of a cross-section. Much of the notation employed later in the thesis is set up in this chapter.

Let us consider a cross-section perpendicular to the longitudinal axis of a tree stem as a closed and bounded set in $\mathbb{R}^2$. This set is *convex* if for every pair of points in it the line segment connecting the points is also contained in it. The *convex closure* of the set is the intersection of all the closed convex sets in $\mathbb{R}^2$ that contain the set (Fig. 1); from the definition it immediately follows that the cross-section is convex if and only if it equals its convex closure (Santaló 1976, Kelly and Weiss 1979). The boundary of the convex closure forms a closed convex curve (Santaló 1976), the length of which is here referred to as the *convex perimeter* of the cross-section and denoted by C. The area of the convex closure is here termed the *convex area* of the cross-section and denoted by A_C, whereas for the area of the cross-section the expression *true area* and denotation A is used. Clearly, every non-convex cross-section is smaller in area and larger in perimeter than its convex closure, that is, always $A \leq A_C$ and true perimeter $\geq C$.

The concept of convex closure is important in forest mensuration, because the commonly used measuring instruments — girth tape, caliper and relascope — do not detect the possible non-convexity of a cross-section but only provide information on its convex closure: A girth tape stretched around a stem contours the convex closure of a cross-section and gives the convex perimeter as its reading. Caliper and relascope measurements, in turn, are based on observing the tangents of the convex closure of a cross-section (Matérn 1956, Matérn 1990, Loetsch et al. 1973, Bitterlich 1984).

Support function, first applied by Matérn (1956) in a context similar to this, is an invaluable tool for relating a convex closure with its tangents by a straightforward mathematical expression. In order to define the function, we first need to set a rectangular planar coordinate system: the origin is chosen to be an interior point O of the convex closure, and a reference direction (the direction of the positive x-axis) is fixed; as usual, we measure the angles anticlockwise with respect to the reference direction. Now the value $p(\theta)$ of the support function $p:[0, 2\pi)\rightarrow(0, \infty)$ of the convex closure is defined as the length of the normal drawn in direction θ from the origin O to the tangent of the convex closure (Fig. 2) (Matérn 1956, 1990, Santaló 1976; see Kelly and Weiss 1979, Rockafellar 1970, Stoyan and Stoyan 1994, and Webster 1994 for a more general definition). Different selections of O naturally result in different functions (which cannot be transformed to the same form by a simple

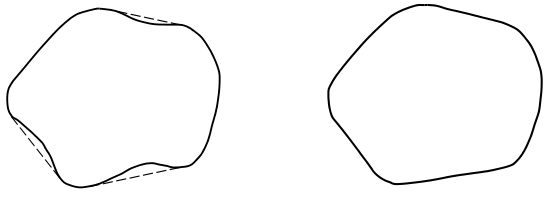

Fig. 1. Non-convex cross-section (left) and its convex closure (right).

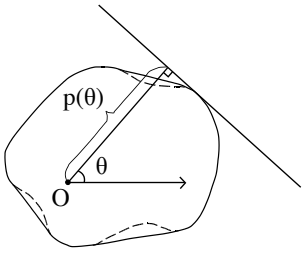

Fig. 2. Definition of the support function p(·) of the convex closure of a cross-section with reference to the interior point O.

phase transition, as is the case with different x-axis direction selections); in other words, the support function of a set is always defined with reference to some inner point of the set.

A necessary and sufficient condition for any twice differentiable nonnegative function p(·) to be a support function of a convex closure is that $p(\theta)+p''(\theta)>0$ for all θ in $[0, 2\pi)$ (Matérn 1956, Santaló 1976). There is a one-to-one correspondence between the shape of a convex closure and its support function, that is, the boundary curve of the closure determines p(·) uniquely and vice versa (Rockafellar 1970, Webster 1994). As suggested above, the family of all the tangents of a convex closure is easy to express in terms of the support function; from the tangents, in turn, a parametric representation for the rectangular Cartesian co-ordinates of the boundary is straightforward to derive; then, knowing the boundary co-ordinates, we can express the perimeter and the area of the convex closure in terms of the support function as

$$C = \int_0^{2\pi} p(\theta)d\theta \,, \tag{1}$$

and

$$\begin{aligned} A_C &= \frac{1}{2}\int_0^{2\pi} p(\theta)[p(\theta)+p''(\theta)]d\theta \\ &= \frac{1}{2}\int_0^{2\pi} [p(\theta)^2 - p'(\theta)^2]d\theta \end{aligned} \tag{2}$$

(Matérn 1956, Santaló 1976, Stoyan and Stoyan 1994). For a more detailed discussion and derivation of these results, see Appendix A.

The crux of the usefulness of the support function in our context is that it lends itself so naturally to the diameter definition common in forestry: the *diameter* of a cross-section is the continuous function $D:[0, \pi)\rightarrow(0, \infty)$,

$$D(\theta) = p(\theta) + p(\theta+\pi) \,. \tag{3}$$

The diameter in direction θ is thus the distance between the two parallel tangents of the convex closure of the cross-section drawn in direction $\theta+\pi/2$, or, equivalently, the length of the orthogonal projection of the convex closure of the cross-section in direction θ (Fig. 3). Accordingly, a diameter defined in this way corresponds to a calipered diameter in practical forest mensuration on one hand (Matérn 1956, 1990), and to the general concept of the width of a closed set in Euclidian n-spaces on the other hand (Kelly and Weiss 1979, Stoyan and Stoyan 1994). Note that there is a clear distinction between this definition and

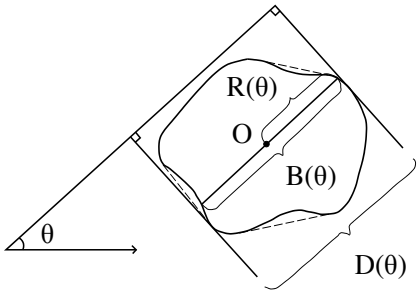

Fig. 3. Diameter D(θ), radius R(θ), and breadth B(θ) of a cross-section in direction θ. The interior point O, with respect to which R(·) and B(·) were determined, was selected to be the centre of gravity of the cross-section.

the usual topological concept of the diameter of a set, which is defined as the supremum of the Euclidian distances between all the pairs of the points in the set (see e.g. Kelly and Weiss 1979, Santaló 1976). Although the support function is always defined with respect to some interior point O of the cross-section, the diameter function is invariant of the selection of this point.

Measuring a diameter of a non-circular cross-section means sampling from an infinite "diameter population" within the cross-section. This can be carried out by selecting a diameter direction θ within the interval $[0, \pi)$. If θ is sampled *randomly*, implying that θ is a random variable with some probability distribution, also the diameter D(θ) becomes a random variable with some probability distribution (as D(θ) is merely a continuous transformation of θ determined by the form of the cross-section). The diameter moments and central moments, which characterise the diameter distribution within the cross-section, can then be expressed by means of the diameter function and the direction distribution: for $k \in \mathbb{Q}_+$,

$$E[D(\theta)^k] = \int_0^\pi D(\theta)^k f_\theta(\theta) d\theta \tag{4}$$

and

$$E\left\{\left\{D(\theta) - E[D(\theta)]\right\}^k\right\} = \int_0^\pi \left\{D(\theta) - E[D(\theta)]\right\}^k f_\theta(\theta) d\theta \,, \tag{5}$$

where $f_\theta(\theta)$ is the probability density function of θ. Note that although we in the following consider diameter moments in a cross-section primarily over the uniform direction distribution in $[0, \pi)$, this distribution is, although perhaps the most natural choice, by no means the only option. For example, if the breast height cross-section of a tree deviates from the circular shape, measuring the breast height diameter parallel or perpendicular to the plot radius direction in relascope sampling corresponds to selecting the diameter direction from a particular non-uniform direction distribution (see Chapter 4, Section 4.2).

As the probability density function of the uniform direction distribution is $1/\pi$ for $\theta \in [0, \pi)$ and zero elsewhere, the *mean diameter* in a cross-section over this distribution becomes

$$\mu_D = E[D(\theta)] = \frac{1}{\pi}\int_0^\pi D(\theta) d\theta \tag{6}$$

(cf. Matérn 1956, 1990, Stoyan and Stoyan 1994). Between the mean diameter and the convex perimeter C there exists the following quite practical relation (obvious from Eqs. 1, 3, and 6):

$$C = \int_0^{2\pi} p(\theta) d\theta = \int_0^\pi [p(\theta) + p(\theta + \pi)] d\theta = \int_0^\pi D(\theta) d\theta = \pi\mu_D \tag{7}$$

(Matérn 1956, 1990). In other words, the mean diameter of a cross-section is obtained by dividing the girth tape measurement by π. This well-known result was originally proved by Augustin Louis Cauchy in 1841 (Matérn 1956; see Santaló 1976 and Stoyan et al. 1986 for a more general representation of the result).

The *diameter variance* in a cross-section over the uniform direction distribution is given by

$$\sigma_D^2 = \mathrm{Var}[D(\theta)] = \mathrm{E}\left\{\left\{ D(\theta) - \mathrm{E}[D(\theta)] \right\}^2\right\} = \frac{1}{\pi}\int_0^{\pi} [D(\theta) - \mu_D]^2 \mathrm{d}\theta \tag{8}$$

(cf. Matérn 1956, 1990, Stoyan and Stoyan 1994). The covariance between the diameters intersecting at angle φ, that is, the *diameter autocovariance function* γ_D:[0, π/2]→[0, ∞) at point φ taken over the uniform direction distribution, is defined as

$$\begin{aligned} \gamma_D(\varphi) &= \mathrm{Cov}[D(\theta), D(\theta+\varphi)] \\ &= \mathrm{E}\left\{\left\{ D(\theta) - \mathrm{E}[D(\theta)] \right\}\left\{ D(\theta+\varphi) - \mathrm{E}[D(\theta+\varphi)] \right\}\right\} \\ &= \frac{1}{\pi}\int_0^{\pi} [D(\theta) - \mu_D][D(\theta+\varphi) - \mu_D]\mathrm{d}\theta \,. \end{aligned} \tag{9}$$

Variance is a special case of covariance, as $\sigma_D^2=\gamma_D(0)$. Further, the correlation between diameters intersecting at angle φ, that is, the *diameter autocorrelation function* ρ_D:[0, π/2]→ [–1, 1] at point φ, φ∈ [0, π/2], is expressed as

$$\rho_D(\varphi) = \frac{\mathrm{Cov}[D(\theta),\ D(\theta+\varphi)]}{\sqrt{\mathrm{Var}[D(\theta)]\mathrm{Var}[D(\theta+\varphi)]}} = \frac{1}{\sigma_D^2\pi}\int_0^{\pi} [D(\theta) - \mu_D][D(\theta+\varphi) - \mu_D]\mathrm{d}\theta \tag{10}$$

(cf. Matérn 1956, 1990, Stoyan and Stoyan 1994). Clearly, $\rho_D(0)=1$. Both $\gamma_D(\cdot)$ and $\rho_D(\cdot)$ run symmetrically around the point φ=π/2, that is, $\gamma_D(\pi/2-\nu)=\gamma_D(\pi/2+\nu)$ and $\rho_D(\pi/2-\nu)=\rho_D(\pi/2+\nu)$ for all ν∈ [0, π/2] — hence the domains of the functions are restricted to [0, π/2].

It is essential to notice that diameter information — however complete and precise concerning the diameter function D(·) — is in general insufficient for making inference about the exact shape and area of a non-circular cross-section. Besides non-convexity, which is ignored in diameter information by definition, one may also encounter problems with the family of *constant-width convex sets*, also referred to as *orbiforms* (a name given by Leonhard Euler; Tiercy 1920, Matérn 1956), in which the diameter is constant in all directions (i.e., $\sigma_D^2=0$). In addition to the circle, the family comprises, for example, the Reuleux polygons (Fig. 4): given a regular (i.e., equiangular and equilateral) polygon with an odd number of sides, the corresponding Reuleux polygon is formed by the circular arcs that are subtended by the sides of the linear polygon and whose centres are the opposite vertices of the linear polygon (Santaló 1976). While the circle is the largest in area of the orbiforms of equal diameter (Hadwiger 1957), the Reuleux triangle is the smallest. By Cauchy's theorem (Eq. 7), the orbiforms of equal diameter are also isoperimetric, that is, their perimeters are equal (this result is sometimes referred to as Barbier's theorem after the French mathematician Joseph Emile Barbier).

The numerical examples provided by Matérn (1956) (Fig. 5, Table 1) illustrate how the above-mentioned diameter characteristics (computed over the uniform direction distribution) relate to the shape of the convex closure of a cross-section (Table 1, Figs. 6, 7 and 8). The mean diameter μ_D is merely a size parameter, whereas the diameter variance σ_D^2 reflects both size, shape and smoothness of the convex closure (Stoyan and Stoyan 1994); the effect

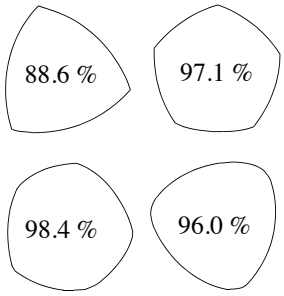

Fig. 4. Four examples of orbiforms — the Reuleux triangle and the Reuleux pentagon in the upper row. The percentage indicates the proportion of the area to the area of the isoperimetric circle (Matérn 1956, Santaló 1976).

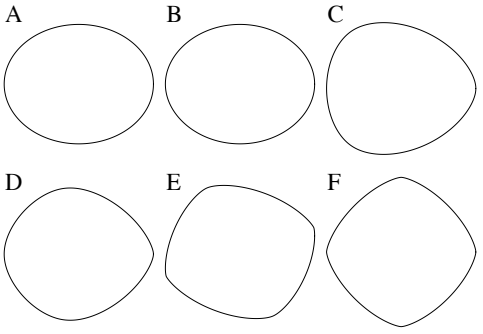

Fig. 5. Six examples of convex shapes provided by Matérn (1956) to illustrate the relation between geometrical shape and some diameter characteristics. Shape A is an ellipse with axis ratio 0.8. See Table 1 and Figs. 6, 7 and 8 for different characteristics of the shapes.

of size can naturally be partialled out from σ_D^2 by using the diameter coefficient of variation $CV_D=\sigma_D/\mu_D$. Even if the diameter autocorrelation function $\rho_D(\cdot)$ does not uniquely relate to the diameter function $D(\cdot)$ — different non-orbiform convex shapes with the same $\rho_D(\cdot)$ can be found (e.g. shapes B and C in Fig. 8; Stoyan and Stoyan 1994) — it evidently characterises some aspects of the shape of a cross-section. Simple inference can be made from the value of $\rho_D(\cdot)$ at the end point $\pi/2$ of the domain, that is, from the autocorrelation of perpendicular diameters (Matérn 1956, 1990, personal communication in November 28, 1995): For an ellipse, $\rho_D(\pi/2)$ is very near –1 — in fact, $\rho_D(\pi/2)$ is a function of the axis ratio in the way that it tends to –1, although very slowly (cf. Matérn 1990, p. 16), as the axis ratio tends to 1. For a circle and other orbiforms, $\sigma_D^2=0$, and $\rho_D(\pi/2)$ thus becomes indefinite. Finally, for a square, $\rho_D(\pi/2)$ tends to +1. The fact that the angle between the minimum and maximum diameters is $\pi/2$ for the ellipse and $\pi/4$ for the square makes these results intuitively plausible. Note that $\rho_D(\pi/2)$ bears also some practical meaning, since if two diameters are measured in a tree, they are usually calipered at right angles to each other.

As mentioned before, the support function and the diameter function derived from it give no information on non-convexity, as they are defined for the convex closure of a cross-section. A polar co-ordinate representation of the boundary of a cross-section provides means for distinguishing between a non-convex cross-section and its convex closure and examining non-convexity. We set the rectangular planar co-ordinate system as before, by choosing an interior point O of the cross-section as the origin and by fixing the positive x-axis. For uniqueness, we need to assume that any ray emanating from O intersects the boundary only once; regarding tree cross-sections, this assumption of *star-shapedness* seems feasible, that is, the origin inside the cross-section can practically always be selected so that the condition is fulfilled. Now the polar co-ordinate representation of the boundary

Table 1. Support function $p(\theta)$, diameter coefficient of variation CV_D, ratio between minimum and maximum diameters D_{min}/D_{max}, and correlation coefficient $\rho_D(\pi/2)$ of the diameters intersecting at right angles for the shapes in Fig. 5 according to Matérn (1956).

Shape	$p(\theta)$	$CV_D(\%)$	D_{min}/D_{max}	$\rho_D(\pi/2)$
A	$(100\cos^2\theta+64\sin^2\theta)^{1/2}$	7.82	0.800	–0.9985
B	$9+\cos(2\theta)$	7.86	0.800	–1.0000
C	$16+\cos(2\theta)+\cos(3\theta)$	4.42	0.882	–1.0000
D	$32+2\cos(2\theta)+\cos(3\theta)+\cos(4\theta)$	4.94	0.871	–0.6000
E	$35+2\cos(2\theta)+2\sin(4\theta)$	5.71	0.817	0.0000
F	$16+\cos(4\theta)$	4.42	0.882	1.0000

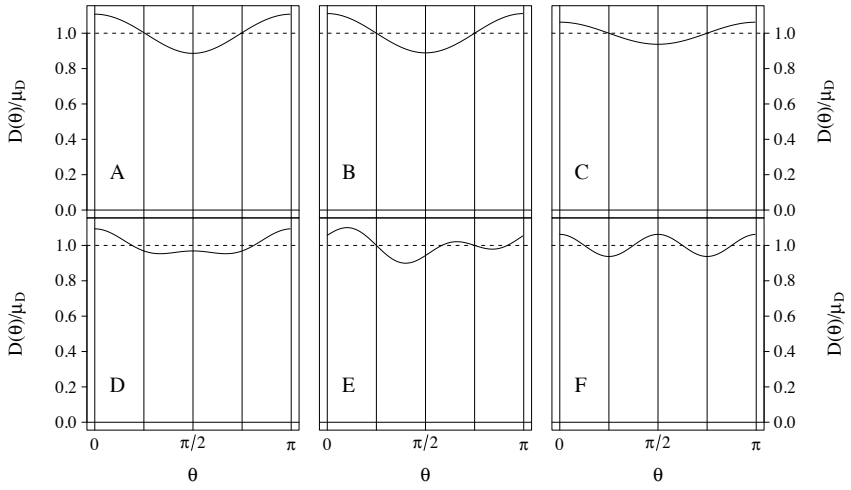

Fig. 6. Diameter functions $D(\theta)$, $\theta \in [0, \pi)$, scaled with the mean diameter μ_D, for the six example shapes in Fig. 5. The positive x-axis, with respect to which the direction θ is determined, runs horizontally through the centre of gravity of the shape; θ increases anticlockwise.

of the cross-section is a continuous function $R:[0, 2\pi)\rightarrow(0, \infty)$, where $R(\theta)$ is the uniquely determined *radius* of the cross-section in direction θ, that is, the distance between O and the point where the ray emanating from O at angle θ intersects the boundary (Fig. 3). By means of $R(\cdot)$, the perimeter of the cross-section can be expressed as

$$C_p = \int_0^{2\pi} \sqrt{R(\theta)^2 + R'(\theta)^2}\, d\theta \tag{11}$$

and the area of the cross-section as

$$A = \frac{1}{2}\int_0^{2\pi} R(\theta)^2\, d\theta \tag{12}$$

(Coxeter 1969, Edwards and Penney 1994).

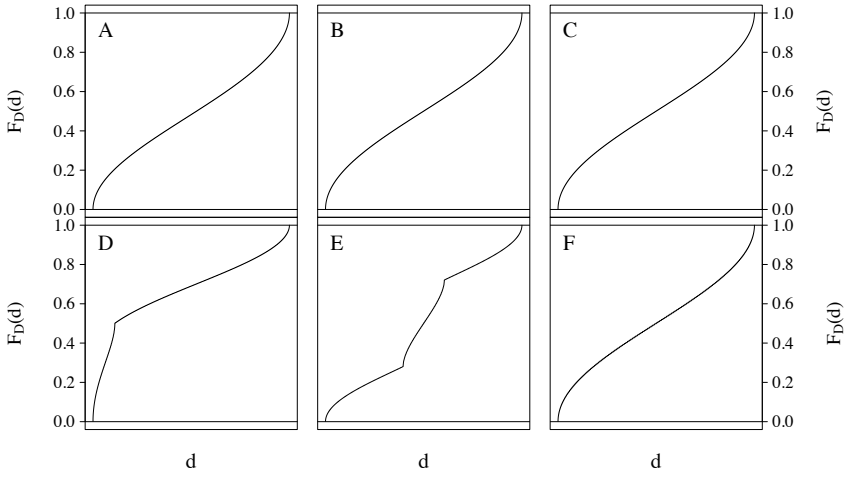

Fig. 7. Cumulative distribution function $F_D(d)=Pr\{(D(\theta)\leq d\}$ of diameter with the uniform direction distribution within $[0, \pi)$ for the example shapes in Fig. 5.

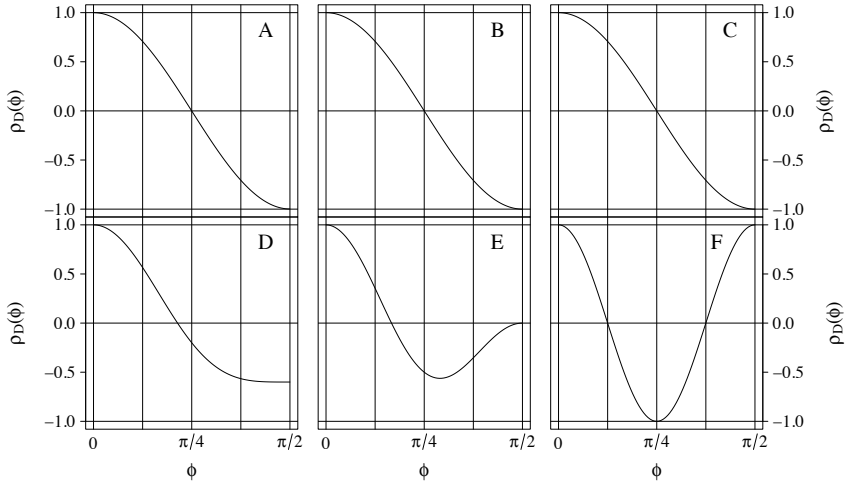

Fig. 8. Diameter autocorrelation function $\rho_D(\varphi)$, $\varphi\in[0, \pi/2]$, over the uniform direction distribution within $[0, \pi)$ for the example shapes in Fig. 5. For the shapes B and C, the autocorrelation functions are congruent.

The sum $B(\theta)=R(\theta)+R(\theta+\pi)$ is here termed the *breadth* of the cross-section in direction θ, $\theta\in[0, \pi)$; it is the length of the chord passing through the point O in direction θ (Fig. 3). Note that the term breadth has sometimes (e.g. Santaló 1976) been used as a synonym for the usual meaning of the width of a set, which, as said before, corresponds to the concept of diameter in this study (in Santaló 1976, however, the width of a convex set is defined as the least of the breadths, i.e., the concept of minimum diameter in this study).

Obviously, the radius and breadth functions depend on the selection of the reference point O. Two examples of a non-arbitrary choice for O are the centre of gravity and the Steiner point (the centre of the mass, distributed over the surface of a convex body, with density

equal to the Gaussian curvature; see Hazewinkel 1992). Given O, the radius function, as opposed to the diameter function, determines the shape of the cross-section uniquely; further, if O is the centre of gravity of the cross-section, the radius function being constant implies that the cross-section be a circle (Matérn 1956, Santaló 1976, Stoyan and Stoyan 1994).

3 Estimation of Cross-Section Area

In this chapter, we consider estimating the area of a tree stem cross-section with the circle area formula and somehow selected diameters; each area estimator is thus characterised by the *diameter selection method*, comprising both the way in which the diameters are selected and the way in which the selected diameters are combined (typically averaged) into the circle formula input. We study how variation in diameter within a non-circular cross-section is reflected to area estimates produced by different estimators; ultimately, we want to find out what can be said about the performance of different estimators without assuming anything about the shape of a cross-section. In the end, we briefly discuss area estimation based on radii.

3.1 Foundations: Source of Randomness and Measures of Estimator Performance

Within a cross-section, we regard the randomness in an area estimator as arising from the procedure of selecting diameters from a fixed, albeit infinite, "diameter population" (cf. the discussion in Chapter 2). Measuring a diameter in a direction sampled from the uniform distribution over $[0, \pi)$ means carrying out simple random sampling in the diameter population, whereas taking a diameter in a direction sampled from some non-uniform distribution means performing random sampling with unequal selection probabilities. Further, measuring an additional diameter perpendicular, or at any fixed angle, to a random diameter is systematic sampling with a random starting point. Yet, naturally, the diameter selection need not involve any randomness at all: taking fixed diameters, such as the maximum or the minimum diameter, or the mean diameter (the girth measurement divided by π), is just selective sampling that entails no randomness when carried out in a fixed diameter population. The area estimators based on a sample of random diameters are of course also random variables, whereas non-randomly selected diameters result in non-random area estimators when viewed from within a cross-section.

The sampling distribution of an area estimator within a cross-section is determined with respect to the diameter sampling design, that is, over all possible samples of diameters. If we select diameters by sampling their directions from a known direction distribution, we obtain the area estimator distribution via this direction distribution and the diameter function. The area estimator can be thought to be composed of a systematic part and a random part:

$$\hat{A}(\boldsymbol{\theta}) = E_{\boldsymbol{\theta}}[\hat{A}(\boldsymbol{\theta})] \; + \; \varepsilon(\boldsymbol{\theta}) \,, \tag{13}$$

where $E_{\boldsymbol{\theta}}[\hat{A}(\boldsymbol{\theta})]$ is the within-cross-section expectation of the area estimator taken over the diameter direction distribution and $\varepsilon(\boldsymbol{\theta})$ is a random error term with zero expectation (and with the distribution determined by the diameter direction distribution and the diameter function). The argument $\boldsymbol{\theta}$ here refers to the source of randomness in general; it can be thought of, for example, as a random vector containing the directions of the diameters included in the estimator.

The *area estimation error* now consists of the *bias* of the estimator and of the random error term:

$$\hat{A}(\boldsymbol{\theta}) - A = \{E_{\boldsymbol{\theta}}[\hat{A}(\boldsymbol{\theta})] - A\} \; + \; \varepsilon(\boldsymbol{\theta}) \,. \tag{14}$$

The bias, measuring how far the expected value of the estimator is from the true area, represents the *systematic error* associated with the estimator; note that this is the "mean error"

to be expected over repeated diameter samplings within a cross-section, not an error being realised in each individual sampling. The random error term, in turn, stands for the *sampling error* resulting from the fact that a diameter sample does not perfectly represent the diameter population but that there is variation between diameter samples that causes variation in estimator values. The usual measure for the magnitude of the sampling error $\varepsilon(\boldsymbol{\theta})$, also termed the *precision* of the estimator, is its variance or standard deviation. The *mean squared error*

$$\begin{aligned} E_{\boldsymbol{\theta}}\{[\hat{A}(\boldsymbol{\theta})-A]^2\} &= \{E_{\boldsymbol{\theta}}[\hat{A}(\boldsymbol{\theta})]-A\}^2 + E_{\boldsymbol{\theta}}[\varepsilon(\boldsymbol{\theta})^2] \\ &= \{E_{\boldsymbol{\theta}}[\hat{A}(\boldsymbol{\theta})]-A\}^2 + Var_{\boldsymbol{\theta}}[\hat{A}(\boldsymbol{\theta})] \end{aligned} \quad (15)$$

combining the squared bias with the precision is a commonly used measure for the *accuracy* of an estimator (e.g. Lindgren 1976).

Trivially, non-random area estimators — those based on girth or fixed diameters, for example — are unaffected by sampling errors: for them, $E_{\boldsymbol{\theta}}[\hat{A}(\boldsymbol{\theta})]=\hat{A}(\boldsymbol{\theta})$ and $Var_{\boldsymbol{\theta}}[\hat{A}(\boldsymbol{\theta})]=0$, and the mean squared error is reduced to the squared bias, that is, to the squared estimation error $[\hat{A}(\boldsymbol{\theta})-A]^2$.

An alternative to the *design-based* thinking discussed above could be a *model-based* approach where cross-sections were regarded as realisations of random figures or as stochastic deformations of a template curve and where stochastic models for the invariant parameters of the random contour functions were then established and estimated in empirical analysis (see e.g. Stoyan and Stoyan 1994 and Hobolth and Jensen 1999). In this thesis, however, we will examine the different area estimators expressly in a design-based way at the within-cross-section level. What was discussed above in terms of diameter-based estimators naturally apply to radius-based estimators as well.

3.2 Effect of Non-Convexity

As already mentioned in Chapter 2, the difference A_C-A between the convex area and the true area of a cross-section is always nonnegative. Aptly, Matérn (1956) termed this difference the *convex deficit* of a cross-section.

From the practical point of view, non-convexity is rather an insidious source of error, since it cannot be observed by a girth tape or a caliper commonly used for measuring standing trees. Thus nothing besides non-negativity can be inferred about convex deficit in an ordinary area estimation situation. It then becomes a valid question whether we had better use the convex area, instead of the true area, as the reference when computing the within-cross-section bias of an area estimator.

3.3 Estimators Based on Diameters and Circle Area Formula

As suggested many times above, an intuitively appealing and the most commonly used way to estimate cross-section area is to apply the circle area formula

$$\hat{A}=\frac{\pi}{4}D^2 , \quad (16)$$

where D is the diameter of the circle that the cross-section is assumed to equate with. As already discussed, D can be chosen in a number of ways within a cross-section. Firstly,

D may be a single measurable diameter: either random, that is, a diameter the direction of which is a random variable usually chosen to be uniformly distributed over [0, π); or systematically sampled, such as the diameter perpendicular to a random diameter; or fixed, such as the minimum diameter or the maximum diameter or the mean diameter derived from the convex perimeter. Secondly, D may be the arithmetic, geometric, or quadratic mean of two or more randomly or systematically sampled or fixed diameters. Using the geometric mean of two diameters in the circle area formula implies the assumption of ellipticity, as this estimator yields the area of an ellipse with the axis lengths equal to the diameters used in the geometric mean. Employing the quadratic mean of two or more diameters, in turn, corresponds to estimating the area as the arithmetic mean of the areas of the circles that have the diameters used in the quadratic mean. Thirdly, D may as well be some other expression constructed from random and non-random diameters, such as the "diameter" involved in the area estimator where the geometric or the quadratic mean of two or more area estimators of the types mentioned above is written in the form of a circle area formula (Matérn 1956, 1990, Loetsch et al. 1973, Kärkkäinen 1974, 1975a, 1984).

In this study, we confine ourselves to estimators where D is a single measurable diameter or a mean of two or more measurable diameters. About the mutual relations between the three types of means, it is useful to remember the following two results: First, for positive variables X_i, i=1, ..., n,

$$\left(\prod_{i=1}^{n} X_i\right)^{\frac{1}{n}} \le \frac{1}{n}\sum_{i=1}^{n} X_i \le \sqrt{\frac{1}{n}\sum_{i=1}^{n} X_i^2}\ , \tag{17}$$

that is, the geometric mean of is never greater than the arithmetic mean, which in turn is never greater than the quadratic mean (see Hardy et al. 1988 for the proofs); the equality between the means holds if all the variables X_i are equal. This implies that the area estimate given by the circle area formula with the geometric mean of unequal diameters be always less than the estimate obtained with the arithmetic mean of the same diameters, which in turn be always less than the estimate obtained with the quadratic mean of the diameters. Second, in the case of *two* positive variables X_1 and X_2, there exists the following relation between the squares of the quadratic, arithmetic and geometric means:

$$\frac{X_1^2 + X_2^2}{2} - 2\left(\frac{X_1 + X_2}{2}\right)^2 + X_1 X_2 = 0\ . \tag{18}$$

This implies that the area estimate based on one of the three diameter means be straightforwardly obtained from the estimates based on the other two (Matérn 1956).

3.3.1 Girth Diameter: Mean Diameter Derived from Convex Perimeter

The non-random area estimator

$$\hat{A}_0 = \frac{\pi}{4}\mu_D^2 = \frac{C^2}{4\pi}\ , \tag{19}$$

where the mean diameter $\mu_D = C/\pi$ (over the uniform direction distribution) derived from the convex perimeter C of the cross-section, termed here the *girth diameter*, is substituted

in the circle area formula, yields the *area of the isoperimetric circle*, that is, the area of the circle that has the perimeter equal to the convex perimeter of the cross-section.

For a non-circular cross-section, this estimator overestimates the convex area irrespective of the shape of the cross-section, because the circle has the largest area among the isoperimetric figures in plane (Hadwiger 1957). Matérn (1956) termed the nonnegative difference $\hat{A}_0 - A_C$ the *isoperimetric deficit* of a cross-section. Regardless of the shape of a cross-section, this deficit can be shown to have the following lower bound depending on diameter variance σ_D^2 within the cross-section:

$$\hat{A}_0 - A_C \geq \frac{3\pi}{4}\sigma_D^2 \tag{20}$$

(see Matérn 1956 for the proof).

Interestingly, $\hat{A}_0$ serves as a baseline for many estimators based on random diameters: in cross-sections with nonnegative correlation between perpendicular diameters, the overestimation error in $\hat{A}_0$ is a lower bound for the within-cross-section bias in those estimators, as we will see in the next section.

3.3.2 Random Diameters with Uniform Direction Distribution

Estimators Involving One or Two Diameters

In the way paved by Matérn (1956), we next consider the area estimators that are of the same form

$$\hat{A} = \frac{\pi}{4} D(\cdot)^2 , \tag{21}$$

but where $D(\cdot)$ is now

1. random diameter $D(\theta)$, $\theta \sim \text{Uniform}(0, \pi)$ ($\hat{A}_1$)
2. arithmetic mean of a random diameter $D(\theta)$ and the diameter $D(\theta+\pi/2)$ perpendicular to it ($\hat{A}_2$)
3. geometric mean of $D(\theta)$ and $D(\theta+\pi/2)$ ($\hat{A}_3$)
4. arithmetic mean of two independent random diameters $D(\theta_1)$ and $D(\theta_2)$, $\theta_1, \theta_2 \sim \text{Uniform}(0, \pi)$ i.i.d. ($\hat{A}_4$)
5. geometric mean of $D(\theta_1)$ and $D(\theta_2)$ ($\hat{A}_5$).

First we focus on the systematic errors, that is, on the within-cross-section biases of these estimators. With the notation introduced before — μ_D denoting the diameter mean, σ_D^2 denoting the diameter variance, and $\rho_D(\pi/2)$ denoting the correlation between perpendicular diameters within a cross-section — the expectations of the estimators over the uniform diameter direction distribution become as follows:

$$\begin{aligned} E(\hat{A}_1) &= \frac{\pi}{4}\mu_D^2 + \frac{\pi}{4}\sigma_D^2 \\ &= \hat{A}_0 + \frac{\pi}{4}\sigma_D^2 , \end{aligned} \tag{22}$$

$$\begin{aligned} E(\hat{A}_2) &= \frac{\pi}{4}\mu_D^2 + \frac{\pi}{8}\sigma_D^2\left[1 + \rho_D\left(\frac{\pi}{2}\right)\right] \\ &= \hat{A}_0 + \frac{\pi}{8}\sigma_D^2\left[1 + \rho_D\left(\frac{\pi}{2}\right)\right], \end{aligned} \tag{23}$$

$$\begin{aligned} E(\hat{A}_3) &= \frac{\pi}{4}\mu_D^2 + \frac{\pi}{4}\sigma_D^2\rho_D\left(\frac{\pi}{2}\right) \\ &= \hat{A}_0 + \frac{\pi}{4}\sigma_D^2\rho_D\left(\frac{\pi}{2}\right), \end{aligned} \tag{24}$$

$$\begin{aligned} E(\hat{A}_4) &= \frac{\pi}{4}\mu_D^2 + \frac{\pi}{8}\sigma_D^2 \\ &= \hat{A}_0 + \frac{\pi}{8}\sigma_D^2 , \end{aligned} \tag{25}$$

and

$$\begin{aligned} E(\hat{A}_5) &= \frac{\pi}{4}\mu_D^2 \\ &= \hat{A}_0 \end{aligned} \tag{26}$$

(cf. Matérn 1956, 1990). (The expectations are obtained by writing the area estimators as sums of squared diameters and diameter products, by taking the expectations separately on each term in the sum, and by applying to these the usual rules that relate means, variances and correlations to each other: $E[D(\theta)^2]=E[D(\theta+\pi/2)^2]=\mu_D^2+\sigma_D^2$, $E[D(\theta)D(\theta+\pi/2)]=\mu_D^2+\sigma_D^2\rho_D(\pi/2)$, $E[D(\theta_1)D(\theta_2)]=E[D(\theta_1)]E[D(\theta_2)]=\mu_D^2$.) Clearly, the estimator $\hat{A}_0$ based on the convex perimeter of a cross-section, which in the previous section was found to overestimate the convex area of a cross-section, now makes a convenient reference. Interestingly, the estimator $\hat{A}_5$ based on the geometric mean of two independent random diameters comprises a bias equal to that of the estimator $\hat{A}_0$. Moreover, the bias of the estimator $\hat{A}_2$ is the arithmetic mean of the biases of the estimators $\hat{A}_1$ and $\hat{A}_3$ (Matérn 1956). In Table 2, the expectations of the estimators are given for the six example shapes of Fig. 5.

Table 2. Expectations of the area estimators $\hat{A}_0$–$\hat{A}_4$ (Eqs. 19 and 22–25) for the shapes in Fig. 5, expressed in permille of true area (cf. Matérn 1956). The expectation of the estimator $\hat{A}_5$ is equal to $\hat{A}_0$ (Eq. 26).

	Shape					
	A	B	C	D	E	F
$\hat{A}_0/A$ (‰)	1019	1019	1022	1017	1030	1030
$E(\hat{A}_1)/A$ (‰)	1025	1025	1024	1020	1034	1032
$E(\hat{A}_2)/A$ (‰)	1019	1019	1022	1018	1032	1032
$E(\hat{A}_3)/A$ (‰)	1013	1013	1020	1016	1030	1032
$E(\hat{A}_4)/A$ (‰)	1022	1022	1023	1019	1032	1031

The mutual ranking of the estimators in terms of bias obviously depends on the values of σ_D^2 and $\rho_D(\pi/2)$ within a cross-section. With the condition $\sigma_D^2>0$ — that is, orbiforms excluded — and by recalling that $-1\leq\rho_D(\pi/2)\leq1$, we can compose the following $\rho_D(\pi/2)$-dependent comparisons between the estimator expectations:

$\rho_D(\pi/2)=-1$:	$E(\hat{A}_3)<\hat{A}_0=E(\hat{A}_5)=E(\hat{A}_2)<E(\hat{A}_4)<E(\hat{A}_1)$
$-1<\rho_D(\pi/2)<0$:	$E(\hat{A}_3)<\hat{A}_0=E(\hat{A}_5)<E(\hat{A}_2)<E(\hat{A}_4)<E(\hat{A}_1)$
$\rho_D(\pi/2)=0$:	$\hat{A}_0=E(\hat{A}_5)=E(\hat{A}_3)<E(\hat{A}_4)=E(\hat{A}_2)<E(\hat{A}_1)$
$0<\rho_D(\pi/2)<½$:	$\hat{A}_0=E(\hat{A}_5)<E(\hat{A}_3)<E(\hat{A}_4)<E(\hat{A}_2)<E(\hat{A}_1)$
$\rho_D(\pi/2)=½$:	$\hat{A}_0=E(\hat{A}_5)<E(\hat{A}_4)=E(\hat{A}_3)<E(\hat{A}_2)<E(\hat{A}_1)$
$½<\rho_D(\pi/2)<1$:	$\hat{A}_0=E(\hat{A}_5)<E(\hat{A}_4)<E(\hat{A}_3)<E(\hat{A}_2)<E(\hat{A}_1)$
$\rho_D(\pi/2)=1$:	$\hat{A}_0=E(\hat{A}_5)<E(\hat{A}_4)<E(\hat{A}_3)=E(\hat{A}_2)=E(\hat{A}_1)$

We find here that with the nonnegative values of $\rho_D(\pi/2)$, all the estimators have expectations greater or equal to that of $\hat{A}_0$; in consequence, all the estimators yield a positive bias, that is, they systematically overestimate the area of a cross-section. With the negative values of $\rho_D(\pi/2)$ this does not hold for the estimator $\hat{A}_3$; however, $E(\hat{A}_3)$ attains its smallest value when $\rho_D(\pi/2)=-1$, and by combining this minimum with the lower bound previously obtained for $\hat{A}_0$ (Eq. 20) we get

$$E(\hat{A}_3) \geq \hat{A}_0 - \frac{\pi}{4}\sigma_D^2 \geq \left(A_C + \frac{3\pi}{4}\sigma_D^2\right) - \frac{\pi}{4}\sigma_D^2 = A_C + \frac{\pi}{2}\sigma_D^2 , \quad (27)$$

which shows that also $\hat{A}_3$ always systematically overestimates the convex area of a cross-section (Matérn 1956). We hence conclude that *regardless of the shape of a non-circular cross-section all these estimators systematically overestimate the convex area of the cross-section*. In the case of orbiforms this conclusion also stands, since a circle is the largest in area among the orbiforms (cf. Fig. 4). (Note that this systematic overestimation motivates the omission of the estimators based on the quadratic mean of diameters, which yield the largest estimates by definition, from our considerations.)

The comparison above also shows that regardless of the value of $\rho_D(\pi/2)$ and thus irrespective of the shape of a cross-section, the estimator $\hat{A}_1$ based on only one random diameter yields the largest bias. The best strategy in terms of bias minimisation, however, depends on the shape of a cross-section: with negatively correlated perpendicular diameters ($-1<\rho_D(\pi/2)<0$), the use of the geometric mean is preferred and, given this, the second diameter is recommended to be taken at right angles to the first one instead of picking it randomly; with mildly positively correlated perpendicular diameters ($0<\rho_D(\pi/2)<½$), the preference of the geometric mean still pertains, but now the second diameter is more advisable to be taken independently at random direction; and finally, with the highly positively correlated perpendicular diameters ($½<\rho_D(\pi/2)<1$), the priority is given to measuring both the diameters independently at random directions, and, conditional on this, to employing the geometric mean. The equalities in the change points are also interesting: if $\rho_D(\pi/2)=-1$ (ellipse-like cross-sections, cf. shapes A–C in Fig. 5 and Table 2), employing the arithmetic mean of two perpendicular diameters is equivalent, in terms of bias, of using the geometric mean of two random diameters; if $\rho_D(\pi/2)=0$ (cf. shape E in Fig. 5 and Table 2), the way of choosing diameters does not matter, but the estimators based on the same type of mean yield an equal bias; if $\rho_D(\pi/2)=½$, using the geometric mean of two perpendicular diameters equals, in terms of bias, using the arithmetic mean of two random diameters; and, if $\rho_D(\pi/2)=1$ (square-like cross-sections, cf. shape F in Fig. 5 and Table 2), the estimators based on two perpendicular diameters yield as large a bias as the estimator based on only one random diameter.

The optimal selection of an estimator may, however, contribute to bias reduction only marginally, since, quoting Matérn (1956), *"the average difference between the 'worst' and the 'best' estimate cannot be greater than the average difference between the 'best' estimate and the area of the convex closure"*: if $0 \le \rho_D(\pi/2) \le 1$, then $\hat{A}_1$ is the worst and $\hat{A}_0$ is the best estimator, and

$$\begin{aligned} E(\hat{A}_1 - \hat{A}_0) &= E(\hat{A}_1) - \hat{A}_0 = \left(\hat{A}_0 + \frac{\pi}{4}\sigma_D^2\right) - \hat{A}_0 = \frac{\pi}{4}\sigma_D^2 \\ &< \frac{3\pi}{4}\sigma_D^2 = \left(A_C + \frac{3\pi}{4}\sigma_D^2\right) - A_C \\ &\le \hat{A}_0 - A_C = E(\hat{A}_0 - A_C); \end{aligned} \tag{28}$$

if, in turn, $-1 \le \rho_D(\pi/2) < 0$, then $\hat{A}_1$ is the worst and $\hat{A}_3$ is the best estimator, and

$$\begin{aligned} E(\hat{A}_1 - \hat{A}_3) &= E(\hat{A}_1) - E(\hat{A}_3) = \left(\hat{A}_0 + \frac{\pi}{4}\sigma_D^2\right) - \left[\hat{A}_0 + \frac{\pi}{4}\sigma_D^2 \rho_D\left(\frac{\pi}{2}\right)\right] \\ &= \frac{\pi}{4}\sigma_D^2\left[1 - \rho_D\left(\frac{\pi}{2}\right)\right] \\ &\le \frac{\pi}{2}\sigma_D^2 = \left(A_C + \frac{\pi}{2}\sigma_D^2\right) - A_C \\ &\le E(\hat{A}_3) - A_C = E(\hat{A}_3 - A_C) \end{aligned} \tag{29}$$

(in both these elaborations, Eq. 20 giving the lower bound for $\hat{A}_0$ is employed, and in the latter derivation also Eq. 27 giving the lower bound for $\hat{A}_3$ is used).

From the systematic errors we proceed into the sampling errors quantified by the within-cross-section variances of the estimators over the uniform direction distribution. Except for the estimator $\hat{A}_5$ based on the geometric mean of two independent diameters, the variances cannot be expressed in terms of the simple parameters μ_D, σ_D^2, and $\rho_D(\pi/2)$, but involve higher moments and product moments of diameters, which make them somewhat difficult to compare with each other:

$$\mathrm{Var}(\hat{A}_1) = \frac{\pi^2}{16}\left\{E[D(\theta)^4] - \left(\mu_D^2 + \sigma_D^2\right)^2\right\}, \tag{30}$$

$$\begin{aligned} \mathrm{Var}(\hat{A}_2) &= \frac{\pi^2}{16}\left\{\frac{1}{8}E[D(\theta)^4] + \frac{1}{2}E\left[D(\theta)^3 D\left(\theta + \frac{\pi}{2}\right)\right] + \frac{3}{8}E\left[D(\theta)^2 D\left(\theta + \frac{\pi}{2}\right)^2\right]\right. \\ &\quad \left. - \frac{1}{4}\left\{2\mu_D^2 + \sigma_D^2\left[1 + \rho_D\left(\frac{\pi}{2}\right)\right]\right\}^2\right\}, \end{aligned} \tag{31}$$

$$\mathrm{Var}(\hat{A}_3) = \frac{\pi^2}{16}\left\{ \mathrm{E}\left[\mathrm{D}(\theta)^2 \mathrm{D}\left(\theta + \frac{\pi}{2} \right)^2 \right] - \left[\mu_D^2 + \sigma_D^2 \rho_D\left(\frac{\pi}{2} \right) \right]^2 \right\}, \tag{32}$$

$$\begin{aligned} \mathrm{Var}(\hat{A}_4) &= \frac{\pi^2}{16}\left\{ \frac{1}{8}\mathrm{E}[\mathrm{D}(\theta)^4] + \frac{1}{2}\mu_D \mathrm{E}[\mathrm{D}(\theta)^3] + \frac{3}{8}\left(\mu_D^2 + \sigma_D^2 \right)^2 \right. \\ &\quad \left. - \frac{1}{4}\left(2\mu_D^2 + \sigma_D^2 \right)^2 \right\}, \end{aligned} \tag{33}$$

and

$$\mathrm{Var}(\hat{A}_5) = \frac{\pi^2}{16}\left\{ \left(\mu_D^2 + \sigma_D^2 \right)^2 - \mu_D^4 \right\}. \tag{34}$$

(The variances are obtained by applying the definition of variance $\mathrm{Var}(X)=\mathrm{E}(X^2)-\mathrm{E}(X)^2$ straightforwardly to the squared mean of diameters in the estimator, by writing the expressions inside the expectation operators as sums of diameter powers and products of diameter powers, by taking the expectations separately on each term in the sums, and by applying to these the usual rules that relate means, variances and correlations to each other: $\mathrm{E}[\mathrm{D}(\theta)^2]=\mathrm{E}[\mathrm{D}(\theta+\pi/2)^2]=\mu_D^2+\sigma_D^2$, $\mathrm{E}[\mathrm{D}(\theta)\mathrm{D}(\theta+\pi/2)]=\mu_D^2+\sigma_D^2\rho_D(\pi/2)$, $\mathrm{E}[\mathrm{D}(\theta)^a\mathrm{D}(\theta+\pi/2)^b]=\mathrm{E}[\mathrm{D}(\theta)^b\mathrm{D}(\theta+\pi/2)^a]$, $\mathrm{E}[\mathrm{D}(\theta_1)^a\mathrm{D}(\theta_2)^b]=\mathrm{E}[\mathrm{D}(\theta_1)^a]\mathrm{E}[\mathrm{D}(\theta_2)^b]$.) We can see that if $\rho_D(\pi/2)=0$, the estimators $\hat{A}_2$ and $\hat{A}_4$, on one hand, and the estimators $\hat{A}_3$ and $\hat{A}_5$, on the other hand, coincide in terms of variance quite as we saw them to do in terms of bias; in other words, if perpendicular diameters in a cross-section are uncorrelated, the way of selecting the diameters does not influence the sampling error but the type of mean used in the area estimator does. In Table 3, the standard deviations (square roots of variances) of the estimators are given for the six example shapes of Fig. 5.

By the procedure known as the delta method (see e.g. Casella and Berger 1990) — based on the linearisation of a non-linear function by Taylor series expansion — the following variance approximations expressible in terms of only μ_D, σ_D^2, and $\rho_D(\pi/2)$ are found:

$$\begin{aligned} \tilde{\mathrm{Var}}(\hat{A}_1) &= \frac{\pi^2}{4}\mu_D^2\sigma_D^2 \\ &= \pi \hat{A}_0 \sigma_D^2, \end{aligned} \tag{35}$$

$$\begin{aligned} \tilde{\mathrm{Var}}(\hat{A}_2) = \tilde{\mathrm{Var}}(\hat{A}_3) &= \frac{\pi^2}{8}\mu_D^2\sigma_D^2\left[1 + \rho_D\left(\frac{\pi}{2} \right) \right] \\ &= \frac{\pi}{2}\hat{A}_0\sigma_D^2\left[1 + \rho_D\left(\frac{\pi}{2} \right) \right], \end{aligned} \tag{36}$$

$$\begin{aligned} \tilde{\mathrm{Var}}(\hat{A}_4) = \tilde{\mathrm{Var}}(\hat{A}_5) &= \frac{\pi^2}{8}\mu_D^2\sigma_D^2 \\ &= \frac{\pi}{2}\hat{A}_0\sigma_D^2. \end{aligned} \tag{37}$$

Table 3. Square roots of the variances (Eqs. 30–34; Sd) and approximate variances (Eqs. 35–37; S̃d) of the area estimators $\hat{A}_1$–$\hat{A}_5$ for the shapes in Fig. 5, expressed in permille of true area (cf. Matérn 1956).

	Shape					
	A	B	C	D	E	F
$Sd(\hat{A}_1)/A$ (‰)	159	160	90	102	118	91
$\tilde{Sd}(\hat{A}_1)/A$ (‰)	159	160	90	101	118	91
$Sd(\hat{A}_2)/A$ (‰)	4	0	0	45	83	91
$Sd(\hat{A}_3)/A$ (‰)	9	4	1	44	83	91
$\tilde{Sd}(\hat{A}_2)/A = \tilde{Sd}(\hat{A}_3)/A$ (‰)	4	0	0	45	83	91
$Sd(\hat{A}_4)/A$ (‰)	113	113	64	72	83	64
$Sd(\hat{A}_5)/A$ (‰)	113	113	64	71	83	64
$\tilde{Sd}(\hat{A}_4)/A = \tilde{Sd}(\hat{A}_5)/A$ (‰)	113	113	64	71	83	64

(For the estimators $\hat{A}_1$–$\hat{A}_4$, Matérn (1956, 1990) presented, without reference to the delta method or any derivation, approximate standard deviations, the squares of which are seen to correspond to these approximate variances.) The nonnegative difference between the actual and approximate variance of the estimator $\hat{A}_5$

$$\mathrm{Var}(\hat{A}_5) - \tilde{\mathrm{Var}}(\hat{A}_5) = \frac{\pi^2}{16}\left[\left(\mu_D^2 + \sigma_D^2\right)^2 - \mu_D^4\right] - \frac{\pi^2}{8}\mu_D^2\sigma_D^2 = \frac{\pi^2}{16}\sigma_D^4 \qquad (38)$$

suggests that these approximate variances might underestimate the true ones; in the example shapes of Fig. 5, however, the approximate variances practically equal the true variances (Table 3).

Unlike the biases and the true variances, the approximate variances are invariant of the type of the mean employed in the estimator — only the number and the way of selecting the diameters influence the approximate sampling error of the estimator; consequently, in terms of approximate variance, it would appear natural to favour the estimators based on the geometric mean, as they yield smaller bias than those based on the arithmetic mean. By the possible values of $\rho_D(\pi/2)$, the variance approximations can be ranked as follows:

$-1 \le \rho_D(\pi/2) < 0$: $\tilde{\mathrm{Var}}(\hat{A}_2) = \tilde{\mathrm{Var}}(\hat{A}_3) < \tilde{\mathrm{Var}}(\hat{A}_4) = \tilde{\mathrm{Var}}(\hat{A}_5) < \tilde{\mathrm{Var}}(\hat{A}_1)$

$\rho_D(\pi/2) = 0$: $\tilde{\mathrm{Var}}(\hat{A}_2) = \tilde{\mathrm{Var}}(\hat{A}_3) = \tilde{\mathrm{Var}}(\hat{A}_4) = \tilde{\mathrm{Var}}(\hat{A}_5) < \tilde{\mathrm{Var}}(\hat{A}_1)$

$0 < \rho_D(\pi/2) < 1$: $\tilde{\mathrm{Var}}(\hat{A}_4) = \tilde{\mathrm{Var}}(\hat{A}_5) < \tilde{\mathrm{Var}}(\hat{A}_2) = \tilde{\mathrm{Var}}(\hat{A}_3) < \tilde{\mathrm{Var}}(\hat{A}_1)$

$\rho_D(\pi/2) = 1$: $\tilde{\mathrm{Var}}(\hat{A}_4) = \tilde{\mathrm{Var}}(\hat{A}_5) < \tilde{\mathrm{Var}}(\hat{A}_2) = \tilde{\mathrm{Var}}(\hat{A}_3) = \tilde{\mathrm{Var}}(\hat{A}_1)$

This comparison suggests that when measuring two diameters in a cross-section, one should take the second diameter at right angles to the first one, if $-1 \le \rho_D(\pi/2) < 0$, and at random direction, if $0 < \rho_D(\pi/2) \le 1$, in order to minimise the approximate sampling error. Noteworthily, this policy agrees with minimising the bias, as was shown by the previous comparison of the within-cross-section expectations of the estimators.

The equalities in the change points of the above comparison are also somewhat interesting: If perpendicular diameters in a cross-section are uncorrelated ($\rho_D(\pi/2)=0$), also the effect of the diameter selection method vanishes: all the two-diameter estimators $\hat{A}_2$, $\hat{A}_3$, $\hat{A}_4$, and $\hat{A}_5$ have the same approximate sampling error, half of that of the estimator $\hat{A}_1$. If, in turn, perpendicular diameters are fully positively correlated ($\rho_D(\pi/2)=1$), taking the

second diameter at right angles to the first one benefits none compared to measuring only one diameter but the approximate variance is halved only by measuring the two diameters independently. Finally, if perpendicular diameters are fully negatively correlated ($\rho_D(\pi/2)=-1$), the approximate sampling error for the estimators $\hat{A}_2$ and $\hat{A}_3$ disappears (cf. shapes B and C in Table 3); hence, for ellipse-like cross-sections, measuring two perpendicular diameters should always lead to an approximately sampling-error-free area estimate.

Generalisation to n Diameters

The area estimators based on a mean of two diameters can naturally be generalised to involve countably many diameters. For the generalised estimators involving the arithmetic mean, the within-cross-section expectations are expressible in terms of the simple parameters μ_D, σ_D^2, and $\rho_D(\pi/2)$: the expectation of the estimator based on the arithmetic mean of $n \in \mathbb{N}$, $n \geq 2$, independent random diameters (a generalisation of $\hat{A}_4$ and thus denoted by $\hat{A}_{G4}$) becomes

$$\begin{aligned} E(\hat{A}_{G4}) &= \frac{\pi}{4}\mu_D^2 + \frac{\pi}{4n}\sigma_D^2 \\ &= \hat{A}_0 + \frac{\pi}{4n}\sigma_D^2 , \end{aligned} \tag{39}$$

and the expectation of the estimator based on the arithmetic mean of n/2, $n=2k$, $k \geq 1$, $k \in \mathbb{N}$, independent random diameters and their n/2 perpendiculars (a generalisation of $\hat{A}_2$ and thus denoted by $\hat{A}_{G2}$) is found to be

$$\begin{aligned} E(\hat{A}_{G2}) &= \frac{\pi}{4}\mu_D^2 + \frac{\pi}{4n}\sigma_D^2\left[1+\rho_D\left(\frac{\pi}{2}\right)\right] \\ &= \hat{A}_0 + \frac{\pi}{4n}\sigma_D^2\left[1+\rho_D\left(\frac{\pi}{2}\right)\right] \end{aligned} \tag{40}$$

(cf. the commonly known theorem about the mean of quadratic forms, to be found in e.g. Kendall and Stuart 1979). If perpendicular diameters are uncorrelated, these general estimators clearly coincide in terms of bias. Further, as n tends to infinity, the expectations of both the general estimators tend to $\hat{A}_0$; the biases of the estimators can hence be reduced by measuring more diameters, but the biases can never fall below that of $\hat{A}_0$.

The expectations of the generalised estimators based on the geometric mean of more than two diameters cannot be expressed in terms of μ_D, σ_D^2, and $\rho_D(\pi/2)$, but involve "fractional diameter moments", that is, expectations of fractional powers of diameters over the uniform direction distribution, which make them difficult to compare with those presented above: the expectation of the estimator based on the geometric mean of n independent random diameters (a generalisation of $\hat{A}_5$ and thus denoted by $\hat{A}_{G5}$) becomes

$$E(\hat{A}_{G5}) = \frac{\pi}{4}\left\{E\left[D(\theta)^{\frac{2}{n}}\right]\right\}^n , \tag{41}$$

and the expectation of the estimator based on the geometric mean of n/2 independent random diameters and their n/2 perpendiculars (a generalisation of $\hat{A}_3$ and thus denoted by $\hat{A}_{G3}$) is found to be

$$E(\hat{A}_{G3}) = \frac{\pi}{4}\left\{ E\left[D(\theta)^{\frac{2}{n}} D\left(\theta + \frac{\pi}{2} \right)^{\frac{2}{n}} \right] \right\}^{\frac{n}{2}} . \tag{42}$$

For the generalised area estimators based on the arithmetic mean, the variances become somewhat intricate:

$$\begin{aligned} \mathrm{Var}(\hat{A}_{G4}) &= \frac{\pi^2}{16n^4}\Big\{ n\,E[D(\theta)^4] + 4n(n-1)\mu_D E[D(\theta)^3] + n(2n-3)\left(\mu_D^2 + \sigma_D^2\right)^2 \\ &\quad + \left[6n(n-1)(n-2) - 2n^2(n-1) \right]\mu_D^2\left(\mu_D^2 + \sigma_D^2\right) \\ &\quad + \left[n(n-1)(n-2)(n-3) - n^2(n-1)^2 \right]\mu_D^4 \Big\} , \end{aligned} \tag{43}$$

and

$$\begin{aligned} \mathrm{Var}(\hat{A}_{G2}) &= \frac{\pi^2}{16n^4}\Bigg\{ n\,E[D(\theta)^4] + 4n\,E\left[D(\theta)^3 D\left(\theta + \frac{\pi}{2} \right) \right] + 3n\,E\left[D(\theta)^2 D\left(\theta + \frac{\pi}{2} \right)^2 \right] \\ &\quad + 4n(n-2)\mu_D \left\{ E[D(\theta)^3] + 3E\left[D(\theta)^2 D\left(\theta + \frac{\pi}{2} \right) \right] \right\} \\ &\quad + 3n(n-2)\left\{ 2\mu_D^2 + \sigma_D^2\left[1 + \rho_D\left(\frac{\pi}{2} \right) \right] \right\}^2 \\ &\quad + 6n(n-2)(n-4)\mu_D^2 \left\{ 2\mu_D^2 + \sigma_D^2\left[1 + \rho_D\left(\frac{\pi}{2} \right) \right] \right\} \\ &\quad + n(n-2)(n-4)(n-6)\mu_D^4 \\ &\quad - \left\{ n\left\{ 2\mu_D^2 + \sigma_D^2\left[1 + \rho_D\left(\frac{\pi}{2} \right) \right] \right\} + n(n-2)\mu_D^2 \right\}^2 \Bigg\} . \end{aligned} \tag{44}$$

For the generalisations based on the geometric mean, the variance expressions are far simpler on the face but again relatively uninformative if one wants to compare them to those above:

$$\mathrm{Var}(\hat{A}_{G5}) = \frac{\pi^2}{16}\left\{ \left\{ E\left[D(\theta)^{\frac{4}{n}} \right] \right\}^n - \left\{ E\left[D(\theta)^{\frac{2}{n}} \right] \right\}^{2n} \right\} , \tag{45}$$

and

$$\mathrm{Var}(\hat{A}_{G3}) = \frac{\pi^2}{16}\left\{ \left\{ E\left[D(\theta)^{\frac{4}{n}} D\left(\theta + \frac{\pi}{2} \right)^{\frac{4}{n}} \right] \right\}^{\frac{n}{2}} - \left\{ E\left[D(\theta)^{\frac{2}{n}} D\left(\theta + \frac{\pi}{2} \right)^{\frac{2}{n}} \right] \right\}^n \right\} . \tag{46}$$

Contrary to these actual variances, the delta method approximations are both uncomplicated and interpretative:

$$\begin{aligned} \widetilde{\mathrm{Var}}(\hat{A}_{G4}) = \widetilde{\mathrm{Var}}(\hat{A}_{G5}) &= \frac{\pi^2}{4n}\mu_D^2\sigma_D^2 \\ &= \frac{\pi}{n}\hat{A}_0\sigma_D^2 , \end{aligned} \tag{47}$$

and

$$\begin{aligned} \widetilde{\mathrm{Var}}(\hat{A}_{G2}) = \widetilde{\mathrm{Var}}(\hat{A}_{G3}) &= \frac{\pi^2}{4n}\mu_D^2\sigma_D^2\left[1+\rho_D\left(\frac{\pi}{2}\right)\right] \\ &= \frac{\pi}{n}\hat{A}_0\sigma_D^2\left[1+\rho_D\left(\frac{\pi}{2}\right)\right]. \end{aligned} \tag{48}$$

Trivially, by measuring more diameters one reduces the true and the approximate variances of the generalised estimators, up to zero as n tends to infinity. Otherwise the generalised estimators share the properties previously demonstrated for the two-diameter estimators: If perpendicular diameters are uncorrelated in a cross-section, the generalised estimators coincide pairwise in terms of true sampling errors ($\mathrm{Var}(\hat{A}_{G3})=\mathrm{Var}(\hat{A}_{G5})$, $\mathrm{Var}(\hat{A}_{G2})=\mathrm{Var}(\hat{A}_{G4})$) and all together in terms of approximate sampling errors ($\widetilde{\mathrm{Var}}(\hat{A}_{G3})=\widetilde{\mathrm{Var}}(\hat{A}_{G5})=\widetilde{\mathrm{Var}}(\hat{A}_{G2})=\widetilde{\mathrm{Var}}(\hat{A}_{G4})$). Further, in the case of an elliptic cross-section, for which $\rho_D(\pi/2)$ is near –1, the approximate variances of $\hat{A}_{G2}$ and $\hat{A}_{G3}$ become close to zero independent of the value of n, and thus increasing the number of diameter measurements within the cross-section should not make much difference in terms of the approximate sampling error.

3.3.3 Minimum and Maximum Diameters

From the estimators involving random diameters with uniformly distributed directions, we proceed to discussing six fixed estimators based on the minimum and maximum diameters of a cross-section. The estimators are still of the form

$$\hat{A} = \frac{\pi}{4}D^2 , \tag{49}$$

where D is now, following Matérn (1956),

6. arithmetic mean of the minimum diameter D_{min} and the maximum diameter D_{max} in the cross-section ($\hat{A}_6$)
7. geometric mean of D_{min} and D_{max} ($\hat{A}_7$)
8. arithmetic mean of D_{min} and its perpendicular ($\hat{A}_8$)
9. geometric mean of D_{min} and its perpendicular ($\hat{A}_9$)
10. arithmetic mean of D_{max} and its perpendicular ($\hat{A}_{10}$)
11. geometric mean of D_{max} and its perpendicular ($\hat{A}_{11}$).

Note that the estimators $\hat{A}_8$–$\hat{A}_{11}$ may not always be well-defined — consider, for example, the situation where D_{min} is attained in two different directions but the diameters perpendicular to these diameters are unequal (Matérn 1956). If the estimators are well-defined,

Table 4. Area estimates produced by the estimators $\hat{A}_6$–$\hat{A}_{11}$ for the shapes in Fig. 5, expressed in permille of true area (cf. Matérn 1956).

Shape	A	B	C	D	E	F
$\hat{A}_6/A$ (‰)	1013	1019	1022	1066	1030	1030
$\hat{A}_7/A$ (‰)	1000	1006	1018	1061	1020	1026
$\hat{A}_8/A$ (‰)	1013	1019	1022	986	921	905
$\hat{A}_9/A$ (‰)	1000	1006	1018	985	919	905
$\hat{A}_{10}/A$ (‰)	1013	1019	1022	1082	1145	1163
$\hat{A}_{11}/A$ (‰)	1000	1006	1018	1078	1143	1163

they are also fixed, as the randomness induced by a selection between the alternative diameters is avoided. In Table 4, the values of the estimators are given for the six example shapes of Fig. 5.

Since the geometric mean is never greater than the arithmetic mean for nonnegative measurements and since D^2 is a monotonously increasing function for $D>0$, the above estimators can be ranked pairwise as $\hat{A}_6 \geq \hat{A}_7$, $\hat{A}_8 \geq \hat{A}_9$, and $\hat{A}_{10} \geq \hat{A}_{11}$. In fact, the larger is the difference between the diameters to be averaged, the more pronounced becomes the reducing effect of using the geometric mean instead of the arithmetic one: if we denote by β the ratio of the smaller diameter to the larger one, the ratio between the estimator involving the arithmetic mean and the estimator involving the geometric mean becomes $(\beta+1)^2/4\beta$ (cf. Matérn 1990), which is a monotonously decreasing function of β in (0, 1]. Furthermore, since the diameter perpendicular to D_{max} cannot be smaller than D_{min} in a cross-section and, similarly, since the diameter perpendicular to D_{min} cannot be larger than D_{max}, we can straightforwardly infer that $\hat{A}_{10} \geq \hat{A}_6 \geq \hat{A}_8$, and $\hat{A}_{11} \geq \hat{A}_7 \geq \hat{A}_9$. The equalities hold for the cross-sections that have D_{max} and D_{min} at right angles to each other. For ellipses, the estimators $\hat{A}_7$, $\hat{A}_9$ and $\hat{A}_{11}$ naturally give the true area, whereas, contrary to what Matérn (1956) claims, the estimators $\hat{A}_6$, $\hat{A}_8$ and $\hat{A}_{10}$ yield the arithmetic mean of the true area and the estimate involving the quadratic mean of D_{max} and D_{min}.

However, no general inference independent of cross-section shape can be made on how these area estimators relate to the estimators based on girth or one or more random diameters with uniformly distributed directions; unlike those estimators, the estimators involving extreme diameters may also underestimate the convex area of a cross-section (cf. estimators $\hat{A}_8$ and $\hat{A}_9$ with shapes D–F in Table 4).

3.4 Estimators Based on Radii

Lastly, we digress a little from the circle area formula and diameters and briefly discuss area estimation based on radial information. In the following, we assume a cross-section to be star-shaped so that all the radii from a suitably chosen interior point O of the cross-section can be uniquely determined (cf. Chapter 2).

The true area of a cross-section, expressed as a function of the polar co-ordinate representation $R(\cdot)$ of the contour of a cross-section (see Chapter 2), can alternatively be viewed as the product of π and the expectation of the squared radius over the uniform direction distribution in $[0, 2\pi)$:

$$A = \frac{1}{2}\int_0^{2\pi} R(\theta)^2 \, d\theta = \pi \frac{1}{2\pi}\int_0^{2\pi} R(\theta)^2 \, d\theta = \pi \, E[R(\theta)^2] \, . \tag{50}$$

These expressions suggest an area estimator of the type

$$\hat{A} = \frac{1}{2}\sum_{i=1}^{n}\left[R(\theta_i)^2 \frac{2\pi}{n} \right] = \frac{\pi}{n}\sum_{i=1}^{n} R(\theta_i)^2 \ , \qquad (51)$$

where $R(\theta_i)$ is the radius of a cross-section measured in direction θ_i, i=1, 2, ..., n. In the first expression, the definite integral of $R(\theta)^2$ is obviously approximated by the sum of n rectangles with the width $2\pi/n$ and the height $R(\theta_i)^2$. This corresponds to estimating the area of the cross-section with the sum of n disjoint, equally wide circular sectors (the area of a circular sector with angle $\Delta\theta_i=2\pi/n$ and side length $R(\theta_i)$ is $\Delta\theta_i R(\theta_i)^2/2=\pi R(\theta_i)^2/n$, and summing up n such sectors then results in the second expression). This expression is straightforwardly seen to be π times the squared quadratic mean of n radii $R(\theta_i)$, a natural estimator for π times the expectation of the squared radius over the uniform direction distribution. The application of this estimator does not require that the radii be measured equidistantly.

Just as the diameters in the estimators based on the circle area formula can be chosen in many ways, also for the radii various selection strategies are naturally available (see e.g. Gregoire and Valentine 1995). The remarkable property of the estimator of Eq. 51 is that it is unbiased if the marginal distribution of each radius direction θ_i is uniform over $[0, 2\pi)$ (Matérn 1956, Gregoire and Valentine 1995). This condition naturally holds if the directions are independently sampled from the uniform distribution over $[0, 2\pi)$, in which case it is also easy to derive analytically the exact variance for the estimator and also to find an unbiased estimator for that variance (Gregoire and Valentine 1995). However, the variance is directly related to the variation in the radii used and thus considerably affected by the choice of the location of O; for decreasing the variance of the estimator, centralising the location of O as well as applying systematic sampling strategies for radii have been suggested (Gregoire and Valentine 1995).

In sum, the bias in area estimation can be avoided, if the cross-sections can be observed "from inside" instead of "from outside", that is, if radii instead of diameters can be measured. For standing trees this is not feasible with the standard measurement equipment, but to estimating the area of end sections of logs — or the area of the crown projection of a tree — for instance, this approach certainly pertains (Matérn 1956).

4 Bitterlich Sampling

Bitterlich sampling — also referred to as relascope sampling, angle-count sampling, horizontal point sampling, variable radius plot sampling, and plotless sampling — was introduced in forestry by the Austrian forester Walter Bitterlich (1948a, 1948b) as a simple counting technique for estimating relative basal area of a tree stand. Nowadays it is also extensively used for sampling trees in forest inventories. The idea in the method is to count, or pick into the sample, those trees in a stand that subtend an angle greater or equal to a fixed angle α when viewed horizontally at breast height from a randomly located point in the stand (Fig. 9). An estimate for the relative basal area at breast height is then obtained by simply multiplying the tally of trees by an α-dependent constant. The procedure may be repeated at several randomly located viewing points in the stand.

There are several alternative ways to formalise Bitterlich sampling. In a model-based approach, the sampling procedure is considered under a model assumed for the structure of the tree stand: in such a model, tree locations are typically regarded as a realisation of a (stationary) spatial point process and tree diameters are treated either as independent random variables with assumed (identical) probability distributions or as the marks of the point process with a mark distribution function involving spatial dependence between the trees; the viewing points need not then be randomly located, but the statistical properties of the estimators of stand totals (typically relative basal area or stem volume) based on angle-count samples are derived given the assumed model (e.g. Holgate 1967, Sukwong et al. 1971, Matérn 1972, Oderwald 1981, and Penttinen 1988). In this study, however, we adopt the usual design-based approach (refer to common textbooks such as e.g. de Vries 1986, Schreuder et al. 1993, and Gregoire and Valentine 2008), where the spatial pattern of tree locations in the region of interest is regarded as fixed and where the randomness in estimators is considered to arise only from the choice of the viewing point locations. Within this design-based context, there are then at least three different unequal probability sample designs for finite population and one formulation for infinite population to choose among (Eriksson 1995); these differ from each other by the definition of sampling unit and population — whether the sampling unit is considered to be the area from which a tree is seen by relascope, the actual tree, or the viewing point in which relascope is used, and,

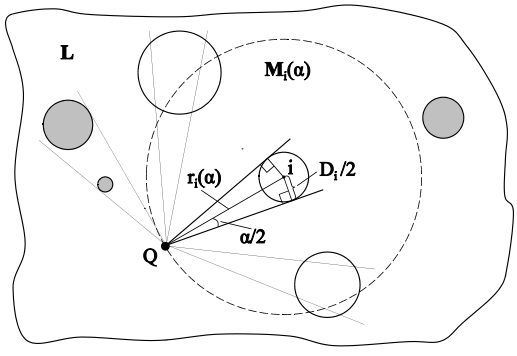

Fig. 9. Selection of trees in region **L** by Bitterlich sampling with viewing angle α: the trees (white cross-sections) that subtend an angle greater or equal to α, when viewed at breast height from a randomly selected point Q in **L**, are included in the sample. The inclusion region $\mathbf{M}_i(\alpha)$ of the tree i with diameter D_i is outlined with the dashed line.

accordingly, whether the population to be sampled then becomes finite or infinite. In this study, we adhere to the classical *Grosenbaugh design*.

In the Grosenbaugh design, the population is finite and consists of the trees reaching above the breast height in the region of interest. A sample is then composed of the trees selected at one randomly located viewing point, and sampling at k independently randomly located viewing points in the region results in k independent samples. The probability of being included in a sample, termed the *inclusion probability* — which in this case equals the probability of being selected at each view, referred to as the *selection probability* — varies according to tree. More precisely — and first realised by the American forester Lewis R. Grosenbaugh (1958), hence the name of the design (Eriksson 1995) — Bitterlich sampling is a method of PPS sampling, that is, sampling with probability proportional to size, meaning that each sampling unit is included in a sample with probability proportional to a covariate, in this case the cross-section area at breast height, which is positively correlated with the variable of interest, in this case typically stem volume.

The estimation of population totals in PPS sampling relies upon the *Horvitz-Thompson theorem*, which is a beautifully general theory for design-based inference from probability samples (Overton and Stehman 1995). The Horvitz-Thompson estimation is based on the inclusion probabilities of the sampling units, by the inverses of which the observed values of the characteristics of interest are weighted. The theorem is explained in more detail in Appendix B.

Our interest focuses on how non-circularity in the breast height cross-sections of trees affects stand or tree characteristic estimation based on Bitterlich sampling. In order to avoid the complications irrelevant from this point of view, we make the following three assumptions, which are independent of our chosen sampling strategy consisting of the Grosenbaugh design and the Horvitz-Thompson estimator: First, we assume the ground level to be horizontal. Second, we assume the viewer's eye to be at breast height (1.3 m) from the ground level and the viewer to sight trees horizontally. And third, we assume the region of interest to be such that the edge effects on the inclusion probabilities of trees need not be considered (for example, we assume the borders of the region to be set in the manner that each tree taken to belong to the stand is located farther than its inclusion radius (Eq. 52) from the borders; for some methods of dealing with the edge effect in Bitterlich sampling, see Grosenbaugh 1958, Haga and Maezawa 1959, Barrett 1964, and Schmid 1969).

4.1 Estimation of Stand Totals

We start by explaining how stand totals, that is, sums of tree characteristics within a stand, are estimated from a Bitterlich sample of trees, when the tree cross-sections at breast height are circular. Then we investigate the errors that emerge when the estimators based on the circularity assumption are applied to trees with non-circular of cross-sections. Finally, we examine the estimation of relative basal area in both these aspects.

In addition to the general simplifying presumptions stated above, we assume the characteristics of the trees in the sample to be measured or estimated without error. For the notation, let $\mathbf{L}$ denote the region of interest in the ground plane, $|\mathbf{L}|$ the area of this region, and $\mathbf{I}$ the set of the trees growing in $\mathbf{L}$ and reaching above breast height. Further, let Q denote a uniformly randomly located viewing point in $\mathbf{L}$ and $\alpha \in (0, \pi)$ the viewing angle used in a relascope.

4.1.1 Principle under Assumption of Circular Cross-Sections

If the cross-sections of the trees are circular at breast height, the maximum distance, determined from the tree pith, at which the tree $i \in \mathbf{I}$ with breast height diameter D_i is taken into the Bitterlich sample becomes

$$r_i(\alpha) = \frac{D_i}{2} \cdot \frac{1}{\sin(\alpha/2)} \tag{52}$$

by a straightforward trigonometric consideration (Fig. 9). In other words, the *inclusion region* $\mathbf{M}_i(\alpha)$ within which the tree $i \in \mathbf{I}$ is observed in an angle greater or equal to α is a circle with radius $r_i(\alpha)$ and area

$$|\mathbf{M}_i(\alpha)| = \pi r_i(\alpha)^2 = \frac{\pi}{4} D_i^2 \cdot \frac{1}{\sin^2(\alpha/2)} \tag{53}$$

(Fig. 9). The ratio $\kappa_i(\alpha)$ of the cross-section area to the inclusion area for tree $i \in \mathbf{I}$ is now seen to depend only on the viewing angle α and thus have the same value for all the trees in $\mathbf{I}$:

$$\kappa_i(\alpha) = \frac{\frac{\pi}{4} D_i^2}{|\mathbf{M}_i(\alpha)|} = \sin^2(\alpha/2)\,; \tag{54}$$

the ratio is referred to as the *basal area factor*. (Note that the cross-section area and inclusion area are here assumed to be expressed in the same units, so that the units cancel out in $\sin^2(\alpha/2)$; to express the basal area factor in m^2/ha or ft^2/ac, $\sin^2(\alpha/2)$ has to be multiplied with 10 000 or 43 560, respectively.)

The *inclusion probability* $\pi_i(\alpha)$ of a tree $i \in \mathbf{I}$ is the probability that the viewing point Q is located in the inclusion region $\mathbf{M}_i(\alpha)$; on account of the uniform distribution of Q in $\mathbf{L}$, the probability is given by the simple area ratio

$$\pi_i(\alpha) = \frac{|\mathbf{M}_i(\alpha)|}{|\mathbf{L}|} = \frac{\pi}{4} D_i^2 \cdot \frac{1}{\sin^2(\alpha/2)\,|\mathbf{L}|}\,. \tag{55}$$

(Note that the inclusion region is here defined to contain the ground-level cross-section of the stem, although the viewing point Q cannot be located within the cross-section.) Accordingly, the probability of a tree to be included in a sample is proportional to its cross-section area (squared diameter) at breast height and inversely proportional to the area of the region of interest; further, the smaller the viewing angle (and, consequently, the smaller the basal area factor) the larger the probability, as $\sin^2(\alpha/2)$ is monotonously increasing for $\alpha \in (0, \pi)$.

Let now $\mathbf{s}_Q(\alpha) \subseteq \mathbf{I}$ denote the sample of trees obtained with the relascope angle α at the viewing point $Q \in \mathbf{L}$. From each tree i in $\mathbf{s}_Q(\alpha)$, we measure the breast height diameter D_i and the value Y_i of the characteristic of interest. As is apparent from Eq. 55, we need the diameter measurements for the inclusion probabilities of the sample trees, which then enable us to apply the Horvitz-Thompson theorem for an unbiased estimation of the total amount of the characteristic of interest in the region $\mathbf{L}$. The sum $Y = \Sigma_{i \in \mathbf{I}} Y_i$ is estimated by

$$\hat{Y}_{HT} = \sum_{i \in \mathbf{s}_Q(\alpha)} \frac{Y_i}{\pi_i(\alpha)} = |\mathbf{L}| \sin^2(\alpha/2) \sum_{i \in \mathbf{s}_Q(\alpha)} \frac{Y_i}{\frac{\pi}{4} D_i^2}, \quad (56)$$

that is, as a weighted sum of the sample tree measurements with the inverses of the cross-section areas (squared diameters) as weights and with a quantity depending on the viewing angle (or the basal area factor) and the area of the region of interest as the scaling coefficient.

The randomness in $\hat{Y}_{HT}$ stems from the placement of the viewing point Q in the region **L**, as this determines the sample $\mathbf{s}_Q(\alpha)$. By the Horvitz-Thompson theorem (Appendix B), $\hat{Y}_{HT}$ is unbiased with respect to the sampling design, that is, $E(\hat{Y}_{HT})=Y$, where the expectation is taken over the probability distribution of all possible samples $\mathbf{s}_Q(\alpha)$ resulting from all possible locations of Q.

The variance of $\hat{Y}_{HT}$ depends on the spatial pattern of the trees in the stand, as it involves the joint inclusion probabilities for all the pairs of the trees in the population (Appendix B). The joint inclusion probability $\pi_{ij}(\alpha)$ for trees i, j$\in$**I** is the probability that both the trees are included in a sample, and in Bitterlich sampling this probability is proportional to the overlapping area of the tree inclusion regions. For the unbiased variance estimator given in Appendix B (Eq. B9) and based on a sample of trees taken at one viewing point, these probabilities need not only be known but also positive for all the pairs of trees in the sample. In a Bitterlich sample, the positivity requirement is invariably fulfilled, as the inclusion regions of the trees in the same sample necessarily overlap. The requirement of knowing the spatial pattern of the trees in the sample can be circumvented by repeating Bitterlich sampling at k randomly and independently selected viewing points $Q_j \in \mathbf{L}$, j=1, ..., k: The estimators $\hat{Y}_{HT}[\mathbf{s}_{Qj}(\alpha)]$ obtained from the k samples are independent and identically distributed, and hence have the same variance $Var\{\hat{Y}_{HT}[\mathbf{s}_{Qj}(\alpha)]\} \equiv Var(\hat{Y}_{HT})$ for all Q_j. An unbiased estimator for this variance is given by the sample variance of the k estimators:

$$\hat{Var}(\hat{Y}_{HT}) = \frac{1}{k-1} \sum_{j=1}^{k} \left\{ \hat{Y}_{HT}[\mathbf{s}_{Q_j}(\alpha)] - \bar{Y}_{HT} \right\}^2, \quad (57)$$

where $\bar{Y}_{HT}$ is the mean of the k independent estimators $\hat{Y}_{HT}[\mathbf{s}_{Qj}(\alpha)]$. The population total Y is estimated with $\bar{Y}_{HT}$, the variance of which is $Var(\bar{Y}_{HT})=Var(\hat{Y}_{HT})/k$. An unbiased estimator of the variance of $\bar{Y}_{HT}$ then becomes

$$\hat{Var}(\bar{Y}_{HT}) = \frac{1}{k} \hat{Var}[\hat{Y}_{HT}] = \frac{1}{k(k-1)} \sum_{j=1}^{k} \left\{ \hat{Y}_{HT}[\mathbf{s}_{Q_j}(\alpha)] - \bar{Y}_{HT} \right\}^2 \quad (58)$$

(cf. de Vries 1986, Schreuder et al. 1993, Eriksson 1995, Gregoire and Valentine 2008).

A model-based approach provides an alternative way of estimating the variance of a stand total estimator — in fact, the model-based studies referred to in the beginning of this chapter expressly address this problem. Under a certain class of models for the random mechanism generating forest stands, analytical expressions for the variance can be found; under other models, the variance can be estimated via simulations.

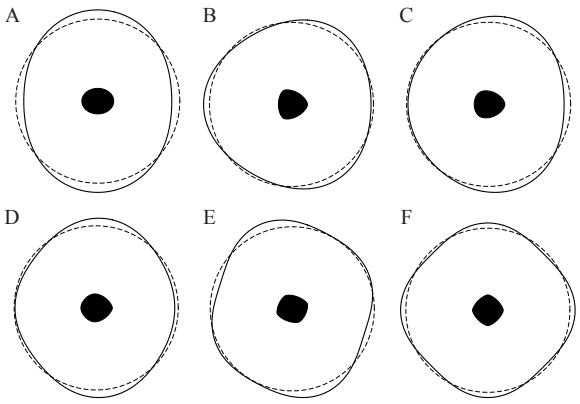

Fig. 10. Inclusion regions obtained with the viewing angle α=20° for five of the six example shapes discussed in Chapter 2 (A and C–F in. Fig. 5 and Table 1) and for an orbiform (B, cf. Fig. 4). The dashed line indicates the inclusion region of the circle that has the same area as the cross-section.

4.1.2 Effect of Non-Circularity of Cross-Sections

Since Bitterlich sampling operates with the tangents of the convex closures of breast height cross-sections, non-convexity in the cross-sections is unobservable and thus does not influence the selection of trees. Therefore, when examining how non-circularity in the breast height cross-sections of trees affects stand total estimation by Bitterlich sampling, we confine ourselves to considering the *convex closures* of the cross-sections of arbitrary non-circular shape.

If the convex closure of the breast height cross-section of a tree $i \in \mathbf{I}$ is not a circle, the maximum distance at which the tree is counted with a certain viewing angle α varies by the direction in which the tree is being viewed. Ergo, the inclusion region becomes non-circular (Fig. 10; cf. Grosenbaugh 1958, Bitterlich 1984). The size and shape of the inclusion region depend not only on the size and shape of the breast height cross-section but also on the viewing angle α used (Fig. 11). Using the support function $p_i(\cdot)$ of the breast height cross-section in tree i, now defined in a co-ordinate system with the origin set in the centre of gravity of the convex closure of the cross-section (or in the pith of the cross-section), we attain the following parametric representation for the length of the radius of the inclusion region:

$$r_i(\theta; \alpha) = \frac{1}{\sin\alpha}\sqrt{p_i(\theta)^2 + p_i(\theta+\pi-\alpha)^2 + 2p_i(\theta)p_i(\theta+\pi-\alpha)\cos\alpha}\ , \qquad (59)$$

where $\alpha \in (0, \pi)$ and $\theta \in [0, 2\pi)$ (see Appendix C for the derivation). (Note that in this parametrisation, θ does not indicate the direction of the radius, but the direction is a function of θ and α (Appendix C); consequently, the area of the inclusion region is not obtained straightforwardly by integrating $r_i(\theta; \alpha)^2$ from 0 to 2π (cf. Eq. 12 in Chapter 2).) We see that as α tends to zero, the numerator of $r_i(\theta; \alpha)$ tends to $p_i(\theta)+p_i(\theta+\pi)=D_i(\theta)$ (and the denominator tends to 0); accordingly, for the trees with an orbiform breast height cross-section (constant diameter function $D(\cdot)$ at breast height), the limiting shape of the inclusion region is a circle (e.g. Fig. 11 B). As α tends to π, the viewer draws closer and closer to the stem, and the radii $r_i(\theta; \alpha)$ are finally found to tend to the radii of the convex closure of the breast height cross-section; in other words, the inclusion region tends to the convex closure of the breast height cross-section (cf. Matérn 1956, p. 24).

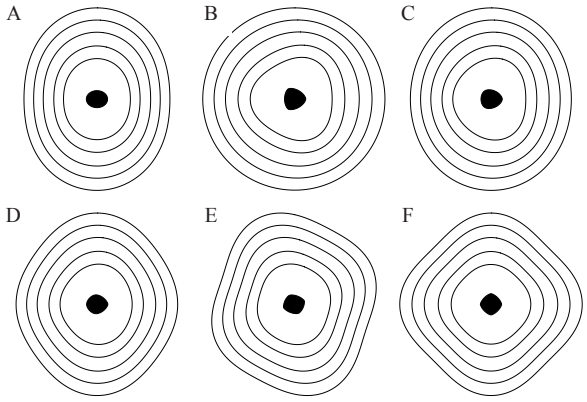

Fig. 11. Effect of viewing angle α on the shape of the inclusion region in the six example shapes in Fig. 10. The regions were produced with viewing angles α=30°(innermost), α=20°, α=10°, α=5° and α=1°(outermost), and rescaled with factors 1, 0.875, 0.550, 0.325, and 0.075, respectively, to facilitate perception of the change in shape.

The area of the inclusion region of the tree i∈ **I** can be expressed as

$$|\mathbf{M}_i(\alpha)| = \frac{1}{\sin^2\alpha}\int_0^{2\pi}[p_i(\theta)^2 + p_i(\theta)p_i(\theta+\pi-\alpha)\cos\alpha + p_i(\theta)p_i'(\theta+\pi-\alpha)\sin\alpha]d\theta \quad (60)$$

(cf. Matérn 1956; see Appendix C for the derivation). If $p_i(\cdot)$ is multiplied with a constant, so is $p_i'(\cdot)$, and $|\mathbf{M}_i(\alpha)|$ thus becomes multiplied with the square of the constant. A similar reasoning pertains to the convex area of the breast height cross-section

$$A_{Ci} = \frac{1}{2}\int_0^{2\pi}[p_i(\theta)^2 - p_i'(\theta)^2]d\theta \quad (61)$$

(Eq. 2 in Chapter 2). In the basal area factor $\kappa_i(\alpha)$ for tree i, then, defined as

$$\kappa_i(\alpha) = \frac{A_{Ci}}{|\mathbf{M}_i(\alpha)|}, \quad (62)$$

the multiplying constant cancels out. Now if $p_i(\cdot)$ is defined with reference to the centre of gravity of the convex closure of the breast height cross-section, the size of the cross-section influences $p_i(\cdot)$ only by a multiplying constant. Consequently, *the basal area factor of a tree is a function of the viewing angle α that depends on the shape but not on the size of the breast height cross-section*.

For example, if the breast height cross-section of the tree i is a circle with radius R_i, for which $p_i(\theta)=R_i$ for all θ, the convex area of the cross-section is naturally $A_{Ci}=\pi R_i^2$, and the area of the inclusion region is given by

$$|\mathbf{M}_i(\alpha)| = \frac{1}{\sin^2(\alpha)} \int_0^{2\pi} (R_i^2 + R_i^2 \cos\alpha)\, d\theta = \frac{2\pi R_i^2 (1+\cos\alpha)}{\sin^2 \alpha}\,, \tag{63}$$

whereby the basal area factor becomes

$$\kappa_i(\alpha) = \frac{A_{Ci}}{|\mathbf{M}_i(\alpha)|} = \frac{\sin^2 \alpha}{2(1+\cos\alpha)} = \sin^2(\alpha/2) \tag{64}$$

– a result already established, in a different way, in the previous section (cf. Eq. 54; $R_i=D_i/2$, $\cos\alpha=2\cos^2(\alpha/2)-1$, $\sin\alpha=2\sin(\alpha/2)\cos(\alpha/2)$). Patently, the ratio does not depend on the radius R_i of the cross-section but is $\sin^2(\alpha/2)$ for every tree with circular cross-section at breast height. For any other convex shape irrespective of size, the basal area factor is then another function of α, although not necessarily very much different from $\sin^2(\alpha/2)$ (cf. Fig. 12).

As in the circular case (cf. Eq. 55), the inclusion probability of the non-circular tree $i \in \mathbf{I}$ is proportional to the convex area of the breast height cross-section:

$$\pi_i(\alpha) = \frac{|\mathbf{M}_i(\alpha)|}{|\mathbf{L}|} = \frac{A_{Ci}}{\kappa_i(\alpha)\,|\mathbf{L}|}\,, \tag{65}$$

where the proportionality coefficient $1/\kappa_i(\alpha)$ just varies according to the shape of the cross-section. The Horvitz-Thompson estimator of the sum $Y=\Sigma_{i\in\mathbf{I}} Y_i$ then becomes

$$\begin{aligned} \hat{Y}_{HT} &= \sum_{i \in \mathbf{s}_Q(\alpha)} \frac{Y_i}{\pi_i(\alpha)} \\ &= |\mathbf{L}| \sum_{i \in \mathbf{s}_Q(\alpha)} \kappa_i(\alpha) \frac{Y_i}{A_{Ci}}\,, \end{aligned} \tag{66}$$

that is, a weighted sum of the sample tree measurements with $\kappa_i(\alpha)/A_{Ci}$ as weights and with the area of the region of interest as the scaling coefficient (cf. Eq. 56).

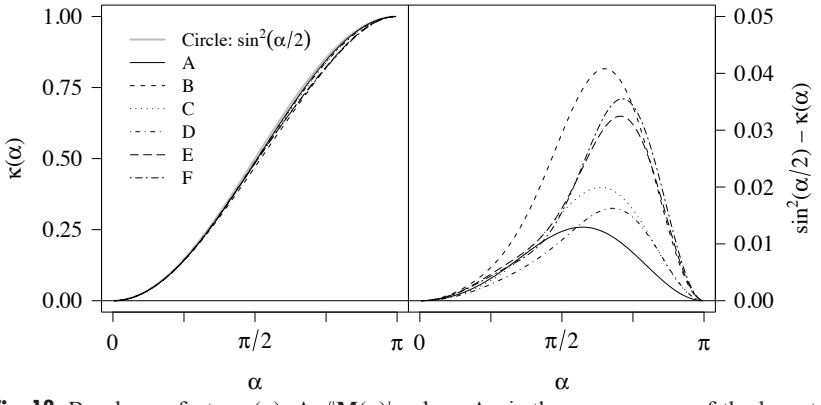

Fig. 12. Basal area factor $\kappa(\alpha)=A_C/|\mathbf{M}(\alpha)|$, where A_C is the convex area of the breast height cross-section and $|\mathbf{M}(\alpha)|$ is the inclusion area of the tree, as a function of viewing angle α for the six example shapes in Fig. 10, with reference to the basal area factor $\sin^2(\alpha/2)$ of a circle.

Yet in practice, both the shapes and the convex areas of the cross-sections usually remain unknown, and the inclusion probabilities are estimated by applying the formula of the circular case (Eq. 55) also to non-circular cross-sections. The resulting estimator (cf. Eq. 56)

$$\begin{aligned}\hat{Y} &= \sum_{i\in \mathbf{s}_Q(\alpha)} \frac{Y_i}{\hat{\pi}_i(\alpha)} \\ &= \sum_{i\in \mathbf{s}_Q(\alpha)} \frac{Y_i}{\frac{\pi}{4}D_i^2 \cdot \frac{1}{\sin^2(\alpha/2)\,|\mathbf{L}|}} \\ &= |\mathbf{L}|\sin^2(\alpha/2) \sum_{i\in \mathbf{s}_Q(\alpha)} \frac{Y_i}{\frac{\pi}{4}D_i^2},\end{aligned} \tag{67}$$

where D_i now denotes the diameter selected in some fashion at breast height in a non-circular tree i, is not necessarily unbiased with respect to the sampling design.

To unveil the possible bias caused by the estimated inclusion probabilities, we bring in the random variable

$$\delta_i[\mathbf{s}_Q(\alpha)] = \begin{cases} 1, & i \in \mathbf{s}_Q(\alpha) \\ 0, & i \notin \mathbf{s}_Q(\alpha) \end{cases} \tag{68}$$

indicating whether a tree $i \in \mathbf{I}$ is included in the sample $\mathbf{s}_Q(\alpha)$; obviously, $E\{\delta_i[\mathbf{s}_Q(\alpha)]\}=\pi_i(\alpha)$, the expectation being taken over the probability distribution of all possible samples (see Appendix B). Now

$$\begin{aligned}E(\hat{Y}) &= E\left[\sum_{i\in \mathbf{s}_Q(\alpha)} \frac{Y_i}{\hat{\pi}_i(\alpha)}\right] \\ &= E\left\{\sum_{i\in \mathbf{I}} \delta_i[\mathbf{s}_Q(\alpha)] \frac{Y_i}{\hat{\pi}_i(\alpha)}\right\} \\ &= \sum_{i\in \mathbf{I}} E\left\{\delta_i[\mathbf{s}_Q(\alpha)]\right\} \frac{Y_i}{\hat{\pi}_i(\alpha)} \\ &= \sum_{i\in \mathbf{I}} Y_i \frac{\pi_i(\alpha)}{\hat{\pi}_i(\alpha)} \\ &= \sum_{i\in \mathbf{I}} Y_i \frac{A_{Ci} \cdot \frac{1}{\kappa_i(\alpha)\,|\mathbf{L}|}}{\frac{\pi}{4}D_i^2 \cdot \frac{1}{\sin^2(\alpha/2)\,|\mathbf{L}|}} \\ &= \sum_{i\in \mathbf{I}} Y_i \frac{A_{Ci}}{\frac{\pi}{4}D_i^2} \cdot \frac{\sin^2(\alpha/2)}{\kappa_i(\alpha)}.\end{aligned} \tag{69}$$

Here we see that the possible bias in the estimator ensues from two tree-specific flaws in the estimated inclusion probabilities: First, the diameter D_i selected to be measured in the

Table 5. Within-cross-section expectation of $A_C/[\pi D(\boldsymbol{\theta})^2/4]$ for the example shapes in Fig. 10, when the diameter $D(\boldsymbol{\theta})$ is measured with methods 1–5 (used in area estimators $\hat{A}_1$–$\hat{A}_5$, see Section 3.3.2). For a reference, the ratio obtained with the girth diameter ($A_C/\hat{A}_0$, diameter selection method 0) is shown. The values are given as 100-fold.

Diameter selection method	Shape					
	A	B	C	D	E	F
0	98.16	96.00	97.85	98.29	97.06	97.07
1	100.00	96.00	98.43	98.98	98.02	97.64
2	98.16	96.00	97.85	98.43	97.54	97.64
3	98.77	96.00	98.04	98.62	97.70	97.64
4	99.07	96.00	98.14	98.64	97.54	97.36
5	98.77	96.00	98.04	98.62	97.70	97.64

non-circular breast height cross-section of tree i may not yield the true convex area A_{Ci} when substituted in the circle area formula. Second, the deviation of the true basal area factor $\kappa_i(\alpha)=A_{Ci}/|\mathbf{M}_i(\alpha)|$ from that of the circle, that is, from $\sin^2(\alpha/2)$, produces an error the magnitude of which depends on the relascope angle α and the shape of the breast height cross-section. (Note that if the selection of diameters D_i involves randomness, $E(\hat{Y})$ becomes a random variable the expectation of which over the (multidimensional) diameter direction distribution should be used as the measure for the goodness of the estimator.)

The two-fold errors resulting from the estimated inclusion probabilities tend to be systematic and of opposite signs. With the diameter derived from the girth, the circle area formula was previously (Section 3.3.1) found to overestimate the convex area of a cross-section of any shape; this is the case also when the maximum diameter is used. This overestimation in all the trees then causes $\hat{Y}$ to underestimate Y on average. Also with random diameters, the circle area formula was found to overestimate the convex area on average, that is, in terms of the expectation over the uniform direction distribution within cross-section (Section 3.3.2). However, $A_{Ci}/E_{\boldsymbol{\theta}}[\pi D_i(\boldsymbol{\theta})^2/4] \leq 1$ does not imply that $E_{\boldsymbol{\theta}}\{A_{Ci}/[\pi D_i(\boldsymbol{\theta})^2/4]\} \leq 1$. Yet for the example shapes in Fig. 10, also the latter inequality holds with the diameter selection methods 1–5 (Table 5), but the order of $E_{\boldsymbol{\theta}}\{A_{Ci}/[\pi D_i(\boldsymbol{\theta})^2/4]\}$ does not follow the order of $A_{Ci}/E_{\boldsymbol{\theta}}[\pi D_i(\boldsymbol{\theta})^2/4]$.

The basal area factor $\kappa_i(\alpha)$, in turn, can be shown to be not larger than $\sin^2(\alpha/2)$ irrespective of the shape of the breast height cross-section of tree i: Matérn (1956) proved that for any (convex) shape of breast height cross-section

$$\left| \sin^2(\alpha/2)\,|\mathbf{M}_i(\alpha)| - \hat{A}_{0i} \right| \leq \hat{A}_{0i} - A_{Ci}\,, \tag{70}$$

where $\hat{A}_{0i}$ is the area estimator based on the convex perimeter at breast height in the tree i; we can rephrase this (setting $|\mathbf{M}_i(\alpha)|=A_{Ci}/\kappa_i(\alpha)$ according to Eq. 62) to get

$$1 \leq \frac{\sin^2(\alpha/2)}{\kappa_i(\alpha)} \leq 1 + \frac{2(\hat{A}_{0i} - A_{Ci})}{A_{Ci}}\,. \tag{71}$$

The basal area factor being smaller than $\sin^2(\alpha/2)$ in all the trees then causes $\hat{Y}$ to overestimate Y on average.

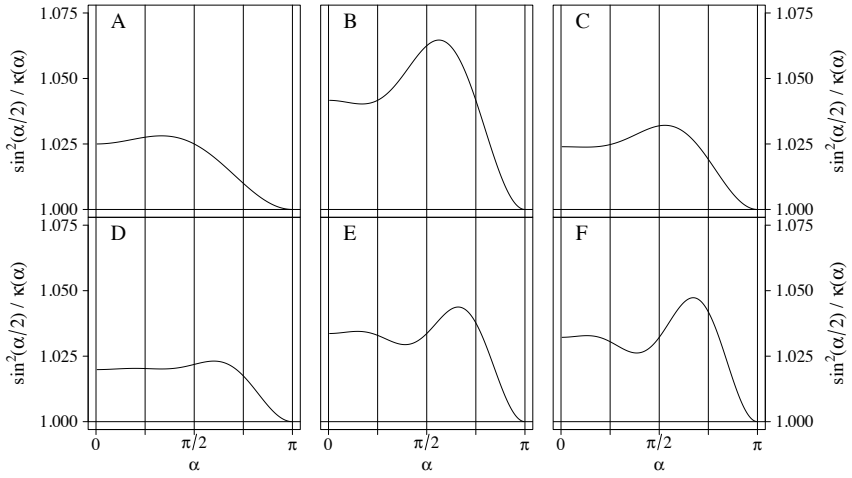

Fig. 13. Ratio of the basal area factor of a circle, $\sin^2(\alpha/2)$, to the basal area factor of a non-circular cross-section, $\kappa(\alpha)=A_C/|\mathbf{M}(\alpha)|$, as a function of the viewing angle α for the six example shapes in Fig. 10 (cf. Matérn 1956, p. 25).

In Fig. 13, the ratio $\sin^2(\alpha/2)/\kappa_i(\alpha)$ is drawn as a function of α for the six example shapes of Fig. 10. With the viewing angles used in practice (α around 1–2°, not more than 5°), each tree with such a non-circular breast height cross-section and with the area A_{Ci} correctly estimated with $\pi D_i^2/4$ appears to contribute to the stand total estimate with an amount that is 2.5–4 % too large. For ellipses, the overestimation increases substantially along with eccentricity (Fig. 14; cf. the results by Grosenbaugh (1958) showing that for an ellipse with axis ratio 0.5 the overestimation amounts to over 25 % with α =1.74°, 3.81°, 45° or 90°). As for more exotic cross-section shapes, we can deduce from the results given by Bitterlich (1984) that for a half circle the overestimation becomes 38 % with α=2.29°.

Grosenbaugh (1958) examined the combined error $\sin^2(\alpha/2)/\kappa_i(\alpha)\cdot A_{Ci}/(\pi D_i^2/4)$ in the ellipses with axis ratio 0.9 or 0.5 by employing the girth diameter or the quadratic, arithmetic or geometric mean of D_{min} and D_{max} as D_i and by applying the values 90°, 45°, 3.81° and 1.74° for α. He found that in all those cases, the combined error was larger or equal to 1,

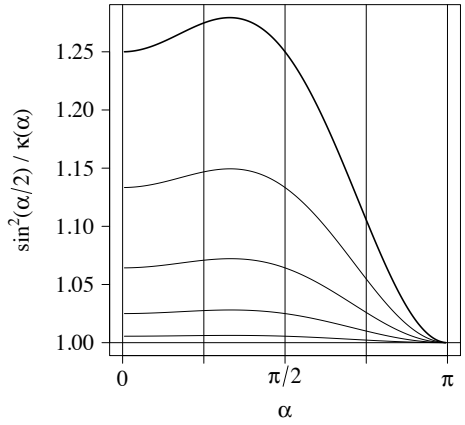

Fig. 14. Ratio of the basal area factor of a circle, $\sin^2(\alpha/2)$, to the true basal area factor, $\kappa(\alpha)$, as a function of the viewing angle α, for ellipses with axis ratio of 0.5 (uppermost curve), 0.6, 0.7, 0.8, and 0.9 (lowermost curve).

Table 6. Contribution of a sample tree to bias in stand total estimation from Bitterlich sample ($\sin^2(\alpha/2)/\kappa(\alpha)\cdot A_C/(\pi D^2/4)$, see Eq. 69), if the breast height cross-section of the tree is one of the shapes in Fig. 10 and if its diameter is measured with methods 0–11 used in area estimators $\hat{A}_0$–$\hat{A}_{11}$ (see Section 3.3). Results with viewing angles α=1° and α=30° (in parentheses) are given; with α=2° and α=5°, the results were similar to those obtained with α=1°. For the diameter selection methods 1–5, the expectation of $A_C/(\pi D^2/4)$ over the uniform direction distribution (Table 5) was used in the computation. The values are given as 100-fold.

Diameter selection method	Shape					
	A	B	C	D	E	F
0	100.61 (100.75)	100.00 (99.87)	100.20 (100.19)	100.24 (100.29)	100.33 (100.40)	100.20 (100.24)
1	102.50 (102.64)	100.00 (99.87)	100.79 (100.79)	100.95 (100.99)	101.32 (101.40)	100.79 (100.83)
2	100.61 (100.76)	100.00 (99.87)	100.20 (100.19)	100.39 (100.43)	100.82 (100.90)	100.79 (100.83)
3	101.24 (101.38)	100.00 (99.87)	100.39 (100.38)	100.58 (100.62)	100.99 (101.06)	100.79 (100.83)
4	101.55 (101.69)	100.00 (99.87)	100.49 (100.48)	100.60 (100.65)	100.82 (100.90)	100.49 (100.54)
5	101.24 (101.38)	100.00 (99.87)	100.39 (100.38)	100.58 (100.62)	100.99 (101.06)	100.79 (100.83)
6	101.23 (101.38)	100.00 (99.87)	100.20 (100.19)	95.71 (95.75)	100.33 (100.40)	100.20 (100.24)
7	102.50 (102.64)	100.00 (99.87)	100.59 (100.58)	96.16 (96.20)	101.35 (101.43)	100.20 (100.63)
8	101.23 (101.38)	100.00 (99.87)	100.20 (100.19)	103.45 (103.50)	112.19 (112.27)	114.00 (114.05)
9	102.50 (102.64)	100.00 (99.87)	100.59 (100.58)	103.56 (103.60)	112.46 (112.54)	114.00 (114.05)
10	101.23 (101.38)	100.00 (99.87)	100.20 (100.19)	94.26 (94.30)	90.25 (90.32)	88.75 (88.79)
11	102.50 (102.64)	100.00 (99.87)	100.59 (100.58)	94.61 (94.65)	90.42 (90.49)	88.75 (88.79)

implying an overestimating bias in $\hat{Y}$. Not unexpectedly, the quadratic mean yielded the smallest combined error (in fact, an error of negligible magnitude when the two smallest values of the viewing angle were used): the quadratic mean in $\pi D_i^2/4$ results in the largest overestimation of A_{Ci}, which then most effectively counterbalances the overestimation of $\kappa_i(\alpha)$ by $\sin^2(\alpha/2)$ (which, in turn, does not depend on diameter selection). In Table 6, the combined errors produced by the diameter selection methods 0–11 and viewing angles 1° and 30° are given for the example shapes of Fig. 10. Manifestly, Grosenbaugh's findings on elliptical cross-section cannot be generalised, but with different shapes and diameter selection methods the combined error may very well result in underestimation. In a majority of the shapes, however, the most common diameter selection methods 0–5 result in overestimation smaller than 1 %. Within the range applied, the viewing angle appears to influence the error only negligibly.

If we choose to measure the girth diameter at breast height from each tree included in Bitterlich sample, we obtain the following bounds for the expectation of $\hat{Y}$ (the stand total estimator involving inclusion probabilities that were estimated as if the cross-sections were circular, Eq. 67):

$$\sum_{i\in\mathbf{I}} Y_i \frac{A_{Ci}}{\hat{A}_{0i}} \;\le\; E(\hat{Y}) \;\le\; \sum_{i\in\mathbf{I}} Y_i \left(2 - \frac{A_{Ci}}{\hat{A}_{0i}} \right) \tag{72}$$

(combine Eqs. 69 and 71 and set $\pi D_i^2/4 = \pi\mu_{Di}^2/4 = \pi(C_i/\pi)^2/4 = \hat{A}_{0i}$). The bounds of the bias are now ascribed to the deviations of the cross-section area estimates $\hat{A}_{0i}$ from the convex areas A_{Ci} at breast height in the stems of the stand. The lower bound evidently falls below the true value $Y=\Sigma_{i\in\mathbf{I}} Y_i$, and hence $\hat{Y}$ with girth diameters may even systematically underestimate Y.

If, in turn, we choose to measure from each tree in the sample one random diameter with uniformly distributed direction, we attain a point approximation for the expectation of $\hat{Y}$: Matérn (1956) proved that for any (convex) shape of breast height cross-section

$$\left| \sin^2(\alpha/2)\,|\mathbf{M}_i(\alpha)| - E_{\boldsymbol{\theta}}(\hat{A}_{1i}) \right| \;\le\; \left[E_{\boldsymbol{\theta}}(\hat{A}_{1i}) - A_{Ci} \right] \tan^2(\alpha/2)\,, \tag{73}$$

where $E_{\boldsymbol{\theta}}(\hat{A}_{1i})$ is the expectation, over the uniform direction distribution, of the area estimator $\hat{A}_1$ involving one random diameter at breast height in tree i; by rephrasing this, the basal area factor $\kappa_i(\alpha)$ is found to satisfy

$$\begin{aligned} &\frac{E_{\boldsymbol{\theta}}(\hat{A}_{1i})}{A_{Ci}} - \tan^2(\alpha/2)\left[\frac{E_{\boldsymbol{\theta}}(\hat{A}_{1i})}{A_{Ci}} - 1 \right] \\ \le\; &\frac{\sin^2(\alpha/2)}{\kappa_i(\alpha)} \\ \le\; &\frac{E_{\boldsymbol{\theta}}(\hat{A}_{1i})}{A_{Ci}} + \tan^2(\alpha/2)\left[\frac{E_{\boldsymbol{\theta}}(\hat{A}_{1i})}{A_{Ci}} - 1 \right]. \end{aligned} \tag{74}$$

With the usually employed relascope angles α of the magnitude 1–2°, $\tan^2(\alpha/2)$ assumes the values 0.000076–0.00030, and hence $\sin^2(\alpha/2)/\kappa_i(\alpha)$ becomes very close to $E_{\boldsymbol{\theta}}(\hat{A}_{1i})/A_{Ci}$. Consequently,

$$\begin{aligned} E(\hat{Y}) \;&= \sum_{i\in\mathbf{I}} Y_i \frac{\sin^2(\alpha/2)}{\kappa_i(\alpha)} \cdot \frac{A_{Ci}}{\hat{A}_{1i}} \\ &\approx \sum_{i\in\mathbf{I}} Y_i \frac{E_{\boldsymbol{\theta}}(\hat{A}_{1i})}{A_{Ci}} \cdot \frac{A_{Ci}}{\hat{A}_{1i}} \\ &= \sum_{i\in\mathbf{I}} Y_i \frac{E_{\boldsymbol{\theta}}(\hat{A}_{1i})}{\hat{A}_{1i}}\,, \end{aligned} \tag{75}$$

that is, the bias in the stand total estimator $\hat{Y}$ is attributable to the deviation of the area estimates based on one random diameter from their within-cross-section expectations in the stems of the stand.

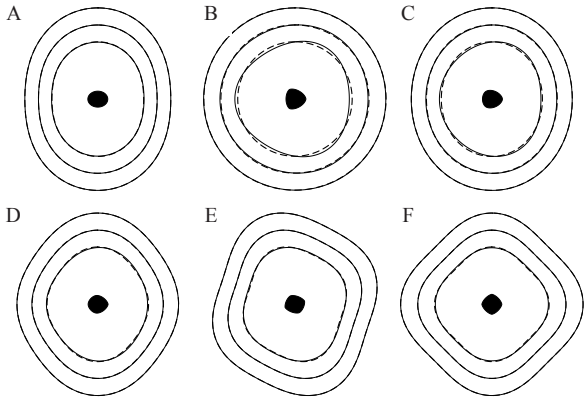

Fig. 15. Approximation (dashed line) of the inclusion region (solid line) by computing the inclusion region radii as $r=D(\xi+\pi/2)/[2\sin(\alpha/2)]$ (cf. Eq. 52), where $D(\xi+\pi/2)$ is the tree diameter taken perpendicular to the plot radius direction and α is the viewing angle, for the six example shapes in Fig. 10. The inclusion regions were produced with $\alpha=1°$ (outermost), $\alpha=5°$ and $\alpha=20°$ (innermost) and rescaled with factors 0.08, 0.325 and 1.25, respectively. Note that for the orbiform with constant diameter (shape B), the approximated inclusion regions are naturally circles irrespective of the value of the viewing angle.

When the viewing point is located close to the boundary of the inclusion region of a tree with non-circular (breast height) cross-section, it is not a straightforward task to check whether the tree should be included in the Bitterlich sample, as the critical distance varies according to the viewing direction (cf. Eq. 59). Contrary to what Grosenbaugh (1958) reasoned, the convention of measuring diameter D perpendicular to the viewing direction and computing the critical distance with the circle formula (Eq. 52) as

$$r(\alpha) = \frac{D}{2} \cdot \frac{1}{\sin(\alpha/2)} \tag{76}$$

appears to give a good approximation with the viewing angles used in practice (α around 1–2°, not more than 5°) (Fig. 15). For ellipses, Grosenbaugh (1958) recommended computing the critical distance as the radius of a circle with the same area as the inclusion area (for ellipses this can be easily determined as a function of D_{min}, D_{max} and α); however, if applied only when the viewing point appears to be near the inclusion region boundary (and not routinely to all sample trees), this practice is likely to result in an inclusion region that is the union of the true inclusion region and the approximating circle (Fig. 16) and is thus not something to advocate.

4.1.3 Special Case: Relative Basal Area

We complete our examination of stand total estimation by Bitterlich sampling by applying the theory presented above to the estimation of relative basal area. As non-convexity of cross-sections cannot be observed with relascope, we define the relative basal area of a stand

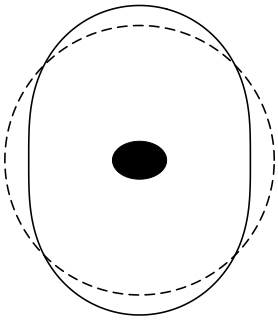

Fig. 16. Approximating the inclusion region (solid line) with a circle of the same area (dashed line), when the cross-section of a tree is an ellipse. If we determine the critical distance at which the tree is included in a sample as the radius of this circle (Grosenbaugh 1958) and if we then apply this critical distance only if the tree appears to be a "borderline case" (the inclusion of which we are uncertain about on the basis of viewing), we risk employing the union of the regions as the inclusion region: when the viewing point is located outside the true inclusion region but inside the circle, applying this critical distance causes the tree to be included in the sample, and the inclusion region then becomes dilated in the parts where the circle reaches farther than the true inclusion region; when the viewing point is located inside the true inclusion region but outside the circle, we do not necessarily realise to make the checking (because the tree does not appear to be a "borderline case" but obviously seems to be included in the sample), and the inclusion region is then not reduced as it should in the parts where the true inclusion region ranges farther than the circle. The problem can be eliminated by applying the critical distance systematically to all the trees.

I growing in region **L** as the sum of the *convex areas* of the breast height cross-sections of the trees in the stand divided by the area of the region:

$$G = \frac{1}{|\mathbf{L}|}\sum_{i\in\mathbf{I}} A_{Ci} \ . \tag{77}$$

If the cross-sections of the trees are circular at breast height — let D_i again stand for the breast height diameter of a tree $i \in \mathbf{I}$ — the relative basal area can be expressed as

$$G = \frac{1}{|\mathbf{L}|}\sum_{i\in\mathbf{I}} \frac{\pi}{4} D_i^2 \ , \tag{78}$$

and its Horvitz-Thompson estimator becomes (cf. Eq. 56)

$$\begin{aligned} \hat{G}_{HT} &= \frac{1}{|\mathbf{L}|}\sum_{i\in s_Q(\alpha)} \frac{\frac{\pi}{4}D_i^2}{\pi_i(\alpha)} \\ &= \frac{1}{|\mathbf{L}|}|\mathbf{L}|\sin^2(\alpha/2)\sum_{i\in s_Q(\alpha)} \frac{\frac{\pi}{4}D_i^2}{\frac{\pi}{4}D_i^2} \\ &= n\sin^2(\alpha/2) \ , \end{aligned} \tag{79}$$

where n is the number of trees in the sample $\mathbf{s}_Q(\alpha)$ obtained at point $Q \in \mathbf{L}$ with viewing angle α. Thus, an unbiased (with respect to the sampling design) estimate for the relative basal area is indeed attained by just counting the number of trees subtending the relascope angle — the fact perceived by Walter Bitterlich, at first only empirically (Bitterlich 1984)! The result follows from the fact that the inclusion area, and thereby also the inclusion probability, of each sampled tree i is proportional to $\pi D_i^2/4$ with $1/\sin^2(\alpha/2)$ as the proportionality coefficient. (Note that $\hat{G}_{HT}$ here is unitless, i.e., the cross-section areas and the area of the region **L** are assumed to be expressed in the same units; as mentioned before, the basal area factor $\sin^2(\alpha/2)$ is usually multiplied by 10 000 or 43 560 so as to express $\hat{G}_{HT}$ in m^2/ha or ft^2/ac, respectively.)

If counting of trees is repeated at k randomly and independently selected viewing points $Q_j \in \mathbf{L}$, j=1, ..., k, G is unbiasedly estimated with the mean $\bar{G}_{HT}$ of the k independent estimators $\hat{G}_{HTj}$; an unbiased estimator for the variance of $\bar{G}_{HT}$ is given by

$$\begin{aligned} \hat{\mathrm{Var}}(\bar{G}_{HT}) &= \frac{1}{k(k-1)} \sum_{j=1}^{k} (\hat{G}_{HT_j} - \bar{G}_{HT})^2 \\ &= \frac{\sin^4(\alpha/2)}{k(k-1)} \sum_{j=1}^{k} (n_j - \bar{n})^2 \ , \end{aligned} \tag{80}$$

where $\bar{n}$ is the arithmetic mean of the numbers of trees n_j counted at the k separate viewing points.

If the convex closures of the breast height cross-sections of the trees are non-circular, the basal area estimator $\hat{G}=n\sin^2(\alpha/2)$ is biased (when considered over the probability distribution of all possible tree samples):

$$\begin{aligned} E(\hat{G}) &= \sin^2(\alpha/2)\, E(n) \\ &= \sin^2(\alpha/2)\, E\left\{ \sum_{i \in \mathbf{I}} \delta_i[\mathbf{s}_Q(\alpha)] \right\} \\ &= \sin^2(\alpha/2) \sum_{i \in \mathbf{I}} \pi_i(\alpha) \\ &= \sin^2(\alpha/2) \sum_{i \in \mathbf{I}} \frac{|\mathbf{M}_i(\alpha)|}{|\mathbf{L}|} \\ &= \frac{1}{|\mathbf{L}|} \sum_{i \in \mathbf{I}} \sin^2(\alpha/2)\, |\mathbf{M}_i(\alpha)| \\ &= \frac{1}{|\mathbf{L}|} \sum_{i \in \mathbf{I}} \frac{\sin^2(\alpha/2)}{\kappa_i(\alpha)} A_{Ci} \\ &\equiv \frac{1}{|\mathbf{L}|} \sum_{i \in \mathbf{I}} \tilde{A}_i(\alpha) \ . \end{aligned} \tag{81}$$

Clearly, the bias of $\hat{G}$ owing to the non-circular shapes of tree cross-sections manifests itself in the deviation of $\tilde{A}_i(\alpha)$ from A_{Ci} (Matérn 1956), that is, in the deviation of $\sin^2(\alpha/2)/\kappa_i(\alpha)$ from 1. As $\sin^2(\alpha/2)/\kappa_i(\alpha)$ was found to be larger or equal to 1 (Eq. 71) for all convex shapes, *$\hat{G}$ tends to overestimate G systematically*.

The inequalities proved by Matérn (1956) and introduced in the previous section (Eqs. 70 and 73) give bounds for the overestimating bias in $\hat{G}$ (originally, the inequalities were derived

expressly for the case of estimating relative basal area by relascope). The first inequality

$$\left| \tilde{A}_i(\alpha) - \hat{A}_{0i} \right| \leq \hat{A}_{0i} - A_{Ci} \quad \Leftrightarrow \quad A_{Ci} \leq \tilde{A}_i(\alpha) \leq A_{Ci} + 2(\hat{A}_{0i} - A_{Ci}) \tag{82}$$

implies that, irrespective of the shape of a cross-section, $\tilde{A}(\alpha)$ be always greater or equal to the convex area of the cross-section, and that the error of $\tilde{A}(\alpha)$ never exceed double the isoperimetric deficit. Accordingly, no matter what shapes breast height cross-sections assume,

$$G \leq E(\hat{G}) \leq G + \frac{2}{|\mathbf{L}|}\sum_{i\in\mathbf{I}}(\hat{A}_{0i} - A_{Ci}) \,. \tag{83}$$

The second inequality

$$\left| \tilde{A}(\alpha) - E_{\boldsymbol{\theta}}(\hat{A}_1) \right| \leq \left[E_{\boldsymbol{\theta}}(\hat{A}_1) - A_C \right] \tan^2(\alpha/2) \tag{84}$$

shows that in practice — α being of the magnitude 1–2°, and $\tan^2(\alpha/2)$ thus 0.000076–0.00030 — $\tilde{A}(\alpha)$ becomes very close to the within-cross-section expectation $E_{\boldsymbol{\theta}}(\hat{A}_1)$ of the estimator based one random diameter. Accordingly,

$$E(\hat{G}) \approx \frac{1}{|\mathbf{L}|}\sum_{i\in\mathbf{I}} E_{\boldsymbol{\theta}}(\hat{A}_{1i}) \,, \tag{85}$$

which implies that, regardless of the shapes of breast height cross-sections, the overestimating bias of the basal area estimator by relascope be approximately equal to the bias obtained by calipering all the trees in **I** in a random direction and applying the circle area formula (Matérn 1956).

Relative basal area may, of course, be estimated using diameter measurements, if they are available on the trees included in the Bitterlich sample. Then it is possible to apply different area estimators, say $\hat{A}_X$ and $\hat{A}_Y$, in the inclusion probability estimation versus the cross-section area estimation: the estimator with estimated inclusion probabilities becomes (cf. Eq. 67)

$$\begin{aligned} \hat{G} &= \frac{1}{|\mathbf{L}|}\sum_{i\in\mathbf{s}_Q(\alpha)} \frac{\hat{A}_{Yi}}{\hat{\pi}_i(\alpha)} \\ &= \frac{1}{|\mathbf{L}|}\sum_{i\in\mathbf{s}_Q(\alpha)} \frac{\hat{A}_{Yi}}{\hat{A}_{Xi} \cdot \dfrac{1}{|\mathbf{L}|\sin^2(\alpha/2)}} \\ &= \sin^2(\alpha/2)\sum_{i\in\mathbf{s}_Q(\alpha)} \frac{\hat{A}_{Yi}}{\hat{A}_{Xi}} \,, \end{aligned} \tag{86}$$

and its expectation over the probability distribution of all possible tree samples is (cf. Eq. 69)

$$
\begin{aligned}
E(\hat{G}) &= \sum_{i\in\mathbf{I}} \hat{A}_{Yi} \frac{\pi_i(\alpha)}{\hat{\pi}_i(\alpha)} \\
&= \sum_{i\in\mathbf{I}} \hat{A}_{Yi} \frac{A_{Ci} \cdot \dfrac{1}{\kappa_i(\alpha)\,|\mathbf{L}|}}{\hat{A}_{Xi} \cdot \dfrac{1}{\sin^2(\alpha/2)\,|\mathbf{L}|}} \\
&= \sum_{i\in\mathbf{I}} \hat{A}_{Yi} \frac{A_{Ci}}{\hat{A}_{Xi}} \cdot \frac{\sin^2(\alpha/2)}{\kappa_i(\alpha)} \,.
\end{aligned}
\tag{87}
$$

For elliptical cross-sections, Grosenbaugh (1958) recommended using the geometric mean of D_{min} and D_{max} in the circle area formula for $\hat{A}_Y$ and the quadratic mean ditto for $\hat{A}_X$ to minimise the bias. This is a most natural choice: the geometric mean in the circle area formula yields the true area A_C of an ellipse, whereas the quadratic mean gives the largest overestimation and thus minimises the combined error $\sin^2(\alpha/2)/\kappa(\alpha)\cdot A_C/\hat{A}_X$.

4.2 Bitterlich Diameters: Diameters Measured Parallel or Perpendicular to Plot Radius Direction

When a tree to be investigated is selected by Bitterlich sampling, it is a common practice to measure its breast height diameter parallel or perpendicular to the plot radius, that is, parallel or perpendicular to the line segment from the viewing point to the assumed centre of gravity, or pith, of the breast height cross-section (Fig. 17). This diameter is then usually regarded as "random", implying a correspondence to the diameter with the uniform direction distribution, which is the way in which "random diameter" is usually understood in colloquial language. Although practically sensible and seemingly sound, this practice involves a likely pitfall if the breast height cross-section of the tree is non-circular: Plot radius direction in Bitterlich sampling is a random variable the value of which depends on the outcome of the random experiment of placing the viewing point in the inclusion region. If the inclusion region of a stem deviates from a circle, the probability of a viewing point to be located in a certain direction when viewed from the tree pith varies according to the direction. In Fig. 17, for example, it is more probable to place the viewing point in the way that the plot radius direction becomes t_Q than in the way that it becomes t_R — simply because the line segment from the pith to the inclusion region boundary is longer through the point Q than through the point R. Accordingly, the distribution of the plot radius direction — and, in consequence, the distribution of the diameter measurement direction — is *not* uniform over $[0, 2\pi)$ — or over $[0, \pi)$, respectively — when viewed from the pith of the tree. In other words, contrary to the usual implicit assumption or belief, *the diameter taken parallel or perpendicular to relascope plot radius direction does not correspond to a random diameter with the uniform direction distribution, if the cross-section of a tree is non-circular*. In Fig. 17, for example, measuring diameters near $D(t_Q)$ is more probable than measuring diameters near $D(t_R)$ if the measurement practice is to take the diameter parallel to the plot radius, and less probable if the practice is to take the diameter perpendicular to the plot radius.

In the following, we first derive the direction distributions for these *Bitterlich diameters*, that is, for the diameters measured parallel or perpendicular to plot radius in Bitterlich sampling. Then we derive the expectations, variances and approximate variances of the area estimators similar to those dealt with in Section 3.3.2 but with Bitterlich diameters involved.

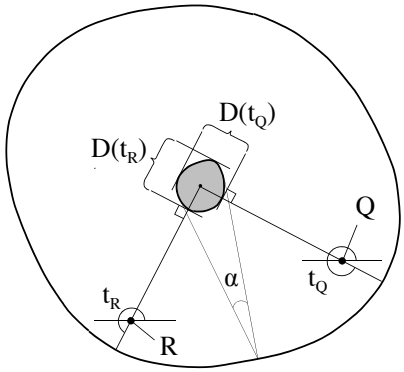

Fig. 17. In a tree with a non-circular breast height cross-section and, hence, with a non-circular inclusion region, measuring diameter in the plot radius direction does not result in a random diameter with the uniform direction distribution: here it is more probable to place the viewing point in the way that the plot radius direction becomes t_Q than in the way that it becomes t_R, because the line segment from the pith to the inclusion region boundary is longer through the point Q than through the point R; hence the diameter measurement is more likely to give a value $D(t_Q)$ than $D(t_R)$.

4.2.1 Direction Distributions of Bitterlich Diameters

The tree-specific probability distribution of the plot radius direction $\tau \in [0, 2\pi)$ is obtained from the inclusion region $\mathbf{M}(\alpha)$ of the tree via geometrical probability. The density mass of τ between directions t_1 and t_2, $t_1<t_2$, is the probability that the viewing point is located in the sector of $\mathbf{M}(\alpha)$ edged by the rays emanating from the tree pith in directions t_1 and t_2 (Fig. 18); since the viewing point is uniformly randomly located in the region of interest, the probability equals the area of the sector divided by the total area of $\mathbf{M}(\alpha)$, that is,

$$\Pr\left\{t_1 \le \tau \le t_2; \alpha\right\} = \frac{|\mathbf{M}(\alpha)_{t_1}^{t_2}|}{|\mathbf{M}(\alpha)|}. \tag{88}$$

The plot radius directions τ and $\tau+\pi$ result in the same diameter of the cross-section, and hence the probability that the direction $\xi \in [0, \pi)$ of the diameter taken *parallel* to plot radius is between t_1 and t_2 is the sum of the probabilities of τ being between t_1 and t_2 or between $t_1+\pi$ and $t_2+\pi$ (Fig. 19), that is,

$$\begin{aligned}\Pr\left\{t_1 \le \xi \le t_2; \alpha\right\} &= \Pr\left\{t_1 \le \tau \le t_2; \alpha\right\} + \Pr\left\{t_1 + \pi \le \tau \le t_2 + \pi; \alpha\right\} \\ &= \frac{|\mathbf{M}(\alpha)_{t_1}^{t_2}|}{|\mathbf{M}(\alpha)|} + \frac{|\mathbf{M}(\alpha)_{t_1+\pi}^{t_2+\pi}|}{|\mathbf{M}(\alpha)|}.\end{aligned} \tag{89}$$

Setting $t_1=0$ and $t_2=t$ and restricting $t \in [0, \pi)$, we obtain the cumulative distribution function of ξ:

$$\begin{aligned} F_\xi(t;\alpha) &= \Pr\{\xi \le t;\alpha\} \\ &= \Pr\{0 \le \xi \le t;\alpha\} \\ &= \Pr\{0 \le \tau \le t;\alpha\} + \Pr\{\pi \le \tau \le \pi + t;\alpha\} \\ &= \frac{|\mathbf{M}(\alpha)_0^t|}{|\mathbf{M}(\alpha)|} + \frac{|\mathbf{M}(\alpha)_\pi^{\pi+t}|}{|\mathbf{M}(\alpha)|}. \end{aligned} \tag{90}$$

Although the inclusion region boundary co-ordinates (Eq. C9 in Appendix C) or radii (Eq. 59) can straightforwardly be expressed as functionals of the support function $p(\cdot)$, the sector area of the inclusion region cannot, or at least this is rather troublesome; the difficulty lies in the determination of the integration limits (see Appendix D). Therefore, when computing the Bitterlich direction distribution, we resort to numerical integration.

The probability density function $f_\xi(t;\alpha)=F_\xi'(t;\alpha)$ may be approximated with

$$f_\xi(t;\alpha) \approx \frac{F_\xi(t+\Delta t;\alpha) - F_\xi(t;\alpha)}{\Delta t}, \tag{91}$$

where Δt is small (0.5°, for example). For the example shapes of Fig. 10, the approximated density functions with viewing angles 1°, 20° and 30° are shown in Fig. 20.

The direction distribution of the diameter taken *perpendicular* to plot radius in Bitterlich sampling is obtained from $F_\xi(t\,;\alpha)$ by a location shift of $-\pi/2$:

$$F_{\xi+\pi/2}(t;\alpha) = \Pr\{\xi + \pi/2 \le t;\alpha\} = \Pr\{\xi \le t - \pi/2;\alpha\} = F_\xi(t - \pi/2;\alpha). \tag{92}$$

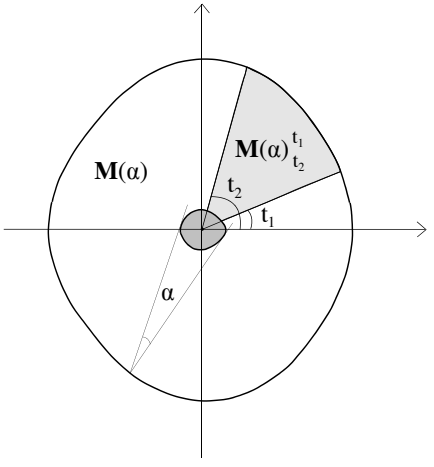

Fig. 18. Illustration of the probability distribution of the plot radius direction τ in Bitterlich sampling with α as the viewing angle: the density mass between directions t_1 and t_2 is the probability of the viewing point to be located in the hatched sector of the inclusion region $\mathbf{M}(\alpha)$.

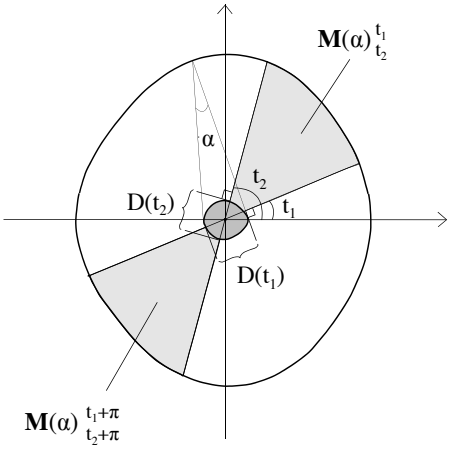

Fig. 19. Illustration of the probability distribution of the direction ξ of the diameter measured parallel to plot radius direction in Bitterlich sampling with α as the viewing angle: the density mass between directions t_1 and t_2 is the probability of the viewing point to be located in either of the hatched sectors of the inclusion region $\mathbf{M}(\alpha)$; $D(t_1)$ and $D(t_2)$ are the diameters in directions t_1 and t_2.

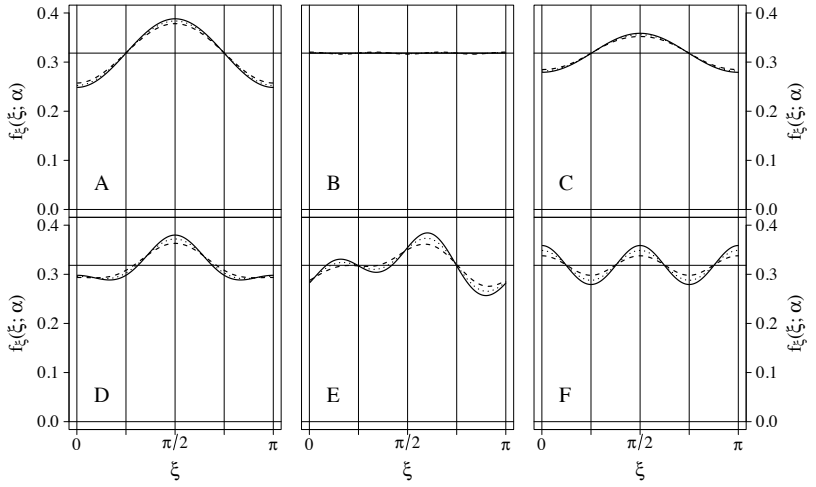

Fig. 20. (Approximated) probability density function $f_\xi(\xi; \alpha)$ of the direction ξ of the diameter taken parallel to plot radius in Bitterlich sampling for the six example shapes in Fig. 10. The distributions were determined with viewing angles α=1° (continuous line), α=20° (dotted line) and α=30° (dashed line). The positive x-axis, with respect to which the direction ξ is determined, runs horizontally through the centre of gravity of the shape; ξ increases anticlockwise. The horizontal line marks the density function $1/\pi$ of the uniform direction distribution.

Table 7. Means ($\mu_{D(\xi)}$, $\mu_{D(\xi+\pi/2)}$) and variances ($\sigma_{D(\xi)}^2$, $\sigma_{D(\xi+\pi/2)}^2$) of Bitterlich diameters ($D(\xi)$ taken parallel and $D(\xi+\pi/2)$ taken perpendicular to plot radius direction) in relation to the same characteristics computed over the uniform direction distribution (μ_D, σ_D^2) for five of the six example shapes in Fig. 10 (the orbiform B with constant diameter in every direction is omitted). The direction distributions of the Bitterlich diameters were determined with the viewing angles α=1° and α=30° (in parentheses).

	Shape				
	A	C	D	E	F
$\mu_{D(\xi)}/\mu_D$ (%)	98.79 (98.95)	99.61 (99.66)	99.70 (99.71)	100.00 (99.88)	100.39 (100.19)
$\mu_{D(\xi+\pi/2)}/\mu_D$ (%)	101.21 (101.05)	100.39 (100.34)	100.50 (100.39)	100.65 (100.44)	100.39 (100.19)
$\sigma_{D(\xi)}^2/\sigma_D^2$ (%)	98.20 (98.66)	99.32 (99.44)	97.08 (96.55)	99.76 (99.80)	99.32 (99.74)
$\sigma_{D(\xi+\pi/2)}^2/\sigma_D^2$ (%)	96.98 (97.61)	99.32 (99.44)	106.71 (104.99)	99.11 (99.52)	99.32 (99.74)

In the example shapes of Fig. 10, taking the Bitterlich diameter perpendicular to plot radius results in larger (or equal; shape F) values on average than taking it parallel to plot radius (Table 7), even though the differences are rather small (about 2.5 % in the ellipse A, less than 1 % in the other shapes). Compared to the diameters with the uniform direction distribution, the Bitterlich diameters parallel to plot radius are on average smaller in a majority

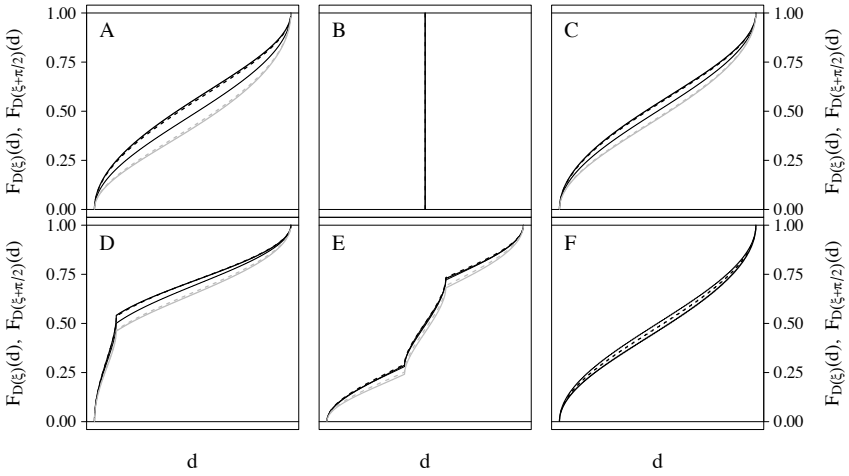

Fig. 21. (Approximated) cumulative distribution functions of the Bitterlich diameters taken parallel ($F_{D(\xi)}(d)$, black) or perpendicular ($F_{D(\xi+\pi/2)}(d)$, grey) to plot radius for the six example shapes in Fig. 10. The distributions were determined with viewing angles α=1° (continuous line) and α=30° (dashed line). For reference, the cumulative distribution function of the diameter with uniformly distributed direction within [0, π) is also shown (thin black line).

of the shapes, whereas the Bitterlich diameters perpendicular to plot radius are on average larger in all the shapes. Interestingly, in all the shapes but one, both types of the Bitterlich diameters seem to have a smaller variance than the diameters with the uniform direction distribution. The correlations between the Bitterlich diameters are the same (up to the third decimal) as the correlations between perpendicular diameters over the uniform direction distribution (Table 1; note that the shape B in this table is not the orbiform in Fig. 10 but the ellipse-like shape in Fig. 5).

From the direction distribution, we get the diameter distribution in a general manner: $F_{D(\xi)}(d) = \Pr\{D(\xi) \le d; \alpha\}$, where $\Pr\{D(\xi) \le d; \alpha\}$ is the probability mass of directions in which diameter is not larger than d. For the example shapes of Fig. 10, the Bitterlich diameter distributions are shown in Fig. 21.

4.2.2 Estimation of Cross-Section Area by Bitterlich Diameters and Circle Area Formula

As mentioned above, Bitterlich diameters (i.e., the diameters measured parallel or perpendicular to plot radius in Bitterlich sampling) are often used as if they were random diameters with the uniform direction distribution. As the direction distributions of the Bitterlich diameters are actually not uniform if the breast height cross-sections of trees are non-circular, we consider the cross-section area estimators similar to $\hat{A}_1$–$\hat{A}_5$ discussed in Section 3.3.2 but now involving Bitterlich diameters. The estimators are of the form

$$\hat{A} = \frac{\pi}{4} D(\cdot)^2 \ , \tag{93}$$

where $D(\cdot)$ is

1ξ. diameter $D(\xi)$ taken parallel to plot radius direction, $\xi \sim F_\xi(\xi; \alpha)$ ($\hat{A}_{1\xi}$)

2ξ. arithmetic mean of diameters $D(\xi)$ and $D(\xi+\pi/2)$ taken parallel and perpendicular to plot radius direction ($\hat{A}_{2\xi}$)

3ξ. geometric mean of $D(\xi)$ and $D(\xi+\pi/2)$ ($\hat{A}_{3\xi}$)

4ξ. arithmetic mean of $D(\xi)$ and an independent random diameter $D(\theta)$, $\xi \sim F_\xi(\xi; \alpha)$, $\theta \sim \text{Uniform}(0, \pi)$ ($\hat{A}_{4\xi}$)

5ξ. geometric mean of $D(\xi)$ and $D(\theta)$ ($\hat{A}_{5\xi}$)

Hardly surprisingly, the within-cross-section expectations, variances and variance approximations of these estimators closely resemble those of the random estimators $\hat{A}_1$–$\hat{A}_5$ (Eqs. 22–26 and 30–37 in Section 3.3.2). If we denote the expectations of $D(\xi)$ and $D(\xi+\pi/2)$ taken over the distribution $F_\xi(\xi; \alpha)$ by $\mu_{D(\xi)}$ and $\mu_{D(\xi+\pi/2)}$, the variances by $\sigma_{D(\xi)}^2$ and $\sigma_{D(\xi+\pi/2)}^2$, and the correlation by $\rho_{D(\xi)}(\pi/2)$ (note that for brevity, the viewing angle α affecting the distribution is omitted in the notation) — and recall that μ_D and σ_D^2 stand for the expectation and the variance of $D(\theta)$ over the uniform distribution of θ — the expectations of the estimators become as follows:

$$\mathrm{E}(\hat{A}_{1\xi}) = \frac{\pi}{4}\mu_{D(\xi)}^2 + \frac{\pi}{4}\sigma_{D(\xi)}^2 , \tag{94}$$

$$\begin{aligned}\mathrm{E}(\hat{A}_{2\xi}) &= \frac{\pi}{4}\left(\frac{\mu_{D(\xi)} + \mu_{D(\xi+\pi/2)}}{2}\right)^2 \\ &\quad + \frac{\pi}{16}\left[\sigma_{D(\xi)}^2 + \sigma_{D(\xi+\pi/2)}^2 + 2\sigma_{D(\xi)}\sigma_{D(\xi+\pi/2)}\rho_{D(\xi)}\left(\frac{\pi}{2}\right)\right],\end{aligned} \tag{95}$$

$$\mathrm{E}(\hat{A}_{3\xi}) = \frac{\pi}{4}\mu_{D(\xi)}\mu_{D(\xi+\pi/2)} + \frac{\pi}{4}\sigma_{D(\xi+\pi/2)}\sigma_{D(\xi)}\rho_{D(\xi)}\left(\frac{\pi}{2}\right), \tag{96}$$

$$\mathrm{E}(\hat{A}_{4\xi}) = \frac{\pi}{4}\left(\frac{\mu_{D(\xi)} + \mu_D}{2}\right)^2 + \frac{\pi}{16}\left(\sigma_{D(\xi)}^2 + \sigma_D^2\right), \tag{97}$$

and

$$\mathrm{E}(\hat{A}_{5\xi}) = \frac{\pi}{4}\mu_{D(\xi)}\mu_D . \tag{98}$$

Unlike with the expectations of the random estimators $\hat{A}_1$–$\hat{A}_5$, it is not easy to see whether these expectations overestimate or underestimate the convex area of a cross-section (because the relationship between $\pi\mu_{D(\xi)}^2/4$, or $\pi\mu_{D(\xi+\pi/2)}^2/4$, and A_C is not straightforward to derive with no assumptions about cross-section shape; cf. Eq. 20 in Section 3.3.2). The exact variances are given by

$$\mathrm{Var}(\hat{A}_{1\xi}) = \frac{\pi^2}{16}\left\{\mathrm{E}[D(\xi)^4] - \left(\mu_{D(\xi)}^2 + \sigma_{D(\xi)}^2\right)^2\right\}, \tag{99}$$

$$\begin{aligned}\mathrm{Var}(\hat{A}_{2\xi}) &= \frac{\pi^2}{16}\left\{\frac{1}{16}\mathrm{E}[D(\xi)^4]+\frac{1}{16}\mathrm{E}\left[D\left(\xi+\frac{\pi}{2}\right)^4\right]+\frac{1}{4}\mathrm{E}\left[D(\xi)^3 D\left(\xi+\frac{\pi}{2}\right)\right]\right.\\ &\quad+\frac{1}{4}\mathrm{E}\left[D(\xi)D\left(\xi+\frac{\pi}{2}\right)^3\right]+\frac{3}{8}\mathrm{E}\left[D(\xi)^2 D\left(\xi+\frac{\pi}{2}\right)^2\right]\\ &\quad-\frac{1}{16}\left[\left(\mu_{D(\xi)}+\mu_{D(\xi+\pi/2)}\right)^2+\sigma^2_{D(\xi)}+\sigma^2_{D(\xi+\pi/2)}\right.\\ &\quad\left.\left.+2\sigma_{D(\xi)}\sigma_{D(\xi+\pi/2)}\rho_{D(\xi)}\left(\frac{\pi}{2}\right)\right]^2\right\},\end{aligned} \tag{100}$$

$$\begin{aligned}\mathrm{Var}(\hat{A}_{3\xi}) &= \frac{\pi^2}{16}\left\{\mathrm{E}\left[D(\xi)^2 D\left(\xi+\frac{\pi}{2}\right)^2\right]\right.\\ &\quad\left.-\left[\mu_{D(\xi)}\mu_{D(\xi+\pi/2)}+\sigma_{D(\xi)}\sigma_{D(\xi+\pi/2)}\rho_{D(\xi)}\left(\frac{\pi}{2}\right)\right]^2\right\},\end{aligned} \tag{101}$$

$$\begin{aligned}\mathrm{Var}(\hat{A}_{4\xi}) &= \frac{\pi^2}{16}\left\{\frac{1}{16}\mathrm{E}[D(\xi)^4]+\frac{1}{16}\mathrm{E}[D(\theta)^4]+\frac{1}{4}\mu_D\mathrm{E}[D(\xi)^3]\right.\\ &\quad+\frac{1}{4}\mu_{D(\xi)}\mathrm{E}[D(\theta)^3]+\frac{3}{8}\left(\mu^2_{D(\xi)}+\sigma^2_{D(\xi)}\right)\left(\mu^2_D+\sigma^2_D\right)\\ &\quad\left.-\frac{1}{16}\left[\left(\mu_{D(\xi)}+\mu_D\right)^2+\sigma^2_{D(\xi)}+\sigma^2_D\right]^2\right\},\end{aligned} \tag{102}$$

and

$$\mathrm{Var}(\hat{A}_{5\xi}) = \frac{\pi^2}{16}\left[\left(\mu^2_{D(\xi)}+\sigma^2_{D(\xi)}\right)\left(\mu^2_D+\sigma^2_D\right)-\mu^2_{D(\xi)}\mu^2_D\right]. \tag{103}$$

Finally, the variance approximations by the delta method become

$$\widetilde{\mathrm{Var}}(\hat{A}_{1\xi}) = \frac{\pi^2}{4}\mu^2_{D(\xi)}\sigma^2_{D(\xi)}, \tag{104}$$

$$\widetilde{\mathrm{Var}}(\hat{A}_{2\xi}) = \frac{\pi^2}{16}\left(\frac{\mu_{D(\xi)}+\mu_{D(\xi+\pi/2)}}{2}\right)^2\left[\sigma^2_{D(\xi)}+\sigma^2_{D(\xi+\pi/2)}+2\sigma_{D(\xi)}\sigma_{D(\xi+\pi/2)}\rho_{D(\xi)}\left(\frac{\pi}{2}\right)\right], \tag{105}$$

$$\begin{aligned}\widetilde{\mathrm{Var}}(\hat{A}_{3\xi}) &= \frac{\pi^2}{16}\left[\mu^2_{D(\xi)}\sigma^2_{D(\xi+\pi/2)}+\mu^2_{D(\xi+\pi/2)}\sigma^2_{D(\xi)}\right.\\ &\quad\left.+2\mu_{D(\xi)}\mu_{D(\xi+\pi/2)}\sigma_{D(\xi)}\sigma_{D(\xi+\pi/2)}\rho_{D(\xi)}\left(\frac{\pi}{2}\right)\right],\end{aligned} \tag{106}$$

$$\widehat{\mathrm{Var}}(\hat{A}_{4\xi}) = \frac{\pi^2}{16}\left(\frac{\mu_{D(\xi)} + \mu_D}{2}\right)^2 \left(\sigma^2_{D(\xi)} + \sigma^2_D\right), \tag{107}$$

and

$$\widehat{\mathrm{Var}}(\hat{A}_{5\xi}) = \frac{\pi^2}{16}\left(\mu^2_D\, \sigma^2_{D(\xi)} + \mu^2_{D(\xi)}\, \sigma^2_D\right). \tag{108}$$

Note that these variance approximations depend not only on the way of selecting the diameters — as with the estimators $\hat{A}_1$–$\hat{A}_5$ — but also on the type of mean employed in the estimator. For the estimator $\hat{A}_{5\xi}$, the approximate variance is easily seen to underestimate the true variance, exactly as was the case with the estimator $\hat{A}_5$ involving two diameters with the uniform direction distribution (cf. Eq. 38 in Section 3.3.2).

In practice, it is often more convenient to measure the (first) diameter perpendicular to plot radius than parallel to it. This practice results in three more area estimators of the form above to be considered: the modifications $\hat{A}_{1\xi 90}$, $\hat{A}_{4\xi 90}$ and $\hat{A}_{5\xi 90}$ of $\hat{A}_{1\xi}$, $\hat{A}_{4\xi}$ and $\hat{A}_{5\xi}$ involving $D(\xi+\pi/2)$ instead of $D(\xi)$. The within-cross-section expectations and variances of the these estimators are obtained from those of $\hat{A}_{1\xi}$, $\hat{A}_{4\xi}$ and $\hat{A}_{5\xi}$ by substituting the moments of $D(\xi+\pi/2)$ for the moments of $D(\xi)$.

In Tables 8 and 9, the expectations, variances and approximate variances of the estimators $\hat{A}_{1\xi}$–$\hat{A}_{5\xi}$, $\hat{A}_{1\xi 90}$, $\hat{A}_{4\xi 90}$ and $\hat{A}_{5\xi 90}$ are given for the example shapes in Fig. 10; the distributions of ξ (and $\xi+\pi/2$) were determined with viewing angles 1° and 30°. None of the

Table 8. Expectations of the area estimators $\hat{A}_{1\xi}$–$\hat{A}_{5\xi}$, $\hat{A}_{1\xi 90}$, $\hat{A}_{4\xi 90}$ and $\hat{A}_{5\xi 90}$ (Eqs. 94–98) for the example shapes in Fig. 10 (the orbiform B with constant diameter in every direction is omitted, because in it all the estimators yield the same estimate, 1.042 times the true area), expressed in permille of true area. The distributions of the directions ξ and $\xi+\pi/2$ of the Bitterlich diameters were determined with the viewing angles α=1° and α=30° (in parentheses).

	Shape				
	A	C	D	E	F
$E(\hat{A}_{1\xi})/A$ (‰)	1000 (1003)	1016 (1017)	1014 (1014)	1034 (1031)	1040 (1036)
$E(\hat{A}_{2\xi})/A$ (‰)	1019 (1019)	1022 (1022)	1019 (1018)	1037 (1034)	1038 (1034)
$E(\hat{A}_{3\xi})/A$ (‰)	1013 (1013)	1020 (1020)	1018 (1017)	1037 (1034)	1040 (1036)
$E(\hat{A}_{4\xi})/A$ (‰)	1010 (1011)	1019 (1020)	1016 (1016)	1032 (1031)	1035 (1033)
$E(\hat{A}_{5\xi})/A$ (‰)	1006 (1008)	1018 (1019)	1014 (1014)	1030 (1029)	1034 (1032)
$E(\hat{A}_{1\xi 90})/A$ (‰)	1050 (1046)	1032 (1031)	1030 (1028)	1047 (1043)	1040 (1036)
$E(\hat{A}_{4\xi 90})/A$ (‰)	1034 (1033)	1027 (1026)	1024 (1023)	1039 (1037)	1035 (1033)
$E(\hat{A}_{5\xi 90})/A$ (‰)	1031 (1029)	1026 (1025)	1022 (1021)	1037 (1035)	1034 (1032)

estimators systematically underestimates the true area. As could be expected on the basis of diameter means (Table 7), the estimators involving the Bitterlich diameter parallel to plot radius ($\hat{A}_{1\xi}$, $\hat{A}_{4\xi}$ and $\hat{A}_{5\xi}$) yield smaller overestimating biases than those involving the Bitterlich diameter perpendicular to plot radius ($\hat{A}_{1\xi 90}$, $\hat{A}_{4\xi 90}$ and $\hat{A}_{5\xi 90}$). In all the shapes but F, the former estimators perform better, in terms of bias, than the estimators that were earlier found to be the best ($\hat{A}_0$ and $\hat{A}_3$; Table 8 vs. Table 2). As to the estimator variance, the type of the Bitterlich diameter involved in the estimator appears to have practically no effect (Table 9). The approximated variances virtually equal the true variances, which in turn hardly deviate from the variances obtained with the diameters with the uniform direction distribution (Table 9 vs. Table 3).

Table 9. Square roots of the variances (Eqs. 99–103; Sd) and approximate variances (Eqs. 104–108; $\tilde{\text{Sd}}$) of the area estimators $\hat{A}_{1\xi}$–$\hat{A}_{5\xi}$, $\hat{A}_{1\xi 90}$, $\hat{A}_{4\xi 90}$ and $\hat{A}_{5\xi 90}$ for the example shapes in Fig. 10 (the orbiform B with constant diameter in every direction is omitted, because in it the variances are identically zero), expressed in permille of true area. The distributions of the directions ξ and $\xi+\pi/2$ of the Bitterlich diameters were determined with the viewing angle $\alpha=1°$; with $\alpha=30°$ the results were the same (up to a difference of 1 permille in a handful of cases).

	Shape				
	A	C	D	E	F
$\text{Sd}(\hat{A}_{1\xi})$/A (‰)	157	90	101	118	91
$\tilde{\text{Sd}}(\hat{A}_{1\xi})$/A (‰)	156	90	99	118	91
$\text{Sd}(\hat{A}_{2\xi})$/A (‰)	4	0	45	83	91
$\tilde{\text{Sd}}(\hat{A}_{2\xi})$/A (‰)	4	0	45	83	91
$\text{Sd}(\hat{A}_{3\xi})$/A (‰)	9	1	44	83	91
$\tilde{\text{Sd}}(\hat{A}_{3\xi})$/A (‰)	5	0	45	83	91
$\text{Sd}(\hat{A}_{4\xi})$/A (‰)	112	64	71	83	64
$\tilde{\text{Sd}}(\hat{A}_{4\xi})$/A (‰)	112	64	70	83	64
$\text{Sd}(\hat{A}_{5\xi})$/A (‰)	112	64	71	83	64
$\tilde{\text{Sd}}(\hat{A}_{5\xi})$/A (‰)	112	64	70	83	64
$\text{Sd}(\hat{A}_{1\xi 90})$/A (‰)	157	90	106	118	91
$\tilde{\text{Sd}}(\hat{A}_{1\xi 90})$/A (‰)	159	90	104	118	91
$\text{Sd}(\hat{A}_{4\xi 90})$/A (‰)	112	64	73	83	64
$\tilde{\text{Sd}}(\hat{A}_{4\xi 90})$/A (‰)	113	64	72	83	64
$\text{Sd}(\hat{A}_{5\xi 90})$/A (‰)	113	64	72	83	64
$\tilde{\text{Sd}}(\hat{A}_{5\xi 90})$/A (‰)	113	64	72	83	64

5 Estimation of Stem Volume

Analogously to the previous discussion on cross-section area estimation in Chapter 3, we now want to explore how diameter variation in non-circular cross-sections is reflected, via different diameter selection methods, to stem volume estimates or predictions. We consider three volume estimation methods — a volume equation, a theoretical general estimator (a definite integral of a cross-section area estimation function), and a definite integral of a non-parametric stem curve (a special case of the general estimator) — in which the input consists of tree height and diameters taken at two or more known (non-random) heights. Our interest is in the *application* of the volume estimation methods: we want to quantify how much of the estimation bias and error variance is attributable to uncertainty in the explanatory variables (diameters) and therefore seek to distinguish the error component due to diameter variation from the components related to other sources of uncertainty, such as model specification, parameter estimation and residual variation. The theoretical discussion in this chapter is a preliminary to the empirical part of the study, where the three types of volume estimators are investigated with real stems.

5.1 Practical Volume Estimator: Laasasenaho Volume Equation

The volume equations constructed by Laasasenaho (1982) are commonly used in Finland for predicting stem volume of standing trees from basic field measurements. We consider here the three-variable equation, with which the volumes of the sample trees are predicted for example in the Finnish national forest inventory (Tomppo et al. 1997). The model is of the form

$$\begin{aligned} V &= \beta_1 D(\cdot, 1.3)^2 + \beta_2 D(\cdot, 1.3)^2 H + \beta_3 D(\cdot, 1.3)^3 H + \beta_4 D(\cdot, 1.3)^2 H^2 \\ &\quad + \beta_5 \left[D(\cdot, 1.3)^2 + D(\cdot, 1.3) D(\cdot, 6) + D(\cdot, 6)^2 \right] + \beta_6 D(\cdot, 6)^2 (H - 6) + \varepsilon_L \,, \end{aligned} \tag{109}$$

where V denotes the stem volume, $D(\cdot, 1.3)$ is the breast height diameter, $D(\cdot, 6)$ is the upper diameter taken at the height of 6 m, H stands for the stem height, and ε_L is a random error with certain properties discussed in more detail below. As indicated by the denotations $D(\cdot, 1.3)$ and $D(\cdot, 6)$, the diameters in the model have not been explicitly specified (in which direction they should be measured, whether they should be computed as a mean of two or more diameters etc.). We fix them here as those yielding the true cross-section areas when substituted in the circle area formula, denoted by $D_A(1.3)$ and $D_A(6)$:

$$\begin{aligned} V &= \beta_1 D_A(1.3)^2 + \beta_2 D_A(1.3)^2 H + \beta_3 D_A(1.3)^3 H + \beta_4 D_A(1.3)^2 H^2 \\ &\quad + \beta_5 \left[D_A(1.3)^2 + D_A(1.3) D_A(6) + D_A(6)^2 \right] + \beta_6 D_A(6)^2 (H - 6) + \varepsilon_L \,. \end{aligned} \tag{110}$$

This specification, albeit not very feasible in practice, is well motivated by the geometrical background of the model (see Laasasenaho 1982, p. 35–39) and also serves our purpose of extracting the effect of non-circularity on prediction error.

The model was constructed on the basis of data on 5053 trees sampled from all over Finland (Laasasenaho 1982), and hence it may be considered to express the dependence of stem volume on diameters and height in the Finnish tree population, with different parameter values β_1, ..., β_6 for different species. This population is finite but so large that sampling from it more or less corresponds to sampling from a theoretical infinite population.

Randomness arises from choosing a tree in the population, and both the response variable and the explanatory variables may be regarded as random variables, the joint distribution of which is generated by repeated independent samplings from the population. As usual with random explanatory variables, the distributional properties of the error term ε_L are defined conditional on the explanatory variables: given any possible combination of values of $D_A(1.3)$, $D_A(6)$ and H in the population, ε_L is assumed to have zero expectation and variance proportional to $D_A(1.3)^4H^2$ (Laasasenaho 1982, p. 36 and p. 43–44); further, ε_L's of separate trees are assumed to be independent. From the zero conditional expectation of ε_L it follows that the expectation of ε_L is zero also marginally, that is, over the joint distribution of $D_A(1.3)$, $D_A(6)$ and H in the population.

We *assume the equation to express the relation correctly*, that is, the functional form as well as the values of the coefficients β_1, ..., β_6 to be true in the population of our interest, and wish to use it to *predict* the volume of a (randomly selected) tree in this population, when the two diameters and the height of the tree are known. The best predictor is the model without the error term, that is, the conditional expectation of the volume:

$$\begin{aligned}\tilde{V}_L &= E[V \mid D_A(1.3), D_A(6), H] \\ &= \beta_1 D_A(1.3)^2 + \beta_2 D_A(1.3)^2 H + \beta_3 D_A(1.3)^3 H + \beta_4 D_A(1.3)^2 H^2 \\ &\quad + \beta_5 \left[D_A(1.3)^2 + D_A(1.3) D_A(6) + D_A(6)^2 \right] + \beta_6 D_A(6)^2 (H-6) .\end{aligned} \tag{111}$$

As there is no estimation error in the parameter values, the *prediction error* $V-\tilde{V}_L$ naturally equals the random error ε_L and follows the assumptions made on ε_L (i.e., $E[V-\tilde{V}_L \mid D_A(1.3), D_A(6), H] = E[V-\tilde{V}_L]=0$ and $Var[V-V_L \mid D_A(1.3), D_A(6), H] \propto D_A(1.3)^4H^2$).

If we then view volume prediction *within the tree of interest*, the setting becomes very similar to that of cross-section area estimation in Chapter 3: volume is now a fixed property of the tree that we estimate by a fixed estimator $\tilde{V}_L$, and the *estimation error* $V-\tilde{V}_L$ becomes a non-random scalar (a realisation of ε_L). We adopt this within-tree view for a while to deal with volume predictors involving random diameters.

Consider estimating the stem volume of the tree by using some diameters other than $D_A(1.3)$ and $D_A(6)$, measured without error at the heights of 1.3 m and 6 m. Denote these diameters by $D(\boldsymbol{\theta}, 1.3)$ and $D(\boldsymbol{\theta}, 6)$, $\boldsymbol{\theta}$ referring here to the diameter direction selection method in general. As the height H is known, the estimator can now be written as a function of the diameters only:

$$\hat{V}_L(\boldsymbol{\theta}) = c_1 D(\boldsymbol{\theta},1.3)^2 + c_2 D(\boldsymbol{\theta},1.3)^3 + c_3 D(\boldsymbol{\theta},1.3) D(\boldsymbol{\theta},6) + c_4 D(\boldsymbol{\theta},6)^2 , \tag{112}$$

where $c_1=\beta_1+\beta_2H+\beta_4H^2+\beta_5$, $c_2=\beta_3H$, $c_3=\beta_5$, and $c_4=\beta_5+\beta_6(H-6)$. If the selection of $D(\boldsymbol{\theta}, 1.3)$ and $D(\boldsymbol{\theta}, 6)$ involves randomness, the estimator becomes a random variable, the within-tree distribution of which is determined by the diameter selection method and the shape of the cross-sections at the heights of 1.3 m and 6 m. As with random area estimators (Section 3.3.2), the random volume estimator can be thought to consist of a systematic part and a stochastic part — the within-tree expectation over the diameter direction distribution and a random sampling error with zero expectation over the same distribution:

$$\hat{V}_L(\boldsymbol{\theta}) = E_{\boldsymbol{\theta}}[\hat{V}_L(\boldsymbol{\theta})] + \nu_L(\boldsymbol{\theta}) . \tag{113}$$

As the estimator is a linear combination of the second and third powers of diameters and their cross-product, its within-tree expectation and variance are obtained by means of the

corresponding diameter moments and product moments taken over the diameter direction distribution:

$$\begin{aligned} E_{\boldsymbol{\theta}}[\hat{V}_L(\boldsymbol{\theta})] &= c_1 E_{\boldsymbol{\theta}}[D(\boldsymbol{\theta},1.3)^2] + c_2 E_{\boldsymbol{\theta}}[D(\boldsymbol{\theta},1.3)^3] \\ &\quad + c_3 E_{\boldsymbol{\theta}}[D(\boldsymbol{\theta},1.3)D(\boldsymbol{\theta},6)] + c_4 E_{\boldsymbol{\theta}}[D(\boldsymbol{\theta},6)^2] , \end{aligned} \tag{114}$$

and

$$\begin{aligned} \mathrm{Var}_{\boldsymbol{\theta}}[\nu_L(\boldsymbol{\theta})] &= \mathrm{Var}_{\boldsymbol{\theta}}[\hat{V}_L(\boldsymbol{\theta})] \\ &= E_{\boldsymbol{\theta}}[\hat{V}_L(\boldsymbol{\theta})^2] - \left\{ E_{\boldsymbol{\theta}}[\hat{V}_L(\boldsymbol{\theta})] \right\}^2 \\ &= c_2^2 E_{\boldsymbol{\theta}}[D(\boldsymbol{\theta},1.3)^6] + 2c_1c_2 E_{\boldsymbol{\theta}}[D(\boldsymbol{\theta},1.3)^5] + c_1^2 E_{\boldsymbol{\theta}}[D(\boldsymbol{\theta},1.3)^4] \\ &\quad + 2c_2c_3 E_{\boldsymbol{\theta}}[D(\boldsymbol{\theta},1.3)^4 D(\boldsymbol{\theta},6)] + 2c_2c_4 E_{\boldsymbol{\theta}}[D(\boldsymbol{\theta},1.3)^3 D(\boldsymbol{\theta},6)^2] \\ &\quad + 2c_1c_3 E_{\boldsymbol{\theta}}[D(\boldsymbol{\theta},1.3)^3 D(\boldsymbol{\theta},6)] + (c_3^2 + 2c_1c_4) E_{\boldsymbol{\theta}}[D(\boldsymbol{\theta},1.3)^2 D(\boldsymbol{\theta},6)^2] \\ &\quad + 2c_3c_4 E_{\boldsymbol{\theta}}[D(\boldsymbol{\theta},1.3)D(\boldsymbol{\theta},6)^3] + c_4^2 E_{\boldsymbol{\theta}}[D(\boldsymbol{\theta},6)^4] \\ &\quad - \left\{ E_{\boldsymbol{\theta}}[\hat{V}_L(\boldsymbol{\theta})] \right\}^2 . \end{aligned} \tag{115}$$

Each diameter selection method can in principle be applied either *dependently* or *independently* at the two observation heights within the stem: in the former, the diameter direction is selected at breast height, and the upper diameter is then measured in the same direction; in the latter, the diameter directions at the two heights are selected independently. In Bitterlich sampling, however, the idea of selecting diameters parallel or perpendicular to plot radius independently at the two heights is unfeasible (the plot radius direction is determined only once, from one viewing point at the breast height level); therefore, only dependent selection can be considered with the methods involving Bitterlich diameters. In the above expressions of within-tree expectation and variance, independent and dependent selection differ from each other only in terms of the product moments $E[D(\boldsymbol{\theta}, 1.3)^k D(\boldsymbol{\theta}, 6)^p]$, k, $p \in \mathbb{Q}_+$, which in the independent case reduce to the products of moments $E[D(\boldsymbol{\theta}, 1.3)^k]E[D(\boldsymbol{\theta}, 6)^p]$. In Appendices E and F, more elaborate method-specific versions of the above general expressions of within-tree expectation and variance are given for the diameter selection methods involving randomness and considered previously in area estimation (methods 1–5 involving the uniform direction distribution, see Section 3.3.2; methods 1ξ–5ξ, 1ξ90, 4ξ90 and 5ξ90 involving Bitterlich diameter direction distribution, see Section 4.2.2).

No matter if we are viewing volume determination at the within-tree level (volume estimation) or at the population level (volume prediction), the volume error $V–\hat{V}_L(\boldsymbol{\theta})$ may be thought to consist of two components — the error term inherent in the model (the difference between the true volume V and the best predictor/estimator $\tilde{V}_L$) and the error due to diameter selection (the difference between the best predictor/estimator $\tilde{V}_L$ and the predictor/estimator $\hat{V}_L(\boldsymbol{\theta})$ obtained with the particular diameter selection method $\boldsymbol{\theta}$); further, the error due to diameter selection can be divided into two components — the within-tree bias $\tilde{V}_L–E_{\boldsymbol{\theta}}[\hat{V}_L(\boldsymbol{\theta})]$ taken with respect to the best predictor/estimator and a random sampling error $\nu_L(\boldsymbol{\theta})$:

$$\begin{aligned} V - \hat{V}_L(\boldsymbol{\theta}) &= (V - \tilde{V}_L) + \left[\tilde{V}_L - \hat{V}_L(\boldsymbol{\theta}) \right] \\ &= \varepsilon_L + \left\{ \tilde{V}_L - \left\{ E_{\boldsymbol{\theta}}[\hat{V}_L(\boldsymbol{\theta})] + \nu_L(\boldsymbol{\theta}) \right\} \right\} \\ &= \varepsilon_L + \left\{ \tilde{V}_L - E_{\boldsymbol{\theta}}[\hat{V}_L(\boldsymbol{\theta})] \right\} - \nu_L(\boldsymbol{\theta}) \,. \end{aligned} \tag{116}$$

At the within-tree level (conditional on the selected tree), only the within-tree diameter sampling error $\nu_L(\boldsymbol{\theta})$ is a random variable (with zero expectation, variance $\mathrm{Var}_{\boldsymbol{\theta}}[\nu_L(\boldsymbol{\theta})]=\mathrm{Var}[\hat{V}_L(\boldsymbol{\theta})]$, and the distribution determined by the diameter sampling method and the shapes of the cross-sections at 1.3 m and 6 m), whereas the model error ε_L and the within-tree systematic error due to diameter selection $\tilde{V}_L - E_{\boldsymbol{\theta}}[\hat{V}_L(\boldsymbol{\theta})]$ are non-random scalars and may in principle be compared to each other. At the population level, however, all the prediction error components are random variables. Yet we have only made assumptions on the model error ε_L. In any event, the prediction bias $E[V - \hat{V}_L(\boldsymbol{\theta})]$ at the population level consists of only the between-trees expectation $E\{\tilde{V}_L - E_{\boldsymbol{\theta}}[\hat{V}_L(\boldsymbol{\theta})]\}$ of the within-tree bias due to diameter selection, as $E(\varepsilon_L)=0$ by assumption and $E[\nu_L(\boldsymbol{\theta})]=E_{\mathrm{tree}}\{E_{\boldsymbol{\theta}}[\nu_L(\boldsymbol{\theta}) \mid \mathrm{tree}]\}=0$. The prediction error variance $\mathrm{Var}[V - \hat{V}_L(\boldsymbol{\theta})]$, in turn, comprises the variances of all the error components (ε_L, $\tilde{V}_L - E_{\boldsymbol{\theta}}[\hat{V}_L(\boldsymbol{\theta})]$ and $\nu_L(\boldsymbol{\theta})$) taken over their marginal distributions as well as double the pairwise covariances computed over their joint distribution.

Above we assumed the model (Eq. 110) to be true. If, however, the true values for the parameters $\beta_1, \ldots, \beta_6$ were unknown and we had to use estimates obtained from any subpopulation, the prediction error $V - \tilde{V}_L$ would also contain a component due to the parameter estimation error (see e.g. Fox 1984; cf. Gregoire and Williams 1992): even if the parameters were unbiasedly estimated, the prediction bias at the population level would be zero only when averaged over (infinitely many) repeated parameter estimations; furthermore, the prediction error variance would increase by a non-zero term depending on the variances and covariances of the parameter estimates and the values of the predicting variables.

5.2 General Volume Estimator: Definite Integral of Cross-Section Area Estimation Function

The true volume of a stem is attained as a definite integral of the cross-section area function — a continuous and bounded function $A:[0, H] \rightarrow [0, \infty)$ expressing how the cross-section area perpendicular to the vertical stem axis changes along the position in the axis:

$$V = \int_0^H A(h)\,dh \,. \tag{117}$$

Substituting for the area function an estimate $\hat{A}(h; \boldsymbol{\theta})$ (where $\boldsymbol{\theta}$ just generally refers to the features of the function distinguishing it from other area estimation functions) results in a volume estimator of the form

$$\hat{V}_G(\boldsymbol{\theta}) = \int_0^H \hat{A}(h; \boldsymbol{\theta})\,dh \,. \tag{118}$$

Estimators of this kind, where no presumptions (besides boundedness) are necessarily made on $\hat{A}(h; \boldsymbol{\theta})$, are here referred to as *general volume estimators*. (We can not require continuity of $\hat{A}(h; \boldsymbol{\theta})$, if we want to allow it to be constructed from random diameters selected independently of each other at all the heights $h \in [0, H]$; see the discussion below.)

Unlike with the volume equation earlier, we now choose to disregard the tree population level — although many population level models for the area estimation function (cross-section area taper models) are to be found in the literature (for a statistical consideration of prediction by such models, without uncertainty in the explanatory variables, refer e.g. to Gregoire et al. 2000). Instead, we adopt the within-tree view and simply regard the stem volume as a fixed property of our tree of interest, which we then want to estimate by means of an estimated cross-section area function (typically derived from either fixed or random diameters taken at predetermined heights) and the tree height. Within-tree randomness in the volume estimator then arises from randomness in the estimated area function (typically stemming from the use of random diameters in the construction of the function).

If $\hat{A}(h; \boldsymbol{\theta})$ is a random function ($\boldsymbol{\theta}$ now referring to the source of randomness, typically the selection method of random diameter directions), it can equivalently be regarded as a continuous parameter stochastic process $\{\hat{A}(h; \boldsymbol{\theta}), h \in [0, H]\}$ within the tree (cf. Rao 1979, p. 2). We are interested in the definite integrals of this process (to get the volume estimator) and of its transformation, the area estimation error process $\{\hat{A}(h; \boldsymbol{\theta})–A(h), h \in [0, H]\}$ (to get the volume estimation error). The definite integrals are well-defined (as limits, in the sense of convergence in mean square, of the sequences of approximating sums (Riemann sums) over [0, H] or any of its sub-intervals), if the processes satisfy the following sufficient (but not necessary!) conditions (Parzen 1962, p. 78–79): First, the processes should have finite second moments. In our case, this is necessarily true, as both $\{\hat{A}(h; \boldsymbol{\theta})\}$ and $\{A(h)\}$ are bounded. Second, the processes should have continuous mean and covariance functions $\mu_{\hat{A}}(h; \boldsymbol{\theta})=E_{\boldsymbol{\theta}}[\hat{A}(h; \boldsymbol{\theta})]$, $\mu_{\Delta\hat{A}}(h; \boldsymbol{\theta})=E_{\boldsymbol{\theta}}[\hat{A}(h; \boldsymbol{\theta})–A(h)]$ and $\gamma_{\hat{A}}(h, k; \boldsymbol{\theta})=Cov_{\boldsymbol{\theta}}[\hat{A}(h; \boldsymbol{\theta}), \hat{A}(k; \boldsymbol{\theta})]=Cov_{\boldsymbol{\theta}}[\hat{A}(h; \boldsymbol{\theta})–A(h), \hat{A}(k; \boldsymbol{\theta})–A(k)]=\gamma_{\Delta\hat{A}}(h, k; \boldsymbol{\theta})$. Although $\hat{A}(h; \boldsymbol{\theta})$ based on diameters taken in independent random directions at each height is not necessarily continuous, its mean and covariance functions are, as they consist of diameter means, variances and covariances that change with height within a stem smoothly, with no discontinuity. Hence, we can assume that our processes fulfil also the second condition.

For processes satisfying the above conditions, the expectation and variance of their definite integrals are given by the definite integrals of the mean and covariance functions (Parzen 1962, p. 79). Accordingly, for the area estimation process and the area estimation error process

$$\begin{aligned} E_{\boldsymbol{\theta}}[\hat{V}_G(\boldsymbol{\theta})] &= E_{\boldsymbol{\theta}}\left[\int_0^H \hat{A}(h; \boldsymbol{\theta})dh\right] \\ &= \int_0^H \mu_{\hat{A}}(h; \boldsymbol{\theta})dh\,, \end{aligned} \tag{119}$$

$$\begin{aligned} E_{\boldsymbol{\theta}}\left[\hat{V}_G(\boldsymbol{\theta}) - V\right] &= E_{\boldsymbol{\theta}}\left[\int_0^H \hat{A}(h; \boldsymbol{\theta})dh - \int_0^H A(h)dh\right] \\ &= E_{\boldsymbol{\theta}}\left\{\int_0^H \left[\hat{A}(h; \boldsymbol{\theta}) - A(h)\right]dh\right\} \\ &= \int_0^H \mu_{\Delta\hat{A}}(h; \boldsymbol{\theta})dh\,, \end{aligned} \tag{120}$$

and

$$\begin{aligned}
\mathrm{Var}_{\boldsymbol{\theta}}[\hat{V}_G(\boldsymbol{\theta})] &= \mathrm{Var}_{\boldsymbol{\theta}}\left[\int_0^H \hat{A}(h;\boldsymbol{\theta})\,dh\right] \\
&= \int_0^H\int_0^H \gamma_{\hat{A}}(h,k;\boldsymbol{\theta})\,dh\,dk \\
&= \int_0^H\int_0^H \gamma_{\Delta\hat{A}}(h,k;\boldsymbol{\theta})\,dh\,dk \\
&= \mathrm{Var}_{\boldsymbol{\theta}}\left\{\int_0^H \left[\hat{A}(h;\boldsymbol{\theta}) - A(h)\right]dh\right\} \\
&= \mathrm{Var}_{\boldsymbol{\theta}}\left[\hat{V}_G(\boldsymbol{\theta}) - V\right].
\end{aligned} \tag{121}$$

In other words, the within-tree expectation and variance of a general volume estimator are attained by integrating the mean and covariance functions of the underlying area estimation process; further, the within-tree bias is obtained by integrating the mean function of the area estimation error process.

A theoretical upper bound for the within-tree variance of a general volume estimator is attained by assuming that the elements of the area estimation process are fully positively correlated, that is, by assuming that $\rho_{\hat{A}}(h, k)=\mathrm{Corr}_{\boldsymbol{\theta}}[\hat{A}(h;\boldsymbol{\theta}), \hat{A}(k;\boldsymbol{\theta})]=1$ for all h and k in [0, H]. In this case, the covariance function of the area estimation process becomes

$$\gamma_{\hat{A}}(h,k;\boldsymbol{\theta}) = \sqrt{\sigma^2_{\hat{A}}(h;\boldsymbol{\theta})\,\sigma^2_{\hat{A}}(k;\boldsymbol{\theta})}\ , \tag{122}$$

where $\sigma_{\hat{A}}^2:[0, H]\rightarrow[0, \infty)$, $\sigma_{\hat{A}}^2(h;\boldsymbol{\theta})=\mathrm{Var}_{\boldsymbol{\theta}}[\hat{A}(h;\boldsymbol{\theta})]$ is the variance function of the area estimation process, and this yields

$$\mathrm{Var}_{\boldsymbol{\theta}}[\hat{V}_G(\boldsymbol{\theta}) \mid \rho_{\hat{A}}(h, k) = 1] = \left[\int_0^H \sqrt{\sigma^2_{\hat{A}}(h;\boldsymbol{\theta})}\,dh\right]^2 \tag{123}$$

as the volume estimator variance.

An area estimation process with uncorrelated elements makes another interesting special case. Envisage a process where the correlation between elements $\hat{A}(h;\boldsymbol{\theta})$ and $\hat{A}(k;\boldsymbol{\theta})$ decreases with an increasing distance between h and k, finally to vanish with distances larger than some threshold value. It can be shown that as the threshold distance is diminished toward zero, that is, as the correlations between elements nearer and nearer each other are made vanish, the variance of the corresponding volume estimator (the variance of the integral of the process) tends to zero. The "limiting process" with mutually uncorrelated elements, that is, with $\mathrm{Corr}_{\boldsymbol{\theta}}[\hat{A}(h;\boldsymbol{\theta}), \hat{A}(k;\boldsymbol{\theta})]=0$ for *all* $h\neq k$ in [0, H], is necessarily discontinuous and possesses a discontinuous covariance function with non-zero values ($\sigma_{\hat{A}}^2(h;\boldsymbol{\theta})$) only within the diagonal line k=h. In our tree stem context, this kind of process would arise, for example, if $\hat{A}(h;\boldsymbol{\theta})$ was based on diameters taken in independent random directions at *all* the heights $h\in[0, H]$. In practice, however, this process has no natural construction: we may well generate individual process elements (area estimators) that are uncorrelated with each other — by independent selection of random diameter directions, for example — but only sparsely, at a finite number of observation heights, not at the infinite number of all possible heights. To obtain a volume estimate, we need to know the values of the area estimation process at all the heights $h\in[0, H]$, and these we attain by assuming continuity — and, thus, some degree of correlation — between our finite number of observed values. Ergo, from

a practical point of view, an area estimation process with uncorrelated elements is just an abstraction that cannot indeed exist in our tree stem context.

A natural practice would be to assume a model for the area estimation function $\hat{A}(h; \boldsymbol{\theta})$ in a tree and derive from it (empirical) approximations of $\mu_{\Delta\hat{A}}(h; \boldsymbol{\theta})$, $\gamma_{\hat{A}}(h, k; \boldsymbol{\theta})$, and $\sigma_{\hat{A}}^2(h; \boldsymbol{\theta})$ (cf. Section 5.3). In the empirical part of this study, however, we will construct crude approximations of $\mu_{\Delta\hat{A}}(h; \boldsymbol{\theta})$, $\gamma_{\hat{A}}(h, k; \boldsymbol{\theta})$, and $\sigma_{\hat{A}}^2(h; \boldsymbol{\theta})$ in a data-driven manner, without an explicit model for $\hat{A}(h; \boldsymbol{\theta})$: We will consider area estimation processes where the area estimator at each height is one of the area estimators discussed in Sections 3.3 and 4.2.2. For each process, we will approximate $\mu_{\Delta\hat{A}}(h; \boldsymbol{\theta})$, $\gamma_{\hat{A}}(h, k; \boldsymbol{\theta})$, and $\sigma_{\hat{A}}^2(h; \boldsymbol{\theta})$ by just interpolating between discrete observations of the process mean, covariance and variance in the stem — between the elements of a vector containing the within-cross-section biases $(E_{\boldsymbol{\theta}}[\hat{A}(h; \boldsymbol{\theta})]–A(h))_{h\in \mathbf{H}}$, a matrix containing the between-cross-sections covariances $(\mathrm{Cov}_{\boldsymbol{\theta}}[\hat{A}(h; \boldsymbol{\theta}), \hat{A}(k; \boldsymbol{\theta})])_{h,\, k\in \mathbf{H}}$, and a vector containing the within-cross-section variances $(\mathrm{Var}_{\boldsymbol{\theta}}[\hat{A}(h; \boldsymbol{\theta})])_{h\in \mathbf{H}}$ of the area estimator observed at fixed heights $\mathbf{H}=\{h_{(1)}, h_{(2)}, ..., h_{(m)}\}$ in the stem. Evidently, a unique area estimation function $\hat{A}(h; \boldsymbol{\theta})$ that would exactly correspond to the obtained $\mu_{\Delta\hat{A}}(h; \boldsymbol{\theta})$, $\gamma_{\hat{A}}(h, k; \boldsymbol{\theta})$, and $\sigma_{\hat{A}}^2(h; \boldsymbol{\theta})$ may not even exist, whereas there are likely to be many whose mean, covariance and variance functions are reasonably adequately approximated by the obtained functions.

5.3 Volume Estimator Based on Non-Parametric Stem Curve: Definite Integral of Interpolating Cubic Splines

Irrespective of the variation in cross-section shape in the stem, the area estimation function in the integral expression of stem volume (Eq. 117) can equivalently be written as $A(h)=\pi D_A(h)^2/4$, where $D_A:[0, H]\rightarrow[0, \infty)$ is a continuous and bounded function expressing the true area diameter (i.e., the diameter that yields the true cross-section area when substituted in the circle area formula) at height h. The true volume of a stem is thus given by

$$V = \frac{\pi}{4}\int_0^H D_A(h)^2\,dh\,, \tag{124}$$

and $D_A(\cdot)$ is referred to as the *true stem curve*.

A plethora of methods have been suggested to predict or estimate $D_A(\cdot)$ (see Sterba 1980, and, for instance, Laasasenaho 1982 and Lappi 1986). In this study, we consider *cubic spline interpolation* between diameters measured at several non-random heights in a stem: the stem curve is composed of piecewise defined 4th order (3rd degree) polynomials of height, one polynomial for each interval between two adjacent measurement heights; each polynomial is required to pass through the endpoints of its domain (the observed (height, diameter)-points), and the smoothness of the whole interpolant is ensured by requiring its first and second derivatives to be continuous over the whole domain [0, H], that is, also in every point of junction of the polynomials. The number of diameter measurements permitting, this approach has quite commonly been used in Finland to estimate stem volume for research purposes (see e.g. Laasasenaho 1982, Lappi 1986, Ojansuu 1993, and Mäkinen et al. 2002).

We are now to examine how diameter selection within cross-sections at predetermined heights affects volume estimation by cubic-spline-interpolated stem curves. As with the family of general volume estimators in Section 5.2, the members of which these estimators patently are, we adopt the within-tree view: we regard the stem volume as a fixed property

of a tree and randomness in volume estimation as arising from diameter selection within the cross-sections at the non-random observation heights.

We omit discussing the potential difficulties in the practical use of interpolating cubic splines — how to determine the initial values optimally and how to avoid non-monotonicity or oscillation, for example, which aspirations manifest themselves in the empirical rules about the required number and distribution (along the vertical axis) of the measurement heights (see Lahtinen and Laasasenaho 1979, and Lahtinen 1988) — but simply assume that we have at our disposal an adequate set of error-free diameter measurements from an adequate set of fixed heights.

Let us denote by $S_3(h; \mathbf{D}, \mathbf{H})$ the interpolating cubic spline based on a vector of diameters $\mathbf{D}=(D(h_{(1)}), D(h_{(2)}), ..., D(h_{(m)}))$ taken (by some selection method) at predetermined heights $\mathbf{H}=(h_{(1)}, h_{(2)}, ..., h_{(m)})$. Presumably the best stem volume estimate is given by the stem curve obtained from the observed true area diameters $\mathbf{D}_A=(D_A(h_{(1)}), D_A(h_{(2)}), ..., D_A(h_{(m)}))$:

$$\tilde{V}_S = \frac{\pi}{4}\int_0^H S_3(h; \mathbf{D}_A, \mathbf{H})^2 dh \ . \tag{125}$$

The estimation error in $\tilde{V}_S$ now results from the interpolation procedure, that is, from the deviation of the estimated stem curve $S_3(\cdot\,; \mathbf{D}_A, \mathbf{H})$ from the true stem curve $D_A(\cdot)$ in other points than those included in $\mathbf{D}_A$.

In practice, not knowing the cross-section areas at the observation heights, we have to do with other diameters than the true area ones; let us denote a vector of such diameters by $\mathbf{D}(\boldsymbol{\theta})=(D(\boldsymbol{\theta}, h_{(1)}), D(\boldsymbol{\theta}, h_{(2)}), ..., D(\boldsymbol{\theta}, h_{(m)}))$, $\boldsymbol{\theta}$ referring to the diameter selection method. If the selection method involves randomness, $\mathbf{D}(\boldsymbol{\theta})$ is a random vector and the interpolated stem curve $S_3[h; \mathbf{D}(\boldsymbol{\theta}), \mathbf{H}]$ becomes a random function. Naturally, the volume estimator

$$\hat{V}_S(\boldsymbol{\theta}) = \frac{\pi}{4}\int_0^H S_3[h; \mathbf{D}(\boldsymbol{\theta}), \mathbf{H}]^2 dh \tag{126}$$

is then also a random variable. Following the theory presented in Section 5.2 for the family of general volume estimators, we could now attempt to estimate the within-tree expectation and variance of this estimator by integrating the mean and covariance functions $\mu_{\hat{A}}(h; \boldsymbol{\theta})$ and $\gamma_{\hat{A}}(h, k; \boldsymbol{\theta})$ of the area estimation process $\{\hat{A}(h; \boldsymbol{\theta}), h\in[0, H]\}=\{\pi S_3[h; \mathbf{D}(\boldsymbol{\theta}), \mathbf{H}]^2/4, h\in[0, H]\}$ in a stem. However, the functions appear to be difficult to derive analytically, as the coefficients determining the values of $S_3[h; \mathbf{D}(\boldsymbol{\theta}), \mathbf{H}]$ between any two elements of $\mathbf{H}$ (the observation heights) are nonlinear functions of the elements of $\mathbf{D}(\boldsymbol{\theta})$. Thus, instead of pursuing the mean and covariance functions of $\{\pi S_3[h; \mathbf{D}(\boldsymbol{\theta}), \mathbf{H}]^2/4, h\in[0, H]\}$, we consider estimating the within-tree expectation and variance of $\hat{V}_S(\boldsymbol{\theta})$ by means of a number of repeated estimations (realisations of the volume estimator).

In principle, to obtain a realisation $\hat{V}_S(\boldsymbol{\theta}_i)$ of the volume estimator, we draw a vector of diameter directions $\boldsymbol{\theta}_i=(\theta_i(h_{(1)}), \theta_i(h_{(2)}), ..., \theta_i(h_{(m)}))$ from the joint distribution of the diameter directions at the fixed observation heights (the distribution is specific to the diameter selection method), measure the corresponding diameters $\mathbf{D}(\boldsymbol{\theta}_i)=(D[\theta_i(h_{(1)}), h_{(1)}], D[\theta_i(h_{(2)}), h_{(2)}], ..., D[\theta_i(h_{(m)}), h_{(m)}])$ at different heights, interpolate between the diameters, and integrate the square of the resulting stem curve realisation $S_3[h; \mathbf{D}(\boldsymbol{\theta}_i), \mathbf{H}]$.

If the diameter selection method involves such dependence between the diameters that the measurement direction chosen at one height determines the measurement directions at the other heights, that is, if all the elements of the direction vector $\boldsymbol{\theta}_i$ are transformations of the direction $\theta_i(h_{(k)})$ associated to one observation height $h_{(k)}\in H$, the multidimensional direction distribution reduces into a one-dimensional one. This is the case, for example,

when the diameters at different heights are measured in the same direction decided upon at breast height (cf. the dependent selection in Section 5.1). The expectation and variance of the volume estimator are then obtained by numerical integration over the one-dimensional direction distribution: we select values for $\theta_i(h_{(k)})$, i=1, ..., n, *equidistantly* within [0, π), estimate from the direction distribution a weight w_i associated to each $\theta_i(h_{(k)})$ as the probability of selecting a direction not farther than half the equi-interval from $\theta_i(h_{(k)})$, derive from each $\theta_i(h_{(k)})$ the direction vector $\boldsymbol{\theta}_i$ and determine the corresponding diameter vector $\mathbf{D}(\boldsymbol{\theta}_i)$, compute the volume estimator realisation $\hat{V}_S(\boldsymbol{\theta}_i)$ associated to each $\mathbf{D}(\boldsymbol{\theta}_i)$, and then estimate the within-tree expectation and variance of the volume estimator as the weighted mean and variance of the n realisations:

$$\begin{aligned}\hat{E}_{\boldsymbol{\theta}}[\hat{V}_S(\boldsymbol{\theta})] &= \sum_{i=1}^{n} w_i \hat{V}_S(\boldsymbol{\theta}_i) \Big/ \sum_{i=1}^{n} w_i \\ &= \sum_{i=1}^{n} w_i \left\{ \frac{\pi}{4} \int_0^H S_3[h; \mathbf{D}(\boldsymbol{\theta}_i), \mathbf{H}]^2 dh \right\} \Big/ \sum_{i=1}^{n} w_i ,\end{aligned} \tag{127}$$

and

$$\hat{Var}_{\boldsymbol{\theta}}[\hat{V}_S(\boldsymbol{\theta})] = \sum_{i=1}^{n} w_i \left\{ \hat{V}_S(\boldsymbol{\theta}_i) - \hat{E}_{\boldsymbol{\theta}}[\hat{V}_S(\boldsymbol{\theta})] \right\}^2 \Big/ \sum_{i=1}^{n} w_i . \tag{128}$$

Naturally, if the one-dimensional direction distribution is uniform, all the weights w_i are equal and the expectation and variance can be estimated with simple (non-weighted) mean and variance.

If the diameter selection method involves no simplifying dependence between the diameters at the different heights, we resort to Monte Carlo integration, where the direction vectors $\boldsymbol{\theta}_i$, i=1, ..., n, are sampled independently from the multidimensional direction distribution. In this case, the within-tree expectation and variance of the volume estimator are then estimated simply with the mean and variance of the n realisations (Robert and Casella 2000):

$$\hat{E}_{\boldsymbol{\theta}}[\hat{V}_S(\boldsymbol{\theta})] = \frac{1}{n} \sum_{i=1}^{n} \hat{V}_S(\boldsymbol{\theta}_i) , \tag{129}$$

and

$$\hat{Var}_{\boldsymbol{\theta}}[\hat{V}_S(\boldsymbol{\theta})] = \frac{1}{n} \sum_{i=1}^{n} \left\{ \hat{V}_S(\boldsymbol{\theta}_i) - \hat{E}_{\boldsymbol{\theta}}[\hat{V}_S(\boldsymbol{\theta})] \right\}^2 . \tag{130}$$

Interestingly, there is a straightforward connection between these estimates (Eqs. 127–130) and the estimates obtained by integrating the mean and covariance functions $\mu_{\hat{A}}(h; \boldsymbol{\theta})$ and $\gamma_{\hat{A}}(h, k; \boldsymbol{\theta})$ of the area estimation process $\{\hat{A}(h; \boldsymbol{\theta}), h \in [0, H]\} = \{\pi S_3[h; \mathbf{D}(\boldsymbol{\theta}), \mathbf{H}]^2/4, h \in [0, H]\}$ (Eqs. 119 and 121), namely, the above estimates imply certain approximations for $\mu_{\hat{A}}(h; \boldsymbol{\theta})$ and $\gamma_{\hat{A}}(h, k; \boldsymbol{\theta})$: Estimating the expectation of $\hat{V}_S(\boldsymbol{\theta})$ as the (weighted) mean of the volume estimates computed from a sample of diameter vectors (Eqs. 127 and 129) corresponds to approximating $\mu_{\hat{A}}(h; \boldsymbol{\theta})$ at each h by the (weighted) mean of a sample of area estimation function realisations (stem curve realisations) $\hat{A}(h; \boldsymbol{\theta}_i) = \pi S_3[h; \mathbf{D}(\boldsymbol{\theta}_i), \mathbf{H}]^2/4$, i=1, ..., n:

$$
\begin{aligned}
\hat{E}_{\boldsymbol{\theta}}[\hat{V}_S(\boldsymbol{\theta})] &= \sum_{i=1}^{n} w_i \hat{V}_S(\boldsymbol{\theta}_i) \Big/ \sum_{i=1}^{n} w_i \\
&= \sum_{i=1}^{n} w_i \left[\int_0^H \hat{A}(h; \boldsymbol{\theta}_i) dh \right] \Big/ \sum_{i=1}^{n} w_i \\
&= \int_0^H \left[\sum_{i=1}^{n} w_i \hat{A}(h; \boldsymbol{\theta}_i) \Big/ \sum_{i=1}^{n} w_i \right] dh \\
&\equiv \int_0^H \hat{\mu}_{\hat{A}}(h) dh \\
&\approx \int_0^H \mu_{\hat{A}}(h) dh \\
&= E_{\boldsymbol{\theta}}[\hat{V}_G(\boldsymbol{\theta})] .
\end{aligned}
\tag{131}
$$

Similarly, estimating the variance of $\hat{V}_S(\boldsymbol{\theta})$ as the (weighted) variance of the volume estimates computed from a sample of diameter vectors (Eqs. 128 and 130) corresponds to approximating $\gamma_{\hat{A}}(h, k; \boldsymbol{\theta})$ by the (weighted) covariance computed at each (h, k) from a sample of area estimation function realisations (stem curve realisations):

$$
\begin{aligned}
\hat{Var}_{\boldsymbol{\theta}}[\hat{V}_S(\boldsymbol{\theta})] &= \sum_{i=1}^{n} w_i \left\{ \hat{V}_S(\boldsymbol{\theta}_i) - \hat{E}_{\boldsymbol{\theta}}[\hat{V}_S(\boldsymbol{\theta})] \right\}^2 \Big/ \sum_{i=1}^{n} w_i \\
&= \sum_{i=1}^{n} w_i \left\{ \int_0^H \hat{A}(h; \boldsymbol{\theta}_i) dh - \int_0^H \hat{\mu}_{\hat{A}}(h) dh \right\}^2 \Big/ \sum_{i=1}^{n} w_i \\
&= \sum_{i=1}^{n} w_i \left\{ \int_0^H \left[\hat{A}(h; \boldsymbol{\theta}_i) - \hat{\mu}_{\hat{A}}(h) \right] dh \right\}^2 \Big/ \sum_{i=1}^{n} w_i \\
&= \sum_{i=1}^{n} w_i \left\{ \int_0^H \int_0^H \left[\hat{A}(h; \boldsymbol{\theta}_i) - \hat{\mu}_{\hat{A}}(h) \right] \left[\hat{A}(k; \boldsymbol{\theta}_i) - \hat{\mu}_{\hat{A}}(k) \right] dh\, dk \right\} \Big/ \sum_{i=1}^{n} w_i \\
&= \int_0^H \int_0^H \left\{ \sum_{i=1}^{n} w_i \left[\hat{A}(h; \boldsymbol{\theta}_i) - \hat{\mu}_{\hat{A}}(h) \right] \left[\hat{A}(k; \boldsymbol{\theta}_i) - \hat{\mu}_{\hat{A}}(k) \right] \Big/ \sum_{i=1}^{n} w_i \right\} dh\, dk \\
&\equiv \int_0^H \int_0^H \hat{\gamma}_{\hat{A}}(h, k) dh\, dk \\
&\approx \int_0^H \int_0^H \gamma_{\hat{A}}(h, k) dh\, dk \\
&= Var_{\boldsymbol{\theta}}[\hat{V}_G(\boldsymbol{\theta})] .
\end{aligned}
\tag{132}
$$

In other words, at each point (h, k), the definite integrals in $\mu_{\hat{A}}(h; \boldsymbol{\theta}) = E_{\boldsymbol{\theta}}[\hat{A}(h; \boldsymbol{\theta})]$ and $\gamma_{\hat{A}}(h, k; \boldsymbol{\theta}) = Cov_{\boldsymbol{\theta}}[\hat{A}(h; \boldsymbol{\theta}), \hat{A}(k; \boldsymbol{\theta})]$ taken over the multidimensional direction distribution (the joint distribution of the diameter directions at the fixed observation heights) are approximated with sums, sums of the squares or sums of the products of n area estimates $\hat{A}(h; \boldsymbol{\theta}_i) = \pi S_3[h; \mathbf{D}(\boldsymbol{\theta}_i), \mathbf{H}]^2/4$ based on n direction vector realisations $\boldsymbol{\theta}_i$ drawn from the distribution.

In Section 5.2 we discovered that as the elements of a stochastic area estimation process become uncorrelated, the within-tree variance of the corresponding generalised volume estimator becomes zero; moreover, we noted that such a discontinuous process is an abstraction that cannot really be generated in a tree stem context (by e.g. independent diameter selection at a finite number of observation heights). Evidently, cubic spline interpolation between uncorrelated (independently selected) random diameters at the observation heights does not result in a volume estimator with zero variance, often quite the contrary: the area estimators at the observation heights are of course mutually independent, but the interpolated curve imposes continuity and induces short-distance dependence (non-zero covariance between heights close to each other) for the area estimators at the heights in between (via spline coefficients involving common diameters), thus making the integral of the resulting covariance function deviate from zero.

As with the volume equation in Section 5.1, the volume estimation error $V-\hat{V}_S(\boldsymbol{\theta})$ can be divided into the two distinct additive components — the error $V-\tilde{V}_S=\varepsilon_S$ inherent in the best estimator $\tilde{V}_S$ and the error $\tilde{V}_S-\hat{V}_S(\boldsymbol{\theta})$ attributable to diameter selection by method $\boldsymbol{\theta}$ — the latter of which further consists of two components — the within-tree bias $\tilde{V}_S-E_{\boldsymbol{\theta}}[\hat{V}_S(\boldsymbol{\theta})]$ with respect to the best estimator and a random sampling error $\nu_S(\boldsymbol{\theta})$:

$$\begin{aligned} V-\hat{V}_S(\boldsymbol{\theta}) &= (V-\tilde{V}_S)+[\tilde{V}_S-\hat{V}_S(\boldsymbol{\theta})] \\ &= \varepsilon_S+\left\{\tilde{V}_S-\left\{E_{\boldsymbol{\theta}}[\hat{V}_S(\boldsymbol{\theta})]+\nu_S(\boldsymbol{\theta})\right\}\right\} \\ &= \varepsilon_S+\left\{\tilde{V}_S-E_{\boldsymbol{\theta}}[\hat{V}_S(\boldsymbol{\theta})]\right\}-\nu_S(\boldsymbol{\theta})\,. \end{aligned} \tag{133}$$

At the within-tree level only $\nu_S(\boldsymbol{\theta})$ is a random variable (with zero expectation and variance $\mathrm{Var}_{\boldsymbol{\theta}}[\nu_S(\boldsymbol{\theta})]=\mathrm{Var}_{\boldsymbol{\theta}}[\hat{V}_S(\boldsymbol{\theta})]$), whereas at the population level all the estimation error components are random variables. The interpretation of the error ε_S contained in the best non-parametric estimator $\tilde{V}_S$, however, does not straightforwardly parallel that of the model error term ε_L of the parametric volume equation: In our "model" $V=\tilde{V}_S+\varepsilon_S$, we have incorporated no distributional assumptions on ε_S that would then have governed the estimation of $\tilde{V}_S$. In particular, the population expectation of ε_S may well deviate from zero, whereupon the estimation bias $E[V-\hat{V}_S(\boldsymbol{\theta})]$ at the population level may involve not only the between-trees expectation $E\{\tilde{V}_S-E_{\boldsymbol{\theta}}[\hat{V}_S(\boldsymbol{\theta})]\}$ of the within-tree bias due to diameter selection but also the population expectation $E(\varepsilon_S)$.

6 Material

The material of the study consists of a small subset of the sample trees felled and measured in 1991 for the nationwide tree quality investigation (VAPU) of the Finnish Forest Research Institute. In the investigation, the forest stand population of Finland was divided into the strata of Scots pine, Norway spruce and silver/pubescent birch dominated stands, in each of which the following four-stage sampling was then performed: First, a subset of 20 clusters were systematically chosen among the clusters of plots placed systematically all over Finland in the 7th National Forest Inventory (for the sampling design of the inventory, see Kuusela and Salminen 1980 and Kuusela et al. 1986). Second, two plots among the total of 28 in each cluster were systematically selected for tree sampling. Third, 20 tally trees were picked in each selected plot (first the four trees growing closest to the plot centre, and then the 16 dominant or codominant trees next closest to the centre); the trees had to fulfill certain selection criteria (living trees of species Scots pine, Norway spruce or silver/pubescent birch with no visible biotic or abiotic defects and with breast height diameter not less than 7 cm). Fourth, six sample trees to be felled in each plot were randomly chosen among the 20 tally trees (three trees among all the tally trees and three trees among the tally trees of dominant species and dominant crown class). Among the sample trees taken from the stratum of the Scots pine dominated stands, a *judgement sample* was then drawn for this study, resulting in a total of 81 trees from 16 plots in 11 clusters (Fig. 22, Table 10).

The geographical distribution of the selected trees was somewhat uneven in both the north–south and east–west directions, in which some noteworthy variation in stem form is known to occur in Finland (e.g. Lappi 1986): in Southern Finland (Fig. 22) 26 stems were measured on six plots, while in Northern Finland 55 stems were taken on ten plots; further, east of the centre meridian 27° of the Finnish national uniform co-ordinate system, only 14 stems were measured on three plots, whereas west of it 67 stems were taken on 13 plots.

All the 16 plots were located in naturally regenerated one-storey stands; while ten of these were pure Scots pine stands, four contained some Norwegian spruce mixture and two silver/pubescent birch mixture. A majority of the stands grew on mineral soil (Table 10); of

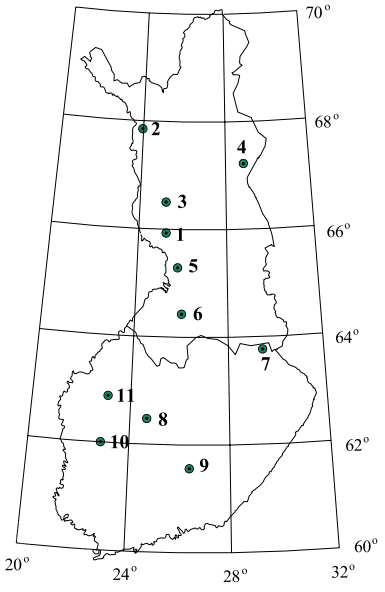

Fig. 22. Locations of the 11 clusters of plots in which the 81 trees investigated in this study were felled (degrees east longitude and north latitude). The line across the country marks the division between Southern Finland and Northern Finland. For the information of the plots in the clusters, see Table 10.

Table 10. Some site and stand characteristics of the plots in which the 81 investigated trees were felled (G is basal area, H_{dom} dominant height, and D_{gM} diameter of the basal area median tree). For the locations of the clusters, see Fig. 22.

Plot	Cluster	Ground class[1]	Site fertility[2]	Stand development stage[3]	G (m^2/ha)	H_{dom} (m)	D_{gM} (cm)	Number of felled trees
301	1	3	4	3	6	6.0	11	6
303	2	3	4	3	2	7.0	11	6
304	2	3	4	4	6	9.5	13	6
305	3	3	4	4	2	5.5	10	5
306	3	3	4	3	1	4.3	8	3
307	4	1	4	4	14	12.0	15	6
308	4	1	4	3	4	4.8	9	6
310	5	3	3	4	9	9.0	12	6
311	6	1	4	4	13	9.5	13	5
312	6	1	4	4	8	8.5	10	6
313	7	2	4	4	5	9.0	13	2
316	8	1	2	3	1	6.6	8	5
317	8	1	2	4	12	9.0	12	6
318	9	1	2	5	24	24.0	25	4
321	10	1	3	5	22	22.0	21	4
322	11	1	4	4	8	9.5	12	5

[1] 1 mineral soil
2 spruce/hardwoods peatland
3 pine peatland
4 open bog

[2] 1 very rich
2 rich
3 medium
4 quite poor
5 poor
6 very poor

[3] 1 open regeneration site
2 young seedling stand
3 advanced seedling stand
4 young (thinning) stand
5 advanced (thinning) stand
6 mature stand
7 shelterwood stand
8 seedtree stand

the seven stands located in peatland, five were drained — in two of these the drainage had been completed so recently that the drainage effect could not yet be discovered in ground vegetation or in trees, whereas in the other three the drainage effect was clearly visible although the ground vegetation was still characterised by the original peatland type. The sites were mainly of the two fertility classes — medium or quite poor — that are the most typical of Scots pine stands in Finland; the three deviating stands grew on rich sites (Table 10). Except for two advanced stands, where one or two thinnings had been carried out, the stands were young stands or advanced seedling stands, where no silvicultural treatments had been applied or cuttings performed since the regeneration (Table 10).

Naturally, given the stage of development of the stands, pulpwood-size trees dominated in the size distribution of the trees (Fig. 23): a total of 72 trees fell into that category (breast height diameter ≤ 17 cm, height ≤ 13 m), whereas only eight trees could be considered sawlog-size (breast height diameter ≥ 22 cm, height ≥ 20 m). Further, one tree (from the plot 304 in the northernmost cluster) appeared to be a slight anomaly with its breast height diameter of 20 cm and height of 13 m; however, this tree was included only in the examination of cross-section shape and cross-section area estimation (and not in the examination of stem volume estimation or Bitterlich sampling), as not more than two discs were measured from it.

Of the large number of characteristics (on stem dimensions, stem quality, growth, crown structure and biomass; Valtakunnallisen puututkimuksen (VAPU) ja kasvunvaihtelututkimuksen maastotyöohjeet 1991) measured in the field on each felled sample tree, only the following were employed in this study: plot radius direction with respect to N–S direction

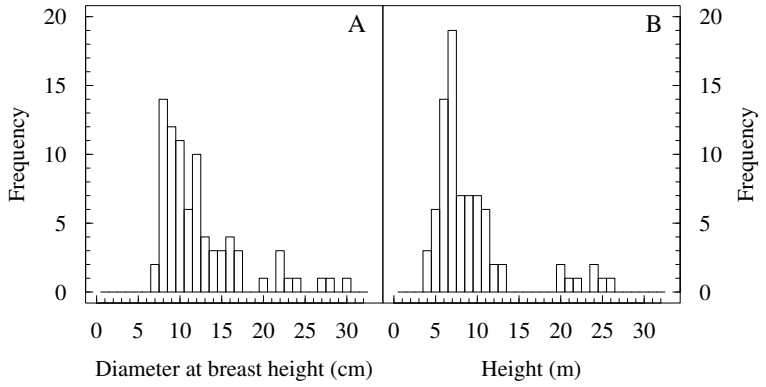

Fig. 23. Frequency distributions of breast height diameter (taken perpendicular to plot radius direction; A) and tree height (B) in the data of the 81 trees investigated in this study.

Table 11. Distribution of the 81 stems of this study according to the number of discs obtained in the stem.

	Number of discs obtained in the stem									
	1	2	3	4	5	6	7	8	9	10
Number of stems	0	1	0	0	0	1	3	25	30	21

Table 12. Number of discs obtained at each observation height in the 81 stems of this study (cf. the diagonal of the Table 13).

	Height									
	1%	2.5%	7.5%	15%	30%	50%	70%	85%	1.3 m	6 m
Number of discs	28	75	77	79	80	79	81	81	80	51

at breast height (i.e., compass bearing of the tree taken from the plot centre to the assumed pith of the tree at breast height), tree height determined with respect to the ground level, and stump height ditto.

In each of the 81 stems, discs of thickness of 3 cm were sawn at two fixed — 1.3 m and 6 m — and eight relative — 1%, 2.5%, 7.5%, 15%, 30%, 50%, 70% and 85% — heights in the way that the lower surface of the disc was located at the cutting height determined from the ground level; were there branches at the proposed height, the cutting height was shifted to the nearest location where a disc free from branches could be obtained, and this new height was recorded. On each disc, a mark indicating the plot radius direction was painted. A complete set of ten discs could not, even in theory, be obtained in every stem: 16 trees were shorter than 6 m, and no disc at the height of 6 m hence existed in them; in two trees, a relative height (15% or 30%) also coincided with a fixed one (1.3 m). Besides, a number

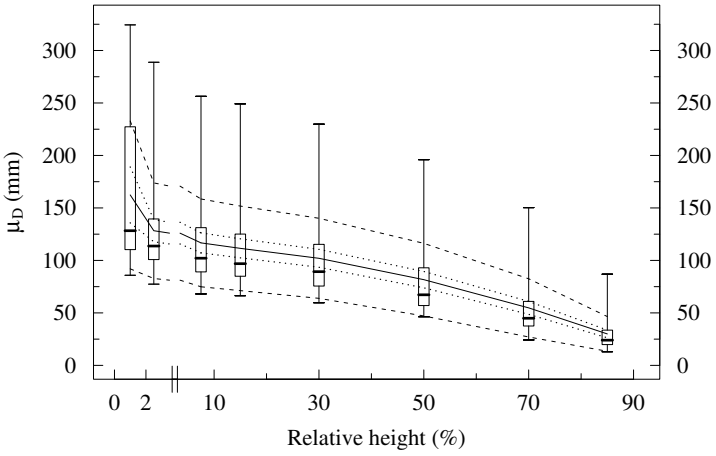

Fig. 24. Summarised distributions, at the eight relative observation heights, of the mean diameter (μ_D) in the discs of the 81 trees of this study. The box depicts the inter-quartile range bisected by the median, and the whiskers reach out to the minimum and maximum values in the data; the solid line denotes the arithmetic mean, whereas the dashed and dotted lines below and above the mean indicate the sample standard deviation and twice the standard error of the mean (i.e., twice the sample standard deviation divided by the square root of the number of observations, see Table 12), respectively.

Table 13. Number of stems, among the 81 stems of this study, in which discs were obtained at both the observation heights in each combination of observation heights.

Height 2	Height 1									
	1%	2.5%	7.5%	15%	30%	50%	70%	85%	1.3 m	6 m
1%	28	28	28	28	28	28	28	28	28	21
2.5%	28	75	74	75	75	74	75	75	75	47
7.5%	28	74	77	77	77	76	77	77	77	49
15%	28	75	77	79	79	78	79	79	79	50
30%	28	75	77	79	80	79	80	80	80	51
50%	28	74	76	78	79	79	79	79	79	50
70%	28	75	77	79	80	79	81	81	80	51
85%	28	75	77	79	80	79	81	81	80	51
1.3 m	28	75	77	79	80	79	80	80	80	51
6 m	21	47	49	50	51	50	51	51	51	51

of discs, especially those taken at 1% height, were broken when sawing or transporting to the laboratory or had to be discarded due to inadequate identification information. In all, a total of 709 cross-sections representing 711 observation heights were included in the study; see Tables 11, 12 and 13 for the summaries of the distribution of the discs between the stems and Fig. 24 for the disc size distributions at the relative observation heights.

The discs were photographed, and the photographs were turned into vectorised digital images, from which the characteristics of the cross-sections were then computed (cf. e.g.

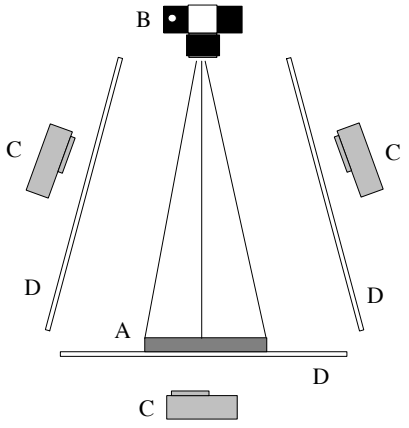

Fig. 25. System with which the discs were photographed: disc (A), camera (B), flashlight with a "slave switch" (C), and plexiglass plate dispersing light evenly (D).

Thies and Harvey 1979, Biging and Wensel 1984, Drake et al. 1988, Jonsson 1992, Saint-André 1998, and Saint-André and Leban 2000). This approach enabled us to exploit shape information to as large an extent as we ever desired and helped us eliminate measurement errors, which could badly confound the possibly subtle influences of non-circularity. Before photographing, the discs were debarked up to the cambium layer in order to eliminate the problems that bark irregularities could cause in the computational extraction of the characteristics from the images. Thus, *all the characteristics computed from the images are under-bark*.

The discs were photographed in a laboratory with fixed lighting by using an ordinary 25-mm film camera with a 50-mm objective and panchromatic black-and-white film of the sensitivity of 100 ASA; in addition to the flashlight attached to the camera, three extra flashlights with "slave switches" (i.e., flashlights that react, with a marginal delay, to the actual camera flashlight) were employed to increase the contrast between the disc and the background (Fig. 25). A ruler showing the scale and a slip of paper with a mark indicating the plot radius direction were placed on the same plane as the lower surface of the disc (Fig. 26 A). Two fixed distances between the camera lens and the plane under the disc were applied — 60 cm for the discs with the diameter up to 15 cm, and 100 cm for the discs larger than that. In order to take into account the possible variation in disc thickness, which would affect the distance between the camera lens and the upper surface of the disc (Fig. 25) later needed in scale determination, thickness was measured (in mm) in four points at the edge of each disc (at regular rotation angle intervals of 90° starting from the plot radius direction).

The film negatives were developed and printed to photographs (Fig. 26 A) with some extra contrasting between the disc edge and the light background (i.e., with some artificial increase in tone value differences). The photographs were transformed into grey-scale digital raster images with an optical scanner of the resolution of 300 dpi; it was expressly owing to the low resolution of the apparatus available that the scanning was performed on the prints instead of the negatives. In each raster image, the length of a 10-cm piece of the ruler beside the disc (Fig. 26 A) was measured (with pixel edge length as the unit) for scale computation, after which the image was manually cropped to contain only the disc and the mark indicating the plot radius direction (Fig. 26 A). In order to facilitate the computational feature extraction, the grey-scale pixels were then classified into two categories — the "information" (black) and the "background" (white) (Fig. 26 B): in each image, the threshold for the intensity values of the information class pixels was set by visual assess-

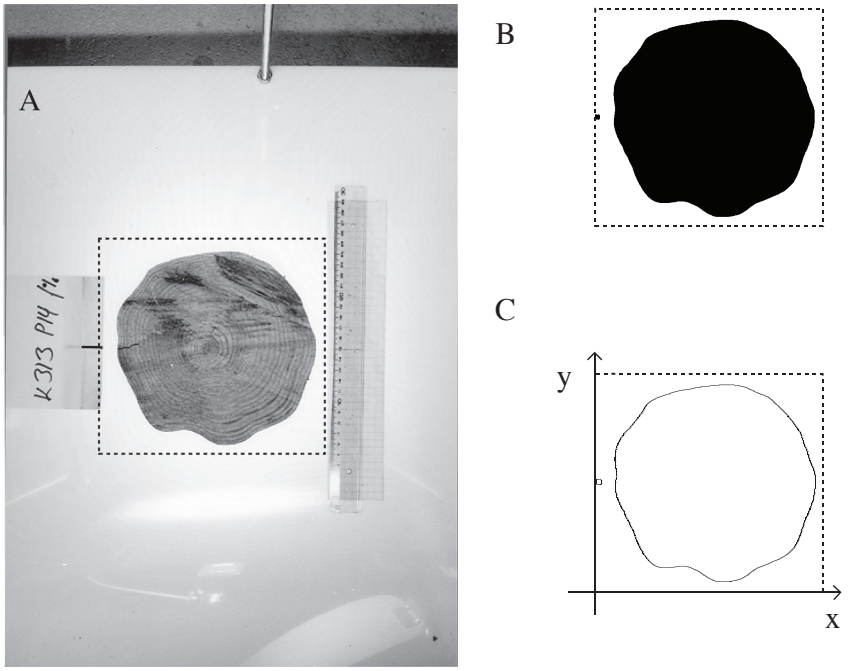

Fig. 26. An example of the photograph of a disc (A) with the area of the cropped digital image demarcated by broken line — note the ruler showing the scale, and the piece of paper containing, in addition to the identification information, the mark indicating the plot radius direction; the one-bit raster image obtained by classifying the pixels of the scanned photograph (B); and the vectorised image of the contour of the disc and the mark indicating the plot radius direction, with co-ordinate axes (C).

ment with the aim of locating the edge of the cross-section correctly and forming connected sets of pixels; due to the high and homogeneous contrasts in the photographs, very little adjustment in the threshold value was needed between the images. Unfortunately, the pith locations were not recorded in the procedure.

From each classified raster image, the boundary pixels of the cross-section and of the mark indicating the plot radius direction were extracted, and the image consisting of these pixels was vectorised (i.e., transformed into a set of co-ordinates of discrete contour points) with smoothing: at each change in direction, the two midpoints of the outer edge of the corner pixel were taken, and the line segment connecting the points was used to outline the corner in the resultant vector image (Fig. 27, Fig. 26 C). Further, the vector image of the convex closure of the cross-section was computed as the convex hull of the discrete contour points of the cross-section.

From the vector image of a cross-section, the following characteristics were determined: centres of gravity of the cross-section (as a substitute for the pith) and the mark indicating the plot radius direction; area of the cross-section; 360 radii from the centre of gravity of the cross-section at regular rotation angle intervals of 1° starting from the N–S direction; and 180 breadths ditto. (To check the effect of the smoothing in vectorisation, the centre of gravity and the area of the cross-section were also computed from the non-vectorised classified raster image: the differences were negligible in all the cross-sections.) From the vector image of the convex closure, in turn, the following properties were computed: area

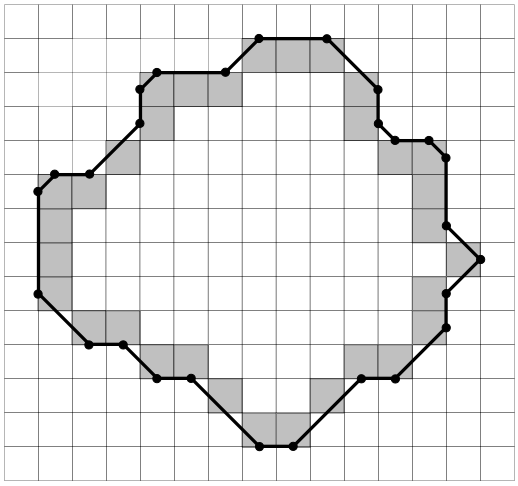

Fig. 27. Principle of the smoothing applied in the vectorisation of the raster image of the cross-section contour pixels: the circles indicate the discrete vertex points that determine the vector image. (Note that this coarse raster figure was created for illustration only; in the actual raster images, the pixel size was much smaller in relation to the cross-section size.)

of the convex closure; convex perimeter (girth); 360 radii from the centre of gravity of the cross-section at regular rotation angle intervals of 1° starting from the N–S direction; 180 breadths ditto; 180 diameters ditto; and, with viewing angles 1.146°, 1.621°, 2.292° and 3.624° (corresponding in circular cross-sections to the basal area factors 1, 2, 4 and 10 m^2/ha), the contour of the inclusion region in a discretised form consisting of 3600 points; the areas of the 360 sectors of the inclusion region, of angular width 1° and with the first sector midline in the N–S direction; and the total area of the inclusion region.

The boundary pixel identification and extraction, the vectorisation and the computation of centres of gravity, convex perimeter, and true and convex area were performed with the GRASS 4.1 and Mathematica 2.2 software (GRASS User's Reference Manual 1993, Guide to Standard Mathematica Packages 1993). For the computation of radii, breadths, diameters, and inclusion area, Fortran code was written, the basic ideas of which are presented in Appendices G and H.

In the computation of the characteristics from the images, the pixel edge length was used as a natural measurement unit. While this unit was fully appropriate for the examination of the *relative* quantities related to the shape of cross-sections and the errors of various area estimation methods, the true scale was needed for the investigation of volume estimation errors. The scale was computed for each cross-section by means of the basic lens formula in optics, the four thickness measurements taken on each disc, and the length measurement of a 10-cm piece of the ruler in the unclassified raster image. See Appendix I for a detailed account of the scale computation.

7 Methods

With the 709 cross-sections from the 81 Scots pine stems in the data, we empirically investigated (i) the variation in cross-section shape, (ii) the effect of the within-cross-section variation in diameter on cross-section area estimates given by the estimators discussed in Sections 3.3 and 4.2.2, (iii) the influence of the within-cross-section variation in diameter on stem volume estimates given by Laasasenaho volume equation, cubic-spline-interpolated stem curve and generalised volume estimator considered in Chapter 5, and (iv) the bias inflicted by non-circular cross-section shape on stand total estimators in Bitterlich sampling as discussed in Section 4.1.2.

As the stems in the data were few in number and did not make up any actual probability sample (the sampling design was not probabilistic in the last stage of subsampling among the trees felled for the nationwide tree quality investigation; see Chapter 6), the data did not really permit confirmatory analysis (hypothesis testing, model building) concerning any meaningful Scots pine population. Instead, we contented ourselves with explorative analysis, considering the empirical distributions of relevant within-cross-section and within-tree characteristics in our data. To enable meaningful, size-independent comparisons between cross-sections or stems, the characteristics were usually turned relative (expressed as percentages). The hierarchical structure of the data resulting from the multi-stage sampling in the data collection (cross-sections being interdependent within a stem, stems interdependent within a plot, plots interdependent within a cluster) was largely disregarded in these considerations: the distributions of the within-cross-section characteristics were examined in the subsets formed by height classes as well as in the set of all the cross-sections, whereas the distributions of the within-tree characteristics were studied in the set of all the stems.

As already pointed out in Chapter 6, the discs were debarked before photographing, and, hence, *all our empirical examinations pertain to cross-sections and stems without bark*.

7.1 Cross-Section Shape

Variation in cross-section shape was examined in three aspects: (i) variation in shape of convex closure, (ii) amount and directional location of non-convexity, and (iii) variation in true shape. The interest in the shape of convex closure was motivated by our interest in area and volume estimation based on measurements made from the outside of a tree: with caliper, tape and height meter, no non-convexity can be registered but only the convex closure of a tree cross-section is observed.

The scalar and functional characteristics (shape indices) computed for each cross-section to analyse shape are summarised in Tables 14 and 15, respectively.

Table 14. Scalar shape indices computed for each cross-section.

Index	Meaning
D_{min}/D_{max}	Ratio between minimum and maximum diameters
CV_D	Diameter coefficient of variation
$\rho_D(\pi/2)$	Correlation between perpendicular diameters
b_e/a_e	Girth-area ellipse ratio
$\lvert\theta_{Dmin}-\theta_{Dmax}\rvert$	Absolute angle between minimum and maximum diameters
$(A_C-A)/A_C$	Relative convex deficit
$(\hat{A}_0-A_C)/A_C$	Relative isoperimetric deficit; relative bias of estimator $\hat{A}_0$ based on girth diameter $C/\pi=\mu_D$ with respect to convex cross-section area

Table 15. Functional shape indices computed for each cross-section from the discretely observed diameter, breadth, and radius functions.

Characteristic	Meaning
$[D(j\cdot 1°)–D_{Ac}]/D_{Ac}$, j=0, ..., 179	Variation in diameter around convex area diameter; "diameter measurement error" with respect to direction
$[B_C(j\cdot 1°)–B(j\cdot 1°)]/\overline{B}$, j=0, ..., 179	Relative difference between breadths of convex closure and cross-section; occurrence of non-convexity with respect to direction
$[R(j\cdot 1°)–\overline{R}_q]/\overline{R}_q=R^*(j\cdot 1°)–1$, j=0, ..., 359	Relative variation in cross-section radius around its quadratic mean; deviation of pre-shape radii from 1 with respect to direction

7.1.1 Shape of Convex Closure

Shape Indices

Mainly for comparison with previous empirical studies (especially that by Matérn in 1990), we investigated the shapes of the convex closures of the cross-sections by means of the following three simple diameter-based indices (which are invariant of scale, translations and rotations, i.e., independent of the size as well as the position and the orientation of the cross-section in the chosen rectangular co-ordinate system): the ratio D_{min}/D_{max} between the minimum and the maximum diameters, with which the deviation of cross-section shape from a circle has mostly been examined in previous empirical studies; the coefficient of variation of diameter $CV_D=\sigma_D/\mu_D$ (the ratio of diameter standard deviation to diameter mean), which better than the extreme diameters describe the magnitude of diameter variation in a cross-section and help detect the possible orbiforms in the data; and the correlation $\rho_D(\pi/2)$ between perpendicular diameters (the diameter autocorrelation at angle $\pi/2$), which gives information on possible ellipticity or square-shapedness of cross-sections (see Chapter 2).

These indices were estimated from the 180 diameters computed systematically (at regular rotation angle intervals of 1° and starting from the N–S direction) in each cross-section (see Chapter 6). D_{min} and D_{max} were determined as the minimum and the maximum of these diameters. In CV_D, the exact value for the mean diameter μ_D was attained by dividing the convex perimeter C by π, whereas the standard deviation σ_D was estimated as the square root of the variance of the 180 diameters:

$$\hat{\sigma}_D^2 = \frac{1}{180}\sum_{j=0}^{179}\left[D(j\cdot 1°)-\mu_D\right]^2 \tag{134}$$

(for unbiasedness, the denominator n=180 instead of the usual n–1=179 was used in this sample variance, as the population mean was not estimated by a sample mean but known exactly). Further, the correlation between perpendicular diameters was estimated as

$$\hat{\rho}_D\left(\frac{\pi}{2}\right) = \frac{1}{\hat{\sigma}_D^2}\cdot\frac{1}{90}\sum_{j=0}^{89}\left[D(j\cdot 1°)-\mu_D\right]\left\{D[(j+90)\cdot 1°]-\mu_D\right\}. \tag{135}$$

An ellipse has often been assumed to approximate cross-section shape better than a circle, with the ratio D_{min}/D_{max} as a simple estimate for the ellipse axis ratio. We tried also another axis ratio estimate, that of an ellipse with the perimeter and area equal to the convex

perimeter C and convex area A_C of the cross-section: since $C \approx \pi[3(a_e+b_e)/2-(a_e b_e)^{1/2}]$ and $A_C=\pi a_e b_e$ for an ellipse with a_e and b_e as the lengths of the long and the short semi-axes, the axis ratio estimate, here referred to as the *girth-area ellipse ratio*, became

$$\frac{b_e}{a_e} = \frac{A_C}{\pi a_e^2}, \tag{136}$$

where

$$a_e = \frac{1}{3}\left(\frac{C}{\pi} + \sqrt{\frac{A_C}{\pi}}\right) + \sqrt{\frac{1}{9}\left(\frac{C}{\pi} + \sqrt{\frac{A_C}{\pi}}\right)^2 - \frac{A_C}{\pi}} \tag{137}$$

(Stoyan and Stoyan 1994); it is not difficult to see that for a circle $b_e/a_e=1$. (Note that there are of course many other alternatives for estimating the axis ratio of the approximating ellipse; these include e.g. the ratio of D_{max} and the diameter perpendicular to it, $A_C/(\pi D_{max}^2/4)$ derived from D_{max} and A_C via the ellipse area formula, the ratio of the semi-axis lengths estimated by a least squares fitting of the ellipse contour equation to the discretely observed contour co-ordinates, and the ratio of the semi-axis lengths estimated by a least squares fitting of the ellipse radius autocovariance function to the sample autocovariances computed from the discretely observed radii; see e.g. Stoyan and Stoyan 1994, Skatter and Høibø 1998, Saint-André and Leban 2000)

Estimating the ellipse ratio with D_{min}/D_{max} or b_e/a_e disregards the requirement that the principal axes be at right angles to each other. To find out whether the extreme diameters would be perpendicular to each other in our cross-sections, we computed the absolute angle $|\theta_{Dmin}-\theta_{Dmax}|$ ($\in [0, 90°]$) between D_{min} and D_{max}. In addition, we examined the change in the orientation of the extreme diameters along with height in a stem by comparing the directions of D_{min} and D_{max} at each height to those at the lowest observed height in the stem.

The association between the size and shape of convex closure was examined by ordinary product moment correlations and accompanying scatterplots between the mean diameter μ_D and the shape indices. Also the interrelations of the indices were examined by pairwise correlations and scatterplots.

Since an ellipse has been much used as a model for cross-section shape, we finally compared the values of the shape indices in the cross-sections with their values in ellipses. This with keeping in mind that the indices impart by no means unique or unambiguous information on shape, but visually quite dissimilar shapes may assume very similar index values (for instance, think of a rhombus and an ellipse with the same D_{min}/D_{max}, or consider the shapes C and F with the same CV_D in Fig. 5 in Chapter 2). Hence, the information given by the indices can only evidence against the ellipticity hypothesis but not for it (for an extensive discussion on some indices and their philosophy, see e.g. Exner 1987 and Stoyan and Stoyan 1994).

Directional Variation in Diameter

Diameter variation with respect to direction within a cross-section was studied by means of the relative deviation $[D(\cdot)-D_{Ac}]/D_{Ac}$ of the discretely observed diameter function $D(j\cdot 1°)$, $j=0, ..., 179$, from the convex area diameter $D_{Ac}=2(A_C/\pi)^{1/2}$ yielding the convex area when substituted in the circle area formula. The choice of D_{Ac}, instead of, say, the mean diameter μ_D, as the reference was motivated by the idea that error in area estimation might be equated

with error in diameter selection: besides diameter variation, the relative differences would then provide information on the preferable choice of diameter direction in area estimation.

The diameter direction was expressed with respect to the N–S direction or with respect to the direction of D_{max} and set to increase anticlockwise. With the N–S direction as the reference direction, the idea was to study whether large-scale exogenous factors (prevailing winds, amount of solar radiation etc.) could affect trees in a somewhat uniform way regardless of the very local growing conditions and thus beget any pattern in the diameter variation. With the direction of D_{max} (which was considered more stable than the other natural option, the direction of D_{min}) as the reference direction, in turn, the idea was to examine if the diameter variation would show an internal pattern reflecting a degree of similarity in reactions of trees to their varying local conditions.

The empirical distribution of the discretely observed functionals $[D(\cdot)–D_{Ac}]/D_{Ac}$ in each height class was summed up simply with the mean, median and variance functions (Ramsay and Silverman 1997): these were estimated with the pointwise averages, medians and variances across the cross-sections in the height class (i.e., with the averages, medians and variances of the cross-sectionwise $[D(j\cdot 1°)–D_{Ac}]/D_{Ac}$ at every observed direction $j\cdot 1°$, j=0, 1, ..., 179).

7.1.2 Non-Convexity

Convex Deficit

As a measure of the amount of non-convexity, the relative convex deficit $[A_C–A]/A_C$, where A is the true area and A_C is the convex area of the cross-section, was computed in each cross-section. Sometimes this characteristic has also been regarded as a shape index (for instance, it is referred to as "convexity ratio" in Stoyan and Stoyan 1994 and as "roundness" in Glasbey and Horgan 1995). Its relation to the scalar shape indices discussed above on one hand, and to the size of a cross-section (the mean diameter μ_D) on the other hand, were examined by pairwise correlations and accompanying scatterplots.

Directional Variation in Breadth

In each cross-section, the occurrence of non-convexity with respect to direction was investigated by means of the relative difference $[B_C(\cdot)–B(\cdot)]/\overline{B}$ between the discretely observed breadth function of the convex closure $B_C(j\cdot 1°)$, j=0, ..., 179, and that of the cross-section $B(j\cdot 1°)$, j=0, ..., 179, with the mean breadth $\overline{B}$ of the cross-section as the denominator. The breadth functions were employed instead of radius functions in order to "encapsulate" the directional information, as in a standard measurement situation we would be interested in the non-convexity occurring in "both ends" of the diameter measurement. As in the examination of diameter variation, the direction was determined both with respect to the N–S direction and in respect of the direction of D_{max}. Also similarly to the diameter variation case, the empirical distribution of the relative difference functions of individual cross-sections in each height class was summed up by the mean, median and variance functions computed pointwise over the cross-sections.

7.1.3 True Shape

The true shapes of cross-sections were studied by means of the discretely observed radius functions $R(j\cdot 1°)$, j=0, ..., 359; in other words, the (discretely, but more densely) observed contour of each cross-section was reduced to 360 equiangular points in polar coordinates. In shape analysis literature, such points are referred to as *(pseudo)landmarks* and the set of them depicting a figure as a *landmark configuration* (Stoyan and Stoyan 1994, Dryden and Mardia 1998). We denote the landmark configuration vector of cross-section i by $\mathbf{R}_i=(R_i(j\cdot 1°))_{j=0,\,1,\,...,\,359}$.

Prior to estimating the average shape and examining the shape variability in our set of cross-sections, we rendered the landmark configurations with different locations, orientations and sizes commensurate by turning each configuration $\mathbf{R}_i$ into its *centred pre-shape* $\mathbf{R}_i^*=(R_i^*(j\cdot 1°))_{j=0,\,1,\,...,\,359}$ (Dryden and Mardia 1998) with the Euclidian similarity transformations (translations, rotations and scaling): First, the configuration was centred, that is, the origin of the Cartesian co-ordinate system was set into the centre of gravity of the configuration; actually, this involved no action, as (not surprisingly considering the large number of landmarks in the configuration) the centre of gravity of the configuration was found to virtually coincide with that of the cross-section (computed from *all* the contour points of the vector image; see Chapter 6) relative to which the radius function had been defined. Second, the configuration was rotated in the way that either the radius to the north of the origin or the maximum radius R_{max} coincided with the positive y-axis; the advantage of fixing the reference axis along with R_{max} was that similar or congruent shapes would be considered equal after the similarity transformations. Third, the configuration was scaled to constant size (centroid size) by dividing the landmarks (radii) by their quadratic average in the cross-section:

$$R_i^*(j\cdot 1°)=\frac{R_i(j\cdot 1°)}{\overline{R}_{qi}}\,, \tag{138}$$

j=0, ..., 359, where

$$\overline{R}_{qi}=\sqrt{\frac{1}{360}\sum_{j=0}^{359}R_i(j\cdot 1°)^2}\;; \tag{139}$$

in other words, the configuration of the cross-section i expressed in polar co-ordinates was dilated by the factor $1/\overline{R}_{qi}$; as a result, in each cross-section, the square root of the sum of squared Euclidean distances from the dilated landmarks to the centre became constant $360^{1/2}$ (this is how the centroid size is defined; Dryden and Mardia 1998).

The deviation of each centred pre-shape configuration from the unit circle was investigated with the difference

$$R_i^*(j\cdot 1°)-1=\frac{R_i(j\cdot 1°)-\overline{R}_{qi}}{\overline{R}_{qi}}\,, \tag{140}$$

j=0, ..., 359. The empirical distribution of these pre-shape deviations (discretely observed relative radius error functions with respect to the quadratic mean of the radii) in each height class was summarised with the mean, median and variance functions computed pointwise over the cross-sections in the height class.

Mean Shape

In each height class, we estimated the mean configuration $\boldsymbol{\mu}_{R^*}=(\mu_{R^*}(j\cdot 1°))_{j=0,\,1,\,...,\,359}$ with the pointwise mean of the pre-shape configurations of the n cross-sections in the class:

$$\hat{\mu}_{R^*}(j\cdot 1°)=\frac{1}{n}\sum_{i=1}^{n}R_i^*(j\cdot 1°)=\frac{1}{n}\sum_{i=1}^{n}\frac{R_i(j\cdot 1°)}{\bar{R}_{qi}}\ , \tag{141}$$

j=0, ..., 359. The deviation of this estimated mean configuration from the unit circle

$$\hat{\mu}_{R^*}(j\cdot 1°)-1=\frac{1}{n}\sum_{i=1}^{n}\frac{R_i(j\cdot 1°)-\bar{R}_{qi}}{\bar{R}_{qi}}\ , \tag{142}$$

j=0, ..., 359, corresponds to the pointwise mean function of the pre-shape deviations (Eq. 140) in the particular height class.

By estimating the mean shape in this way, we assumed that the pre-shape configurations $\mathbf{R}^*$ in each height class follow the model

$$\mathbf{R}^*=\boldsymbol{\mu}_{R^*}+\boldsymbol{\varepsilon}\ , \tag{143}$$

where $\boldsymbol{\varepsilon}=(\varepsilon(j\cdot 1°))_{j=0,\,1,\,...,\,359}$ is the vector of independent random errors with zero mean (cf. Dryden and Mardia 1998, p. 88). The model implies that each pre-shape configuration be generated from the common mean by just random disturbance (measurement error) and not with any translations, rotations or rescaling.

(As opposed to *full generalised Procrustes analysis,* where several landmark configurations are matched to their mean shape with translation, rotation and scaling, and where this unknown mean shape is estimated as the configuration that minimises the sum of the so-called full Procrustes distances between it and the observed configurations (Dryden and Mardia 1998, p. 87–92), we performed here a restricted version, where we reduced translation into mere superimposition of centres of gravity and rotation into alignment of N–S or R_{max} directions.)

Shape Variability

In each height class, we explored shape variability around the estimated mean shape with a principal component analysis of the 360 residual variables $R^*(j\cdot 1°)-\hat{\mu}_{R^*}(j\cdot 1°)$, j=0, 1, ..., 359 (cf. Stoyan and Stoyan 1994, Dryden and Mardia 1998; for the principal component analysis in general, refer e.g. to Dillon and Goldstein 1984, Jolliffe 1986, or Jackson 1991). The analysis involved estimating the covariance matrix of the variables and then extracting its positive eigenvalues and the corresponding eigenvectors. The use of the covariance matrix, as opposed to the correlation matrix, was justified by the variation in the variables being of the same order of magnitude. The elements of the covariance matrix were estimated with the sample covariances of the variables over the n cross-sections at the particular height; the estimation was based on considerably different numbers of observations, as the number of cross-sections in the height classes varied from 28 to 81 (see Table 12 in Chapter 6). The n–1 positive eigenvalues of the estimated covariance matrix gave the variances $Var(PC_{(k)})$ of the n–1 principal components $PC_{(k)}$, k=1, ..., n–1, and the corresponding eigenvectors gave the coefficients $a_{(k)j}$ of the 360 variables in the n–1 principal components, j=0, 1, ..., 359, k=1, ..., n–1.

Each estimated principal component $PC_{(k)}=\Sigma_j[R^*(j\cdot 1°)-\hat{\mu}_{R^*}(j\cdot 1°)]a_{(k)j}$, k=1, ..., n–1, was visualised in plane by drawing the following contours:

$$\hat{\mu}_{R*}(j\cdot 1°) + c\cdot a_{(k)j}\sqrt{\mathrm{Var}(PC_{(k)})} \tag{144}$$

for c=±2, ±4, ±6 and j=0, 1, ..., 359. (Usually, the values for the coefficient c are selected in the way that they would cover the full potential range of the standardised principal component scores $c_{(k)i}=PC_{(k)i}/\mathrm{Var}(PC_{(k)})^{1/2}=\Sigma_j[R^*_i(j\cdot 1°)-\hat{\mu}_{R*}(j\cdot 1°)]a_{(k)j}/\mathrm{Var}(PC_{(k)})^{1/2}$, k=1, ..., n–1, i=1, ..., n, in the data: if the variables $R^*(j\cdot 1°)-\hat{\mu}_{R*}(j\cdot 1°)$, j=0, 1, ..., 359, follow a multivariate normal distribution, the standardised principal component scores approximately follow the normal distribution with mean 0 and variance 1, for which 99.7% of the probability mass is within [–3, 3]; accordingly, c=±1, ±2, ±3 would be an adequate range. In our data, however, the shape variability was found to be so small that the range of c had to be magnified in order to easily visualise the effect of each principal component. See Dryden and Mardia 1998, p. 48–49 and p. 97, for a more detailed explanation of the rationale behind this common way of visualisation.) The idea was to illustrate the magnitude ($[\mathrm{Var}(PC_{(k)})^{1/2}]$) and the direction (coefficients $a_{(k)j}$) of the variability around the mean shape in each principal component estimated from our set of cross-sections. Since the correlation of the jth variable with the kth principal component is known to be

$$\mathrm{Corr}\left[R^*(j\cdot 1°)-\hat{\mu}_{R*}(j\cdot 1°),\, PC_{(k)}\right] = \frac{a_{(k)j}\sqrt{\mathrm{Var}(PC_{(k)})}}{\sqrt{\mathrm{Var}\left[R^*(j\cdot 1°)-\hat{\mu}_{R*}(j\cdot 1°)\right]}}\,, \tag{145}$$

the visualisation contours can equivalently be written as

$$\hat{\mu}_{R*}(j\cdot 1°) + c\cdot\sqrt{\mathrm{Var}\left[R^*(j\cdot 1°)-\hat{\mu}_{R*}(j\cdot 1°)\right]}\cdot\mathrm{Corr}\left[R^*(j\cdot 1°)-\hat{\mu}_{R*}(j\cdot 1°),\, PC_{(k)}\right]. \tag{146}$$

Hence, another interpretation of the visualisation is that the contour portrays the correlations of the radius residual variables to the principal component, each correlation being weighted with c times the standard deviation of the pertinent radius residual variable.

In order to detect severely deviating cross-sections (outliers) and their effect on the shape analysis at each height, the standardised principal component scores $c_{(k)i}=PC_{(k)i}/\mathrm{Var}(PC_{(k)})^{1/2}$ of the n cross-sections (i=1, ..., n) for each principal component (k=1, ..., n–1) were examined; they were plotted against the within-cross-section means of the 360 pre-shape residuals $\Sigma_j[R^*_i(j\cdot 1°)-\hat{\mu}_{R*}(j\cdot 1°)]/360$ (good indicators of within-cross-section radial variation and, thus, of non-circularity) as well as against the sizes of the cross-sections as indicated by the expected diameters μ_{Di}.

7.2 Estimation of Cross-Section Area

The effect of within-cross-section diameter variation on area estimation was examined with the area estimators for which the theoretical properties had previously been established (see Sections 3.3 and 4.2.2). The estimators were of the form

$$\hat{A} = \frac{\pi}{4}D(\cdot)^2\,, \tag{147}$$

where D(·) was

0. girth diameter $C/\pi=\mu_D$ (mean diameter of over the uniform direction distribution) ($\hat{A}_0$)
1. a random diameter with the uniform direction distribution within $[0, \pi)$ ($\hat{A}_1$)

2. arithmetic mean of a random diameter and the diameter perpendicular to it ($\hat{A}_2$)
3. geometric mean of a random diameter and the diameter perpendicular to it ($\hat{A}_3$)
4. arithmetic mean of two independent random diameters ($\hat{A}_4$)
5. geometric mean of two independent random diameters ($\hat{A}_5$)
6. arithmetic mean of D_{min} and D_{max} ($\hat{A}_6$)
7. geometric mean of D_{min} and D_{max} ($\hat{A}_7$)
8. arithmetic mean of D_{min} and the diameter perpendicular to it ($\hat{A}_8$)
9. geometric mean of D_{min} and the diameter perpendicular to it ($\hat{A}_9$)
10. arithmetic mean of D_{max} and the diameter perpendicular to it ($\hat{A}_{10}$)
11. geometric mean of D_{max} and the diameter perpendicular to it ($\hat{A}_{11}$)

1ξ. diameter parallel to plot radius in Bitterlich sampling ($\hat{A}_{1\xi}$)

2ξ. arithmetic mean of the diameters parallel and perpendicular to plot radius in Bitterlich sampling ($\hat{A}_{2\xi}$)

3ξ. geometric mean of the diameters parallel and perpendicular to plot radius in Bitterlich sampling ($\hat{A}_{3\xi}$)

4ξ. arithmetic mean of a random diameter and the diameter parallel to plot radius in Bitterlich sampling ($\hat{A}_{4\xi}$)

5ξ. geometric mean of a random diameter and the diameter parallel to plot radius in Bitterlich sampling ($\hat{A}_{5\xi}$)

1ξ90. diameter perpendicular to plot radius in Bitterlich sampling ($\hat{A}_{1\xi 90}$)

4ξ90. arithmetic mean of a random diameter and the diameter perpendicular to plot radius in Bitterlich sampling ($\hat{A}_{4\xi 90}$)

5ξ90. geometric mean of a random diameter and the diameter perpendicular to plot radius in Bitterlich sampling ($\hat{A}_{5\xi 90}$)

min. D_{min} ($\hat{A}_{min}$)

max. D_{max} ($\hat{A}_{max}$).

The comparison between the estimators actually meant a comparison between different ways of selecting diameter under the circularity assumption (estimators $\hat{A}_0$, $\hat{A}_1$, $\hat{A}_2$, $\hat{A}_4$, $\hat{A}_{1\xi}$, $\hat{A}_{2\xi}$, $\hat{A}_{4\xi}$, $\hat{A}_{1\xi 90}$, $\hat{A}_{4\xi 90}$, $\hat{A}_6$, $\hat{A}_8$, $\hat{A}_{10}$, $\hat{A}_{min}$, $\hat{A}_{max}$) and different ways of determining principal axes under the ellipticity assumption (estimators $\hat{A}_3$, $\hat{A}_5$, $\hat{A}_{3\xi}$, $\hat{A}_{5\xi}$, $\hat{A}_{5\xi 90}$ $\hat{A}_7$, $\hat{A}_9$, $\hat{A}_{11}$,). $\hat{A}_{min}$ and $\hat{A}_{max}$ were included in the consideration mainly to obtain the lower and upper bounds for the estimates.

The estimators were compared by means of their estimated *relative* within-cross-section bias, standard deviation (the square root of the variance) and root mean squared error (RMSE, the square root of the sum of the variance and the squared bias; cf. Eq. 15 in Section 3.1); these characteristics, computed in each cross-section, are summarised in Table 16. Whether the errors should be expressed relative to the true area or to the convex area is not a straightforward question: as many times pointed out, non-convexity cannot be discerned by caliper or tape and is thus a matter of indirect observation of cross-section shape rather than a question of diameter measurement error or diameter sampling error; hence, it may appear unjustifiable to include into the area estimation error the bias induced by non-convexity that is inherent in the diameter population and thus present in the population total however precisely all the members of the population were ever measured. We circumvented this problem by proportioning the estimation error both to the true area and to the convex area.

For the fixed estimators ($\hat{A}_0$, $\hat{A}_6$–$\hat{A}_{11}$, $\hat{A}_{min}$, and $\hat{A}_{max}$), the relative within-cross-section biases were directly given by the relative estimation errors $[\hat{A}–A]/A$ and $[\hat{A}–A_C]/A_C$. The within-cross-section variances were naturally zero, and the relative root mean squared error thus equalled the absolute value of the relative bias. D_{min} and D_{max} were determined as the minimum and the maximum of the 180 diameters computed systematically (at regular rota-

Table 16. Characteristics estimated for each cross-section to examine the performance of different area estimators (combinations of the circle area formula and a diameter selection method).

Characteristic	Meaning
$[E(\hat{A}_j)–A]/A$, $[E(\hat{A}_j)–A_C]/A_C$, j=0–11, 1ξ–5ξ, 1ξ90, 4ξ90, 5ξ90	Relative within-cross-section bias of estimator $\hat{A}_j$ (circle area formula and diameter selection method j) with respect to true or convex cross-section area
$Var(\hat{A}_j)^{1/2}/A$, $Var(\hat{A}_j)^{1/2}/A_C$, j=1–5, 1ξ–5ξ, 1ξ90, 4ξ90, 5ξ90	Within-cross-section standard deviation of estimator $\hat{A}_j$ relative to true or convex cross-section area
$\tilde{Var}(\hat{A}_j)^{1/2}/A$, $\tilde{Var}(\hat{A}_j)^{1/2}/A_C$, j=1–5, 1ξ–5ξ, 1ξ90, 4ξ90, 5ξ90	Delta method approximation of within-cross-section standard deviation of estimator $\hat{A}_j$ relative to true or convex cross-section area
$RMSE(\hat{A}_j, A)/A$, $RMSE(\hat{A}_j, A_C)/A_C$, j=0–11, 1ξ–5ξ, 1ξ90, 4ξ90, 5ξ90	Relative within-cross-section root mean squared error of estimator $\hat{A}_j$ with respect to true or convex cross-section area; $RMSE(\hat{A}_j, A)/A = \{[E(\hat{A}_j)–A]^2/A^2 + Var(\hat{A}_j)/A^2\}^{1/2}$

tion angle intervals of 1° and starting from the N–S direction) in each cross-section; also the diameters perpendicular to D_{min} and D_{max} were then taken among the 180 systematic diameters.

For the random estimators ($\hat{A}_1$–$\hat{A}_5$, $\hat{A}_{1\xi}$–$\hat{A}_{5\xi}$, $\hat{A}_{1\xi 90}$, $\hat{A}_{4\xi 90}$, and $\hat{A}_{5\xi 90}$), the relative biases $[E(\hat{A})–A]/A$ and $[E(\hat{A})–A_C]/A_C$, relative standard deviations $Var(\hat{A})^{1/2}/A$ and $Var(\hat{A})^{1/2}/A_C$, and relative approximate standard deviations $\tilde{Var}(\hat{A})^{1/2}/A$ and $\tilde{Var}(\hat{A})^{1/2}/A_C$ were estimated by inserting the estimated diameter moments and product moments in the analytical expressions of the within-cross-section expectations $E(\hat{A})$, variances $Var(\hat{A})$ and approximate variances $\tilde{Var}(\hat{A})$ (Eqs. 22–26, 30–34 and 35–37 in Section 3.3.2; Eqs. 94–98, 99–103 and 104–108 in Section 4.2.2). As for the approximate variances, the interest was in their deviation from the true variances: in practice, we would prefer to use the approximate expressions for their simplicity (they only involve diameter means μ_D, $\mu_{D(\xi)}$ and $\mu_{D(\xi+\pi/2)}$, variances σ_D^2, $\sigma_{D(\xi)}^2$ and $\sigma_{D(\xi+\pi/2)}^2$, and correlations $\rho_D(\pi/2)$ and $\rho_{D(\xi)}(\pi/2)$ between perpendicular diameters), if only they do not deviate too much from the true variances.

For the random estimators involving only diameters with the uniform direction distribution ($\hat{A}_1$–$\hat{A}_5$), the mean diameter μ_D was obtained from the convex perimeter as C/π, whereas the other moments and product moments were estimated as simple means from the 180 systematic diameters in each cross-section: σ_D^2 and $\rho_D(\pi/2)$ were obtained with Eqs. 134 and 135, and the other (product) moments generally from

$$\hat{E}\left[D(\theta)^k D\left(\theta+\frac{\pi}{2}\right)^p \right] = \frac{1}{180}\sum_{j=0}^{179} D(j\cdot 1°)^k D[(j+90)\cdot 1°]^p \ , \qquad (148)$$

k=0, ..., 4, p=0, ..., 4. (Note that for j+90≥180, $D[(j+90)\cdot 1°]=D[(j–90)\cdot 1°]$.)

For the random estimators involving Bitterlich diameters (diameters parallel or perpendicular to plot radius in Bitterlich sampling; $\hat{A}_{1\xi}$–$\hat{A}_{5\xi}$, $\hat{A}_{1\xi 90}$, $\hat{A}_{4\xi 90}$, and $\hat{A}_{5\xi 90}$), the non-uniform direction distributions were determined for each cross-section using (i) the inclusion region of the individual cross-section or (ii) the inclusion region of the breast height cross-section

of the tree in which the cross-section was located. The first approach is naturally unfeasible in practice (plot radius direction in Bitterlich sampling cannot be determined separately for different observation heights), and it was considered mainly as a "thinking experiment" — to examine area estimation errors in the case that all the 709 cross-sections of the data had been taken at breast height. The inclusion regions were determined with the viewing angles 1.146°, 1.621°, 2.292° and 3.624° (corresponding, with circular cross-sections, to the basal area factors 1, 2, 4, and 10 m^2/ha, respectively). The direction distributions were estimated in a discretised form, with a point probability (probability mass) associated to each of the 180 systematic diameter directions starting from the N–S direction: for each direction $j\cdot 1°$, j=0, ..., 179, the probability mass $w(j\cdot 1°)$ was estimated as the summed area of the two sectors, of angular width 1°, around the directions $j\cdot 1°$ and $(j+180)\cdot 1°$ divided by the total inclusion area (see Appendix H, Fig. H2). The expectations of the Bitterlich diameters were then estimated as weighted means

$$\begin{aligned}\hat{\mu}_{D(\xi)} &= \sum_{j=0}^{179} w(j\cdot 1°)D(j\cdot 1°)\,,\\ \hat{\mu}_{D(\xi+\pi/2)} &= \sum_{j=0}^{179} w(j\cdot 1°)D[(j+90)\cdot 1°]\,,\end{aligned} \tag{149}$$

the variances as weighted variances

$$\begin{aligned}\hat{\sigma}^2_{D(\xi)} &= \sum_{j=0}^{179} w(j\cdot 1°)\left[D(j\cdot 1°)-\hat{\mu}_{D(\xi)}\right]^2\,,\\ \hat{\sigma}^2_{D(\xi+\pi/2)} &= \sum_{j=0}^{179} w(j\cdot 1°)\left\{D[(j+90)\cdot 1°]-\hat{\mu}_{D(\xi+\pi/2)}\right\}^2\,,\end{aligned} \tag{150}$$

the correlation as

$$\begin{aligned}\hat{\rho}_{D(\xi)}\left(\frac{\pi}{2}\right) &= \frac{1}{\sqrt{\hat{\sigma}^2_{D(\xi)}}}\frac{1}{\sqrt{\hat{\sigma}^2_{D(\xi+\pi/2)}}}\cdot\\ &\quad \sum_{j=0}^{89} w(j\cdot 1°)\left[D(j\cdot 1°)-\hat{\mu}_{D(\xi)}\right]\left\{D[(j+90)\cdot 1°]-\hat{\mu}_{D(\xi+\pi/2)}\right\}\,,\end{aligned} \tag{151}$$

and the other moments generally as

$$\hat{E}\left[D(\xi)^k D\left(\xi+\frac{\pi}{2}\right)^p\right] = \sum_{j=0}^{179} w(j\cdot 1°)D(j\cdot 1°)^k D[(j+90)\cdot 1°]^p\,, \tag{152}$$

k=0, ..., 4, p=0, ..., 4. (Note that the probability masses $w(j\cdot 1°)$, j=0, ..., 179, sum to one, and that for $j+90\geq 180$, $D[(j+90)\cdot 1°]=D[(j-90)\cdot 1°]$.)

The distributions of the relative within-cross-section biases, standard deviations and RMSEs were examined in the whole set of the cross-sections and in the subsets determined by height classes. Whether the performance of an area estimator was related to cross-section size was examined by computing the correlations of the cross-section areas with the biases, standard deviations and RMSEs of each estimator. Since the relative bias of

the reference estimator $\hat{A}_0$ with respect to the convex area (i.e., the relative isoperimetric deficit $[\hat{A}_0 - A_C]/A_C$) may also be regarded as a shape index (as e.g. in Stoyan and Stoyan 1994, where it is referred to as "area-perimeter ratio"), its correlations with the scalar shape indices of Section 7.1 (Table 14) and with the cross-section size indicated by the mean diameter μ_D were examined.

7.3 Estimation of Stem Volume

The effect of diameter selection on volume estimation was investigated by applying the 22 diameter selection methods listed in Section 7.2 to the three volume estimation methods (Laasasenaho volume equation, cubic-spline-interpolated stem curve and generalised volume estimator) discussed in Chapter 5. The diameter selection methods were applied both *dependently* and *independently* at the separate observation heights within a stem: in the former, the diameter direction was selected at breast height, and the diameters at the other heights were then measured in the same direction; in the latter, the diameter directions were selected at each height independently of the other heights. However, with Bitterlich diameters (diameter selection methods 1ξ–5ξ, $1\xi 90$, $4\xi 90$ and $5\xi 90$) only dependent selection was applied, as independent selection could not be considered realistic: in Bitterlich sampling, it is not feasible to think of viewing a tree from different viewing points at different heights. The direction distributions of the Bitterlich diameters in each tree were then naturally determined from the inclusion region of the breast height cross-section (i.e., the distribution obtained at breast height was applied also to the cross-sections at the other heights in the tree). The inclusion regions of the trees were determined with the viewing angles 1.146°, 1.621°, 2.292° and 3.624° (corresponding, with circular cross-sections, to the basal area factors of 1, 2, 4, and 10 m^2/ha, respectively).

For each resulting volume estimator $\hat{V}_{Xj}$ (a combination of the volume estimation method X and the diameter selection method j), the within-tree expectation $E(\hat{V}_{Xj})$ and variance $\mathrm{Var}(\hat{V}_{Xj})$ were estimated. From these, the relative within-tree mean squared error (MSE), consisting of the squared relative within-tree bias and the relative within-tree variance, was computed with respect to a volume-estimation-method-specific reference volume $\tilde{V}_X$:

$$\frac{E\left[(\hat{V}_{Xj} - \tilde{V}_X)^2\right]}{\tilde{V}_X^2} = \left[\frac{E(\hat{V}_{Xj}) - \tilde{V}_X}{\tilde{V}_X}\right]^2 + \frac{\mathrm{Var}(\hat{V}_{Xj})}{\tilde{V}_X^2} \,. \tag{153}$$

(Note that for the Laasasenaho volume equation, the prediction errors were now defined as the opposite numbers of those in the theoretical considerations in Section 5.1; note also that for the general volume estimator, the within-tree bias was estimated "directly" without computing the within-tree expectation of the estimator.) *The idea of varying the reference volume according to the volume estimation method was to separate out, in the best possible way, the diameter selection effect from the other sources of error in the volume estimator*. The within-tree characteristics computed for each volume estimator in each tree are summarised in Table 17; the variances and the MSEs were considered in the square root scale (as standard deviations and root mean squared errors, RMSEs), to make them easy to interpret.

The investigation was carried out on the 79 stems within which 7 or more cross-sections had been observed; this requirement was due to the method used for estimating the true stem volume (see Section 7.3.1). However, the Laasasenaho volume equation could be examined only with the 50 stems in which the discs at both the heights of 1.3 m and 6 m had been observed.

Table 17. Characteristics estimated for each stem to examine the performance of different volume estimators (combinations of a volume estimation method and a diameter selection method). In independent selection (IS), diameter measurement directions at different observation heights within a stem were selected independently of each other; in dependent selection (DS), diameters at all observation heights were measured in the direction selected at breast height.

Volume estimation method	Diameter selection methods	Characteristic	Meaning
Laasasenaho (1982) volume equation re-estimated	j=0, 1–11 (IS, DS), 1ξ–5ξ, 1ξ90, 4ξ90, 5ξ90 (DS)	$[E(\hat{V}_{Lj})-\tilde{V}_L]/\tilde{V}_L$, $E[(\hat{V}_{CLj}-\tilde{V}_{CL})/\tilde{V}_{CL}]$	Relative within-tree bias of prediction (by the equation and diameter selection method j) with respect to the best prediction by the equation
(i) with true area diameters and estimated true volume and (ii) with convex area diameters and estimated convex volume	j=1–5 (IS, DS), 1ξ–5ξ, 1ξ90, 4ξ90, 5ξ90 (DS)	$Var(\hat{V}_{Lj})^{1/2}/\tilde{V}_L$, $Var(\hat{V}_{CLj})^{1/2}/\tilde{V}_{CL}$	Within-tree standard deviation of prediction relative to the best prediction by the equation
	j=0, 1–11 (IS, DS), 1ξ–5ξ, 1ξ90, 4ξ90, 5ξ90 (DS)	$RMSE(\hat{V}_{Lj}, \tilde{V}_L)/\tilde{V}_L$, $RMSE(\hat{V}_{CLj}, \tilde{V}_{CL})/\tilde{V}_{CL}$	Relative within-tree root mean squared error of prediction with respect to the best prediction by the equation; $RMSE(\hat{V}_{Lj}, \tilde{V}_L)/\tilde{V}_L = \{[E(\hat{V}_{Lj})-\tilde{V}_L]^2/\tilde{V}_L{}^2+Var(\hat{V}_{Lj})/\tilde{V}_L{}^2\}^{1/2}$
		$(\tilde{V}_L-\tilde{V})/\tilde{V}_L$, $(\tilde{V}_{CL}-\tilde{V}_C)/\tilde{V}_{CL}$	Relative error of the best prediction by the equation with respect to estimated true or convex volume (relative residual); error inherent in the Laasasenaho equation
Cubic-spline-interpolated stem curve	j=0, 1–11 (IS, DS), 1ξ–5ξ, 1ξ90, 4ξ90, 5ξ90 (DS)	$[E(\hat{V}_{Sj})-\tilde{V}]/\tilde{V}$ $[E(\hat{V}_{Sj})-\tilde{V}_C]/\tilde{V}_C$	Relative within-tree bias of the estimator (the stem curve with diameter selection method j) with respect to estimated true or convex volume
	j=1–5 (IS, DS), 1ξ–5ξ, 1ξ90, 4ξ90, 5ξ90 (DS)	$Var(\hat{V}_{Sj})^{1/2}/\tilde{V}$ $Var(\hat{V}_{Sj})^{1/2}/\tilde{V}_C$	Within-tree standard deviation of the estimator relative to estimated true or convex volume
	j=0, 1–11 (IS, DS), 1ξ–5ξ, 1ξ90, 4ξ90, 5ξ90 (DS)	$RMSE(\hat{V}_{Sj}, \tilde{V})/\tilde{V}$, $RMSE(\hat{V}_{Sj}, \tilde{V}_C)/\tilde{V}_C$,	Relative within-tree root mean squared error of the estimator with respect to estimated true or convex volume; $RMSE(\hat{V}_{Sj}, \tilde{V})/\tilde{V} = \{[E(\hat{V}_{Sj})-\tilde{V}]^2/\tilde{V}^2+Var(\hat{V}_{Sj})/\tilde{V}^2\}^{1/2}$
General volume estimator	j=0, 1–5 (DS), 6–11 (IS, DS), 1ξ–5ξ, 1ξ90, 4ξ90, 5ξ90 (DS)	$E(\hat{V}_{Gj}-V)/\tilde{V}$ $E(\hat{V}_{Gj}-V_C)/\tilde{V}_C$	Relative within-tree bias of the estimator (with diameter selection method j) with respect to true or convex volume and proportioned to estimated true or convex volume
	j=1–5, 1ξ–5ξ, 1ξ90, 4ξ90, 5ξ90 (DS)	$Var(\hat{V}_{Gj})^{1/2}/\tilde{V}$ $Var(\hat{V}_{Gj})^{1/2}/\tilde{V}_C$	Within-tree standard deviation of the estimator relative to estimated true or convex volume
	j=0, 1–5 (DS), 6–11 (IS, DS), 1ξ–5ξ, 1ξ90, 4ξ90, 5ξ90 (DS)	$RMSE(\hat{V}_{Gj},V)/\tilde{V}$, $RMSE(\hat{V}_{Gj},V_C)/\tilde{V}_C$,	Within-tree root mean squared error of the estimator with respect to true or convex volume and relative to estimated true or convex volume; $RMSE(\hat{V}_{Gj}, V)/\tilde{V} = \{[E(\hat{V}_{Gj}-V)]^2/\tilde{V}^2+Var(\hat{V}_{Gj})/\tilde{V}^2\}^{1/2}$

The distributions of the relative within-tree biases, standard deviations and RMSEs produced by the different volume estimators were examined in the set of all the stems. Further, the associations of these characteristics with tree size (as expressed by the estimated true stem volume) as well as with growing site location (in terms of the cluster co-ordinates in N-S and E-W directions) were examined by computing their correlations and by plotting them with respect to each other.

7.3.1 True Volume

The true stem volume V between the stump height h_s and the total height H (both measured in the field with respect to the ground level, see Chapter 6) was estimated for each tree with the method that was regarded as the most accurate among those available: from the true area diameters $\mathbf{D}_A=(D_A(h))_{h\in \mathbf{H}}=(2[A(h)/\pi]^{1/2})_{h\in \mathbf{H}}$ observed at heights $\mathbf{H}=(h_{(1)}, ..., h_{(m)}, H)$, a stem curve $S_3(h; \mathbf{D}_A, \mathbf{H})$ was estimated with interpolating cubic splines, and the volume was then obtained as the solid of revolution of the curve as

$$\tilde{V} = \frac{\pi}{4}\int_{h_s}^{H} S_3(h; \mathbf{D}_A, \mathbf{H})^2 dh \ . \qquad (154)$$

(Instead of the symbol $\tilde{V}_S$ used in Eq. 125 in Section 5.3, the volume estimate is here denoted as $\tilde{V}$, because it will serve as the reference volume not only for the cubic-spline-interpolated stem curve method but also for the generalised volume estimator and be used to assess the model error component independent of diameter selection in the Laasasenaho volume equation). The computations were performed with the Fortran 77 subroutines written by Mr Carl-Gustaf Snellman in the Finnish Forest Research Institute and based on the work of Lahtinen and Laasasenaho (1979).

By their empirical experience, Lahtinen and Laasasenaho (1979, p. 54) recommended that the stem curve estimation be based on not fewer than 7 observation points along the stem. In the 79 trees included in the volume investigation, the number of observation heights varied between 7 and 10, and thus, with the tree height H and the assumed top diameter $D_A(H)=0.4$ cm included, the interpolation was based on 8–11 observation points. The initial values (required for a unique solution of the system of the spline equations) were determined via estimated second derivatives of the stem curve at the lowest and highest observation heights (cf. Lahtinen and Laasasenaho 1979, p. 19, 31); the derivatives were estimated by approximating the stem curve at both ends of the stem with interpolating parabolas passing through the three lowermost and uppermost observation points.

As the squared cubic splines consist of piecewise polynomials of the observation heights, the squared stem curve could be integrated analytically. In addition to the total volume, the volume of the stem segment between the lowermost and the uppermost observation heights $h_{(1)}$ and $h_{(m)}$ was estimated; this *partial volume*, also denoted by $\tilde{V}$, was required as the reference volume for the general volume estimators. In the same way, the total and partial *convex volumes*, both denoted by $\tilde{V}_C$, were estimated for each stem from the convex area diameters $(D_{Ac}(h))_{h\in \mathbf{H}}=(2[A_C(h)/\pi]^{1/2})_{h\in \mathbf{H}}$.

In 11 stems of the total of 79, there were one or two intervals between adjacent observation heights where the true area was larger at the upper height than at the lower height; in 10 of these 11 stems this was the case also with the convex area. Such non-monotonicity might result in an aberrant oscillation in a cubic spline function. However, the taper curves obtained for the said 11 stems were regarded as acceptable — the three worst ones are shown

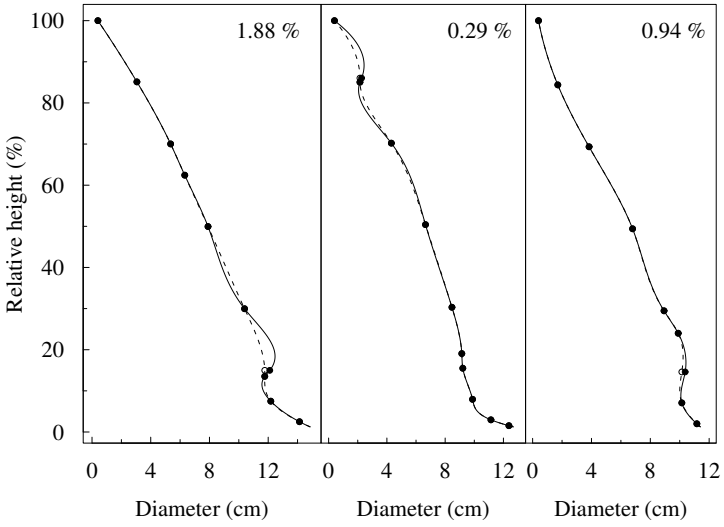

Fig. 28. The three worst cases of oscillating cubic-spline-interpolated stem curves among the 11 stems (of the total 79) in which the observed true area diameters increased upwards in one or more measurement intervals. The continuous line indicates the stem curve obtained from the observed true area diameters (filled circles) and employed for estimating the true volume; the dashed line shows the stem curve obtained by forcing monotonicity from below (i.e., by coercing the larger upper diameter to have the value of the smaller lower diameter; open circles); the percentage gives the relative difference between the volumes obtained with the two stem curves.

in Fig. 28 — and thus none of the known improvements for the algorithm (Lahtinen 1988 and 1993) were considered necessary to implement.

7.3.2 Laasasenaho Volume Equation

Stem volume estimation for standing trees was imitated by applying the 22 different diameter selection methods (see Section 7.2) to the Laasasenaho (1982) three-variable volume equation where the originally unspecified diameters at the heights of 1.3 m and 6 m were fixed as the true area diameters (cf. the discussion in Section 5.1):

$$\begin{aligned} V \;&= \beta_1 D_A(1.3)^2 + \beta_2 D_A(1.3)^2 H + \beta_3 D_A(1.3)^3 H + \beta_4 D_A(1.3)^2 H^2 \\ &\quad + \beta_5 \left[D_A(1.3)^2 + D_A(1.3) D_A(6) + D_A(6)^2 \right] + \beta_6 D_A(6)^2 (H-6) + \varepsilon_L \; . \end{aligned} \tag{155}$$

In Laasasenaho's original specification, the stem volume was defined to extend from the top of the tree either to the highest root collar affecting cutting, or, if the collar did not exist or was located below the height of 10 cm, to the height of 10 cm (Laasasenaho 1982). This is how the cutting point (stump height h_S) of each tree was determined also in this study, and thus the estimated true volume in this study (see Section 7.3.1) agreed well with the definition of the stem volume in the original work.

Table 18. Original parameter estimates of the Laasasenaho (1982) three-variable volume equation for Scots pine (Eq. 155), and the estimates used in this study (obtained from the 50 stems in the data with both the 1.3 m and 6 m cross-sections available).

Parameter	Data		
	2326 stems in the study by Laasasenaho (1982)	$\tilde{V}$, $D_A(1.3)$, $D_A(6)$, H in 50 stems of this study	$\tilde{V}_C$, $D_{Ac}(1.3)$, $D_{Ac}(6)$, H in 50 stems of this study
β_1	0.268621	0.202318	0.201441
β_2	–0.0145543	–0.0109918	–0.0108715
β_3	–0.0000478628	–0.000279395	–0.000284556
β_4	0.000334101	0.000831394	0.000844558
β_5	0.0973148	0.115504	0.115359
β_6	0.0440716	0.0294864	0.0291432

Instead of employing Laasasenaho's parameter estimates based on the data of 2326 Scots pine sample trees from all over Finland, we re-estimated the parameters from the 50 stems of our data in which the cross-section had been observed at both the heights of 1.3 m and 6 m; this was to make the error inherent in the model (the random error term ε_L, also referred to as the model error) as small as possible. The estimation was performed both *without and with the assumption of cross-section convexity*: in the former, the estimated true volume $\tilde{V}$ was employed as the response variable and the true area diameters $D_A(1.3)$ and $D_A(6)$ (as well as the height H) were used as the explanatory variables; in the latter, the response variable was the estimated true convex volume $\tilde{V}_C$ and the explanatory variables comprised the convex area diameters $D_{Ac}(1.3)$ and $D_{Ac}(6)$. As the error terms were assumed heteroscedastic (variance proportional to $D_A(1.3)^4H^2$, or to $D_{Ac}(1.3)^4H^2$; refer to Section 5.1), a weighted least squares estimation was performed with $1/[D_A(1.3)^4H^2]$, or $1/[D_{Ac}(1.3)^4H^2]$, as the weight of each observation (stem); this corresponds to the ordinary least squares estimation of a form factor model carried out in the original work (Laasasenaho 1982, p. 43–44). As in the original study, the within-plot and within-cluster interdependencies of the stems, which at least in principle breached the model assumptions, were disregarded in the estimation. Judging from the residual plots, the models fitted well in the data; also, the relative root mean squared errors (the standard deviations of the relative residuals adjusted with the number of parameters) were in concordance with that in the original data (3.59% and 3.60% vs. 3.53%; Laasasenaho 1982, p. 43). The original and the re-estimated parameter values are given in Table 18. In the following, we will deal with the volume estimation without the convexity assumption; the particularities related to the estimation with the convexity assumption will be considered in the end of the section.

We assumed the re-estimated model to be correct and thus disregarded the effects of using estimated parameters instead of the true ones (cf. the discussion in Section 5.1). As the reference volume (to which the estimators by different diameter selection methods were to be compared) we used the best estimate

$$\begin{aligned}\tilde{V}_L &= \hat{\beta}_1 D_A(1.3)^2 + \hat{\beta}_2 D_A(1.3)^2 H + \hat{\beta}_3 D_A(1.3)^3 H + \hat{\beta}_4 D_A(1.3)^2 H^2 \\ &\quad + \hat{\beta}_5 \left[D_A(1.3)^2 + D_A(1.3) D_A(6) + D_A(6)^2 \right] + \hat{\beta}_6 D_A(6)^2 (H-6)\,;\end{aligned} \tag{156}$$

this was because we wanted to distinguish the error component caused by diameter selection from the error component inherent in the model (the model error that is present even if the

diameters were measured "correctly", i.e., even if the true area diameters at the heights of 1.3 m and 6 m in the stem were known). The model error in each stem was then estimated as the relative error of this best estimate $\tilde{V}_L$ with respect to the estimated true volume $\tilde{V}$ (i.e., as the relative residual $(\tilde{V}_L - \tilde{V})/\tilde{V}_L$ of the estimated model). The purpose of the diameter specification as true area diameters (to comply with the estimation of true volume) and the parameter re-estimation was expressly to make this error as small as possible, that is, to set the reference volume as close to our estimated true volume as possible.

Applying the different diameter selection methods to the volume equation resulted in the volume estimators (here written as a function of the diameters only)

$$\hat{V}_{Lj} = \hat{c}_1 D_j(1.3)^2 + \hat{c}_2 D_j(1.3)^3 + \hat{c}_3 D_j(1.3) D_j(6) + \hat{c}_4 D_j(6)^2 \ , \tag{157}$$

where $\hat{c}_1 = \hat{\beta}_1 + \hat{\beta}_2 H + \hat{\beta}_4 H^2 + \hat{\beta}_5$, $\hat{c}_2 = \hat{\beta}_3 H$, $\hat{c}_3 = \hat{\beta}_5$, and $\hat{c}_4 = \hat{\beta}_5 + \hat{\beta}_6 (H - 6)$, and where $D_j(1.3)$ and $D_j(6)$ are the diameters selected with method j at the heights of 1.3 m and 6 m.

With the diameter selection methods involving only fixed diameters (methods 0, 6–11, min and max; independent and dependent selection), there was naturally no within-tree variation in the estimator values, whereby the within-tree expectation of the estimator equalled the constant estimate itself (i.e., $E(\hat{V}_{Lj}) = \hat{V}_{Lj}$ and $Var(\hat{V}_{Lj}) = 0$).

With the diameter selection methods involving random diameters (methods 1–5, independent and dependent selection; methods 1ξ–5ξ 1ξ90, 4ξ90 and 5ξ90, dependent selection), the within-tree expectation and variance of the volume estimator were estimated by means of estimated diameter moments and product moments:

$$\begin{aligned} \hat{E}[\hat{V}_{Lj}] \ &= \hat{c}_1 \hat{E}[D_j(1.3)^2] + \hat{c}_2 \hat{E}[D_j(1.3)^3] \\ &\quad + \hat{c}_3 \hat{E}[D_j(1.3) D_j(6)] + \hat{c}_4 \hat{E}[D_j(6)^2] \ , \end{aligned} \tag{158}$$

and

$$\begin{aligned} \hat{Var}[\hat{V}_{Lj}] \ &= \hat{c}_2^2 \hat{E}[D_j(1.3)^6] + 2\hat{c}_1 \hat{c}_2 \hat{E}[D_j(1.3)^5] + \hat{c}_1^2 \hat{E}[D_j(1.3)^4] \\ &\quad + 2\hat{c}_2 \hat{c}_3 \hat{E}[D_j(1.3)^4 D_j(6)] + 2\hat{c}_2 \hat{c}_4 \hat{E}[D_j(1.3)^3 D_j(6)^2] \\ &\quad + 2\hat{c}_1 \hat{c}_3 \hat{E}[D_j(1.3)^3 D_j(6)] + (\hat{c}_3^2 + 2\hat{c}_1 \hat{c}_4) \hat{E}[D_j(1.3)^2 D_j(6)^2] \\ &\quad + 2\hat{c}_3 \hat{c}_4 \hat{E}[D_j(1.3) D_j(6)^3] + \hat{c}_4^2 \hat{E}[D_j(6)^4] \\ &\quad - \left\{ \hat{E}[\hat{V}_{Lj}] \right\}^2 \ ; \end{aligned} \tag{159}$$

refer to Appendices E and F for the more detailed method-specific expressions. The diameter moments and product moments were estimated as explained in Section 7.2: With the methods 1–5 involving the uniform direction distribution, the moment estimates were obtained as simple means from the 180 systematic diameters in each cross-section. With methods 1ξ–5ξ, 1ξ90, 4ξ90 and 5ξ90 involving the non-uniform direction distributions of the Bitterlich diameters, the moments were estimated as weighted means from the 180 systematic diameters, the weights being determined as the relative sector areas of the inclusion region of the breast height cross-section.

The assumption of cross-section convexity influenced the reference volume, the estimated model error, and the within-tree expectations and variances of the estimators: The convex reference volume $\tilde{V}_{CL}$ was obtained from the volume equation estimated with true convex volume $\tilde{V}_C$ and the convex area diameters, and the relative model error $[\tilde{V}_{CL} - \tilde{V}_C]/\tilde{V}_{CL}$

was naturally determined as the relative residual of this model. Since the diameters of a non-convex cross-section and its convex closure coincide, the within-tree expectation and variance of the estimator $\hat{V}_{CLj}$ produced by each diameter selection method j were obtained by using the same diameters and diameter moment estimates as in the non-convex case, but with the parameter estimates $\hat{c}_1$, $\hat{c}_2$, $\hat{c}_3$ and $\hat{c}_4$ of the volume equation estimated with the true convex volume and the convex area diameters.

7.3.3 Cubic-Spline-Interpolated Stem Curve

Stem volume estimation for a felled sample tree was mimicked by applying each of the 22 diameter selection methods (see Section 7.2) at the 7–10 observation heights in a stem and constructing the cubic-spline-interpolated stem curves from the resulting diameter vectors (with the assumed diameter of 0.4 cm at the top of the tree added in them). Let us denote with $\mathbf{D}_j$ the diameter vector obtained with the diameter selection method j, with $\mathbf{H}$ the vector containing the observation heights (plus the tree height) and with $S_3[h; \mathbf{D}_j, \mathbf{H}]$ the interpolated stem curve. The volume estimate by each diameter selection method was then obtained as the solid of revolution of the stem curve from the recorded stump height h_s to the height H of the tree:

$$\hat{V}_{Sj} = \frac{\pi}{4}\int_{h_s}^{H} S_3[h; \mathbf{D}_j, \mathbf{H}]^2 dh \ . \tag{160}$$

Technically the volume estimation was carried out in the same manner as the estimation of the true volume (see Section 7.3.1; however, potential oscillation in the stem curves due to diameter increase within short distances upward was not controlled here). All the 79 stems with cross-sections observed at 7 or more heights were included in the investigation.

With the diameter selection methods involving fixed diameters (methods 0, 6–11, min and max; independent and dependent selection), there was no within-tree variation in the volume estimates (i.e., $\mathrm{Var}(\hat{V}_{Sj})=0$), and the within-tree expectation was given by the constant volume estimate itself (i.e., $E(\hat{V}_{Sj})=\hat{V}_{Sj}$).

With the diameter selection methods involving random diameters (methods 1–5, independent and dependent selection; methods 1ξ–5ξ, 1ξ90, 4ξ90 and 5ξ90, dependent selection), the diameter vector selection was repeated several times in each stem in order to capture the within-tree variation in volume estimates. The "population" from which the diameter vectors were sampled varied according to the diameter selection method: it consisted of all the diameter vectors that could be formed by the diameter selection method in question from the systematically measured diameters, 180 at each observation height, in the stem.

The *dependent selection* of diameters at the different heights in a stem restricted the diameter vector population so that all the vectors therein could be included in the sample: with the methods where only one diameter direction within a cross-section was actually selected and where the other direction, if taken, was fully determined by the first one (methods 1–3, 1ξ–3ξ and 1ξ90), there were 180 possible diameter vectors; with methods where two diameter directions within a cross-section were selected independently of each other (methods 4, 5, 4ξ, 5ξ, 4ξ90 and 5ξ90), the number of possible diameter vectors was 180^2, as for each first diameter direction selection there were 180 alternatives as the second choice. Using these 180 or 180^2 diameter vectors meant selecting the one diameter direction or the pair of diameter directions equidistantly (by every 1°) within [0°, 180°) or [0°, 180°)×[0°, 180°). To each diameter vector, the estimated selection probability of the one diameter direction or the pair of diameter directions was associated as a weight.

The probability was determined by means of the diameter direction distribution(s): with one direction selection, the weight was the probability of selecting a direction within 0.5° from the chosen direction (the probability mass within 0.5° from the common direction of the diameters in the diameter vector); with two independent direction selections within a cross-section, the weight was the product of such probabilities related to the two chosen directions. The within-tree expectation and variance of each volume estimator (diameter selection method) were then estimated as the weighted mean and variance of the volume estimates obtained with the diameter vectors of the method (cf. Eqs. 127 and 128 and the discussion on numerical integration in Section 5.3). (Thus, with interrelated diameter selection methods (1, 1ξ and 1ξ90; 2, 2ξ and 2ξ90; 3, 3ξ and 3ξ90 etc.), the volume estimates were computed using the same diameter vectors, but the within-tree expectation and variance were estimated with different weights.) With only the uniform direction distribution involved (methods 1–5), the weights associated to each diameter vector became equal, and the weighted mean and variance of the volume estimates were simplified to the simple arithmetic mean and sample variance. With the non-uniform direction distributions of the Bitterlich diameters involved in the first direction selection (methods 1ξ–5ξ, 1ξ90, 4ξ90 and 5ξ90), the weights became unequal and were obtained from the relative sector areas of the inclusion region of the breast height cross-section of the tree (cf. Section 7.2).

In the *independent selection* of diameters at the different heights in a stem (applied only to the diameter selection methods 1–5 involving the uniform direction distribution), the diameter vector population grew so large that all the vectors therein could not be used: with methods 1–3 the number of possible diameter vectors amounted to 180^m and with methods 4–5 to180^{2m}, m being the number of observation heights, total height excluded. Instead, we drew upon Monte Carlo integration where 180^2 diameter direction vectors were to be sampled independently from the multidimensional direction distribution of each diameter selection method. With the uniform marginal distributions of the independent directions, the multidimensional direction distributions became also uniform, implying that all the diameter vectors of generated by the method had the same probability to be chosen. Therefore a simple random sample of 180^2 vectors was drawn from the diameter vector population of each diameter selection method, with replacement for practical ease; in practice, the sampling was carried out by selecting randomly at each observation height the required one or two diameters among the 180 alternatives and by repeating this procedure 180^2 times for each stem. The within-tree expectation and variance of the volume estimator were then estimated as the mean and sample variance of the volume estimates computed from the selected diameter vectors (cf. Eqs. 129 and 130 and the discussion on Monte Carlo integration in Section 5.3).

As the natural reference volume, we employed the estimated true volume $\tilde{V}$ computed with the similar stem curve approach from the true area diameters (see Section 7.3.1). Unlike with the volume equation, the error contained in the reference volume could not now be quantified, as the true volumes of the stems were unknown and no more precise estimates were available. Consequently, the within-tree biases and variances produced by the different diameter selection methods could only be compared with each other; no notion about their magnitude with respect to the "error intrinsic in the volume estimation method" could be gained.

Since the diameters are the same for a non-convex cross-section and its convex closure, assuming cross-section convexity influenced only the reference volume: with the convexity assumption, we employed the convex volume estimate $\tilde{V}_C$ computed from the convex area diameters (see Section 7.3.1) as the reference.

7.3.4 General Volume Estimator

Finally, we considered estimating the volume of the stem segment from the lowermost observation height $h_{(1)}$ to the uppermost one $h_{(m)}$ by means of general volume estimators that involved area estimation functions $\hat{A}_j(h)=\pi D_j(h)^2/4$ arising from the application of each of the 22 diameter selection methods (see Section 7.2; j refers to the diameter selection method) and the circle area formula at a all the heights $h \in [0, H]$ in a stem:

$$\hat{V}_{Gj} = \int_{h_{(1)}}^{h_{(m)}} \hat{A}_j(h)\,dh = \frac{\pi}{4}\int_{h_{(1)}}^{h_{(m)}} D_j(h)^2\,dh \,. \tag{161}$$

We omitted to define explicitly the values of the area estimation functions between the observation heights (and to estimate the stem volumes actually) but focused on "direct" estimation of the bias, covariance and variance functions $\mu_{\Delta\hat{A}j}(h)$, $\gamma_{\hat{A}j}(h, k)$ and $\sigma_{\hat{A}j}^2(h)$ of the area estimation process $\{\hat{A}_j(h), h \in [0, H]\}=\{\pi D_j(h)^2/4, h \in [0, H]\}$ of each diameter selection method in each tree. As explained in Section 5.2, the within-tree bias and variance of each general volume estimator (diameter selection method) in each tree could then be estimated by integrating the estimated treewise bias end covariance functions:

$$\begin{aligned} \hat{E}\left[\hat{V}_{Gj} - V\right] &= \int_{h_{(1)}}^{h_{(m)}} \hat{\mu}_{\Delta\hat{A}_j}(h)\,dh \\ &= \int_{h_{(1)}}^{h_{(m)}} \hat{E}\left[\hat{A}_j(h) - A(h)\right]dh \,, \end{aligned} \tag{162}$$

and

$$\begin{aligned} \hat{Var}(\hat{V}_{Gj}) &= \int_{h_{(1)}}^{h_{(m)}}\int_{h_{(1)}}^{h_{(m)}} \hat{\gamma}_{\hat{A}_j}(h, k)\,dh\,dk \\ &= \int_{h_{(1)}}^{h_{(m)}}\int_{h_{(1)}}^{h_{(m)}} \hat{Cov}[\hat{A}_j(h), \hat{A}_j(k)]\,dh\,dk \,. \end{aligned} \tag{163}$$

Further, an estimate for the theoretical upper bound of the within-tree variance (the variance conditional on fully correlated area estimation process) was given by the definite integral of the estimated variance function:

$$\begin{aligned} \hat{Var}[\hat{V}_{Gj} \mid \rho_{\hat{A}_j}(h, k) = 1] &= \left\{\int_{h_{(1)}}^{h_{(m)}} \sqrt{\hat{\sigma}^2_{\hat{A}_j}(h)}\,dh\right\}^2 \\ &= \left\{\int_{h_{(1)}}^{h_{(m)}} \sqrt{\hat{Var}[\hat{A}_j(h)]}\,dh\right\}^2 \,. \end{aligned} \tag{164}$$

As in the cubic-spline-interpolated stem curves before, all the 79 stems with 7 or more observed cross-sections were included in the examination. For each diameter selection method j in each stem, the bias, variance and covariance functions were estimated from the

discrete observations on the area estimator $\hat{A}_j(h)=\pi D_j(h)^2/4$ along the stem, that is, from the vectors of the estimated within-cross-section biases $(\hat{E}[\hat{A}_j(h)]-A(h))_{h\in \mathbf{H}}$ and variances $(\hat{Var}[\hat{A}_j(h)])_{h\in \mathbf{H}}$ at the 7–10 observation heights $\mathbf{H}=(h_{(1)}, h_{(2)}, ..., h_{(m)})$ and from the matrix of the estimated between-cross-sections covariances $(\hat{Cov}[\hat{A}_j(h), \hat{A}_j(k)])_{h, k\in \mathbf{H}}$ at the 42–90 two-height combinations $\mathbf{H}\times\mathbf{H}$ in the stem.

With the diameter selection methods involving only fixed diameters (methods 0, 6–11, min, max; independent and dependent selection), the variances and covariances of the area estimators at separate heights were naturally zero and the biases were given by the differences between the area estimates and the true area at each height.

With the diameter selection methods involving random diameters, only dependent selection was considered: With Bitterlich diameters (methods 1ξ–5ξ, 1ξ90, 4ξ90 and 5ξ90), independent selection was not feasible, as noted before. With diameters having the uniform direction distribution (methods 1–5), independent selection was to result, by definition, in the same within-cross-section biases and variances of the area estimators as dependent selection, as well as in zero covariances between the area estimators at separate heights, thus providing no information for covariance function estimation (refer to the discussion on an area estimation process with uncorrelated elements in Section 5.2). In all the cross-sections, the biases and the variances of the area estimators had already been estimated when considering cross-section area estimators (Section 7.2). Similarly, the covariances of the area estimators at different heights could be expressed in terms of diameter moments and product moments, which were then estimated from the 180 systematic diameters and their products in each cross-section (cf. Section 7.2): With the methods involving the uniform direction distribution, the moment estimates were obtained as simple means. With the methods involving the non-uniform direction distributions of the Bitterlich diameters, the moment estimates were obtained as weighted means, the weights being determined as the relative sector areas of the inclusion region of the breast height cross-section.

From the discrete estimated values, the bias, variance and covariance functions of the area estimation process in each tree were estimated by *linear interpolation*. Linear interpolation was employed for simplicity and for its assuredly reasonable behaviour: as there were 56 functions to be estimated in each of the 79 stems (3 functions for each of the methods 1–5, 1ξ–5ξ, 1ξ90, 4ξ90 and 5ξ90 with dependent selection; 1 function for the method 0; and 1 function for each of the methods 6–11, min and max with both dependent and independent selection), the use of smoother higher order interpolating splines requiring control and adjustment for possible non-feasible oscillations was regarded as too laborious an approach.

The linear functions could be integrated analytically. The integration limits were set as the lowermost and the uppermost observation heights $h_{(1)}$ and $h_{(m)}$, because the functions could not be justifiably extrapolated to cover the whole stem from the stump height to the very top. Thus, unlike with the other volume estimation methods, the volume bias and variance were computed only for that part of the stem within which cross-sections had been observed. As the reference volume, the estimated true volume $\tilde{V}$ of the stem segment between the lowermost and the uppermost observation heights (see Section 7.3.1) was used.

The assumption of cross-section convexity did not influence the actual area estimation processes $\{\hat{A}_j(h), h\in \mathbf{H}\}$ (based on diameters and the circle area formula, the area estimators $\hat{A}_j(h)$ were the same whether the cross-sections were assumed convex or not) but affected the area estimation error processes $\{\hat{A}_j(h)-A_C, h\in \mathbf{H}\}$, where the errors were now taken with respect to the convex area A_C. Consequently, with the convexity assumption, only the bias functions of the 30 area estimation processes (22 diameter selection methods with dependent selection, 8 methods with independent selection) needed to be re-estimated from the biases taken with respect to the convex area in each stem; the integrals of these functions

were then thought to yield the estimated biases $\hat{E}[\hat{V}_{Gj}-V_C]$ of the general volume estimators with respect to true (partial) convex volume V_C. The reference volume, to which the estimated within-tree volume biases and variances were proportioned, was naturally also changed for the estimated partial convex volume $\tilde{V}_C$ (see Section 7.3.1).

7.4 Estimation of Stand Totals in Bitterlich Sampling

In Bitterlich sampling, applying circularity assumption to non-circular cross-sections was found to inflict potential bias in stand total estimators, due to two tree-specific faults in the estimated inclusion probabilities (see Eq. 69 in Section 4.1.2): (i) deviation of the true basal area factor of the tree $\kappa(\alpha)=A_C/|\mathbf{M}(\alpha)|$ (the ratio of the convex area of the breast height cross-section to the inclusion area) from that of a circle $\sin^2(\alpha/2)$, and (ii) estimation of the convex area of the breast height cross-section with estimator $\hat{A}_j=\pi D_j^2/4$ based on diameter D_j measured in the cross-section by some method j. With the viewing angle α values of 1.146°, 1.621°, 2.292° and 3.624° (corresponding, with circular cross-sections, to the basal area factor values of 1, 2, 4, and 10 m^2/ha, respectively), these errors were investigated in the 80 breast height cross-sections of the data. As a "thinking experiment", the examination was then extended to all the 709 cross-sections, using their own inclusion regions as if they were all breast height cross-sections.

The deviation of the true basal area factor from that of a circle, expressed as the ratio $\sin^2(\alpha/2)/\kappa(\alpha)$, was first computed separately in each cross-section. In the estimation of the relative basal area of a stand by Bitterlich sampling, $\sin^2(\alpha/2)/\kappa(\alpha)-1$ straightforwardly indicates the contribution of the tree to the bias of the basal area estimator, since

$$E(\hat{G})-G=\frac{1}{|\mathbf{L}|}\sum_{i\in\mathbf{I}}A_{Ci}\left[\frac{\sin^2(\alpha/2)}{\kappa_i(\alpha)}-1\right] \tag{165}$$

(cf. Eqs. 77 and 81 in Section 4.1.3). To check Matérn's approximate theoretical result that, with viewing angle α of the magnitude 1°, this bias is the same as we would get by calipering every stem in the stand in a randomly chosen direction, that is,

$$E(\hat{G})-G\approx\frac{1}{|\mathbf{L}|}\sum_{i\in\mathbf{I}}\left[E_{\boldsymbol{\theta}}(\hat{A}_{1i})-A_{Ci}\right] \tag{166}$$

(cf. Eq. 85 in Section 4.1.3), $\sin^2(\alpha/2)/\kappa(\alpha)-1$ in each cross-section was compared to the relative within-cross-section bias $[E_{\boldsymbol{\theta}}(\hat{A}_1)-A_C]/A_C$ of the area estimator $\hat{A}_1$ based on one random diameter, computed already earlier (see Section 7.2).

The combined effect $\sin^2(\alpha/2)/\kappa(\alpha)\cdot A_C/(\pi D_j^2/4)$ was computed with the 22 diameter selection methods (see Section 7.2) in each cross-section. With the methods involving randomness (1–5, 1ξ–5ξ, 1ξ90, 4ξ90 and 5ξ90), the expectation of the effect

$$E\left[\frac{\sin^2(\alpha/2)}{\kappa(\alpha)}\cdot\frac{A_C}{\pi D_j^2/4}\right]=\frac{4}{\pi}\sin^2(\alpha/2)\,|\mathbf{M}(\alpha)|\,E\left[\frac{1}{D_j^2}\right] \tag{167}$$

over the diameter direction distribution was considered. The fractional moments $E[1/D_j^2]$ were estimated in a similar way as moments and product moments in Section 7.2 (cf. Eqs. 148, 149 and 152). With the methods involving the uniform direction distribution (1–5),

the moments were estimated as the simple means of the 180 or 180^2 systematic diameters raised to the power of –2 in each cross-section:

$$\begin{aligned}
&\hat{E}[D(\theta)^{-2}] = \frac{1}{180}\sum_{j=0}^{179} D(j\cdot 1°)^{-2} \ ,\\
&\hat{E}\left\{\left[\frac{D(\theta)+D(\theta+\pi/2)}{2}\right]^{-2}\right\} = \frac{1}{180}\sum_{j=0}^{179}\left\{\frac{D(j\cdot 1°)+D[(j+90)\cdot 1°]}{2}\right\}^{-2} \ ,\\
&\hat{E}\left\{\left[\sqrt{D(\theta)D(\theta+\pi/2)}\ \right]^{-2}\right\} = \frac{1}{180}\sum_{j=0}^{179} D(j\cdot 1°)^{-1}D[(j+90)\cdot 1°]^{-1} \ ,\\
&\hat{E}\left\{\left[\frac{D(\theta_1)+D(\theta_2)}{2}\right]^{-2}\right\} = \frac{1}{180^2}\sum_{k=0}^{179}\sum_{j=0}^{179}\left[\frac{D(j\cdot 1°)+D(k\cdot 1°)}{2}\right]^{-2} \ ,\\
&\hat{E}\left\{\left[\sqrt{D(\theta_1)D(\theta_2)}\ \right]^{-2}\right\} = \frac{1}{180^2}\sum_{k=0}^{179}\sum_{j=0}^{179} D(j\cdot 1°)^{-1}D(k\cdot 1°)^{-1} = \left[\frac{1}{180}\sum_{j=0}^{179} D(j\cdot 1°)^{-1}\right]^2 \ .
\end{aligned} \tag{168}$$

(Note that for $j+90 \geq 180$, $D[(j+90)\cdot 1°] = D[(j-90)\cdot 1°]$.) With the methods involving the non-uniform direction distributions of the Bitterlich diameters (1ξ–3ξ, $1\xi 90$), the moments were estimated as the weighted means of the diameter powers, the weights being determined as the relative sector areas of the inclusion region:

$$\begin{aligned}
&\hat{E}[D(\xi)^{-2}] = \sum_{j=0}^{179} w(j\cdot 1°)D(j\cdot 1°)^{-2} \ ,\\
&\hat{E}\left\{\left[\frac{D(\xi)+D(\xi+\pi/2)}{2}\right]^{-2}\right\} = \sum_{j=0}^{179} w(j\cdot 1°)\left\{\frac{D(j\cdot 1°)+D[(j+90)\cdot 1°]}{2}\right\}^{-2} \ ,\\
&\hat{E}\left\{\left[\sqrt{D(\xi)D(\xi+\pi/2)}\ \right]^{-2}\right\} = \sum_{j=0}^{179} w(j\cdot 1°)D(j\cdot 1°)^{-1}D[(j+90)\cdot 1°]^{-1} \ ,\\
&\hat{E}[D(\xi+\pi/2)^{-2}] = \sum_{j=0}^{179} w(j\cdot 1°)D[(j+90)\cdot 1°]^{-2} \ .
\end{aligned} \tag{169}$$

(Note that the weights $w(j\cdot 1°)$, $j=0, \ldots, 179$, sum to one.) And with the methods involving both types of diameters (4ξ–5ξ, $4\xi 90$–$5\xi 90$), the moments were estimated as the simple means of the weighted means (which in the case of the geometric mean of independent diameters turned into the product of the weighted and the simple mean):

$$\hat{E}\left\{\left[\frac{D(\xi)+D(\theta)}{2}\right]^{-2}\right\}=\frac{1}{180}\sum_{k=0}^{179}\sum_{j=0}^{179}w(j\cdot 1°)\left[\frac{D(j\cdot 1°)+D(k\cdot 1°)}{2}\right]^{-2},$$

$$\hat{E}\left\{\left[\sqrt{D(\xi)D(\theta)}\right]^{-2}\right\}=\left[\sum_{j=0}^{179}w(j\cdot 1°)D(j\cdot 1°)^{-1}\right]\left[\frac{1}{180}\sum_{k=0}^{179}D(k\cdot 1°)^{-1}\right],$$

$$\hat{E}\left\{\left[\frac{D(\xi+\pi/2)+D(\theta)}{2}\right]^{-2}\right\}=\frac{1}{180}\sum_{k=0}^{179}\sum_{j=0}^{179}w(j\cdot 1°)\left\{\frac{D[(j+90)\cdot 1°]+D(k\cdot 1°)}{2}\right\}^{-2}, \quad (170)$$

$$\hat{E}\left\{\left[\sqrt{D(\xi+\pi/2)D(\theta)}\right]^{-2}\right\}=\left\{\sum_{j=0}^{179}w(j\cdot 1°)D[(j+90)\cdot 1°]^{-1}\right\}\left[\frac{1}{180}\sum_{k=0}^{179}D(k\cdot 1°)^{-1}\right].$$

The distributions of $\sin^2(\alpha/2)/\kappa(\alpha)$ and $E[\sin^2(\alpha/2)/\kappa(\alpha)\cdot A_C/(\pi D_j^2/4)]$ were viewed in the set of the breast height cross-sections and in the set of all the cross-sections. The relation between $\sin^2(\alpha/2)/\kappa(\alpha)$ and cross-section shape, as expressed by the scalar shape indices (see Table 14 in Section 7.1), was studied with pairwise correlations and accompanying scatterplots.

8 Results with Discussion

8.1 Caveats on Data

As pointed out before (see Chapters 6 and 7), the trees examined in this study did not make up a proper probability sample, as the last stage of subsampling among the trees felled for the nationwide tree quality investigation was not probabilistic but subjective. This subjectivity manifested itself in the geographically uneven distribution of the plots over Finland (Fig. 22 in Chapter 6), as well as in the largely skewed size distribution of the stems (Fig. 23 in Chapter 6). Consequently, the empirical results reported here cannot really be generalised to the Scots pine population in Finland, but they rather illustrate the ideas of the theoretical part of the study (Chapters 2–5) and give a notion of the magnitude of the effects of non-circularity on cross-section area and stem volume estimation, as well as on stand total estimation from a Bitterlich sample, in Scots pine in Finland.

In comparison to the majority of previous empirical studies, however, our data made a somewhat novel combination of fairly detailed information on a relatively large number of observation units (709 disc contours at 8 relative and 2 fixed heights in 81 stems). Matérn´s (1990) data, presented a bit farther below, compare with our data in terms of the elaborate measurements but involve a considerably smaller number of stems and discs. Otherwise, non-circularity and its effects have typically been studied with simple diameter or radius measurements taken at breast height, or at one or more points in sawlogs, in data sets containing some dozens up to thousands of stems.

In addition to the non-generalisability (and non-repeatability!) of the results due to non-probabilistic sampling, three other, partly related, shortcomings in our data need be noted: First, as already mentioned above, the size distribution of the stems was largely skewed and bimodal, with only a small number of sawlog-size stems (8) and a modest size variation among the pulpwood-size stems. Due to this, the results on the large stems, which would be the most interesting economically, involve larger uncertainty than those on the small stems. Moreover, it was difficult to establish the effect of cross-section size or stem size on shape characteristics and on area and volume estimation errors; also, there was a risk to confound size effect with location effect, as all the sawlog-sized trees were growing in the two southernmost plots. Second, the number of observed cross-sections varied between the heights, with missing discs especially at the heights of 1% and 6 m (see Table 12 in Chapter 6). On this account, the means of cross-section characteristics (shape indices, area estimation errors etc.) became estimated with different precisions at different heights, and the comparisons between heights were based on slightly different sets of stems or on incomplete pairwise samples; clearly, the disc sets at different heights reflected the stem size distribution to different degrees, the height of 1% deviating particularly much from the other heights with its higher proportion (8/28) of the sawlog-size stems. With strongly height-dependent characteristics, in turn, the means and standard deviations taken over all the cross-sections might exhibit rather large biases, for instance because the weight of the 1% height was much lower than it should be due to the large number of missing observations. Also, in the 51 (=79–28) stems without the 1% disc available, the estimated true volume probably contained larger error than in the other stems, as in the butt of the tree the error in diameter has stronger influence on the stem volume estimate than at upper heights (true volume was obtained by integrating the cubic-spline-interpolated stem curve based on true area diameters, and between the stump height and the first observation height this stem curve was approximated with an interpolating parabola passing through the three lowermost observation points; see Section 7.3.1). At the same time, our results may give too optimistic a picture on the diameter selection effect with cubic-interpolated stem curve

and general volume estimator, as the diameter observations from the butt part that is the most irregular in shape were missing in 51 stems out of 79. Third, the dependence structure in the data (the cross-sections being interdependent within a stem, the stems interdependent within a plot, the plots interdependent within a cluster) complicated the assessment of the uncertainty in the means taken over cross-sections or stems: with positive correlations between cross-sections or stems, the standard errors of the means are likely to underestimate the true standard deviations of the means.

The measurements on the discs in the data can be considered practically free from measurement errors, as they were computed from the digital images (instead of being measured by hand or being results from some relatively rough computational approximations, as in the majority of previous studies). The errors due to photographing, print-making of the photographs, scanning, vectorisation of the digital raster images and scale computation can be regarded as practically negligible, except perhaps in the smallest 85% height discs where the modest resolution of scanning (see Chapter 6) may have caused some artefactual roughness in shape. (Nowadays, naturally, the digital images would be taken directly with a digital camera or a scanner with a much higher resolution, thus omitting the laborious and potentially error-prone phases of print-making and scanning.)

The fact that *our empirical results are based on debarked discs* naturally impedes their application into practice. It is not straightforward to assess how over-bark results would differ from the under-bark ones in Scots pine (cf. the empirical results by Matérn (1990)): on one hand, bark may tend to smooth wood undulations, whereupon the effect of diameter selection on area and volume estimation might be less pronounced over bark than under bark; on the other hand, with its irregularities, bark is likely to increase cross-sectional non-convexity, which would increase overestimation error in area and volume estimation.

Before entering into our results, we briefly present the empirical study by Matérn (1990), which provides the best comparison regarding cross-section shape and area estimation. Matérn's material consisted of 17 Scots pine and 22 Norway spruce stems, most of them sawlog-size, felled in 7 temporary plots in central Sweden. From the stems, discs of the thickness of 4 cm were sawn at breast height and at 6 relative heights (1%, 10%, 30%, 50%, 70%, 90%). From a subset of the discs comprising the breast-height discs of all the trees and the relative-height discs of 5 pines and 6 spruces, contour drawings were made both outside and inside bark; in all, a total of 45 pine and 52 spruce under-bark contours, as well as 47 and 58 over-bark contours, were included in the investigation. From each drawing, 36 radii of the cross-section and its convex closure, as well as 36 values of the support function of the cross-section (yielding 18 diameters), were measured in equidistant directions (with angle interval of 10°); as the maximum and the minimum diameter, the largest and the smallest of the 18 observed diameters were employed, whereas the true area, convex area, and convex perimeter were estimated by numerical integration from the observed radii and support function values (presumably by assuming linear course for the functions between the observations) . The shape of the convex closure of a cross-section was examined by means of ratio between the minimum and the maximum diameter D_{min}/D_{max}, diameter coefficient of variation CV_D, and correlation between perpendicular diameters $\rho_D(\pi/2)$ estimated from the 18 observed diameters, whereas the magnitude of non-convexity was assessed by means of the relative convex deficit in each cross-section. As to area estimation based on the circle area formula, Matérn already considered many of the diameter selection methods dealt with in this study (see Section 7.2); he compared the estimators in terms of average (over all cross-sections) relative bias defined with respect to the convex area. In addition to these traditional area estimators, he also considered estimators based on measurements obtained with some less common instruments (e.g. Biltmore stick and sector fork). However, he did not investigate the effect of cross-section shape variation (diameter selection) on stem volume estimation.

8.2 Cross-Section Shape

8.2.1 Shape of Convex Closure

Shape Indices

As pointed out in the methods section (see Section 7.1.1), the five shape indices (diameter coefficient of variation CV_D, ratio between the extreme diameters D_{min}/D_{max}, girth-area ellipse ratio b_e/a_e, correlation between perpendicular diameters $\rho_D(\pi/2)$, and angle between the extreme diameters $|\theta_{Dmax}–\theta_{Dmin}|$) computed on the convex closure of each cross-section do not provide unique or unambiguous information on shape, but very different shapes may have very similar index values. To give a flavour of the association between index values and shapes, examples of the convex closures of actual discs with the extreme index values are presented in Appendix K. In the following, we will summarise the distributions of the index values in the data. Since ellipse has been much used as a model for cross-section shape, we will also compare the values of CV_D and $\rho_D(\pi/2)$ observed in cross-sections to the values in the ellipses with the same axis ratio, realising, however, that due to the above-mentioned ambiguity, the information from the shape indices can only give evidence against the ellipticity hypothesis but not for it.

Judging from the diameter coefficient of determination CV_D, the within-cross-section variation in diameter was in general very moderate in the data (Table 19, Fig. 29); about 16% (110/709) of the convex closures were almost circular (or orbiform) with CV_D smaller than 1%. The observation height seemed to play a role in the diameter variation: in the butt of the stems, the convex closures tended to be more non-circular on average and vary more in shape than in the middle and upper parts of the stems, as indicated by the larger means, medians and standard deviations of CV_D at the two lowest relative heights (Fig. 29 A). This accords with previous findings based on other characteristics than CV_D (e.g. Tiihonen 1961 on Scots pine, Georgopoulos and Gofas 1966 on poplar species, Williamson 1975 on Douglas fir, Mäkinen 1998 on Scots pine, and Saint-André and Leban 2000 on Norway spruce) that cross-sections are more non-circular in the butt, and sometimes also in the top of a stem, than in the middle parts, presumably due to the influence of root and branch formation. The convex closures at 6 m (of which many (20/51) were located higher than the 70% relative height in the small stems of the data) appeared to be more regular on average but also vary more in their shape than those at 1.3 m (Fig. 29 A).

Table 19. Summary statistics of the distributions of diameter coefficient of variation CV_D, ratio between the minimum and the maximum diameter D_{min}/D_{max}, girth-area ellipse ratio b_e/a_e, absolute difference between the directions of the minimum and the maximum diameter $|\theta_{Dmin}–\theta_{Dmax}|$, and correlation between perpendicular diameters $\rho_D(\pi/2)$ in the set of all the discs (n=709).

Statistic	CV_D (%)	D_{min}/D_{max} (%)	b_e/a_e (%)	$\lvert\theta_{Dmax}–\theta_{Dmin}\rvert$ (°)	$\rho_D(\pi/2)$
Mean	1.96	93.7	86.3	65	–0.56
Std. dev.	1.16	3.1	3.7	16	0.42
Minimum	0.37	73.4	67.8	17	–0.99
1st quartile	1.20	92.5	84.9	54	–0.87
Median	1.73	94.4	87.2	68	–0.71
3rd quartile	2.43	95.8	88.9	79	–0.34
Maximum	9.94	98.5	93.4	90	0.78

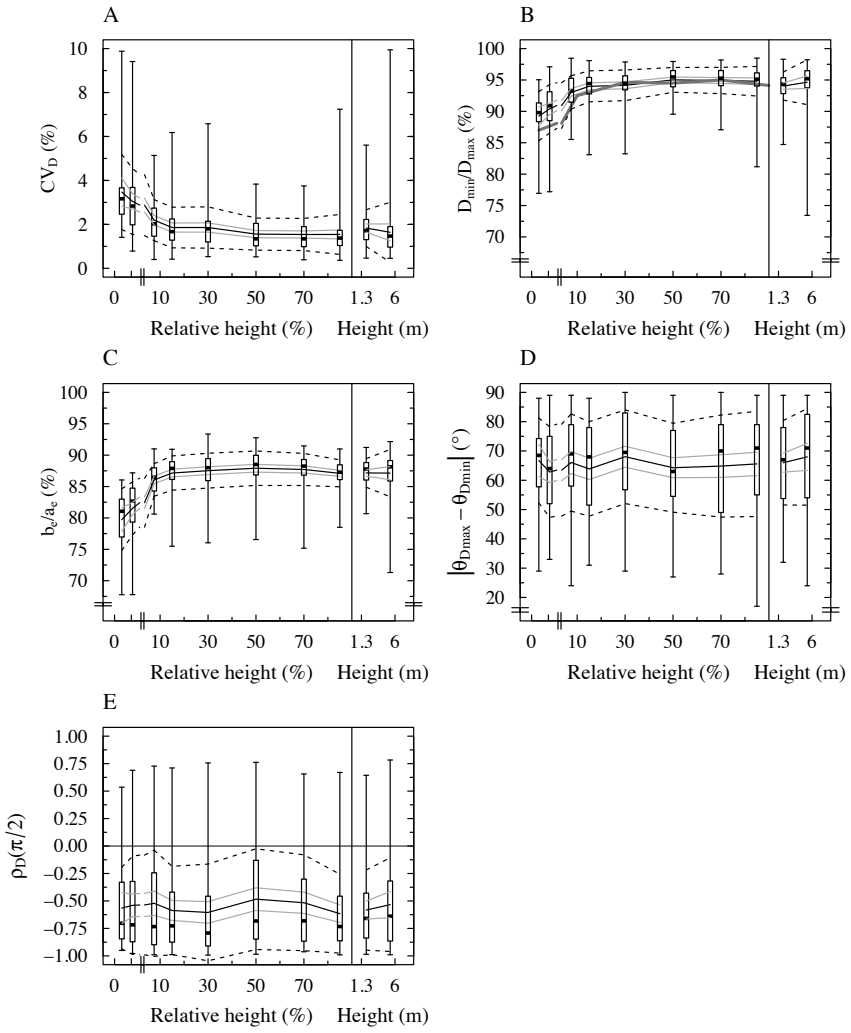

Fig. 29. Summarised distributions of the estimated diameter coefficient of variation CV_D (A), ratio between the minimum and the maximum diameter D_{min}/D_{max} (B), girth-area ellipse ratio b_e/a_e (C), absolute difference between the directions of the minimum and the maximum diameter $|\theta_{Dmin}–\theta_{Dmax}|$ (D), and correlation between perpendicular diameters $\rho_D(\pi/2)$ (E) in the cross-sections at the ten within-stem observation heights; the number of cross-sections varies between the heights (see Table 12 in Chapter 6). The box depicts the inter-quartile range bisected by the median, and the whiskers reach out to the extreme values in the data; the solid line denotes the arithmetic mean, whereas the dashed and thin grey lines below and above the mean indicate the magnitude of the sample standard deviation and twice the standard error of the mean (i.e., twice the sample standard deviation divided by the square root of the number of observations), respectively. The thick grey line in B gives the arithmetic means in the study by Matérn (1990).

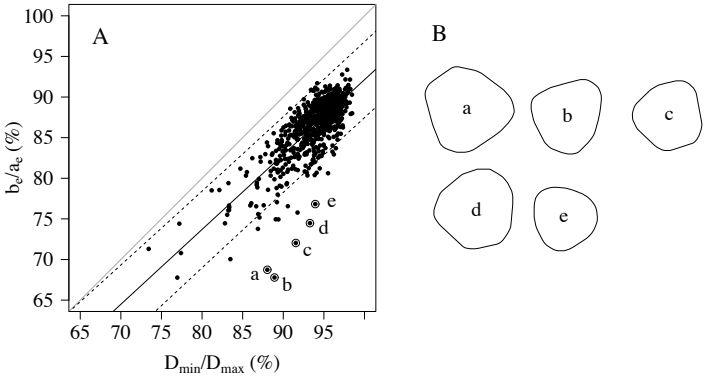

Fig. 30. Two alternative ways of determining ellipse axis ratio — as the ratio between the extreme diameters D_{min}/D_{max}, or as the girth-area ellipse ratio b_e/a_e — yielded very different values in the 709 cross-sections (A); the solid line denotes the regression relationship between the ratios, with the 95% prediction band (assuming normality) given by the dashed lines. The cross-sections with the largest difference between the ratios were characterised by some (tri)angularity (B); diameter coefficients of variation CV_D in these cross-sections were (a) 3.35%, (b) 3.94%, (c) 2.16%, (d) 1.94% and (e) 1.97%, and correlations between perpendicular diameters $\rho_D(\pi/2)$ (a) 0.11, (b) 0.77, (c) 0.69, (d) 0.62 and (e) 0.78; relative to the other discs, the disc in (a) is portrayed in half size.

The distribution of D_{min}/D_{max} (Table 19, Fig. 29 B) echoed the impression given by CV_D on the diameter variation. The difference between D_{min} and D_{max} appeared in general fairly small, being less than 10% in 89% (632/709) of the cross-sections. With respect to relative height, D_{min}/D_{max} behaved like a reflection of CV_D, although in a different scale (Fig. 29 B). This behaviour agreed with the results reported by Matérn (1990) on the basis of 45 cross-sections (Fig. 29 B): from the 30% relative height upwards, our mean values of D_{min}/D_{max} were strikingly similar to those of his, whereas at the lower heights he reported considerably smaller values, indicating more pronounced non-circularity in the lower parts of his 15 Scots pine stems (which were on average larger in size than our stems).

The generally high values of D_{min}/D_{max} would point to rather a modest ellipticity. The clearly lower values of the alternative axis ratio, the girth-area ellipse ratio b_e/a_e (Table 19, Fig. 29 C), however, imply that the non-circularity of the convex closures be more complex than just the ellipticity indicated by the difference in the extreme diameters: judging from their girth and area, the convex closures should be much flatter ellipses than what D_{min}/D_{max} suggest. Plotting b_e/a_e against D_{min}/D_{max} showed that the relationship between these two axis ratios was not simple (Fig. 30): particularly "triangular" cross-sections tended to have low b_e/a_e with high D_{min}/D_{max}. With the relatively larger inter-quartile range and standard deviation (Fig. 29 C), b_e/a_e also indicated larger variation in shape at the height of 1% than what D_{min}/D_{max} and CV_D relying solely on diameter information would suggest.

The distribution of the angle $|\theta_{Dmin}–\theta_{Dmax}|$ between D_{min} and D_{max} (Table 19, Fig. 29 D) did not support the ellipse model either: in only 10% (73/709) of the cross-sections, $|\theta_{Dmin}–\theta_{Dmax}|$ was within (85°, 90°], and irrespective of the observation height, the median and the mean of $|\theta_{Dmin}–\theta_{Dmax}|$ lay between 60° and 70°, with a pronounced vari-

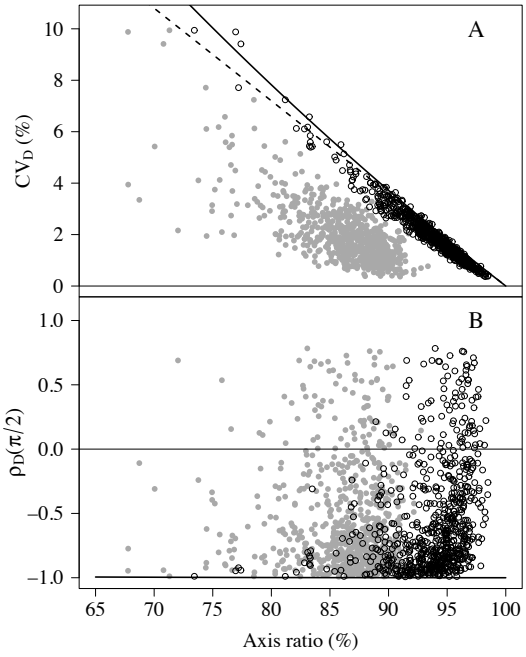

Fig. 31. Comparison of the values of diameter coefficient of variation CV_D (A) and correlation between perpendicular diameters $\rho_D(\pi/2)$ (B) in the 709 cross-sections to the values in an ellipse (thick black line), as a function of axis ratio; in the cross-sections, the axis ratio was determined either as the ratio between the extreme diameters D_{min}/D_{max} (black circles) or as the girth-area ellipse ratio b_e/a_e (grey dots). The linear relationship fitted between CV_D and D_{min}/D_{max} in the data (dashed line in A, with equation $CV_D = 36 - 0.36 \cdot D_{min}/D_{max}$, RMSE = 0.228 (percentage unit) and $R^2 = 0.962$) deviated from the actually curvilinear relationship in an ellipse, the smaller the axis ratio the larger the deviation. Note that in an ellipse $\rho_D(\pi/2)$ is practically constant irrespective of the axis ratio (as axis ratio increases from 65% to 100%, $\rho_D(\pi/2)$ decreases from –0.9945 to –1).

ation between the cross-sections (Fig. 29 D). Some earlier studies (e.g. Müller 1958b on Norway spruce, and Kärkkäinen 1975a on silver birch, pubescent birch and European aspen) have likewise established that D_{min} and D_{max} not be in general perpendicular to each other within a cross-section, whereas some other studies (e.g. Georgopoulos and Gofas 1966 on poplar species) have reported the reverse. If diameter varies little within a cross-section, D_{min} and D_{max} are not very distinct from other diameters and may be located very near each other (e.g. in this study $|\theta_{Dmin}–\theta_{Dmax}|$ assumed its minimum value in the cross-section where D_{min}/D_{max} attained its maximum value; see Figs. K2 A and K4 C in Appendix K).

The orientation of D_{min} and D_{max} with respect to relative height showed no pattern: the means or the medians of the rotation angles with respect to the directions at the lowest observation height exhibited no particular trend, and the variability of the angles was large at all the observation heights. This is consistent with previous results (e.g. Williamson 1975 on Douglas fir, and Kellogg and Barber 1981 on western hemlock) where no system in major axis rotation was found. Yet the sampling of the discs with respect to height may have been too sparse to detect regularity in orientation: the maximum distance between the

Table 20. Comparison of the between-cross-sections means and standard deviations of three shape indices (diameter coefficient of variation CV_D, ratio between the extreme diameters D_{min}/D_{max}, correlation of perpendicular diameters $\rho_D(\pi/2)$) to those reported by Matérn (1990). In the parentheses, Matérn's results from over-bark observations are given; n is the number of observations.

		This study			Matérn (1990)		
		Height			Height		
		1%	10–90%	1.3 m	1%	10–90%	1.3 m
CV_D	Mean[1]	3.85	1.88	2.01	4.66 (3.88)	2.24 (2.04)	2.60 (2.73)
(%)	Std.dev.	1.71	0.86	0.84	2.02 (1.58)	1.16 (1.02)	1.17 (1.04)
D_{min}/D_{max}	Mean	89.2	94.6	94.0	86.9 (89.2)	94.2 (94.4)	92.7 (91.9)
(%)	Std.dev.	3.9	2.3	2.2	6.0 (4.6)	3.1 (2.8)	3.2 (2.8)
$\rho_D(\pi/2)$	Mean	–0.57	–0.56	–0.58	–0.61 (–0.72)	–0.60 (–0.52)	–0.63 (–0.39)
	Std.dev.	0.37	0.42	0.36	0.38 (0.17)	0.41 (0.45)	0.25 (0.38)
n		28	400	80	5 (5)	25 (25)	15 (17)

[1] Quadratic mean

discs, 20% of the total height, typically involved several whorls of branches, which with their spiral phyllotaxis (known to characterise Scots pine) could cause spiral alternation in cross-section shape as well (e.g. through the formation of the water conduits sustaining the branches).

The within-cross-section correlation $\rho_D(\pi/2)$ between perpendicular diameters appears to capture slightly other aspects of shape than what CV_D and D_{min}/D_{max} reflecting mere diameter variation manage to seize (refer e.g. to Fig. 5 and Table 1 in Chapter 2, where the artificial shapes C and F with the same diameter variation assume strikingly different $\rho_D(\pi/2)$ values, or to Fig. K5 in Appendix K, where are portrayed visually rather similar real convex closures with similar magnitude of diameter variation but extremely divergent values of $\rho_D(\pi/2)$). However, the distribution of $\rho_D(\pi/2)$ in the data (Table 19, Fig. 29 E) did not endorse the use of the ellipse as a shape model either: in only 8% (56/709) of the cross-sections, $\rho_D(\pi/2)$ assumed values within [–1, –0.95), and in 13% (89/709) of the cross-sections, $\rho_D(\pi/2)$ was even positive, indicating some degree of squareness. With respect to height, no particular trend in $\rho_D(\pi/2)$ could be discerned (Fig. 29 E); also, in the light of $\rho_D(\pi/2)$, the shapes of the convex closures did not seem to vary more at the lowest relative heights than at the upper heights (Fig. 29 E), contrary to what the results on CV_D, D_{min}/D_{max} and b_e/a_e indicated.

An explicit comparison to ellipses with the same axis ratio (Fig. 31, cf. Table 6 in Matérn 1990), the ratio being determined as D_{min}/D_{max}, showed that while the diameter variation in the cross-sections in terms of CV_D was of the same magnitude as in ellipses, the values of $\rho_D(\pi/2)$ largely deviated from those of ellipses, particularly when the difference between D_{min} and D_{max} was small. If the axis ratio was determined as b_e/a_e, also the CV_D values in the cross-sections deviated substantially from the values in ellipses (Fig. 31). Eventually, few of the 709 cross-sections appeared truly elliptic, judging from these shape indices: the four most elliptic convex closures (selected by determining the axis ratio as D_{min}/D_{max} and by seeing that CV_D be close to that of an ellipse with the same D_{min}/D_{max} (cf. Fig. 31 A), b_e/a_e be close to D_{min}/D_{max}, and $\rho_D(\pi/2)$ be close to –1) are portrayed in Fig. K8 in Appendix K.

A comparison to Matérn's (1990) results (Table 20) showed that in his data (consisting of 45 under-bark cross-sections from 15 Scots pine stems of a larger size on average than those in this study), the within-cross-section variation in diameter, as characterised by

CV_D and D_{min}/D_{max}, was larger on average and varied more between the cross-sections, especially at the heights of 1% and 1.3 m. In D_{min}/D_{max}, the true difference between the studies was presumably even larger, as in Matérn's study the ratio was in all likelihood overestimated (D_{min} overestimated, D_{max} underestimated) due to the sparse sampling of diameters (only 18 diameters measured in each cross-section). The shapes of the convex closures as characterised with $\rho_D(\pi/2)$, however, were on average very similar in the studies, despite the considerable difference in the number of observed cross-sections and in the size of the stems. Interestingly, bark appeared to decrease shape irregularities in Matérn's data, especially at the height of 1%; yet due to the small number of observations this result remains somewhat uncertain. (In Norway spruce, Matérn reported less within-cross-section variation in diameter than in Scots pine, except at the height of 1%, where the variation was clearly larger. At this height, with $\rho_D(\pi/2)$ values closer to zero, the spruce cross-sections also appeared to be further from elliptic than pine cross-sections. In spruce, bark did not much influence the results.)

Besides Matérn's work, quantitative results on CV_D and $\rho_D(\pi/2)$ seem scarce in literature; Matérn mentions Kinashi (1954) who reported a CV_D of 2% for Japanese cedar, based on the observations on 10 stems, and Chacko (1961) who presented for four tree species some estimates of $\rho_D(\pi/2)$, which later, however, proved to refer to the between-stems correlations of the observations of perpendicular diameters. D_{min}/D_{max}, in turn, has been quite frequently quantified, especially in timber scaling studies; however, the measurements have usually been taken with caliper and are therefore likely to involve measurement errors. In general, the results collated by Matérn on D_{min}/D_{max} (see Table 7 in Matérn 1990) suggest that diameter variation be larger in deciduous trees than in coniferous trees; as to Scots pine, the results of this study appeared to agree with the previous results (our mean 93.7% vs. the weighted mean 94.7% of the studies concerning "pine" and listed in Table 7 in Matérn (1990), with the number of cross-sections as weights).

The main finding in the pairwise correlations between the shape indices (Table 21, Fig. 31 A) was that CV_D and D_{min}/D_{max} correlated almost fully negatively, as they did also in Matérn's (1990) data. Indeed, D_{min}/D_{max} may very well be used in these data to predict

Table 21. Correlations between the five shape indices (diameter coefficient of variation CV_D, ratio between the extreme diameters D_{min}/D_{max}, correlation of perpendicular diameters $\rho_D(\pi/2)$, girth-area ellipse ratio b_e/a_e, and absolute difference between the directions of the extreme diameters $|\theta_{Dmin}-\theta_{Dmax}|$) and the expected diameter μ_D in this study (n=709) and in that of Matérn (1990) (n=45). In the parentheses, Matérn's results based on over-bark observations (n=47) are given.

	This study						Matérn (1990)			
	CV_D	D_{min}/D_{max}	$\rho_D(\pi/2)$	μ_D	b_e/a_e	$\lvert\theta_{Dmax}-\theta_{Dmin}\rvert$	CV_D	D_{min}/D_{max}	$\rho_D(\pi/2)$	μ_D
CV_D	1						1			
D_{min}/D_{max}	–0.98	1					–0.98 (–0.93)	1		
$\rho_D(\pi/2)$	–0.35	0.30	1				–0.14 (–0.45)	0.03 (0.28)	1	
μ_D	0.20	–0.22	0.01	1			–0.51 (–0.33)	0.43 (0.14)	–0.05 (0.16)	1
b_e/a_e	–0.73	0.77	–0.04	–0.16	1					
$\lvert\theta_{Dmax}-\theta_{Dmin}\rvert$	0.19	–0.15	–0.60	0.01	0.12	1				

CV_D linearly with $CV_D = 36 – 0.36 \cdot D_{min}/D_{max}$ (Fig. 31 A); Matérn (1990, p. 15) obtained a very similar relationship $CV_D = 37 – 0.37 \cdot D_{min}/D_{max}$, although he computed CV_D and D_{min}/D_{max} from only 18 diameters in each cross-section. Also b_e/a_e exhibited moderate linear dependence on CV_D and D_{min}/D_{max}, whereas $\rho_D(\pi/2)$ did not; this backs up the idea that $\rho_D(\pi/2)$ depicts such aspects of shape that are not attributable to mere diameter variation (interestingly, $\rho_D(\pi/2)$ correlated very modestly with $|\theta_{Dmin}–\theta_{Dmax}|$, which would suggest that $|\theta_{Dmin}–\theta_{Dmax}|$ might have some meaning as a shape index, even with a small within-cross-section variation in diameter). None of the shape indices appeared to co-vary with the size of cross-section (as expressed with the mean diameter μ_D), as was the case also in Matérn's (1990) data. Concerning D_{min}/D_{max}, this agrees with some earlier results (e.g. Tirén 1929 on over-bark cross-sections at breast height in Scots pine and Norway spruce), but contradicts with some others where a slight increase in diameter variation along with size was reported (e.g. Bøhmer 1935 and Kärkkäinen 1975b on Scots pine sawlogs, and Williamson 1975 on Douglas fir sawlogs) or where non-circularity in cross-sections was seen to increase with age (e.g. Saint-André and Leban 2000 on sawlog-size Norway spruce stems, based on data of interpolated tree rings). The correlations did not vary noteworthily along with the observation height.

Directional Variation in Diameter

Since the circle has the smallest perimeter among convex planar figures with area A_C, its diameter D_{Ac} (perimeter divided by π) is smaller than the expected diameter (perimeter divided by π) of any non-circular convex figure with the same area. Therefore it was expected that the discretely observed relative diameter error function $[D(\theta)–D_{Ac}]/D_{Ac}$, $\theta=j\cdot1°$, j=0, ..., 179, would assume clearly more positive values (in magnitude or in number) than negative ones within a cross-section.

With the N–S direction as the reference direction, a clearly systematic directional pattern in diameter errors was observed at the height of 1% (Fig. 32): the diameter errors were on average negative in directions 45°–100° and attained their largest values in directions approximately perpendicular to these directions, that is, in directions 135°–190°. In other words, at this height, the diameters taken approximately between the NW–SE and W–E directions were on average the smallest in the cross-sections and would result in underestimates of the convex area of the magnitude 0–1.6% when substituted in the circle area formula ($[D(\theta)–D_{Ac}]/D_{Ac}=p \Rightarrow [\hat{A}(\theta)–A_C]/A_C=[D(\theta)^2–D_{Ac}^2]/D_{Ac}^2=(p+1)^2–1$), whereas the diameters taken between the SW–NE and S–N directions were on average the largest and would yield overestimates of the magnitude 3.6–5.7%. Apparently, the phenomenon did not occur in some individual cross-sections only, as the behaviour of the mean curve was supported by the median curve. A similar directional pattern, although much feebler in magnitude, could be found at the height of 50%, and with a slight phase transition at the heights of 2.5% and 6 m (Fig. 32).

As the trees included in the study were felled in different parts of Finland (the 28 stems in which the discs at the height of 1% were observed grew in the clusters 1–10; see Fig. 22 in Chapter 6), the phenomenon cannot be attributed to local factors such as site conditions and stand structure (resulting in asymmetric space available for growth around a tree) or small-scale topography. Instead, a plausible explanation might be provided by the south-westerly winds prevailing in Finland, combined with the relatively flat topography of the country: the torsional moment caused by the wind stress results in asymmetric growth, possibly through formation of reaction wood, that strengthens the stem in the directions opposite to the pressure. Some previous studies give support for this explanation: Müller

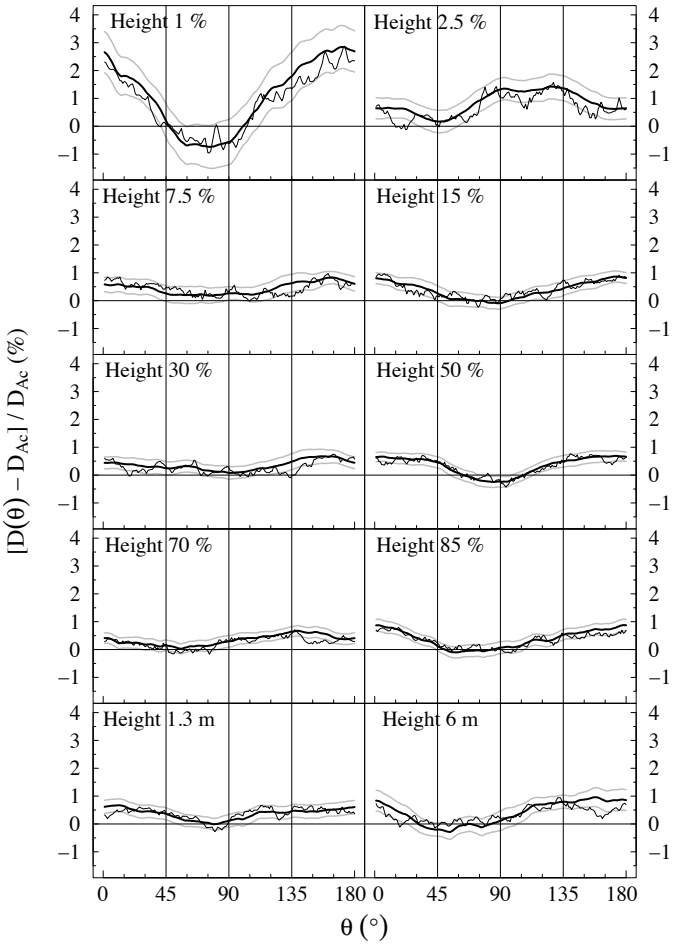

Fig. 32. Mean (thick black line), median (thin black line), and mean ± its standard error (standard deviation divided by the square root of the number of observations; grey line) of the discretely observed diameter error functions $[D(\theta)–D_{Ac}]/D_{Ac}$, $\theta=j\cdot1°$, j=0, ..., 179, at the ten observation heights. The diameter direction θ is determined with respect to the N–S direction and increasing anticlockwise.

(1958a) observed a striking similarity between the wind direction distribution and D_{max} direction distribution in Douglas fir in several places in Germany, whereas Robertson (1990, 1991) found a clear association between the prevailing wind direction and the directionality of compression wood zones, mean wood density, tree-ring width and stem eccentricity in balsam fir in Newfoundland. However, our results somewhat contradict with the observations of Heikkilä (1913), who reported the direction of D_{max} in Scots pine to be most frequently parallel to NW–SE direction in Viitasaari (63°5′N 25°51′E, cf. Fig. 22) and to W–E direction in Evo-Vesijako (61°21′N 25°6′E, cf. Fig. 22); however, he also reported confounding factors (slope, clearcut borderline) affecting the results.

With the direction of D_{max} as the reference direction, the average directional pattern in diameter errors quite predictably became U-shaped at all the observation heights (Fig. 33):

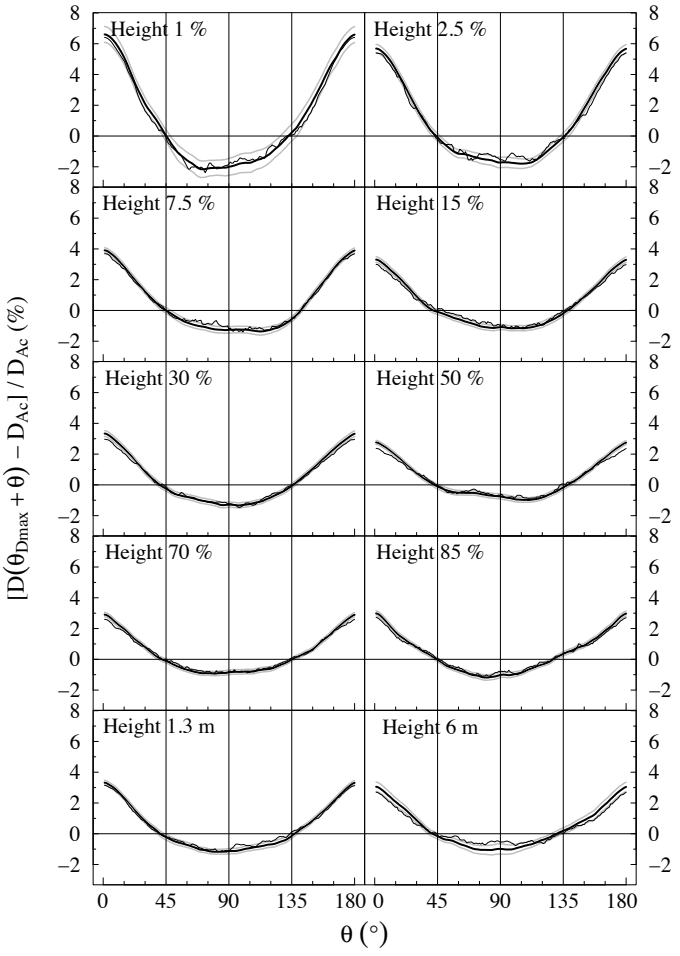

Fig. 33. As Fig. 32, but the diameter direction θ is determined with respect to the direction of the maximum diameter θ_{Dmax} (and increasing anticlockwise).

diameters located approximately within ±45° around D_{max} would on average considerably overestimate convex area when substituted in the circle area formula, whereas diameters located 45°–135° anticlockwise from D_{max} would then yield underestimates of far less pronounced magnitude. The overestimation being far more peaked than the underestimation, especially at the low observation heights, would imply that the change in diameter be far more rapid around D_{max} than around D_{min}. The location of the minimum average diameter error was seen to deviate from 90° and vary with observation height, which well agreed with the results obtained on the angle $|\theta_{Dmin}–\theta_{Dmax}|$ between D_{min} and D_{max} (cf. Fig. 29 D). At all the observation heights, the between-cross-sections variation of the diameter errors was of the same magnitude as above with the N–S direction as the reference direction (note the different scales in Figs. 32 and 33).

8.2.2 Non-Convexity

Convex Deficit

The amount of non-convexity was exiguous in the data (Table 22): in about 87% (614/709) of the cross-sections, the convex deficit was less than 1%. On the other hand, none of the cross-sections was exactly convex, the minimum convex deficit being 0.25%; at least a part of the observed non-convexity may thus be regarded as an artefact caused by the low resolution in the scanning of the photographs (see Chapter 6). Probably ascribable to root and branch formation, the convex deficit was on average larger in the base and in the top of the stems and less pronounced in the middle parts (Fig. 34); the variation between the cross-sections, however, was larger in the base than in the top. The observations at 1.3 m and 6 m parallelled this pattern (Fig. 34), as in many of the stems (20/51) 6 m was located higher than the 70% relative height. The largest convex deficit was found in the disc sawn at the height of 2.5% (see Fig. K6 A in Appendix K).

Compared to the discs of this study, the cross-sections examined by Matérn (1990) appeared on average more non-convex in the base of the stems and less non-convex in the upper parts; further, bark appeared to magnify non-convexity considerably (Table 23, Fig. 34). Recall, however, that Matérn did not measure the true and convex areas of the cross-sections but estimated them from 36 equiangular radii with numerical integration, which together with his small number of observations makes the actual difference between his and our study difficult to establish. (In Norway spruce under bark, Matérn reported similar amount of non-convexity as in Scots pine. In spruce, bark increased non-convexity only little.)

Besides Matérn's work, rather few results on convex deficit appear in literature, here are some examples: Perkal (1948) reported an average value of 0.76% concerning 38 discs in 22 trees (species not mentioned); Kärkkäinen (1975a), in turn, reported the convex deficit to be on average less than 1% in the end sections of 420 silver birch and 240 European aspen logs; Gregoire et al. (1990) found practically no non-convexity in 101 breast height cross-sections of various species of which majority (65/101) were red spruce; finally, Loetsch et al. (1973) presented as an example a teak cross-section with the convex deficit increasing with age and ending up to 8.5% at the age of 120 years.

The amount of non-convexity in a cross-section exhibited no association with the size and shape of the convex closure, as indicated by the low correlations between the convex deficit and the size and shape indices (Table 24). The examination by observation height, however, revealed a slight negative dependence on the size (the larger the size, the smaller

Table 22. Summary statistics of the distribution of relative convex deficit $(A_C–A)/A_C$ in the set of all the discs (n=709).

Statistic	$(A_C–A)/A_C$ (%)
Mean	0.70
Std. dev.	0.29
Minimum	0.25
1st quartile	0.54
Median	0.63
3rd quartile	0.81
Maximum	2.88

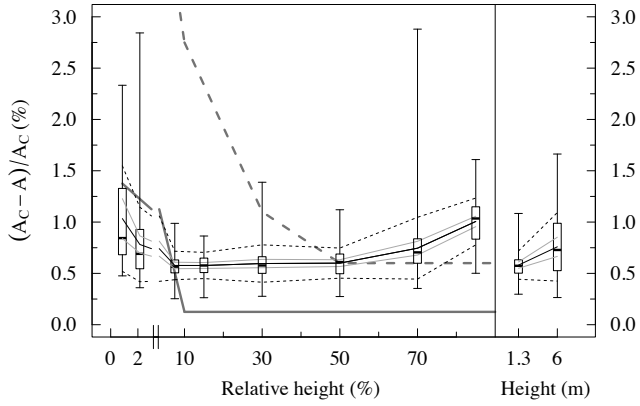

Fig. 34. Summarised distribution of relative convex deficit within a cross-section $(A_C–A)/A_C$ at the ten within-stem observation heights. (For the explanation of the boxplot and the lines, refer to the caption of Fig. 29.) The thick grey lines give the arithmetic means in the study by Matérn (1990); the solid line denotes the results under bark and the dashed line over bark.

Table 23. Comparison of the between-cross-sections means and standard deviations of relative convex deficit $(A_C–A)/A_C$ to those reported by Matérn (1990). In the parentheses, Matérn's results obtained from over-bark observations are given; n is the number of observations.

		This study			Matérn (1990)		
		Height			Height		
		1%	10–90%	1.3 m	1%	10–90%	1.3 m
$(A_C–A)/A_C$ (%)	Mean	1.03	0.71	0.58	1.34 (4.83)	0.15 (1.14)	0.16 (3.18)
	Std.dev.	0.51	0.26	0.14	1.53 (0.93)	0.10 (1.08)	0.15 (1.07)
n		28	400	80	5 (5)	25 (25)	15 (17)

Table 24. Correlation of relative convex deficit $(A_C–A)/A_C$ with the five shape indices depicting the convex closure of a cross-section (diameter coefficient of variation CV_D, ratio between the extreme diameters D_{min}/D_{max}, correlation of perpendicular diameters $\rho_D(\pi/2)$, girth-area ellipse ratio b_e/a_e, and absolute difference between the directions of the extreme diameters $|\theta_{Dmin}–\theta_{Dmax}|$) and with the size of a cross-section (expected diameter μ_D) in this study (n=709) and in that of Matérn (1990) (n=45). In the parentheses, Matérn's results based on over-bark observations (n=47) are given.

	This study						Matérn (1990)			
	CV_D	D_{min}/D_{max}	$\rho_D(\pi/2)$	μ_D	b_e/a_e	$\lvert\theta_{Dmax}–\theta_{Dmin}\rvert$	CV_D	D_{min}/D_{max}	$\rho_D(\pi/2)$	μ_D
$(A_C–A)/A_C$	0.17	–0.20	0.03	–0.39	–0.47	–0.08	0.57 (0.09)	–0.57 (–0.13)	0.26 (0.15)	–0.32 (0.65)

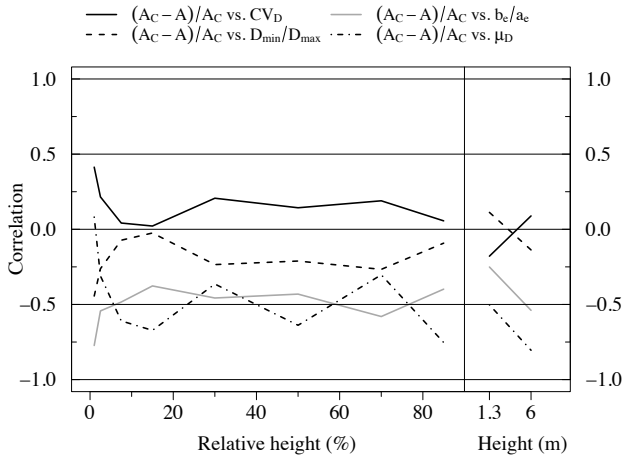

Fig. 35. Correlation of relative convex deficit $(A_C–A)/A_C$ with diameter coefficient of variation CV_D, ratio between the extreme diameters D_{min}/D_{max}, girth-area ellipse ratio b_e/a_e, and mean diameter μ_D at the ten observation heights. (Correlation of convex deficit with correlation between perpendicular diameters $\rho_D(\pi/2)$ is not shown as it was close to 0 at all the observation heights.)

the convex deficit) at the heights of 15%, 50%, 85% and 6 m, as well as a negative correlation with the girth-area ellipse ratio at the height of 1% (Fig. 35). Matérn (1990) found no clear connection between the amount of non-convexity and the size and shape of the convex closure either (Table 24); yet the modest positive correlations he found between the under-bark convex deficit and the diameter variation on one hand (large diameter variation implying irregularity in under-bark shape and thus proneness to under-bark non-convexity), and between the over-bark convex deficit and the disc size on the other hand (the effect of bark being more pronounced in large trees), suggest that in larger stems such associations might exist.

Directional Variation in Breadth

Non-convexity evinced no general dependence on direction, no matter if the direction was taken with respect to the N–S direction or the direction of D_{max}. At each observation height, the between-cross-sections median function of the discretely observed relative breadth difference functions $[B_C(\theta)–B(\theta)]/\overline{B}$, $\theta=j\cdot 1°$, j=0, 1, ..., 179, ran fairly steadily at the level of 0.3–0.5% (higher in the base and in the top of the stems, lower in the middle parts) across the direction θ. The same held for the mean function at all other observation heights except the two lowest ones (at the heights of 1% and 2.5%, the mean function exhibited four peaks of the magnitude of 0.25–0.5% above the median level, but these were caused by few individual cross-sections, as also indicated by the large values of the standard deviation functions).

8.2.3 True Shape

Mean Shape

When the radius direction was determined with respect to the N–S direction, the mean shape $\hat{\mu}_{R^*}(\theta)$ obtained as the average of the pre-shapes $R^*(\theta)=R(\theta)/\overline{R}_q$ of the cross-sections differed little from a circle: at all the observation heights except that of 1%, the mean function of the discretely observed relative radius error functions $[R(\theta)-\overline{R}_q]/\overline{R}_q=R(\theta)/\overline{R}_q-1$, $\theta=j\cdot 1°$, $j=0, 1, ..., 359$, ran approximately within ±1% from the zero, that is, the 360 radii deviated on average less than 1% from their quadratic mean $\overline{R}_q$ (Fig. 36). At the height of 1%, the

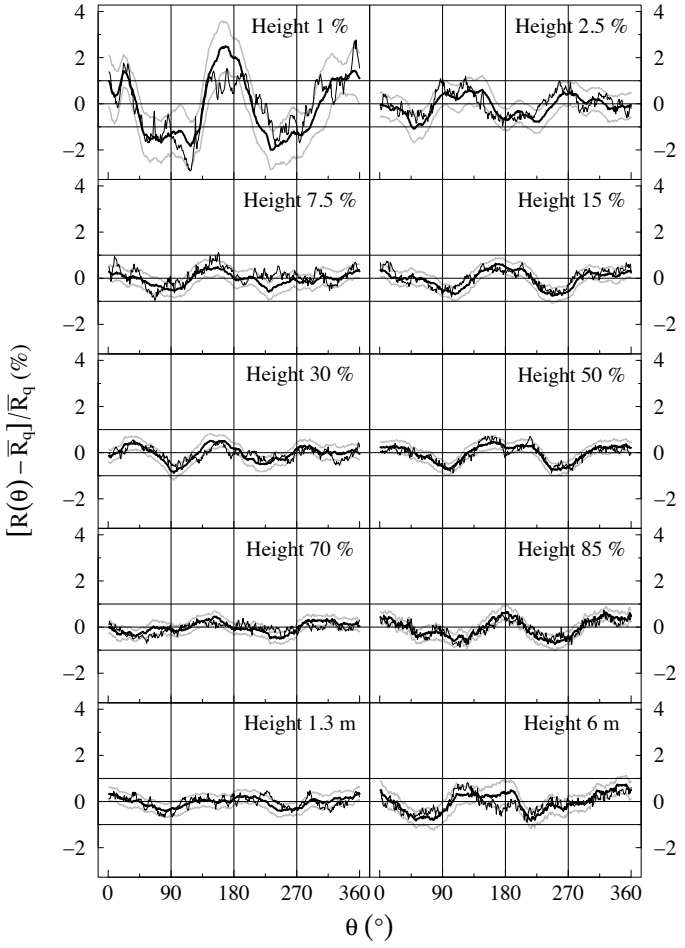

Fig. 36. Mean (thick black line), median (thin black line), and mean ± its standard error (grey line) of the down-scaled pre-shape configurations $R^*(\theta)-1$, $\theta=j\cdot 1°$, $j=0, ..., 179$ (i.e., the discretely observed radius error functions $[R(\theta)-\overline{R}_q]/\overline{R}_q$, where $\overline{R}_q$ is the quadratic mean of the radii $R(\theta)$ within the cross-section), at the ten observation heights. The radius direction θ is determined with respect to the N–S direction and increasing anticlockwise. The mean line equals the estimated mean shape $\hat{\mu}_{R^*}(\theta)$ from which 1 has been subtracted (cf. Fig. 38).

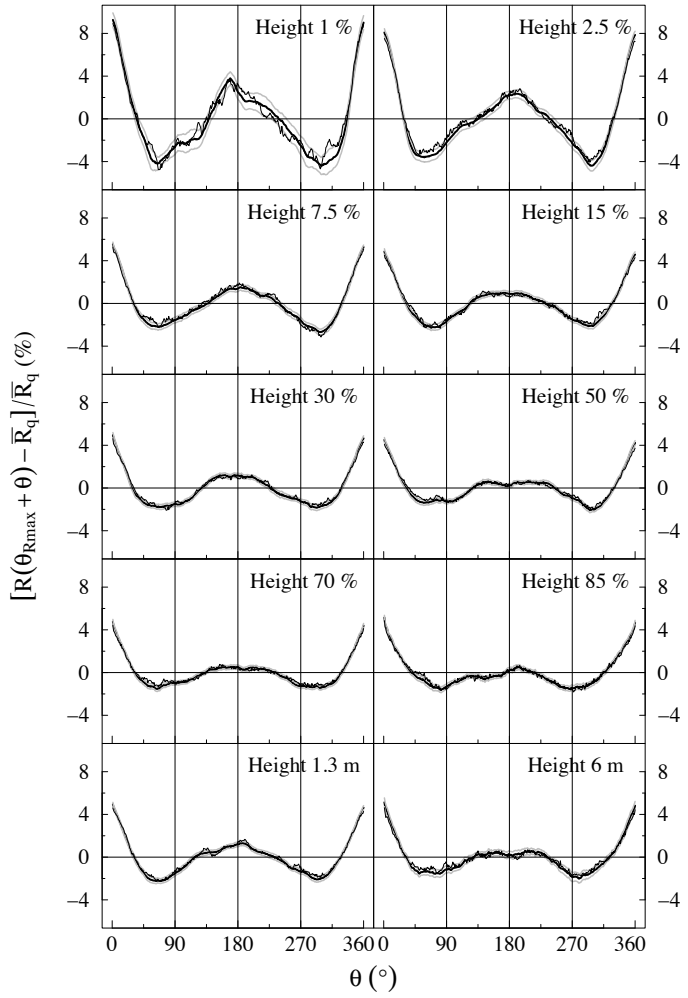

Fig. 37. As Fig. 36, but the radius direction θ is determined with respect to the direction of the maximum radius R_{max} (and increasing anticlockwise).

radii exhibited more than double that range of average relative deviation, but even at that height the mean shape was difficult to differentiate visually from a circle (Fig. 38 A). The directions of the hollows and bulges observed in the mean shape at the height of 1% agreed well with the directional pattern observed earlier in the diameters (cf. Fig. 32).

With the direction of R_{max} as the reference direction, the mean shape simply appeared to reflect the placement of the centre of gravity (from which the radii to the contour were measured) within the discs: at almost all the observation heights, the mean shape stretched outwards from a circle approximately in the directions –30°–30° and 135°–240° anticlockwise from R_{max}, and drew inwards in the intermediate directions, with the swelling being clearly steeper and more pronounced around the R_{max} direction than in the approximately opposite directions (Fig. 37). The two local maxima of the mean function were not 180° from each other but their mutual locations varied with height (Fig. 37). These deviations from a circle, resulting in a slightly asymmetric oviform shape, were large enough to be also visually discerned at the heights of 1% and 2.5% (Fig. 38 B).

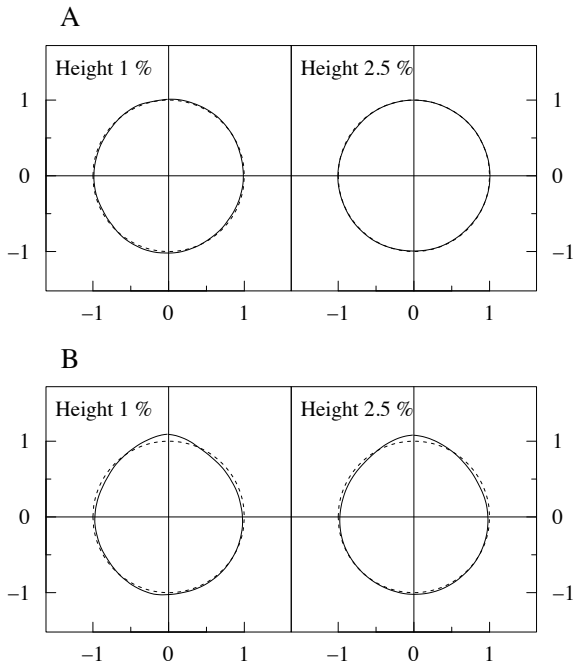

Fig. 38. Estimated mean shape $\hat{\mu}_{R*}(\theta)$ of the cross-sections (black line) illustrated in plane and compared to the unit circle (dashed line) at the two lowest observation heights: y-axis is parallel to the N–S direction (A) or to the direction of the maximum radius R_{max} (B).

Shape Variability

No matter if the radius direction was determined with respect to the N–S direction or with respect to the direction of R_{max}, the variability of the cross-section pre-shapes $R^*(\theta)=R(\theta)/\overline{R}_q$ around the mean shape $\hat{\mu}_{R*}(\theta)$ (i.e., the sum of the variances of the 360 residual variables $R^*(\theta)–\hat{\mu}_{R*}(\theta)$, $\theta=j\cdot 1°$, j=0, ..., 359, in the set of the cross-sections at the particular height) was manifestly the largest at the two lowest observation heights, decreased then along with height, to increase slightly again in the top of the stems (the variance of the pre-shape residuals was larger at the heights of 6 m and 85% than at the heights of 1.3 m and 70%, respectively; Figs. 39 and 40). These results accord well with our previous findings on the shape indices. Quite naturally, employing the R_{max} direction as the reference direction yielded smaller shape variability, only 60–72% of that with the N–S direction as the reference direction (Figs. 39 and 40).

With the N–S direction as the reference direction, the first six principal components at each observation height explained 81–91% of the total variance of the residual variables (Fig. 39). At most of the heights, the first two components captured clearly the largest portions of the variability, but their combined share did not amount to more than 48–61% of the total variance. The slightly dominating first component seemed to embody a regular variation around the SW–NE and NW–SE directions resembling the variation that was earlier found on diameter (cf. Fig. 32) and explained with the prevailing wind directions. The second component, in turn, appeared to include a similar kind of variation with a phase

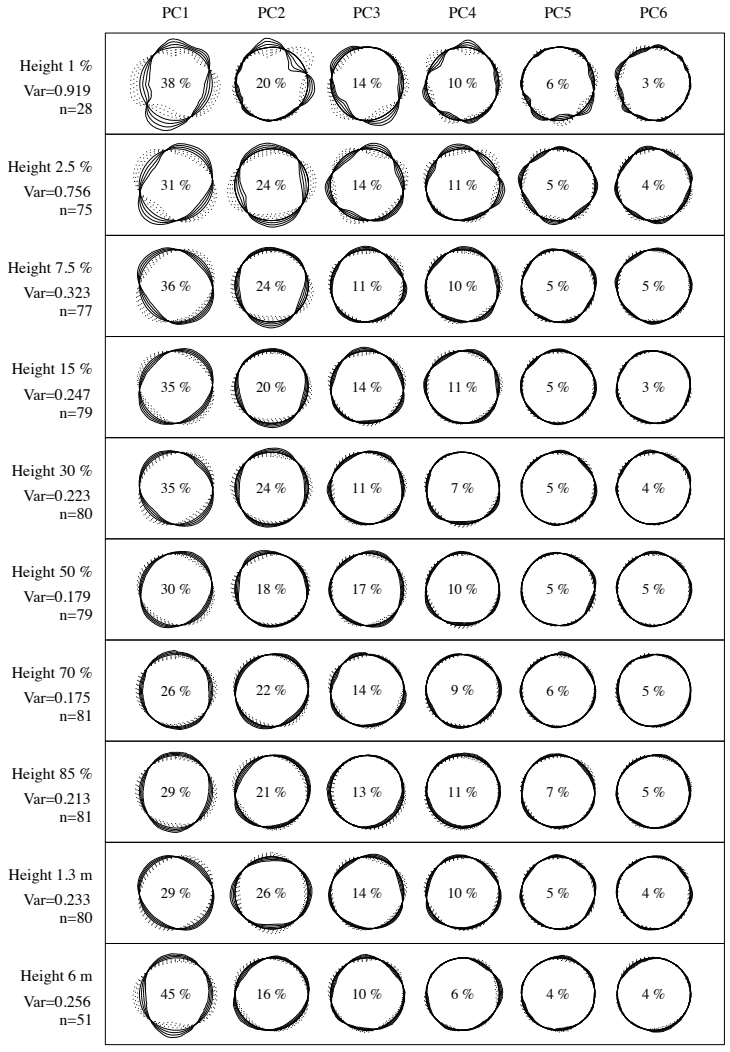

Fig. 39. Visualisation of the first six principal components (PC) estimated from the covariance matrix of the pre-shape residuals $R^*(\theta)–\hat{\mu}_{R*}(\theta)$, $\theta=j\cdot 1°$, j=0, ..., 359, at each of the ten observation heights, the radius direction θ being determined with respect to the N–S direction (y-axis is parallel to the N–S direction and the direction is increasing anticlockwise): around the mean shape (thick line), contours in the direction of the PC coefficient vector are drawn, the coefficients being weighted by 6, 4, 2 (thin line), –2, –4 and –6 (dotted line) standard deviations of the PC (see Eqs. 144 and 146 in Section 7.1.3). The percentage gives the proportion explained by the principal component of the summed variance (Var) of the 360 residual variables at the particular height. The number of observations (n) varied with height.

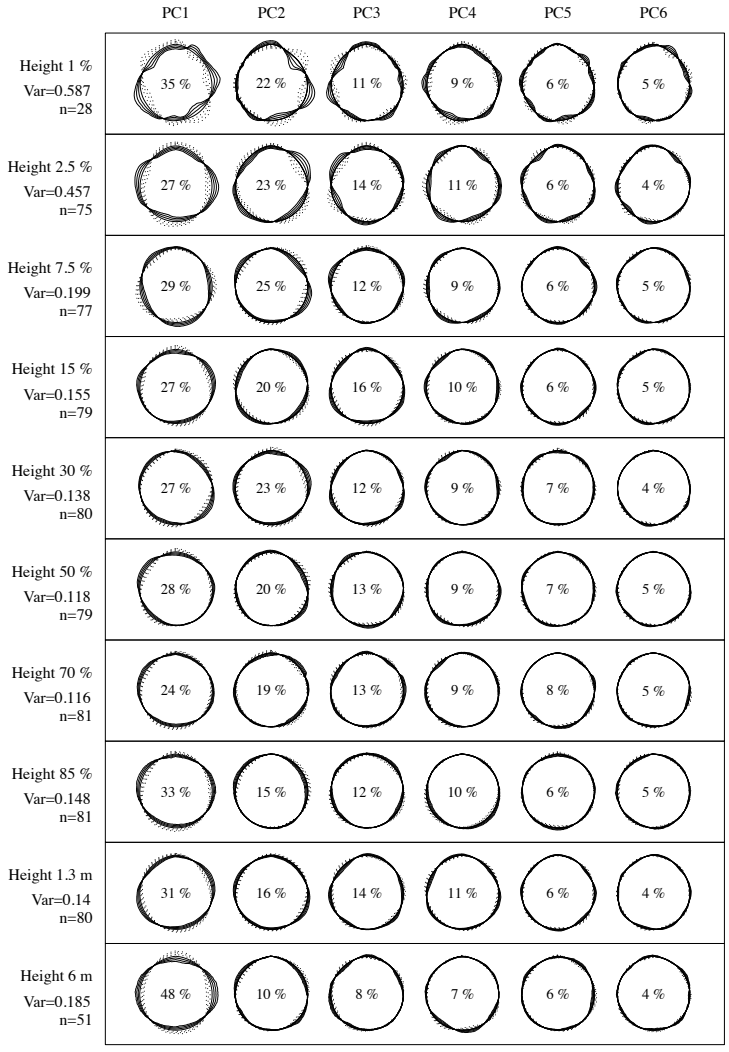

Fig. 40. As Fig. 39, but the radius direction θ is determined with respect to the direction of the maximum radius R_{max} (y-axis is parallel to the direction of R_{max} and the direction is increasing anticlockwise).

transition of approximately 30°–45° — except at the height of 1%, where the second component comprised some strong shape irregularities between the N–S and E–W directions and where the third component then appeared to be the phase transition component. For the rest of the components, interpretations are difficult to give; apart from the heights of 1% and 2.5%, the variability around the mean shape was so small that the visualisations of the components, even if heavily exaggerated as in our figures, were tricky to decipher.

With the R_{max} direction as the reference direction, the first six principal components at each observation height explained 78–88% of the total variance (Fig. 40). The dominance of the first component was weaker than with the N–S direction as the reference direction, and the variability was in general slightly more evenly distributed between the components. No general variability patterns could be found in the components: at the height of 1%, the

visualisations of the first two components resembled strikingly those obtained with the N–S direction as the reference direction, with some phase transition only, as if the R_{max} directions in the separate discs at the lowest height had been fairly close to each other (which was not the case); at many other heights, the first component appeared to reflect somewhat irregular ovality, resulting from radius variation around four main directions, these directions changing along with height but being at approximately 45° angle to each other.

The plots of the standardised principal component scores against each other and against the within-cross-section means of the pre-shape residuals revealed slightly deviating cross-sections with somewhat divergent principal component scores (at the heights of 15%, 85%, 1.3 m and 6 m with the N–S direction as the reference direction, and at the heights of 15%, 30% , 70%, 85%, 1.3 m and 6 m with the R_{max} direction as the reference direction); none of these, however, could be regarded as a true outlier. Cross-section size showed no association with the shape deviation or with the standardised scores.

8.3 Estimation of Cross-Section Area

In the theoretical part of this study (Section 3.3), we found that the area estimator $\hat{A}_0$ involving girth diameter (mean diameter over the uniform direction distribution, obtained by dividing convex perimeter by π) makes an adequate baseline estimator, with respect to which the biases of the estimators $\hat{A}_1$–$\hat{A}_5$ involving diameters with the uniform direction distribution can be expressed. Further, the relative error of $\hat{A}_0$ with respect to convex area (relative isoperimetric deficit $(\hat{A}_0–A_C)/A_C$) may also be regarded as a shape index, "a measure of the deviation from circular form" (Matérn 1990). Due to this special standing of $\hat{A}_0$, we here first examine in more detail its relative errors and their relation to other shape indices, to amount of non-convexity and to cross-section size in our data. After this, we compare all our area estimators $\hat{A}_0$, $\hat{A}_1$–$\hat{A}_{11}$, $\hat{A}_{1\xi}$–$\hat{A}_{5\xi}$, $\hat{A}_{1\xi}$, $\hat{A}_{4\xi}$, $\hat{A}_{5\xi}$, $\hat{A}_{min}$ and $\hat{A}_{max}$ (the combinations of the 22 diameter selection methods and the circle area formula; see Section 7.2) in terms the distributions of their estimated relative within-cross-section biases, standard deviations and RMSEs.

8.3.1 Reference Estimator Based on Girth Diameter

The relative error of the estimator $\hat{A}_0$ with respect to convex area was of the same meagre magnitude as the amount of non-convexity in the data (Table 25; cf. Table 22): in 74% (528/709) of the cross-sections, the isoperimetric deficit was less than 1%, and only in three very non-circular cross-sections it amounted to more than 5% (see Fig. K7 in Appendix K). The behaviour of the isoperimetric deficit with respect to relative height reflected our previous finding that the convex closures were more non-circular on average and more variable in shape in the butt of the stems than in the middle and upper parts (Fig. 41 A). Between the absolute observation heights of 1.3 m and 6 m, however, the difference lay basically only in the maximum value (one individual cross-section), which caused the difference also in variance (Fig. 41 A).

The relative error of $\hat{A}_0$ with respect to true area can be thought to stand for the combined effect of the convex and isoperimetric deficits (with the slight flaw of having true area instead of convex area in the denominator); indeed, the (first order) summary statistics of the distribution of this relative error (Table 25) equalled approximately the sum of the summary statistics of the deficits (Tables 22 and 25). As the deficits were in general small in the data, so was also their combined effect: in 82% (578/709) of the cross-sections, the relative

Table 25. Summary statistics of the distribution of the error of the girth diameter estimator $\hat{A}_0$ with respect to convex area A_C (isoperimetric deficit) or to true area A in the set of all the discs (n=709).

Statistic	$(\hat{A}_0–A_C)/A_C$ (%)	$(\hat{A}_0–A)/A$ (%)
Mean	0.90	1.62
Std. dev.	0.67	0.86
Minimum	0.18	0.46
1st quartile	0.52	1.14
Median	0.71	1.39
3rd quartile	1.01	1.84
Maximum	5.78	8.30

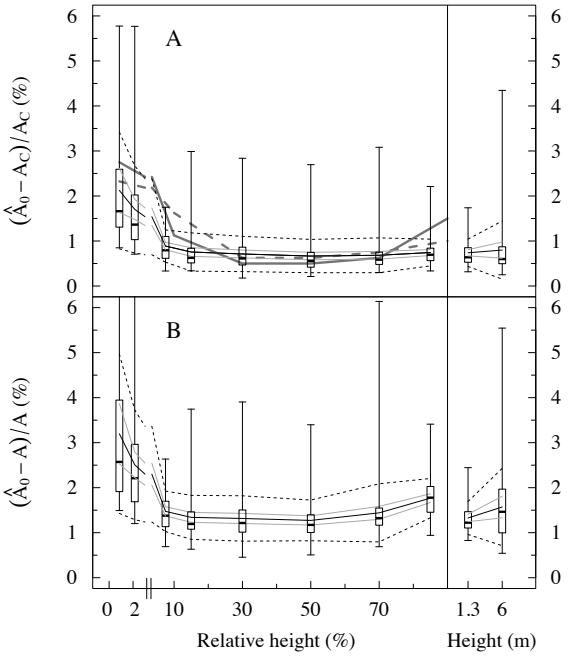

Fig. 41. Summarised distributions of the relative errors of the girth diameter area estimator $\hat{A}_0$ with respect to convex area A_C (A; relative isoperimetric deficit) or true area A (B) at the ten observation heights; the maximum values at the heights of 1% and 2.5% that are not shown in B were 8.30% and 6.86%, respectively. The thick grey lines give the arithmetic means in the study by Matérn (1990): solid line under bark, dashed line over bark. (For the explanation of the boxplot and the lines, refer to the caption of Fig. 29.)

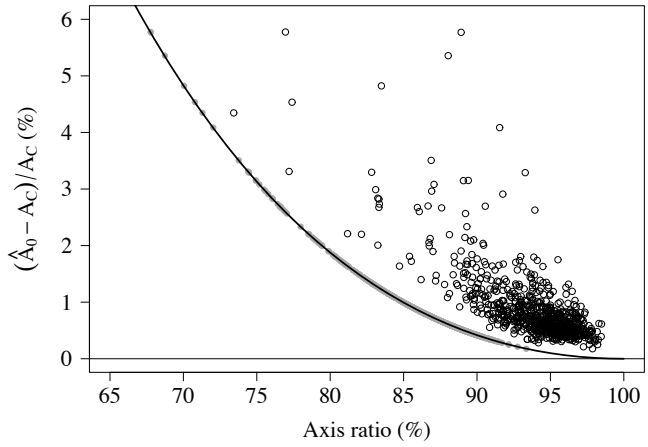

Fig. 42. Comparison of the values of relative isoperimetric deficit $(\hat{A}_0–A_C)/A_C$ in the 709 cross-sections to the values in an ellipse (thick black line), as a function of axis ratio; in the cross-sections, the axis ratio was determined either as the ratio between the extreme diameters D_{min}/D_{max} (black circles) or as the girth-area ellipse ratio b_e/a_e (grey dots).

error of $\hat{A}_0$ with respect to true area was less than 2%. That the amount of non-convexity was on average larger in the base and in the top of the stems and less pronounced in the middle parts in our data was also mirrored in the behaviour of this relative error (Fig. 41 B; cf. Fig. 34).

Compared to ellipses with the same axis ratios, the ratio being determined as the extreme diameter ratio D_{min}/D_{max}, the cross-sections in our data assumed clearly larger isoperimetric deficits (Fig. 42, cf. Table 6 in Matérn 1990); this further corroborates the understanding begotten by the shape indices that ellipse is not an adequate shape model for tree cross-sections but that their non-circularity is of a more intricate kind. When the axis ratio was determined with the girth-area ellipse ratio b_e/a_e, the isoperimetric deficits naturally coincided with the ellipse values (because b_e/a_e is by definition the axis ratio of the ellipse that has the same convex area A_C and perimeter C as the cross-section and, thus, also the same isoperimetric deficit $(\hat{A}_0–A_C)/A_C = (C^2/4\pi–A_C)/A_C$).

In his discs of somewhat larger size, Matérn (1990) reported on average slightly higher and more variable isoperimetric deficits than those in this study (Table 26); differences to our cross-sections appeared to be most pronounced in the base and in the top of the stems (Fig. 41 A). Bark tended to increase isoperimetric deficit, except at the lowermost and uppermost heights, but the difference was negligibly small. (In Norway spruce, Matérn reported similar isoperimetric deficits as in Scots pine, except at the height of 1% where the cross-sections exhibited clearly larger isoperimetric deficits over bark. Otherwise bark did not noteworthily increase isoperimetric deficit in spruce.)

Literature does not seem to abound with such results on isoperimetric deficit where the effect of measurement errors could be to a large extent excluded: Borowski (1960) reported an average value of 1.60% in a total of 564 cross-sections taken from 41 pines (exact species not mentioned, contours drawn under bark); Kärkkäinen (1976), in turn, documented an average value of 1.7% in the debarked end sections of 174 European aspen logs; and Gregoire et al. (1990) studied 101 breast height cross-sections of various conifer species of which majority (65/101) were red spruces, and found the isoperimetric deficit to be on

Table 26. Comparison of the between-cross-sections means and standard deviations of isoperimetric deficit $(\hat{A}_0–A_C)/A_C$ to those reported by Matérn (1990). In the parentheses, Matérn's results obtained from over-bark observations are given; n is the number of observations.

		This study			Matérn (1990)		
		Height			Height		
		1%	10–90%	1.3 m	1%	10–90%	1.3 m
$(\hat{A}_0–A_C)/A_C$ (%)	Mean	2.12	0.71	0.74	2.67 (2.46)	0.89 (0.94)	0.97 (1.74)
	Std.dev.	1.30	0.38	0.30	1.78 (0.96)	0.50 (0.48)	0.53 (0.57)
n		28	400	80	5 (5)	25 (25)	15 (17)

Table 27. Correlation of isoperimetric deficit $(\hat{A}_0–A_C)/A_C$ with shape indices depicting the convex closure of a cross-section (diameter coefficient of variation CV_D, ratio between the extreme diameters D_{min}/D_{max}, girth-area ellipse ratio b_e/a_e, correlation of perpendicular diameters $\rho_D(\pi/2)$, and absolute difference between the directions of the extreme diameters $|\theta_{Dmax}–\theta_{Dmin}|$), with size of a cross-section (expected diameter μ_D), and with convex deficit $(A_C–A)/A_C$ in this study (n=709) and in that of Matérn (1990) (n=45). In the parentheses, the Matérn's results based on over-bark observations (n=47) are given.

	This study							Matérn (1990)				
	CV_D	D_{min}/D_{max}	$\rho_D(\pi/2)$	μ_D	b_e/a_e	$\lvert\theta_{Dmax}–\theta_{Dmin}\rvert$	$(A_C–A)/A_C$	CV_D	D_{min}/D_{max}	$\rho_D(\pi/2)$	μ_D	$(A_C–A)/A_C$
$(\hat{A}_0–A_C)/A_C$	0.72	–0.75	0.03	0.16	–0.96	–0.10	0.48	0.69 (0.45)	–0.68 (–0.46)	0.28 (0.06)	–0.51 (0.03)	0.74 (0.59)

average 2.65% when girths were determined from digitised convex closure contours and 3.10% when girths were measured in the field (in the latter case, the median was 3.20% and the between-cross-sections standard deviation 0.066%; actually, estimation errors were computed with respect to true area, but only four discs were reported to have a measurable convex deficit). As an extremity, Loetsch et al. (1973) cited an early Dutch work (by H.E. Wolff von Wülfing in 1929) on plantation teak in Indonesia, where the average combined effect of convex and isoperimetric deficits ($(\hat{A}_0–A)/A$) was reported to increase with tree size, from 0.8% with breast heigh diameter of 30 cm to 14.9% with breast heigh diameter of 100 cm.

Isoperimetric deficit appeared to be independent of cross-section size and be associated with convex deficit only at the heights of 1% and 70% (Table 27, Fig. 43). Quite expectedly, however, it correlated almost fully negatively with girth-area ellipse ratio at all the observation heights (as mentioned before, both the characteristics are functions of the convex perimeter and convex area of a cross-section and have a slightly curvilinear relationship (Fig. 42), due to which the linear correlation is not exactly perfect) and moderately with the diameter variation within a cross-section at most observation heights (Table 27, Fig. 43). Matérn (1990) found stronger associations with cross-section size (negative correlation, i.e., the larger the cross-section the smaller the isoperimetric deficit) and with convex deficit (Table 27); interestingly, our under-bark results seemed to agree better with his over-bark results than with his under-bark ones.

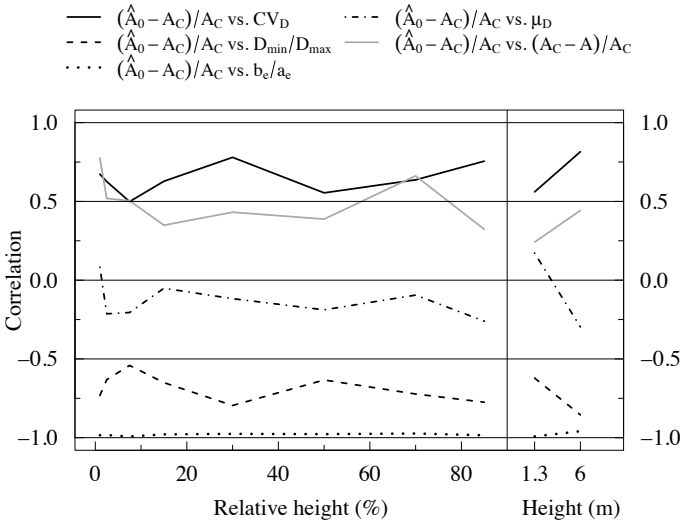

Fig. 43. Correlation of relative isoperimetric deficit $(\hat{A}_0–A_C)/A_C$ with diameter coefficient of variation CV_D, ratio between the extreme diameters D_{min}/D_{max}, girth-area ellipse ratio b_e/a_e, expected diameter μ_D, and convex deficit $(A_C–A)/A_C$ at the ten observation heights. (Correlation of isoperimetric deficit with correlation between perpendicular diameters $\rho_D(\pi/2)$ is not shown as it was close to 0 at all the observation heights.)

8.3.2 Comparison of Area Estimators

The area estimators were compared by means of their estimated within-cross-section biases, standard deviations (square roots of within-cross-section variances) and RMSEs (square roots of the sums of within-cross-section variances and squared biases), proportioned to true or convex cross-section areas and considered in the set of all the discs and in the subsets of height classes. If we were to estimate the total cross-section area of a stand, it would be reasonable to select area estimator primarily on the basis of its average behaviour, expressed by mean within-cross-section bias across trees, whereas variation in estimates within cross-sections and between trees would be of lesser importance (although they affect the precision with which we can expect to be able to estimate the stand total). If, in turn, our interest was to estimate the cross-section area of an individual tree, also variation in estimates at both the levels would equally matter, and therefore not only mean within-cross-section bias and RMSE but also their standard deviations across trees would be useful measures of estimator performance. The smaller the within-cross-section and between-trees variation in estimates, the more feasible it would be to attempt to correct the systematic error of the estimator.

Before entering into the comparison of the estimators, we note that *for the estimators involving Bitterlich diameters* (diameters taken parallel or perpendicular to plot radius in Bitterlich sampling; estimators $\hat{A}_{1\xi}$–$\hat{A}_{5\xi}$, $\hat{A}_{1\xi 90}$, $\hat{A}_{4\xi 90}$, and $\hat{A}_{5\xi 90}$) *we only report the results obtained with viewing angle 1.146° (basal area factor 1 m²/ha with circular cross-sections)*. This is because within the studied range of 1.146°–3.624° (basal area factor range of 1–10 m²/ha with circular cross-sections), viewing angle had practically no influence on the within-cross-section biases, variances and RMSEs. (This was not unexpected in the light of the findings on the example shapes in Fig. 10: see e.g. Fig. 21 where the viewing angles 1°

and 30° were shown to produce almost identical Bitterlich diameter direction distributions in all the shapes, and Tables 8 and 9 where negligible differences in area estimation biases and standard deviations between the same viewing angles were reported). Furthermore, the "thinking experiment" where the Bitterlich direction distribution was determined individually for each cross-section using its own inclusion region (instead of using the inclusion region of the breast height cross-section for all the other cross-sections of a tree) made practically no difference either, except for a slight effect on the within-cross-section biases, which will be discussed in due course below.

Biases

In terms of relative within-cross-section bias, taking one or two random diameters with the uniform direction distribution, or one random diameter and its perpendicular, was as good an approach as measuring girth: the estimators $\hat{A}_1$–$\hat{A}_5$ produced bias distributions very similar to that of the girth diameter estimator $\hat{A}_0$ (Table 28, Fig. 44), the average biases being about 0.9% with respect to convex area and about 1.6% with respect to true area. This was hardly surprising considering the generally small diameter variation found earlier within our discs (see Section 8.2.1): in the bias formulae (Eqs. 22–26 in Section 3.3.2), the terms involving the within-cross-section variance of diameter became close to zero.

In area estimation in our data, Bitterlich diameters practically corresponded to random diameters with the uniform direction distribution: the estimators $\hat{A}_{1\xi}$–$\hat{A}_{5\xi}$, $\hat{A}_{1\xi 90}$, $\hat{A}_{4\xi 90}$ and $\hat{A}_{5\xi 90}$ yielded bias distributions similar to those of the estimators $\hat{A}_0$ and $\hat{A}_1$–$\hat{A}_5$ (Fig. 44, Table 29). This was quite expected, as the breast height cross-sections (whose direction distributions were used for all the other cross-sections in the same tree) deviated rather little from circles and as the other cross-sections in the same tree did not necessarily repeat the shape of the breast height cross-section. In 70% (493/709) of the cross-sections, however, measuring the Bitterlich diameter perpendicular to plot radius resulted in larger bias than taking it parallel to plot radius (as we had found to be the case also with the example shapes of Fig. 10; see Table 8).

While all our random area estimators always yielded overestimating bias with respect to both true and convex area, the fixed area estimators involving D_{min}, D_{max} and their

Table 28. Summarised distributions of the relative within-cross-section biases of the area estimators $\hat{A}_1$–$\hat{A}_5$ with respect to convex area A_C and true area A in the set of all the cross-sections (n=709); for comparison, the results on the estimator $\hat{A}_0$ are also given.

Relative bias	Statistic	Diameter selection method j					
		0	1	2	3	4	5
$[E(\hat{A}_j)–A_C]/A_C$ (%)	Mean	0.90	0.95	0.91	0.86	0.93	0.90
	Std. dev.	0.67	0.73	0.67	0.62	0.70	0.67
	Min.	0.18	0.18	0.18	0.17	0.18	0.18
	Median	0.71	0.74	0.71	0.67	0.72	0.71
	Max.	5.78	6.81	5.80	5.64	6.29	5.78
$[E(\hat{A}_j)–A]/A$ (%)	Mean	1.62	1.67	1.62	1.58	1.64	1.62
	Std. dev.	0.86	0.92	0.87	0.82	0.89	0.86
	Min.	0.46	0.47	0.46	0.45	0.46	0.46
	Median	1.39	1.42	1.40	1.36	1.41	1.39
	Max.	8.30	9.36	8.33	7.30	8.83	8.30

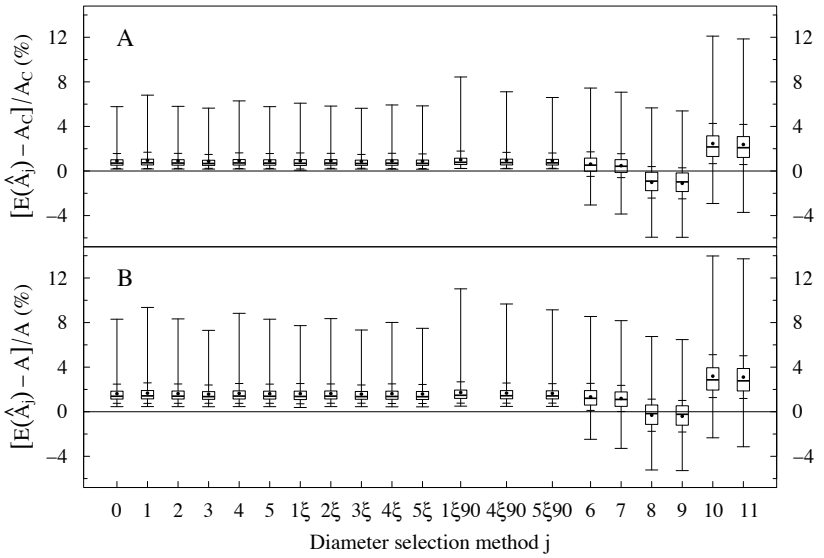

Fig. 44. Summarised distributions of the relative within-cross-section biases of the area estimators $\hat{A}_0$, $\hat{A}_1$–$\hat{A}_5$, $\hat{A}_{1\xi}$–$\hat{A}_{5\xi}$, $\hat{A}_{1\xi 90}$, $\hat{A}_{4\xi 90}$, $\hat{A}_{5\xi 90}$ and $\hat{A}_6$–$\hat{A}_{11}$ with respect to convex area (A) or true area (B) in the set of all the discs (n=709). The Bitterlich diameter direction distribution was determined in the breast height cross-section in each tree with viewing angle 1.146° (basal area factor 1 m^2/ha with circular cross-sections). The box depicts the inter-quartile range bisected by the median, and the whiskers reach out to the extreme values in the data; the filled circle denotes the arithmetic mean, whereas the short horizontal lines below and above the mean indicate the magnitude of the sample standard deviation.

Table 29. Summarised distributions of the relative within-cross-section biases of the area estimators $\hat{A}_{1\xi}$–$\hat{A}_{5\xi}$, $\hat{A}_{1\xi 90}$, $\hat{A}_{4\xi 90}$ and $\hat{A}_{5\xi 90}$ with respect to convex area A_C and true area A in the set of all the cross-sections (n=709); for comparison, the results on the estimator $\hat{A}_0$ are also given. The Bitterlich diameter direction distribution was determined in the breast height cross-section in each tree with viewing angle 1.146° (basal area factor 1 m^2/ha with circular cross-sections).

Relative bias	Statistic	Diameter selection method j								
		0	1ξ	2ξ	3ξ	4ξ	5ξ	1ξ90	4ξ90	5ξ90
$[E(\hat{A}_j)–A_C]/A_C$ (%)	Mean	0.90	0.90	0.91	0.87	0.90	0.88	1.01	0.96	0.93
	Std. dev.	0.67	0.72	0.67	0.62	0.69	0.66	0.78	0.72	0.69
	Min.	0.18	0.07	0.18	0.18	0.16	0.16	0.22	0.20	0.20
	Median	0.71	0.69	0.71	0.67	0.70	0.68	0.78	0.75	0.73
	Max.	5.78	6.09	5.83	5.63	5.93	5.85	8.44	7.11	6.60
$[E(\hat{A}_j)–A]/A$ (%)	Mean	1.62	1.62	1.63	1.58	1.62	1.59	1.73	1.67	1.65
	Std. dev.	0.86	0.91	0.87	0.82	0.88	0.85	0.96	0.90	0.87
	Min.	0.46	0.38	0.46	0.45	0.44	0.44	0.50	0.48	0.48
	Median	1.39	1.37	1.40	1.36	1.37	1.35	1.48	1.44	1.42
	Max.	8.30	7.73	8.35	7.33	8.01	7.48	11.03	9.67	9.14

Table 30. Summarised distributions of the relative within-cross-section errors (biases) of the area estimators $\hat{A}_6$–$\hat{A}_{11}$, $\hat{A}_{min}$, and $\hat{A}_{max}$ with respect to convex area A_C and true area A in the set of all the cross-sections (n=709); for comparison, the results on the estimator $\hat{A}_0$ are also given.

Relative bias	Statistic	Diameter selection method j								
		0	6	7	8	9	10	11	min	max
$[E(\hat{A}_j)–A_C]/A_C$ (%)	Mean	0.90	0.62	0.48	–1.02	–1.11	2.47	2.38	–5.85	7.36
	Std. dev.	0.67	1.10	1.07	1.41	1.39	1.80	1.80	3.21	4.13
	Min.	0.18	–3.05	–3.86	–5.94	–5.95	–2.92	–3.71	–27.33	1.81
	Median	0.71	0.53	0.43	–0.91	–0.98	2.16	2.09	–5.15	6.33
	Max.	5.78	7.44	7.07	5.66	5.39	12.10	11.85	–0.94	34.78
$[E(\hat{A}_j)–A]/A$ (%)	Mean	1.62	1.33	1.19	–0.32	–0.41	3.20	3.11	–5.19	8.13
	Std. dev.	0.86	1.21	1.17	1.44	1.42	1.92	1.91	3.21	4.26
	Min.	0.46	–2.48	–3.29	–5.23	–5.28	–2.34	–3.14	–26.50	2.22
	Median	1.39	1.21	1.09	–0.17	–0.24	2.87	2.78	–4.53	7.09
	Max.	8.30	8.55	8.17	6.75	6.47	13.98	13.72	–0.07	36.32

perpendiculars produced also underestimating biases (Fig. 44). Indeed, the best estimators in terms of average bias were found among these estimators, the actual "winner" varying according to the reference area (Fig. 44, Table 30): with respect to convex area, the estimators $\hat{A}_6$ and $\hat{A}_7$ involving the mean of D_{min} and D_{max} yielded the smallest average bias of 0.5–0.6%; with respect to true area, in turn, the estimators $\hat{A}_8$ and $\hat{A}_9$ involving the mean of D_{min} and its perpendicular resulted in the smallest, this time negative, average bias of 0.3–0.4% (also $\hat{A}_6$ and $\hat{A}_7$ yielded smaller average bias with respect to true area than the random estimators). However, these average-bias-optimal estimators were clearly more unstable (with larger between-cross-section variation of the biases) than the girth diameter estimator and the random estimators (Fig. 44, Tables 28–30).

In general, employing the geometric mean instead of the arithmetic one decreased the overestimation bias (or increased the underestimation bias) only little (Fig. 44, Tables 28–30: $\hat{A}_2$ vs. $\hat{A}_3$, $\hat{A}_4$ vs. $\hat{A}_5$, $\hat{A}_{2\xi}$ vs. $\hat{A}_{3\xi}$, $\hat{A}_{4\xi}$ vs. $\hat{A}_{5\xi}$, $\hat{A}_{4\xi 90}$ vs. $\hat{A}_{5\xi 90}$, $\hat{A}_6$ vs. $\hat{A}_7$, $\hat{A}_8$ vs. $\hat{A}_9$, $\hat{A}_{10}$ vs. $\hat{A}_{11}$). Further, taking the second diameter perpendicular to the first one appeared to produce regularly smaller and less variable biases than taking it in a random direction (as would be expected on the basis of the prevalence of strong negative within-cross-section correlations between perpendicular diameters, see Section 8.2; cf. Eqs. 23–24 in Section 3.3.2 and Eqs. 95–96 in Section 4.2.2), but again the effect was very small (Fig. 44, Tables 28–30: $\hat{A}_2$ vs. $\hat{A}_4$, $\hat{A}_3$ vs. $\hat{A}_5$, $\hat{A}_{2\xi}$ vs. $\hat{A}_{4\xi}$ or $\hat{A}_{4\xi 90}$, $\hat{A}_{3\xi}$ vs. $\hat{A}_{5\xi}$ or $\hat{A}_{5\xi 90}$).

As could be expected from our results on the shapes of the convex closures, the relative within-cross-section biases were found to be larger on average and more variable in the very butt than in the middle and upper parts of the stems (Figs. 45 and 46); for almost all the estimators, the average bias at the height of 1% was double the bias in the other parts of the stems (even triple, when the bias was computed with respect to true area). By contrast, no association was found between cross-section size and relative bias in any area estimator.

A closer examination of the breast height cross-sections showed that Bitterlich diameters indeed deviated from random diameters with the uniform direction distribution (Fig. 47 A), even though the implications of this deviation to relative within-cross-section biases were then very small (as was seen above): If the estimator involved diameter taken perpendicular to plot radius in Bitterlich sampling ($\hat{A}_{1\xi 90}$, $\hat{A}_{2\xi}$, $\hat{A}_{3\xi}$, $\hat{A}_{4\xi 90}$ and $\hat{A}_{5\xi 90}$), the bias was in all the breast height cross-sections larger than if the diameter was taken in a uniformly distributed

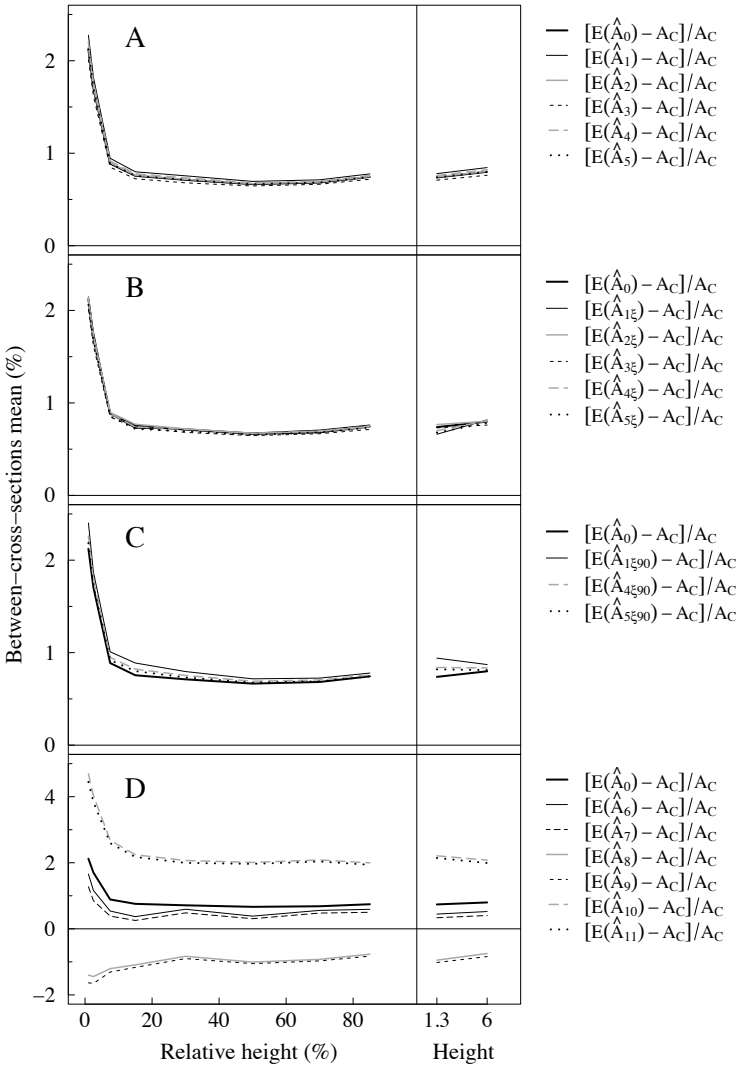

Fig. 45. Means of the relative within-cross-section biases of the area estimators $\hat{A}_0$, $\hat{A}_1$–$\hat{A}_5$, $\hat{A}_{1\xi}$–$\hat{A}_{5\xi}$, $\hat{A}_{1\xi 90}$, $\hat{A}_{4\xi 90}$, $\hat{A}_{5\xi 90}$ and $\hat{A}_6$–$\hat{A}_{11}$ with respect to convex area at the ten observation heights. The Bitterlich diameter direction distribution was determined in the breast height cross-section in each tree with viewing angle 1.146° (basal area factor 1 m^2/ha with circular cross-sections). The results on the estimator $\hat{A}_0$ are shown for comparison in all the panels.

random direction ($\hat{A}_1$–$\hat{A}_5$). If, in turn, the estimator involved diameter taken parallel to plot radius ($\hat{A}_{1\xi}$, $\hat{A}_{4\xi}$ and $\hat{A}_{5\xi}$), in over 90% (73/80) of the cross-sections the bias was smaller than with the random diameter with uniformly distributed direction. (In neither of the cases, however, the differences were statistically significant, not even at the 90% significance level, according to the paired t-tests where the biases of each estimator were assumed normally distributed.) Patently, taking diameter perpendicular to plot radius in Bitterlich sampling yielded larger (in all the breast height cross-sections) and more variable biases than taking

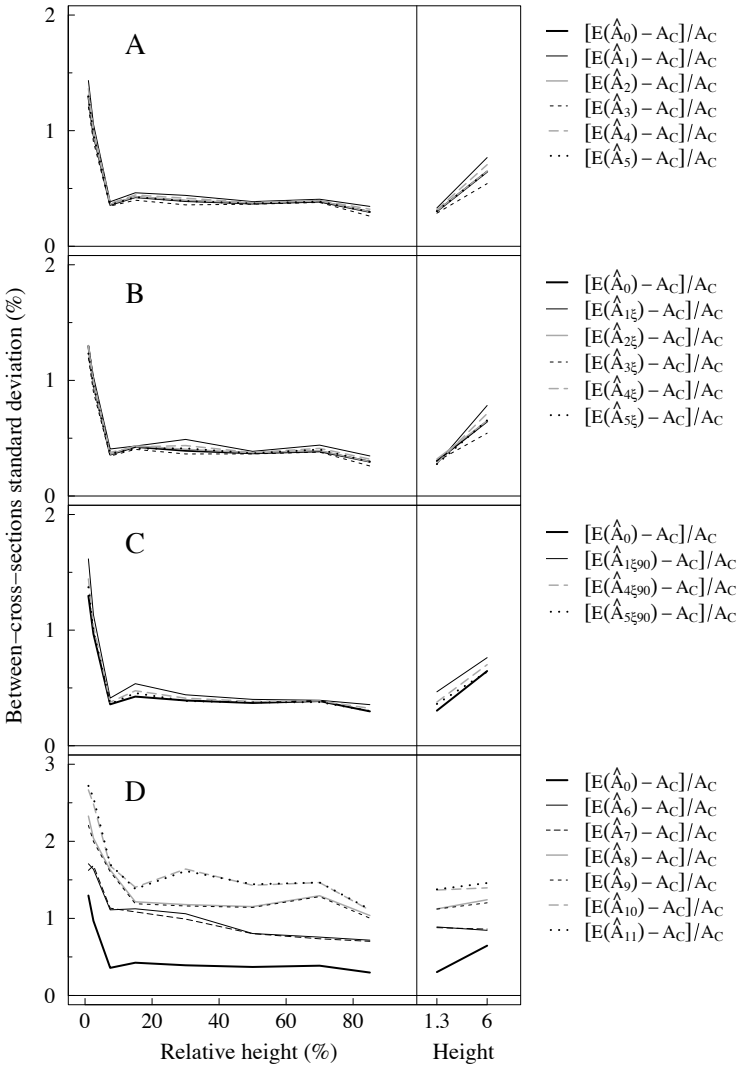

Fig. 46. Standard deviations of the relative within-cross-section biases of the area estimators $\hat{A}_0$, $\hat{A}_1$–$\hat{A}_5$, $\hat{A}_{1\xi}$–$\hat{A}_{5\xi}$, $\hat{A}_{1\xi 90}$, $\hat{A}_{4\xi 90}$, $\hat{A}_{5\xi 90}$ and $\hat{A}_6$–$\hat{A}_{11}$ with respect to convex area at the ten observation heights. The Bitterlich diameter direction distribution was determined in the breast height cross-section in each tree with viewing angle 1.146° (basal area factor 1 m^2/ha with circular cross-sections). The results on the estimator $\hat{A}_0$ are shown for comparison in all the panels.

it parallel, but the differences were small (at the largest, i.e., with $\hat{A}_{1\xi 90}$ vs. with $\hat{A}_{1\xi}$, the difference was about 2.4 percentage units in an individual disc, 0.3 percentage units in average bias and 0.2 percentage units in bias standard deviation).

Extending this examination, as a "thinking experiment", from the breast height cross-sections to all the cross-sections (i.e., determining the Bitterlich diameter direction distributions separately for each cross-section, as if all the cross-sections were breast height cross-sections) produced qualitatively similar results (Fig. 47 B). The differences in biases

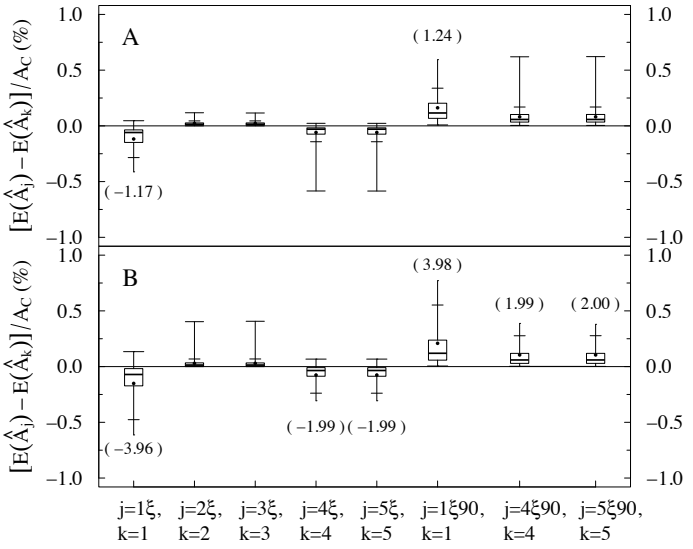

Fig. 47. Summarised distributions of the differences in the relative within-cross-section biases for eight pairs of area estimators in the sets of breast-height cross-sections (A, n=80) and all the cross-sections (B, n=709). The pairs were formed in the way that estimators involving Bitterlich diameters are compared to similar estimators involving random diameters with the uniform direction distribution. The Bitterlich diameter direction distribution was determined separately for each cross-section with viewing angle 1.146° (basal area factor 1 m^2/ha with circular cross-sections). In the parentheses, the extreme values reaching out of the figure are given. (For the explanation of the boxplot, refer to the caption of Fig. 44.)

between the two ways of taking Bitterlich diameters were now slightly more pronounced (at the largest, i.e., with $\hat{A}_{1\xi 90}$ vs. with $\hat{A}_{1\xi}$, the difference was about 7.9 percentage units in an individual disc, 0.4 percentage units in average bias and 0.4 percentage units in bias standard deviation).

In his somewhat larger discs, Matérn (1990) reported more variable and on average larger biases, especially at the height of 1% (Table 31). Interestingly, in his data the estimators $\hat{A}_6$ and $\hat{A}_7$ involving the mean of D_{min} and D_{max} underestimated convex area at the height of 1%; this may be due to the sparse sampling of diameters (D_{min} and D_{max} were determined as the minimum and the maximum of 18 diameters measured at regular angular intervals of 10°) that resulted in the underestimation of D_{max} being larger than the overestimation of D_{min}. While bark appeared to increase, particularly at breast height, the biases of the estimators $\hat{A}_1$–$\hat{A}_3$ involving a random diameter and its perpendicular, at the height of 1% the effect was opposite, there bark decreased and especially stabilised the biases (Table 31); this echoes the earlier findings in Matérn's data on bark attenuating shape irregularities (cf. Table 20 of shape indices) as well as on bark decreasing and stabilising isoperimetric deficits (biases of the estimator $\hat{A}_0$, cf. Table 26) at the lowermost height; as mentioned earlier, these results remain rather uncertain due to the small number of observations at the lowest observation height. (In Norway spruce, Matérn reported biases of similar magnitude as in Scots pine, but with reverse bark effects: at breast height bark did not markedly influence the biases, whereas at the height of 1% bark clearly reduced the biases.)

Table 31. Comparison of the between-cross-sections means and standard deviations of the relative within-cross-section biases (with respect to convex area) of the area estimators $\hat{A}_1$, $\hat{A}_2$, $\hat{A}_3$, $\hat{A}_6$, $\hat{A}_7$, $\hat{A}_9$ and $\hat{A}_{11}$ to those reported by Matérn (1990). In the parentheses, Matérn's results from over-bark observations are given; n is the number of observations.

Diameter selection method j	Statistic of $[E(\hat{A}_j)–A_C]/A_C$	This study			Matérn (1990)		
		Height			Height		
		1%	10–90%	1.3 m	1%	10–90%	1.3 m
1	Mean	2.28	0.75	0.78	2.90 (2.62)	0.94 (0.98)	1.03 (1.82)
	Std.dev.	1.43	0.41	0.33	1.97 (1.06)	0.53 (0.52)	0.59 (0.60)
2	Mean	2.14	0.72	0.74	2.71 (2.48)	0.89 (0.95)	0.98 (1.77)
	Std.dev.	1.31	0.38	0.31	1.92 (0.97)	0.50 (0.49)	0.54 (0.58)
3	Mean	2.01	0.69	0.71	2.53 (2.34)	0.85 (0.91)	0.92 (1.70)
	Std.dev.	1.21	0.35	0.29	1.68 (0.88)	0.49 (0.47)	0.49 (0.56)
6	Mean	1.66	0.50	0.45	–0.51 (1.67)	0.62 (0.88)	0.49 (1.77)
	Std.dev.	1.71	0.91	0.89	1.50 (1.86)	1.09 (0.94)	1.42 (1.34)
7	Mean	1.27	0.41	0.34	–1.10 (1.28)	0.50 (0.77)	0.31 (1.57)
	Std.dev.	1.62	0.88	0.88	1.81 (2.04)	1.13 (0.92)	1.40 (1.36)
9	Mean	–1.64	–0.98	–1.02	–2.60 (0.05)	–0.68 (–0.66)	–1.59 (–1.25)
	Std.dev.	2.21	1.16	1.12	2.68 (2.62)	1.33 (1.14)	1.42 (1.98)
11	Mean	4.45	2.02	2.14	5.06 (4.93)	1.82 (2.34)	2.55 (5.04)
	Std.dev.	2.72	1.41	1.38	5.00 (2.53)	1.46 (1.18)	1.60 (2.28)
n		28	400	80	5 (5)	25 (25)	15 (17)

Besides Matérn's (1990) work, literature does not seem to abound with empirical results on errors of different area estimators (Table 32). Specifically, no within-cross-section biases were available for the random estimators, but we had to content ourselves to area estimation errors (resulting from individual diameter samplings in cross-sections) and their between-cross-sections means (cf. the figures for the estimators $\hat{A}_1$–$\hat{A}_3$ in Table 32). For comparability with the previous studies, we included in our consideration the earlier work (Pulkkinen 1996) where the discs of this study (and 4 other discs) were subjected to random diameter sampling (taking one or two diameters in each disc) and where average estimation errors were then computed across the discs for the random area estimators. Generally, the geometric mean of diameters resulted in smaller average errors or biases than the arithmetic one (just as should be the case); a possible explanation for Chacko's (1961) conflicting results is that he may have used not the same diameters in the estimators $\hat{A}_2$ and $\hat{A}_3$. As for the biases of the fixed estimators ($\hat{A}_6$–$\hat{A}_{11}$), the results of this study accorded finely with Kärkkäinen's (1975a, 1976) findings on silver birch and European aspen logs. As for the average errors of the random estimators ($\hat{A}_1$–$\hat{A}_3$), the differences between the estimators were small in all the studies. However, the average errors did not always comply with the theory on the within-cross-section biases of the random estimators: Gregoire et al. (1990) reported that the estimators $\hat{A}_1$–$\hat{A}_3$ involving one random diameter and its perpendicular underestimated true area on average (whereas the girth diameter estimator $\hat{A}_0$ produced an average overestimation of similar magnitude in their data, cf. Section 8.3.1); further, and similar to the results by Pulkkinen (1996), $\hat{A}_1$ involving one diameter resulted in a smaller average error than $\hat{A}_2$ and $\hat{A}_3$ involving two diameters (whereas the between-cross-sections variation of the errors was then clearly larger for $\hat{A}_1$ than for $\hat{A}_2$ and $\hat{A}_3$ in both the studies).

The last-mentioned phenomenon — that, with the area estimators involving one random diameter or one random diameter and its perpendicular ($\hat{A}_1$ and $\hat{A}_2$, rarely also $\hat{A}_3$), the mean of the relative estimation errors across individual cross-sections (trees) does not

Table 32. Means of the relative errors (Â–A)/A of the area estimators $\hat{A}_1$–$\hat{A}_3$ and $\hat{A}_6$–$\hat{A}_{11}$ with respect to true area A in some previous empirical studies, mostly collated by Matérn (1990). Results are obtained under bark if not otherwise stated; n is the number of cross-sections.

Study	Species	n[1]	Estimator $\hat{A}_1$	$\hat{A}_2$	$\hat{A}_3$	$\hat{A}_6$	$\hat{A}_7$	$\hat{A}_8$	$\hat{A}_9$	$\hat{A}_{10}$	$\hat{A}_{11}$
Chacko 1961	*Shorea robusta*	27 (l)	4.3	4.0	4.2					6.1	
	Albizzia lebbek	27 (l)	2.7	2.4	2.8					4.6	
	Pinus roxburghii	30 (l)	0.6	0.6	0.7					1.6	
	Salmalia malabarica	27 (l)	6.6	6.2	4.7					8.8	
Georgopoulos and Gofas 1966	*Populus* sp.	60 (d)					1.34				0.95
Kärkkäinen 1975a[2]	*Betula pendula*	420 (l)				1.86	1.61	–0.41	–0.56	4.02	3.84
	Populus tremula	240 (l)				1.06	0.84	–0.86	–1.01	2.85	2.69
Kärkkäinen 1976	*Populus tremula*	174 (l)	1.81[3]			1.69	1.50				
Delord 1979	13 coniferous & broad-leaved species	55 (d,ob)	2.15	2.07							
Biging and Wensel 1988	Several coniferous species	50 (d)								1.11	0.98
Gregoire et al. 1990[4]	Several coniferous species, 64 % *Picea rubens*	101 (d, ob)	–3.7/–0.6	–2.4	–2.6						
Matérn 1990[5]	*Pinus sylvestris*	45				0.65	0.47				2.71
	Picea abies	52				0.60	0.50				2.04
	Pinus sylvestris	47 (ob)				5.11	4.91				8.49
	Picea abies	58 (ob)				1.70	1.60				3.45
Pulkkinen 1996	*Pinus sylvestris*	713	1.41	1.69	1.64	1.33	1.18	–0.32	–0.42	3.22	3.13

[1] (d): observations at breast height
(l): observations at one or more heights in a log
(ob): observations over bark
[2] True area was determined as the integral approximation from 16 radii; the error resulting from this procedure was estimated to be 0.4 % on average.
[3] This is actually the mean of the relative errors of the area estimator where the quadratic mean of 8 diameters is substituted in the circle area formula.
[4] Diameters were not taken in random directions with the uniform direction distribution but measured in east–west and north–south directions, which were assumed, after some statistical tests, to correspond to random directions; for the estimator $\hat{A}_1$, the two mean figures pertain to these measurements, respectively.
[5] Relative errors were originally computed with respect to convex area, and their means were then simply transformed by dividing with the average ratio between true and convex area.

necessarily behave as (the mean of) the relative within-cross-section biases, but that these estimators may produce smaller average errors than the girth diameter estimator ($\hat{A}_0$) or even negative average errors — has been reported in many empirical studies (e.g. Müller 1957, 1958a, 1958b, Kennel 1959, 1964; see also the discussion in Matérn 1990, p. 39–40). Referring to time before Matérn's theoretical work (1956), Loetsch et al. (1973) even state it as "the formerly wide-spread opinion that in principle girth measurement yields larger values of cross-sectional area than diameter measurement". The most popular explanation for this puzzling "discrepancy between theory and field practice" (Matérn 1990) has been measurement errors due to handling of a caliper: the higher contact pressure that the caliper exerts on wood compared to a tape (Kennel 1964), or a measurer's unconscious tendency to align the caliper arm with the longer axis of the stem cross-section (Gregoire et al. 1990) or to adjust the caliper direction to avoid protruding ridges in bark (Matérn 1990). Another mensurational reason could be the difficulty in determining the direction of diameter measurement in the way that the direction is truly uniformly distributed: for convenience, diameters in the whole plot may have been taken in a fixed direction (compass direction; e.g. Kennel 1959, 1964, Gregoire et al. 1990), which, in the absence of blatantly eye-catching diameter directionality, has then been assumed to correspond to a uniformly distributed direction within each cross-section; alternatively, diameters may have been taken in the plot radius direction, which we found in the case of Bitterlich sampling and non-circular breast height cross-sections to result in non-uniform direction distributions (see Section 4.2). Yet the phenomenon can naturally occur even without any presence of measurement errors: this is because the mean of the relative area estimation errors resulting from one diameter sampling in each individual cross-section does not necessarily estimate accurately its own expectation over the uniform diameter direction distribution (i.e., the mean, across individual cross-sections, of the relative within-cross-section biases over the uniform diameter direction distribution). If all the n cross-sections in the plot are of the same non-circular shape and have the same orientation, in which case their relative within-cross-section biases are the same and the mean of the biases equals this bias, the mean of the n relative area estimation errors estimates the bias defined over infinite number of diameter directions using a diameter direction sample of size n; the larger the sample size (the number of cross-sections), the narrower becomes the distribution of the mean around its expectation (the bias); with a small sample size and a large diameter variance within the cross-sections, the mean may deviate quite a bit from its expectation and even be negative. If the n cross-sections in the plot then vary in shape, which is the case in reality, the mean of the n relative area estimation errors is likely to vary even more around its expectation over the uniform diameter direction distribution; basically, the within-cross-section bias in each cross-section is in this case estimated with one single area estimation error, and the mean of the biases is then estimated with the mean of these presumably poor bias estimates.

Variances and Variance Approximations

For the area estimators involving randomness ($\hat{A}_1$–$\hat{A}_5$, $\hat{A}_{1\xi}$–$\hat{A}_{5\xi}$, $\hat{A}_{1\xi 90}$, $\hat{A}_{4\xi 90}$ and $\hat{A}_{5\xi 90}$), the diameter sampling errors within the cross-sections were examined in the square root scale, in terms of the relative within-cross-section standard deviations of the estimators. Whether the standard deviations were proportioned with convex area or true area made practically no difference, and therefore in the following only the results with respect to convex area are given.

With the estimators involving only random diameters (and not their perpendiculars), the sampling errors quite notably surpassed the systematic errors: with one random diameter

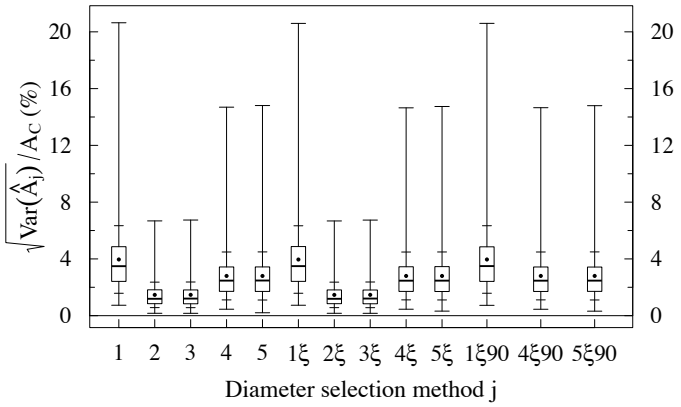

Fig. 48. Summarised distributions of the relative within-cross-section standard deviations of the area estimators $\hat{A}_1$–$\hat{A}_5$, $\hat{A}_{1\xi}$–$\hat{A}_{5\xi}$, $\hat{A}_{1\xi 90}$, $\hat{A}_{4\xi 90}$ and $\hat{A}_{5\xi 90}$ with respect to convex area in the set of all the discs (n=709). The Bitterlich diameter direction distribution was determined in the breast height cross-section in each tree with viewing angle 1.146° (basal area factor 1 m^2/ha with circular cross-sections). (For the explanation of the boxplot, refer to the caption of Fig. 44.)

Table 33. Summarised distributions of the relative within-cross-section standard deviations of the area estimators $\hat{A}_1$–$\hat{A}_5$ with respect to convex area A_C in the set of all the cross-sections (n=709).

Relative std. dev.	Statistic	Diameter selection method j				
		1	2	3	4	5
$\mathrm{Var}(\hat{A}_j)^{1/2}/A_C$ (%)	Mean	3.96	1.47	1.47	2.80	2.80
	Std. dev.	2.38	0.90	0.90	1.69	1.69
	Min.	0.74	0.17	0.17	0.45	0.21
	Median	3.49	1.19	1.21	2.47	2.48
	Max.	20.64	6.68	6.74	14.69	14.81

Table 34. Summarised distributions of the relative within-cross-section standard deviations of the area estimators $\hat{A}_{1\xi}$–$\hat{A}_{5\xi}$, $\hat{A}_{1\xi 90}$, $\hat{A}_{4\xi 90}$ and $\hat{A}_{5\xi 90}$ with respect to convex area A_C in the set of all the cross-sections (n=709). The Bitterlich diameter direction distribution was determined in the breast height cross-section in each tree with viewing angle 1.146° (basal area factor 1 m^2/ha with circular cross-sections).

Relative std. dev.	Statistic	Diameter selection method j							
		1ξ	2ξ	3ξ	4ξ	5ξ	1ξ90	4ξ90	5ξ90
$\mathrm{Var}(\hat{A}_j)^{1/2}/A_C$ (%)	Mean	3.96	1.46	1.47	2.80	2.80	3.96	2.80	2.80
	Std. dev.	2.38	0.90	0.90	1.69	1.69	2.38	1.69	1.69
	Min.	0.74	0.17	0.17	0.45	0.32	0.73	0.45	0.32
	Median	3.49	1.19	1.21	2.47	2.47	3.49	2.47	2.47
	Max.	20.60	6.68	6.74	14.65	14.74	20.60	14.65	14.80

involved (estimators $\hat{A}_1$, $\hat{A}_{1\xi}$, $\hat{A}_{1\xi 90}$), the average relative within-cross-section standard deviation was quadruple the average relative within-cross-section bias (with respect to convex area), whereas with two random diameters (estimators $\hat{A}_4$, $\hat{A}_5$, $\hat{A}_{4\xi}$, $\hat{A}_{5\xi}$, $\hat{A}_{4\xi 90}$, $\hat{A}_{5\xi 90}$) the standard deviation was triple the bias (Tables 33 and 34, Fig. 48; cf. Tables 28 and 29, Fig. 44). It indeed seemed advisable to take the second diameter perpendicular to the first one (estimators $\hat{A}_2$, $\hat{A}_3$, $\hat{A}_{2\xi}$, $\hat{A}_{3\xi}$), as this reduced the average sampling error into half of that obtained by taking the second diameter in a random direction and substantially attenuated the sampling error variation between the cross-sections (Tables 33 and 34, Fig. 48). This can be seen as a reflection of the strong negative within-cross-section correlations between perpendicular diameters that were observed in a clear majority of our discs (see Section 8.2.1): in the variance approximation formulae (Eq. 36 in Section 3.3.2, and Eqs. 105 and 106 in Section 4.2.2), the reducing effect of such correlation is obvious, and later we will see that in our data the approximate variances closely resembled the true ones. Whether the geometric or the arithmetic mean of diameters was employed in the estimator did not affect the sampling errors. Further, using Bitterlich diameters resulted in practically similar sampling errors as using random diameters with the uniform direction distribution (and determining the Bitterlich direction distribution with the inclusion region of each individual cross-section, instead of using the inclusion region of the breast height cross-section for all the cross-sections of the tree, made no practical difference either). With respect to relative height in a stem, the sampling errors behaved fairly similarly to the biases: the relative within-cross-section standard deviations were found to be larger on average and more variable at the lowest observation height than in the other parts of the stems (Figs. 49 and 50).

Noteworthily, as already hinted above, the approximate within-cross-section variances were found to be very close to the true variances with all the estimators (Fig. 51). This implies quite a facilitation in the sampling error estimation, since the much simpler approximate equations (Eqs. 35–37 in Section 3.3.2, Eqs. 104–108 in Section 4.2.2) may be used instead of the complex analytic ones (Eqs. 30–34 in Section 3.3.2, Eqs. 99–103 in Section 4.2.2). Quite consonant with the theory (see Eq. 38 in Section 3.3.2, and Section 4.2.2), the approximate variances of the estimators $\hat{A}_5$, $\hat{A}_{5\xi}$ and $\hat{A}_{5\xi 90}$ underestimated the true variances in all the cross-sections; with the other estimators, the approximate equations yielded both under- and overestimates of the true variances.

RMSEs

Relative within-cross-section RMSE combines the effects of relative within-cross-section bias and relative within-cross-section variance caused by diameter sampling, and therefore it is a particularly relevant measure of estimator performance in single tree estimation. In RMSE, negative bias is not allowed to compensate for sampling variance, as bias is included in the squared form. For the fixed estimators, for which sampling variance is naturally always zero, RMSE equals the absolute value of the area estimation error within each cross-section. With its non-negativity, RMSE penalises equally for negative and positive bias, and therefore its average may give too pessimistic an impression about estimator performance in stand total estimation (where positive and negative errors in different cross-sections should be allowed to cancel out each other); here this is the case with fixed estimators producing both positive and negative estimation errors in different cross-sections. On the other hand, turning negative estimation errors into positive reduces variance, and therefore RMSE variance may give too optimistic an impression about error variation in single tree estimation.

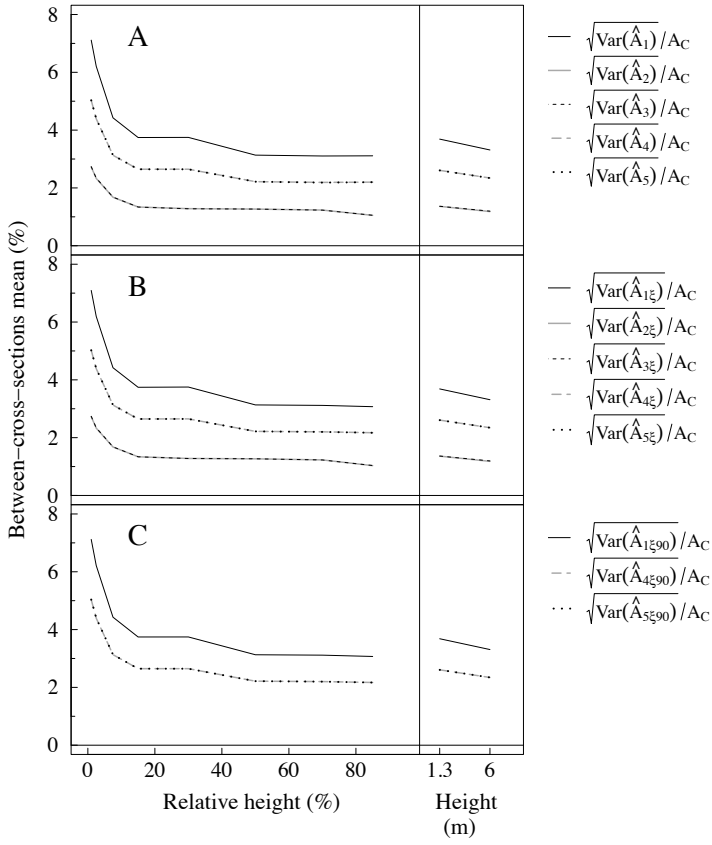

Fig. 49. Means of the relative within-cross-section standard deviations of the area estimators $\hat{A}_1$–$\hat{A}_5$, $\hat{A}_{1\xi}$–$\hat{A}_{5\xi}$, $\hat{A}_{1\xi 90}$, $\hat{A}_{4\xi 90}$ and $\hat{A}_{5\xi 90}$ with respect to convex area at the ten observation heights. The Bitterlich diameter direction distribution was determined in the breast height cross-section in each tree with viewing angle 1.146° (basal area factor 1 m^2/ha with circular cross-sections).

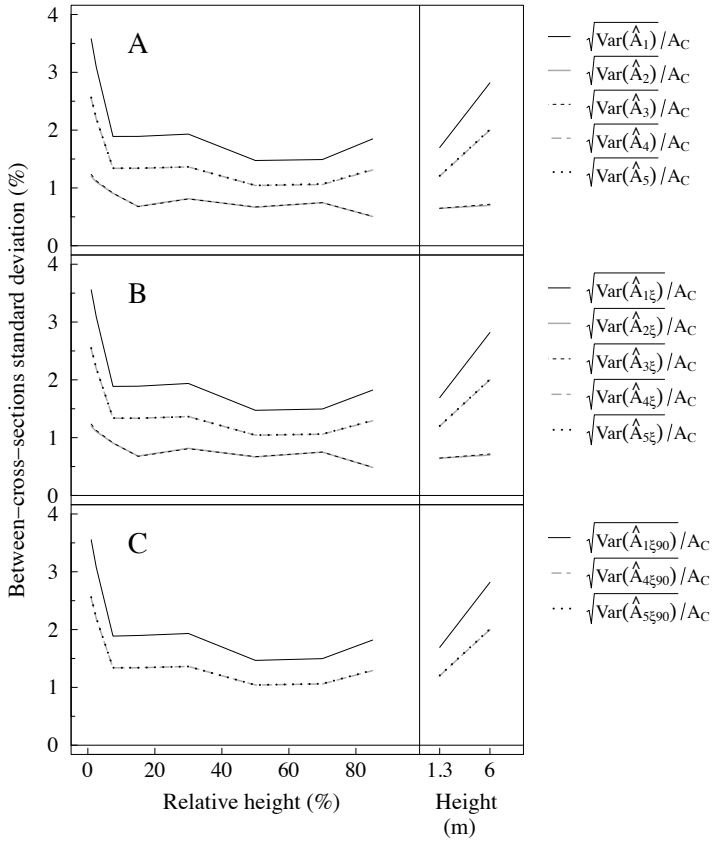

Fig. 50. Standard deviations of the relative within-cross-section standard deviations of the area estimators $\hat{A}_1$–$\hat{A}_5$, $\hat{A}_{1\xi}$–$\hat{A}_{5\xi}$, $\hat{A}_{1\xi 90}$, $\hat{A}_{4\xi 90}$ and $\hat{A}_{5\xi 90}$ with respect to convex area at the ten observation heights. The Bitterlich diameter direction distribution was determined in the breast height cross-section in each tree with viewing angle 1.146° (basal area factor 1 m^2/ha with circular cross-sections).

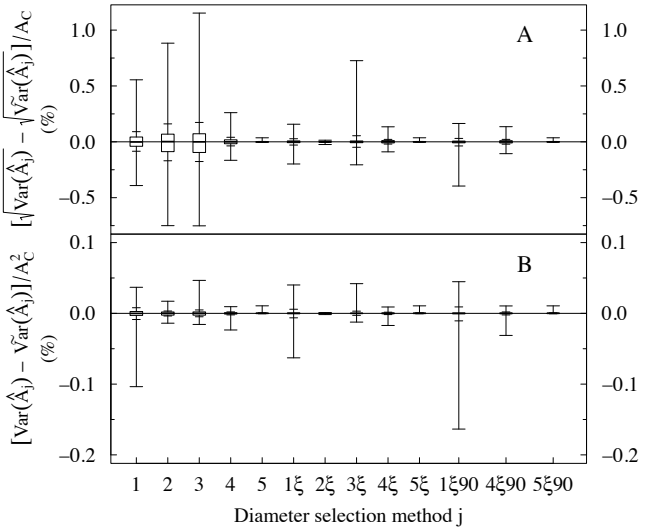

Fig. 51. Summarised distributions of the relative differences between the true and the approximate within-cross-section standard deviations (A) and variances (B) of the area estimators $\hat{A}_1$–$\hat{A}_5$, $\hat{A}_{1\xi}$–$\hat{A}_{5\xi}$, $\hat{A}_{1\xi 90}$, $\hat{A}_{4\xi 90}$ and $\hat{A}_{5\xi 90}$ with respect to convex area in the set of all the discs (n=709). The Bitterlich diameter direction distribution was determined in the breast height cross-section in each tree with viewing angle 1.146° (basal area factor 1 m^2/ha with circular cross-sections). (For the explanation of the boxplot, refer to the caption of Fig. 44; the means were not drawn, as they equalled the medians.)

Table 35. Summarised distributions of the relative within-cross-section RMSEs of the area estimators $\hat{A}_0$ and $\hat{A}_1$–$\hat{A}_5$ with respect to convex area A_C and true area A in the set of all the cross-sections (n=709).

Relative RMSE	Statistic	Diameter selection method j					
		0	1	2	3	4	5
$E\{[\hat{A}_j–A_C]^2\}^{1/2}/A_C$ (%)	Mean	0.90	4.09	1.76	1.73	2.97	2.97
	Std. dev.	0.67	2.46	1.07	1.05	1.79	1.78
	Min.	0.18	0.81	0.38	0.37	0.62	0.52
	Median	0.71	3.59	1.42	1.40	2.59	2.58
	Max.	5.78	21.73	8.30	8.23	15.98	15.89
$E\{[\hat{A}_j–A]^2\}^{1/2}/A$ (%)	Mean	1.62	4.38	2.25	2.22	3.32	3.31
	Std. dev.	0.86	2.48	1.15	1.13	1.82	1.81
	Min.	0.46	1.07	0.56	0.56	0.82	0.78
	Median	1.39	3.81	1.93	1.90	2.88	2.88
	Max.	8.30	23.11	9.53	9.43	17.44	17.28

Table 36. Summarised distributions of the relative within-cross-section RMSEs of the area estimators $\hat{A}_{1\xi}$–$\hat{A}_{5\xi}$, $\hat{A}_{1\xi 90}$, $\hat{A}_{4\xi 90}$ and $\hat{A}_{5\xi 90}$ with respect to convex area A_C and true area A in the set of all the cross-sections (n=709); for comparison, the results on the estimator $\hat{A}_0$ are also given. The Bitterlich diameter direction distribution was determined in the breast height cross-section in each tree with viewing angle 1.146° (basal area factor 1 m^2/ha with circular cross-sections).

Relative RMSE	Statistic	Diameter selection method j								
		0	1ξ	2ξ	3ξ	4ξ	5ξ	1ξ90	4ξ90	5ξ90
$E\{[\hat{A}_j–A_C]^2\}^{1/2}/A_C$ (%)	Mean	0.90	4.08	1.76	1.73	2.97	2.96	4.10	2.98	2.97
	Std. dev.	0.67	2.44	1.07	1.05	1.78	1.77	2.47	1.80	1.79
	Min.	0.18	0.81	0.38	0.37	0.57	0.47	0.80	0.56	0.46
	Median	0.71	3.56	1.42	1.40	2.58	2.57	3.59	2.59	2.59
	Max.	5.78	21.28	8.19	8.13	15.64	15.56	22.13	16.29	16.20
$E\{[\hat{A}_j–A]^2\}^{1/2}/A$ (%)	Mean	1.62	4.36	2.25	2.22	3.31	3.30	4.39	3.34	3.32
	Std. dev.	0.86	2.47	1.15	1.13	1.81	1.79	2.50	1.83	1.82
	Min.	0.46	1.06	0.57	0.56	0.83	0.81	1.07	0.84	0.82
	Median	1.39	3.79	1.92	1.90	2.87	2.86	3.83	2.90	2.88
	Max.	8.30	22.44	9.40	9.30	17.00	16.84	23.68	17.85	17.70

Table 37. Summarised distributions of the relative within-cross-section RMSEs of the area estimators $\hat{A}_6$–$\hat{A}_{11}$ with respect to convex area A_C and true area A in the set of all the cross-sections (n=709); for comparison, the results on the estimator $\hat{A}_0$ are also given.

Relative RMSE	Statistic	Diameter selection method j						
		0	6	7	8	9	10	11
$E\{[\hat{A}_j–A_C]^2\}^{1/2}/A_C$ (%)	Mean	0.90	0.93	0.86	1.34	1.36	2.50	2.43
	Std. dev.	0.67	0.85	0.80	1.12	1.14	1.75	1.74
	Min.	0.18	0.00	0.00	0.00	0.00	0.01	0.04
	Median	0.71	0.72	0.66	1.03	1.06	2.16	2.10
	Max.	5.78	7.44	7.07	5.94	5.94	12.10	11.85
$E\{[\hat{A}_j–A]^2\}^{1/2}/A$ (%)	Mean	1.62	1.43	1.32	1.11	1.11	3.21	3.13
	Std. dev.	0.86	1.09	1.02	0.97	0.97	1.90	1.89
	Min.	0.46	0.00	0.00	0.00	0.00	0.02	0.03
	Median	1.39	1.23	1.15	0.86	0.86	2.87	2.78
	Max.	8.30	8.55	8.17	6.75	6.47	13.98	13.72

As is evident from the variance results above, the sampling error component dominated the within-cross-section RMSEs in our data. Consequently, the advantageousness of using the fixed estimators in single-tree area estimation became fairly obvious: the girth diameter estimator ($\hat{A}_0$, for which the RMSE equalled the bias in each cross-section) produced generally small and the most stable RMSEs, and also the fixed area estimators involving D_{min}, D_{max} and the perpendicular of D_{min} ($\hat{A}_6$–$\hat{A}_9$, which produced both negative and positive biases and the smallest average biases) performed well, on average sometimes even better than the girth diameter estimator (Fig. 52, Table 37). Among the random estimators, the ones involving one random diameter and its perpendicular ($\hat{A}_2$, $\hat{A}_3$, $\hat{A}_{2\xi}$, $\hat{A}_{3\xi}$) proved to

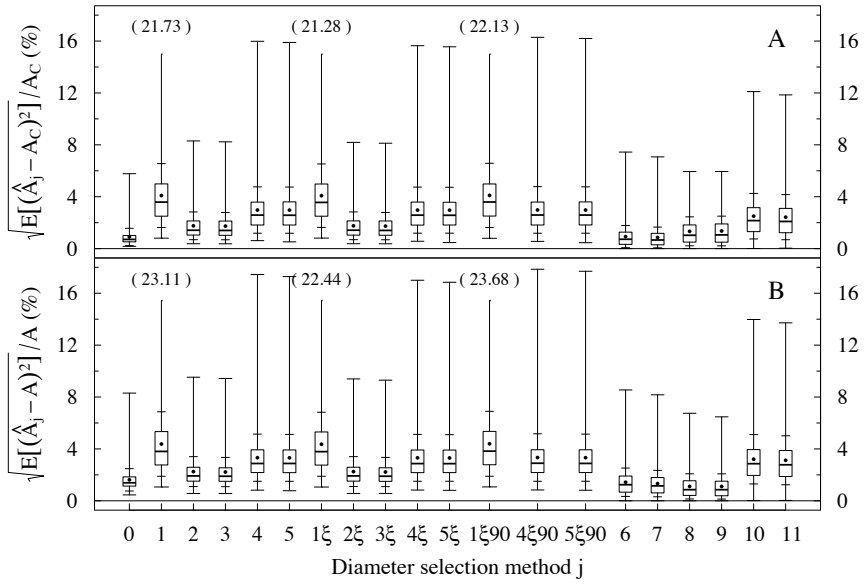

Fig. 52. Summarised distributions of the relative within-cross-section RMSEs of the area estimators $\hat{A}_0$, $\hat{A}_1$–$\hat{A}_5$, $\hat{A}_{1\xi}$–$\hat{A}_{5\xi}$, $\hat{A}_{1\xi 90}$, $\hat{A}_{4\xi 90}$, $\hat{A}_{5\xi 90}$ and $\hat{A}_6$–$\hat{A}_{11}$ with respect to convex area (A) or true area (B) in the set of all the discs (n=709). The Bitterlich diameter direction distribution was determined in the breast height cross-section in each tree with viewing angle 1.146° (basal area factor 1 m^2/ha with circular cross-sections). In the parentheses, the maximum values reaching out of the figure are given. (For the explanation of the boxplot, refer to the caption of Fig. 44.)

be preferred in single-tree estimation: they yielded patently the narrowest RMSE distributions, comparable to the good fixed estimators ($\hat{A}_6$–$\hat{A}_9$) in terms of variation, yet with larger average values (Fig. 52, Tables 35 and 36). With respect to relative height in a stem, the within-cross-section RMSEs followed the patterns of the within-cross-section biases for the fixed estimators (Figs. 53 D and 54 D; cf. Figs. 45 D and 46 D) and the patterns of the within-cross-section sampling errors for the random estimators (Figs. 53 A–C and 54 A–C; cf. Figs. 49 and 50).

8.4 Estimation of Stem Volume

The volume estimation results consist of the distributions of the estimated within-tree biases, standard deviations and RMSEs of the volume estimators — the combinations of the 22 diameter selection methods (see Section 7.2) and the three volume estimation methods — proportioned to the reference volume specific for each volume estimation method (see Section 7.3, Table 17) and considered in the sets of 50 (Laasasenaho volume equation) or 79 stems of the data. The different diameter selection methods were in principle applied both dependently and independently at the different observation heights within a stem (in dependent selection, the common diameter direction to be applied at all the observation heights was determined at breast height); independent selection, however, was not feasible with Bitterlich diameters and could not be meaningfully applied to the general volume

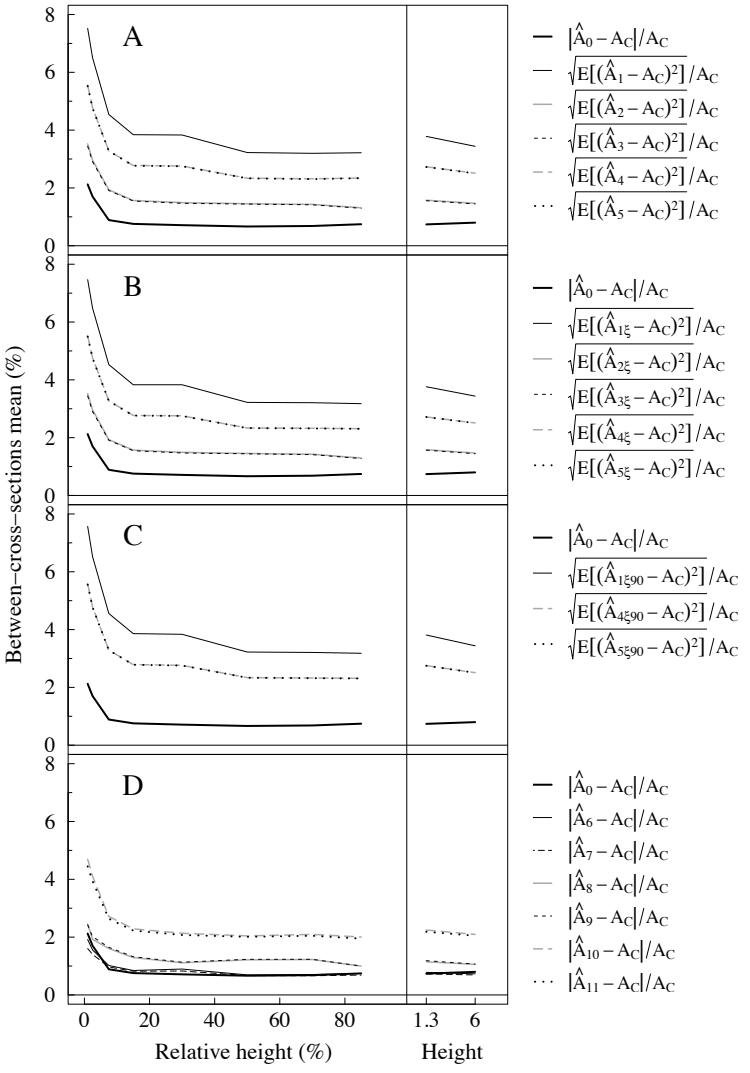

Fig. 53. Means of the relative within-cross-section RMSEs of the area estimators $\hat{A}_0$, $\hat{A}_1$–$\hat{A}_5$, $\hat{A}_{1\xi}$–$\hat{A}_{5\xi}$, $\hat{A}_{1\xi 90}$, $\hat{A}_{4\xi 90}$, $\hat{A}_{5\xi 90}$ and $\hat{A}_6$–$\hat{A}_{11}$ with respect to convex area at the ten observation heights. The Bitterlich diameter direction distribution was determined in the breast height cross-section in each tree with viewing angle 1.146° (basal area factor 1 m^2/ha with circular cross-sections).

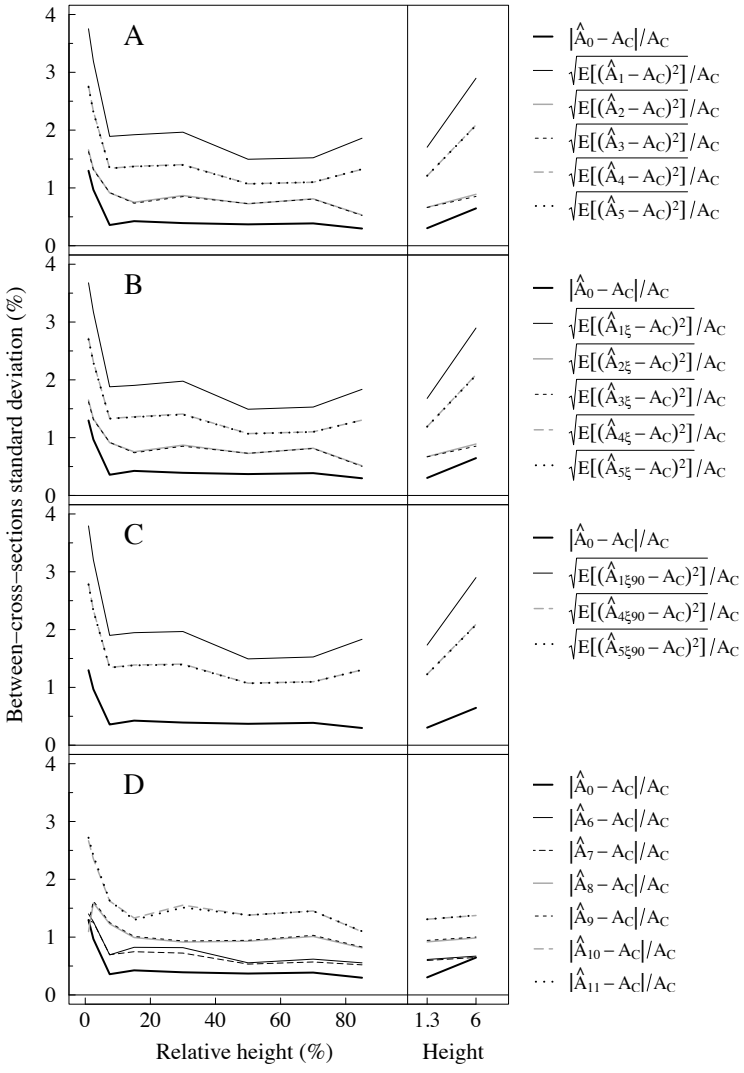

Fig. 54. Standard deviations of the relative within-cross-section RMSEs of the area estimators $\hat{A}_0$, $\hat{A}_1$–$\hat{A}_5$, $\hat{A}_{1\xi}$–$\hat{A}_{5\xi}$, $\hat{A}_{1\xi 90}$, $\hat{A}_{4\xi 90}$, $\hat{A}_{5\xi 90}$ and $\hat{A}_6$–$\hat{A}_{11}$ with respect to convex area at the ten observation heights. The Bitterlich diameter direction distribution was determined in the breast height cross-section in each tree with viewing angle 1.146° (basal area factor 1 m^2/ha with circular cross-sections).

estimator with random diameters either (see the discussion in the beginning of Section 7.3 and in Section 7.3.4). As in the cross-section area estimation, girth diameter served as a "yardstick" to which the other diameter selection methods were compared.

As pointed out earlier (see the discussion on the area estimation in Section 8.3.2), if we wanted to estimate the total stem volume of a stand, it would be sensible to choose volume estimator by its average behaviour, as expressed by mean within-tree bias across trees; variation in estimates within and between trees would then be of lesser importance. If, in turn, we were to estimate the stem volume of an individual tree, also variation in volume estimates within and between trees would count, and therefore both mean within-tree bias and RMSE as well as their standard deviations across trees would be useful measures of estimator performance. The smaller the within-tree and between-trees variation in estimates, the more feasible it would be to try to correct the systematic error of an estimator. For a volume estimator involving no randomness, within-tree RMSE equals the absolute value of the volume estimation error; if the estimator produces both positive and negative estimation errors, the mean and variance of RMSE across trees may then give an erroneous impression about the performance of the estimator in stand total estimation (positive and negative errors in different stems are not allowed to cancel out each other) or about its error variation in single tree estimation (turning negative estimation errors into positive decreases variance), respectively.

As in the area estimation, varying viewing angle within the range of 1.146°–3.624° (basal area factor, with circular cross-sections, within the range of 1–10 m^2/ha) did not practically influence the results of any volume estimators involving Bitterlich diameters. Further, Bitterlich diameters yielded results very similar to those given by dependently selected random diameters with the uniform direction distribution; as pointed out earlier (see Section 8.3.2), this was expected, as the breast height cross-sections deviated little from circles and as the other cross-sections in the same tree did not faithfully echo the shape of the breast height cross-section. *Consequently, we present in the following only the results for random diameters with the uniform direction distribution (diameter selection methods 1–5), but remind that the results from dependent selection pertain to Bitterlich diameters (diameter selection methods 1ξ–5ξ, 1ξ90, 4ξ90 and 5ξ90) with viewing angles 1.146°–3.624° (basal area factors 1–10 m^2/ha with circular cross-sections) as well.*

For the comparison between the different diameter selection methods within each volume estimation method, some questions of interest naturally arise from the theory and results on cross-section area estimation (Chapter 3, Section 4.2 and Section 8.3): we want to find out how the properties of the different diameter selection methods observed in area estimation are reflected in volume estimation (e.g. whether the interrelationships of the methods are preserved in volume estimation, whether assuming cross-sections elliptic vs. circular makes any practical difference, whether the second diameter is advisable to be calipered crosswise rather than in a random direction to minimise bias and sampling error etc.). We also want to see whether the magnitude of error due to diameter selection is much larger or smaller in volume estimation than in area estimation, whether it differs between the different volume estimation methods (e.g. whether the error due to diameter selection is larger in a method where a larger number of diameters within a stem are involved), and whether it is related to the size and the growing site location of a stem; note, however, that although we strove to differentiate the error related to diameter selection from the error inherent in the volume estimation method by varying the reference volume with respect to which the estimator properties were computed, the resulting diameter selection effect may still not carry exactly the same meaning in each of the three volume estimation methods. For the comparison between dependent (the prevailing practice) and independent diameter selection within a stem, theory on volume estimation (Chapter 5) provides some anticipations:

we expect that dependence will affect the within-tree variances more than the within-tree biases of the volume estimators; particularly, dependent selection of random diameters should increase the within-tree variances due to the presumably positive correlation between parallel diameters at adjacent heights, whereas dependent selection of D_{min} and/or D_{max} and their perpendiculars should decrease the within-tree biases due to the fact that the directions of D_{min} and D_{max} vary very much between the heights (see Section 8.2.1). Finally, we are naturally interested in the effect of disregarding non-convexity of cross-sections (as the commonly used measurement equipment only give information on the convex closures of cross-sections); note, however, that the convexity assumption turns up somewhat differently in each of the three volume estimation methods and that its effect cannot thus be assessed fully commensurately in the different methods.

As pointed out earlier (see Section 8.1), the quality of our data sets certain limits to the interpretation of the volume estimation results: Due to the strongly skewed and bimodal stem size distribution with only 8 sawlog-size stems, it was difficult to establish the effect of stem size on volume estimation errors. Also, size effect might be confounded with location effect, as all the sawlog-size trees were growing in the two southernmost plots, where no pulpwood-size trees were taken (see Table 10, Fig. 22). Furthermore, in 51 stems out of 79, the true stem volume was probably estimated less precisely due to the missing discs at the height of 1% (the stem curve was approximated with an interpolating parabola between the stump height and the first observation height), which was then reflected as larger uncertainties both in the model error of the Laasasenaho volume equation and in the diameter selection effect with the cubic-spline-interpolated stem curve. At the same time, not having these 1% discs, which would probably have been more irregular in shape than the upper discs, may have resulted in unrealistically small diameter selection effects with the cubic-spline-interpolated stem curve and the general volume estimator.

The cubic-spline-interpolated stem curve and the general volume estimator could be applied to a larger set of stems than the Laasasenaho volume equation, since there were more stems with observations at seven or more heights (79) than stems with observations at both the heights of 1.3 m and 6 m (50). With all the diameter selection methods except those based on both D_{min} and D_{max} (methods 6 and 7), this difference in the application data slightly affected the results. The effect will be explained in more detail below, but we may conjecture that the results given below for the Laasasenaho volume equation may be slightly over-optimistic, as the within-tree biases and variances obtained with the other two volume estimators for the 50 stems proved to be slightly smaller than those obtained for the whole set of 79 stems.

8.4.1 Laasasenaho Volume Equation

With the Laasasenaho volume equation, the differences in the within-tree volume expectations and variances between the different diameter selection methods followed straightforwardly from the differences in the diameters or the diameter moments between the methods (see Eqs. 158 and 159 in Section 7.3.2 and the method-specific equations in Appendices E and F); particularly, the effect of measuring the diameters at the two heights independently vs. taking them dependently manifested itself explicitly in the diameter product moments. However, as the coefficients $\hat{c}_1, ..., \hat{c}_4$ of the moments were functions of the tree height H and the regression coefficient estimates $\hat{\beta}_1, ..., \hat{\beta}_6$ (Fig. 55), similar differences in diameters or diameter moments produced dissimilar effects in trees of different sizes.

The effect of assuming tree cross-sections convex emerged through the very slightly different coefficient functions $\hat{c}_1, ..., \hat{c}_4$ resulting from the different regression coefficient

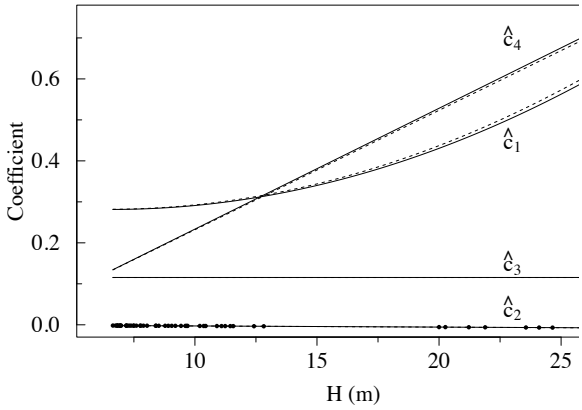

Fig. 55. Coefficient functions employed in the stem volume estimators based on the Laasasenaho volume equation (Eq. 157 in Section 7.3.2). The functions consist of the parameter estimates $(\hat{\beta}_1,\ldots,\hat{\beta}_6)$ of the Laasasenaho equation and of tree height (H): $\hat{c}_1 = \hat{\beta}_1 + \hat{\beta}_2 H + \hat{\beta}_4 H^2 + \hat{\beta}_5$, $\hat{c}_2 = \hat{\beta}_3 H$, $\hat{c}_3 = \hat{\beta}_5$, and $\hat{c}_4 = \hat{\beta}_5 + \hat{\beta}_6 (H - 6)$. The parameters of the Laasasenaho equation were re-estimated in our data with (dashed line) and without (solid line) the assumption of convex cross-sections (for the parameter estimates refer to Table 18 in Section 7.3.2). The points indicate the 50 stems for which both 1.3 m and 6 m discs were available and that could thus be included in the estimation.

estimates $\hat{\beta}_1$, ..., $\hat{\beta}_6$ (Table 18, Fig. 55) and through the different reference volumes with respect to which the within-tree biases were computed and by which both the biases and the variances were proportioned (the best estimate $\tilde{V}_L$ vs. $\tilde{V}_{CL}$ based on true area diameters $D_A(1.3)$ and $D_A(6)$ vs. convex area diameters $D_{Ac}(1.3)$ and $D_{Ac}(6)$ for estimation without vs. with the convexity assumption; see Section 7.3.2).

We used the best estimate $\tilde{V}_L$ (or $\tilde{V}_{CL}$; the fixed part of the model), instead of the estimated true volume $\tilde{V}$ (or the estimated convex volume $\tilde{V}_C$; the response variable of the model), as the reference volume because we strove to distinguish the diameter selection effect from the error inherent in the volume equation; this inherent model error is due to variation in stem tapering and would remain in the volume estimate even if the both the two observed cross-sections of a stem were circular and their diameters were measured without error (see Section 5.1 and Section 7.3.2). The relative model error was estimated in each stem with the relative residual $(\tilde{V}_L - \tilde{V})/\tilde{V}_L$ (or $(\tilde{V}_{CL} - \tilde{V}_C)/\tilde{V}_{CL}$). The distributions of these relative model errors among all the trees where both 1.3 m and 6 m discs were available, as well as in the subsets of pulpwood-size and sawlog-size trees, are summarised in Table 38. The model error was found to be unassociated with the diameter selection effect: the relative within-tree biases, variances and RMSEs produced by the different diameter selection methods (and computed with respect to the reference volume) did not correlate with the model errors (cf. the examples in Fig. 56). In other words, a large model error and a poor performance of any diameter selection method, or vice versa, did not systematically coincide in our trees.

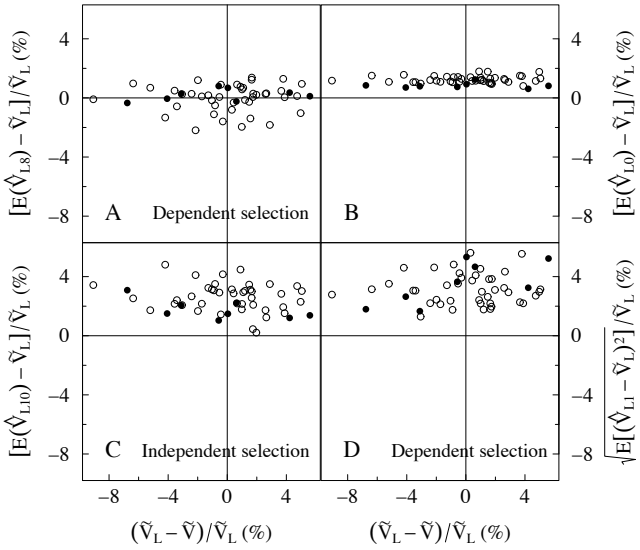

Fig. 56. Examples of the relationship between the relative model error ($(\tilde{V}_L - \tilde{V})/\tilde{V}_L$, cf. Table 38) and the performance of some diameter selection methods with the re-estimated Laasasenaho volume equation in the set of the stems for which both 1.3 m and 6 m discs were available (n=50): the relative within-tree biases obtained with (A) the arithmetic mean of D_{min} and its perpendicular (diameter selection method 8, producing the smallest average within-tree bias among all the methods), (B) girth diameter (method 0, "yard-stick method"), and (C) the arithmetic mean of D_{max} and its perpendicular (method 10, producing the largest average within-tree bias among all the methods), as well as (D) the relative within-tree RMSEs obtained with one random diameter (method 1, producing the largest within-tree variance among all the methods). Sawlog-size trees (cf. Table 38) are denoted with filled circles. Here the volume equation re-estimated without assuming stem cross-sections convex was used; the equation re-estimated with the convexity assumption gave practically similar relationships.

Biases

With random diameters (diameter selection methods 1–5), dependent and independent selection produced practically similar relative within-tree biases (the differences in the distribution statistics were less than one hundredth of percentage unit). This was hardly astonishing, as the bias formulae with dependent and independent selection deviated from each other only in terms of one product moment term (Eq. 158 in Section 7.3.2, Appendix E). *Hence, for these diameter selection methods, we here only present the results obtained with dependent selection.*

As in the area estimation, employing girth diameter (method 0) and random diameters (methods 1–5) in the volume equation resulted in systematic overestimation and produced practically similar bias distributions (Table 39, Fig. 57); compared with the area estimation, the distributions had slightly smaller means (1.2% vs. 1.6% without the convexity assumption, and 0.6% vs. 0.9% with the convexity assumption) and medians and considerably narrower ranges and inter-quartile ranges (cf. Table 28 and Fig. 44). In other words, as in the area estimation, measuring a second diameter, either in a random direction (methods 4 and 5) or crosswise (methods 2 and 3), hardly reduced within-tree prediction bias compared

Table 38. Summarised distributions of the relative model errors (relative residuals) of the two re-estimated Laasasenaho volume equations among all the trees where both 1.3 m and 6 m discs were available (n=50) and in the subsets of small (14 $dm^3 \leq \tilde{V} \leq 127\ dm^3$; n=42) and large (318 $dm^3 \leq \tilde{V} \leq 756\ dm^3$; n=8) trees. The equations were re-estimated (i) with estimated true volume $\tilde{V}$ and true area diameters $D_A(1.3)$ and $D_A(6)$ as the response and explanatory variables (i.e., without convexity assumption on the cross-sections) and (ii) with estimated convex volume $\tilde{V}_C$ and convex area diameters $D_{Ac}(1.3)$ and $D_{Ac}(6)$ as the response and explanatory variables (i.e., with convexity assumption on the cross-sections). $\tilde{V}_L$ and $\tilde{V}_{CL}$ stand for the volume estimates given by the fixed parts of the models.

Statistic	$(\tilde{V}_L-\tilde{V})/\tilde{V}_L$ (%)			$(\tilde{V}_{CL}-\tilde{V}_C)/\tilde{V}_{CL}$ (%)		
	All trees	Small trees	Large trees	All trees	Small trees	Large trees
Mean	0.00	0.10	–0.51	0.00	0.10	–0.51
Std. dev.[1]	3.22	3.07	4.14	3.23	3.09	4.12
Std. dev.[2]	3.59			3.60		
Minimum	–9.07	–9.07	–6.78	–9.06	–9.06	–6.07
1st quartile	–1.92	–1.61	–3.35	–1.95	–1.63	–3.44
Median	0.52	0.78	–0.27	0.52	0.78	–0.26
3rd quartile	1.75	1.75	1.52	1.75	1.75	1.58
Maximum	5.59	5.05	5.59	5.46	5.14	5.46

[1] (n–1) as the denominator
[2] (n–p), p=6, as the denominator

Table 39. Summarised distributions of the relative within-tree biases of the volume estimators based on the re-estimated Laasasenaho volume equations and girth or dependently selected random diameters with the uniform direction distribution (measurement direction determined at the height of 1.3 m for both the heights of 1.3 m and 6 m), among the trees where both the 1.3 m and 6 m discs were available (n=50). The biases were determined with respect to the best volume estimate $\tilde{V}_L$ or the best convex volume estimate $\tilde{V}_{CL}$. Selecting random diameters independently at both the observation heights produced practically similar results.

Relative bias	Statistic	Diameter selection method j					
		Dependent selection					
		0	1	2	3	4	5
$[E(\hat{V}_{Lj})-\tilde{V}_L]/\tilde{V}_L$ (%)	Mean	1.19	1.21	1.19	1.16	1.20	1.18
	Std. dev.	0.27	0.27	0.27	0.27	0.27	0.27
	Min.	0.61	0.63	0.61	0.59	0.62	0.61
	Median	1.16	1.18	1.17	1.15	1.18	1.16
	Max.	1.79	1.81	1.80	1.78	1.80	1.79
$[E(\hat{V}_{CLj})-\tilde{V}_{CL}]/\tilde{V}_{CL}$ (%)	Mean	0.63	0.66	0.64	0.61	0.64	0.63
	Std. dev.	0.19	0.19	0.19	0.18	0.19	0.19
	Min.	0.34	0.35	0.34	0.33	0.34	0.34
	Median	0.58	0.60	0.59	0.55	0.59	0.58
	Max.	1.09	1.11	1.10	1.08	1.10	1.09

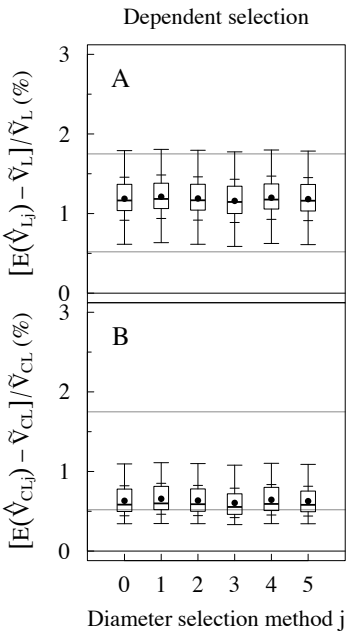

Fig. 57. Summarised distributions of the relative within-tree biases of the volume estimators based on the re-estimated Laasasenaho volume equation and girth (diameter selection method 0) or random diameters (diameter selection methods 1–5) in the set of the stems for which both 1.3 m and 6 m discs were available (n=50). The equation was estimated without (A) or with (B) the assumption of convex cross-sections, and the diameters were selected dependently within a stem with breast height diameter determining the common diameter direction (independent selection gave practically similar results). The box depicts the inter-quartile range bisected by the median, and the whiskers reach out to the extreme points of the data; the filled circle denotes the arithmetic mean, whereas the short horizontal line segments below and above it indicate the magnitude of the sample standard deviation. For comparison, the distribution summary of the relative model errors (relative residuals) in the data are given (to the extent that it fits in the figure, see Table 38): median and 3rd quartile (continuous grey line).

to using only one random diameter (method 1), and the benefit of using the geometric mean instead of the arithmetic one (method 3 vs. 2, 5 vs. 4) was also negligible. Assuming cross-sections convex (disregarding non-convexity) shifted the bias distributions about 0.6 percentage units closer to zero and clearly shortened the ranges, but failed to decrease the variances and narrow the inter-quartile ranges to the same extent (Fig. 57 A vs. B, Table 39). Judging from inter-quartile ranges and the between-trees standard deviations, the systematic error due to diameter selection appeared relatively small compared to the model error (Table 39 vs. Table 38, Fig. 57).

The fact that girth diameter (mean diameter over the uniform direction distribution) resulted in similar biases as random diameters indicates that the second and third moments and the product moment of random diameters were very close to the second and the third powers and the product of mean diameters at the heights of 1.3 and 6 m (cf. Eq. 158 in Section 7.3.2, Appendix E).

Employing fixed diameters (methods 6–11) in the volume equation yielded far more variable biases than using girth and random diameters, in terms of both the between-trees variances (Table 40 vs. Table 39) and the ranges and inter-quartile ranges reaching frequently also to negative values (Fig. 58 vs. Fig. 57). Yet also with these methods, the error due to diameter selection seemed clearly smaller than the model error (Table 40 vs. Table 38, Fig. 58). The same methods that performed well in terms of average bias in the area estimation did well with the volume equation as well: D_{min} and its perpendicular (methods 8 and 9), especially with dependent selection (the upper diameter taken in the same direction as the breast height diameter), yielded on average no additional bias on top of the model error when no convexity was assumed in the equation estimation (Fig. 58 B, Table 40); similarly, D_{min} together with D_{max} (methods 6 and 7) produced on average smaller bias than girth or random diameters, be the diameters selected independently or dependently or the equations estimated with or without the convexity assumption (Table 40, Fig. 58). Generally, dependent

Table 40. Summarised distributions of the relative within-tree biases of the volume estimators based on the re-estimated Laasasenaho volume equations and independently (measurement directions determined independently for the heights of 1.3 m and 6 m) or dependently (measurement direction determined for both the heights at the height of 1.3 m) selected fixed diameters, among the trees where both 1.3 m and 6 m discs were available (n=50). For comparison, the results of the estimator based on girth diameter (diameter selection method 0) are also given.

Relative bias	Statistic	Diameter selection method j								
		Independent selection								
		0	6	7	8	9	10	11	min	max
$[E(\hat{V}_{Lj})-\tilde{V}_L]/\tilde{V}_L$ (%)	Mean	1.19	0.98	0.89	–0.33	–0.39	2.48	2.42	–4.56	6.67
	Std. dev.	0.27	0.67	0.68	0.81	0.81	0.98	0.99	1.72	1.67
	Min.	0.61	–1.40	–1.54	–2.03	–2.12	0.21	0.13	–9.34	2.69
	Median	1.16	1.16	1.02	–0.15	–0.20	2.47	2.43	–4.38	6.60
	Max.	1.79	2.02	1.91	1.14	1.05	4.81	4.75	–1.54	10.37
$[E(\hat{V}_{CLj})-\tilde{V}_{CL}]/\tilde{V}_{CL}$ (%)	Mean	0.63	0.43	0.33	–0.87	–0.94	1.92	1.86	–5.08	6.09
	Std. dev.	0.19	0.66	0.66	0.82	0.81	0.94	0.95	1.69	1.68
	Min.	0.34	–1.89	–2.08	–2.52	–2.61	–0.50	–0.58	–9.86	2.05
	Median	0.58	0.59	0.48	–0.77	–0.81	1.88	1.83	–4.99	6.03
	Max.	1.09	1.46	1.35	0.72	0.64	4.02	3.97	–2.15	9.84
		Dependent selection								
		6	7	8	9	10	11	min	max	
$[E(\hat{V}_{Lj})-\tilde{V}_L]/\tilde{V}$ (%)	Mean	1.08	1.01	0.02	–0.03	2.24	2.19	–3.52	5.80	
	Std. dev.	0.87	0.89	0.86	0.86	1.00	1.00	2.26	1.96	
	Min.	–1.48	–1.68	–2.19	–2.35	0.26	0.18	–9.31	2.12	
	Median	1.16	1.05	0.15	0.10	2.15	2.11	–3.36	5.85	
	Max.	3.15	3.09	1.38	1.37	4.81	4.76	2.46	10.26	
$[E(\hat{V}_{CLj})-\tilde{V}_{CL}]/\tilde{V}_{CL}$ (%)	Mean	0.53	0.45	–0.53	–0.58	1.68	1.63	–4.05	5.23	
	Std. dev.	0.85	0.87	0.86	0.86	0.95	0.96	2.22	1.96	
	Min.	–2.04	–2.23	–2.75	–2.91	–0.46	–0.53	–9.83	1.45	
	Median	0.62	0.51	–0.42	–0.45	1.48	1.45	–3.86	5.37	
	Max.	2.48	2.42	0.80	0.79	4.05	4.04	1.77	9.73	

and independent diameter selection resulted in fairly similar interrelationships between the different diameter selection methods (Fig. 58 A vs. B, C vs. D); dependent selection tended to shift the distributions slightly toward zero, which was expected, as with this approach the true D_{min} or D_{max} at the height of 6 m were not employed. Finally, the effect of assuming convexity parallelled that observed with random diameters: the assumption shifted the bias distributions downwards by some 0.5–0.6 percentage units but did not practically influence the variability (Fig. 58 A vs. C, B vs. D, Table 40).

Tree size appeared to be moderately associated with relative within-tree bias, when girth or random diameters (methods 0 and 1–5; independent and dependent selection) were used — the correlations between the estimated true stem volumes and the relative biases were around –0.5, and the relative biases in the pulpwood-size stems were on average 1.5-fold compared to those in the sawlog-size stems — but only when cross-section non-convexity was taken into account. In other words, the convexity assumption diminished the bias caused by girth or random diameter selection relatively more in the small trees than in the large ones. The volume equations estimated with and without the convexity assumption, however,

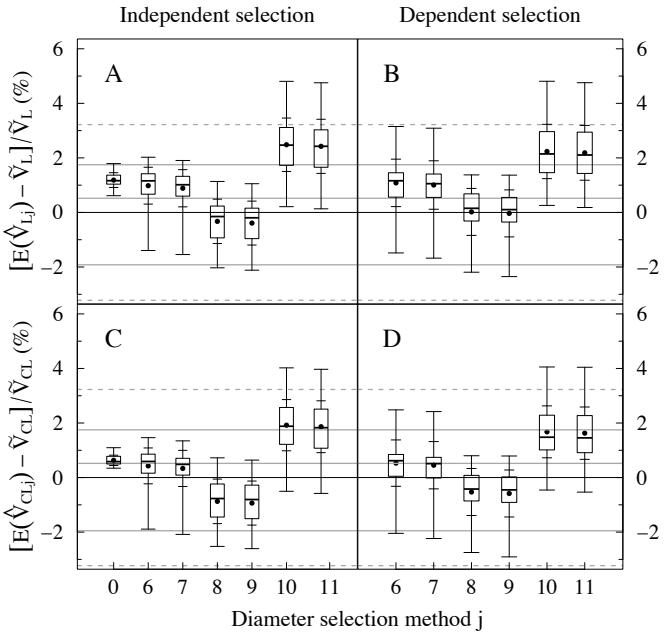

Fig. 58. Summarised distributions of the relative within-tree biases of the volume estimators based on the re-estimated Laasasenaho volume equation and fixed diameters (diameter selection methods 6–11) in the set of the stems for which both 1.3 m and 6 m discs were available (n=50); for comparison, results obtained with girth (diameter selection method 0) are also given. The equation was estimated without (A, B) or with (C, D) the assumption of convex cross-sections, and the diameters were selected independently (A, C) or dependently (B, D) within a stem. For comparison, the distribution summary of the relative model errors (relative residuals) in the data are given (see Table 38): 1st quartile, median and 3rd quartile (continuous grey line), and mean (0) ± standard deviation (dashed grey line). (For the explanation of the boxplot, refer to the caption of Fig. 57.)

gave very similar within-tree volume expectations with the same diameter moments (as the differences in the regression coefficients were small), and hence the size effect was largely attributable to the use of the different reference volumes (with respect to which the relative biases were taken): the breast height and upper cross-sections of the sawlog-size trees in the data were slightly less non-convex than those of the pulpwood-size ones (cf. Fig. 35 in Section 8.2.2, where negative correlation is shown between the convex deficit and the cross-section size particularly at the height of 6 m but also at the height of 1.3 m), which caused the best estimates (reference volumes $\tilde{V}_L$ and $\tilde{V}_{CL}$) to be closer to each other in the sawlog-size trees (as the convex area diameters deviated less from the true area diameters). With other fixed diameters than the girth diameter, no such size effect was found; evidently, the large variation in diameters between the stems of approximately the same size masked the influence of the reference volume.

Geographical location of growing site did not have influence on relative within-tree bias. The seeming beneficiality of growing in the south, resulting in smaller biases with girth or random diameters but not with other methods, proved to be a size-related artefact: the two southernmost plots only involved the 8 sawlog-size trees, and the pulpwood-size

trees taken from the third southernmost plot yielded quite contrasting results. On the basis of the observations made on larger variability in stem tapering in Lapland (Laasasenaho 1982), we would have expected larger variability in within-tree biases in the north than in the south, but this was not found.

The combined effect of diameter selection and model error is given by the bias taken with respect to the estimated true volume (i.e., $[E(\hat{V}_{Lj})–\tilde{V}]/\tilde{V}_L$, or $[E(\hat{V}_{CLj})–\tilde{V}_C]/\tilde{V}_{CL}$, where j stands for the diameter selection method). The first-order summary characteristics (mean, median, quartiles) of the distributions of these biases are approximately obtained by summing the characteristics of the distributions of the two components, that is, of the biases with respect to the best estimate (Tables 39 and 40) and of the model errors (Table 38). In this way, however, the minimums become underestimated and the maximums overestimated, by less than half a percentage unit with random diameters (methods 1–5), but by several percentage units at worst with fixed diameters (methods 6–11, min, max). As for the second-order characteristics (variance, standard deviation), the case is more complicated: With random diameters, the sum of the variances of the two components underestimates the variance of the combined effect, as the positive (although very small) covariance between the components is not taken into account, whereas the sum of the standard deviations of the components very slightly overestimates the standard deviation of the combined effect. With fixed diameters, the variance becomes either underestimated or overestimated (the small covariance between the components can be either positive or negative), but the sum of the standard deviations of the components always overestimates the standard deviation of the combined effect, yet not more than one percentage unit (except for the min and max methods).

Variances

With random diameters (diameter selection methods 1–5), the convexity assumption had no practical influence on the sampling errors in the volume estimates (with and without the assumption, the distribution statistics of the relative within-tree standard deviations were equal up to one hundredth of percentage unit). *Therefore we here present only the results obtained without the convexity assumption.*

As in the area estimation, the different random diameter selection methods entailed manifestly different sampling errors (Table 41, Fig. 59); the distributions of the sampling errors were fairly similar to those in the area estimation, although with slightly smaller means and medians and considerably less variation between the trees (cf. Table 33 and Fig. 48). Again, using a random diameter and its perpendicular (methods 2 and 3) resulted in the least variable sampling errors with clearly the smallest average (1.0% — smaller than the average within-tree bias without the convexity assumption), whereas the other methods entailed double or triple that magnitude of average sampling error and much larger between-trees variation. Indeed, the benefit of taking the second diameter crosswise instead of measuring it in a random direction (method 2 vs. 4, 3 vs. 5) was greater than that gained by measuring two random diameters instead of only one (methods 4 and 5 vs. 1). Behind the superiority of perpendicular diameters lies their negative correlation observed earlier within a majority of the cross-sections (see Section 8.2.1): the correlation manifests itself more clearly in the within-tree variances than in the biases simply because the terms of the form $E[D(\theta, 1.3)^m D(\theta+\pi/2, 1.3)^n]$ and $E[D(\theta, 6)^m D(\theta+\pi/2, 6)^n]$, $m, n \in \mathbb{R}_+$, involving products of the perpendicular diameters are more numerous in the variance expressions (Eq. 159 in Section 7.3.2, Appendix F) than in the bias expressions (Eq. 158 in Section 7.3.2, Appendix E). (Negative correlation between $D(\theta)$ and $D(\theta+\pi/2)$ implies

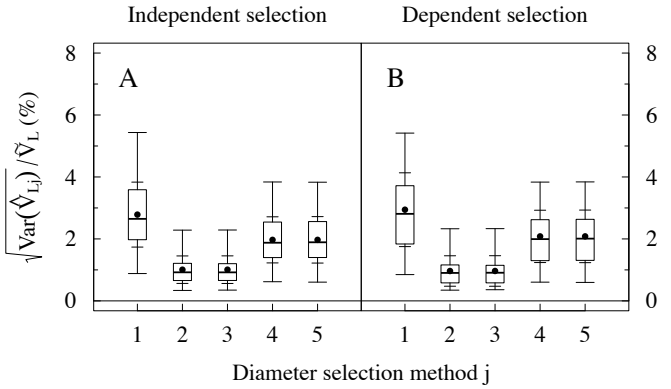

Fig. 59. Summarised distributions of the relative within-tree standard deviations of the volume estimators based on the re-estimated Laasasenaho volume equation and random diameters (diameter selection methods 1–5) in the set of the stems for which both 1.3 m and 6 m discs were available (n=50). The equation estimated without the assumption of convex cross-sections was used (the equation with convexity assumption gave practically similar results), and the diameters were selected independently (A) or dependently (B) within a stem. (For the explanation of the boxplot, refer to the caption of Fig. 57.)

Table 41. Summarised distributions of the relative within-tree standard deviations of the volume estimators based on the Laasasenaho volume equation re-estimated without convexity assumption and on independently or dependently selected random diameters with the uniform direction distribution, among the trees where both the 1.3 m and 6 m discs were available (n=50). The volume equation re-estimated with the convexity assumption gave practically similar results.

Relative std. dev.	Statistic	Diameter selection method j									
		Independent selection					Dependent selection				
		1	2	3	4	5	1	2	3	4	5
$\mathrm{Var}(\hat{V}_{Lj})^{1/2}/\tilde{V}_L$ (%)	Mean	2.79	1.01	1.01	1.97	1.97	2.94	0.96	0.97	2.08	2.08
	Std. dev.	1.05	0.44	0.45	0.74	0.75	1.19	0.49	0.49	0.84	0.85
	Min.	0.88	0.34	0.35	0.62	0.60	0.85	0.35	0.36	0.60	0.60
	Median	2.65	0.92	0.92	1.88	1.89	2.81	0.90	0.91	1.99	2.01
	Max.	5.44	2.28	2.29	3.84	3.83	5.42	2.33	2.33	3.83	3.84

that $E[D(\theta)D(\theta+\pi/2)]<E[D(\theta)]E[D(\theta+\pi/2)]$, which can presumably be generalised into $E[D(\theta)^m D(\theta+\pi/2)^n]<E[D(\theta)^m]E[D(\theta+\pi/2)^n]$, $m, n \in \mathbb{R}_+$.) Whether the geometric or the arithmetic mean of diameters was employed in the estimator did not affect the sampling errors.

Unlike in the biases, dependence in diameter selection within a stem mattered, although only to a very slight extent, in the sampling errors: dependent selection produced slightly larger means and standard deviations as well as wider ranges and inter-quartile ranges than independent selection, except for crosswise calipered diameters, with which the variation increased only marginally and with which the means even slightly decreased (Fig. 59 A vs. B, Table 41). The variance-increasing effect of dependent selection is probably attributable to the positive correlation of breast height diameter and upper diameter taken in the same

direction within a stem. The influence is more discernible in variances than in biases, because the terms of the form $E[D(\theta, 1.3)^m D(\theta, 6)^n]$, $m, n \in \mathbb{R}_+$, are more numerous in the variance expressions (Eq. 159 in Section 7.3.2, Appendix F) than in the bias expressions (Eq. 158 in Section 7.3.2, Appendix E). (Positive correlation between $D(\theta, 1.3)$ and $D(\theta, 6)$ implies that $E[D(\theta, 1.3)D(\theta, 6)] > E[D(\theta, 1.3)]E[D(\theta, 6)]$, which can presumably be generalised into $E[D(\theta, 1.3)^m D(\theta, 6)^n] > E[D(\theta, 1.3)^m]E[D(\theta, 6)^n]$, $m, n \in \mathbb{R}_+$.) With perpendicular diameters, however, their negative within-cross-section correlation (see the discussion above) seems to counteract this influence; why the effect of negative correlation appears to be stronger in dependent selection than in independent selection remains unclear.

Neither tree size nor geographical location of growing site appeared to have an influence on the sampling errors.

RMSEs

As is evident from the results above, with random diameters (diameter selection methods 1–5) the diameter selection method affected the volume equation performance in an individual tree more via the sampling error component than via the bias component: the relative within-tree RMSEs followed the patterns exhibited by the relative within-tree standard deviations, although the differences between the methods were more moderate (Fig. 60, Table 42). The averages resulting from one (method 1) or two random diameters (methods 4 and 5) without convexity assumption were now approximately double or 1.5-fold the 1.6% produced by two perpendicular diameters (methods 2 and 3). Even with the poorest of these methods, however, the total diameter selection effect (the bias and the sampling error combined) appeared clearly smaller than the model error (Fig. 60). Ascribable to the relative within-tree biases, convexity assumption made a discernible difference, shifting the distributions some 0.2–0.4 percentage units closer to zero (Fig. 60 C vs. A and D vs. B, Table 42).

Equally biased but lacking within-tree variance, girth diameter (method 0) distinctly outperformed random diameters (Fig. 60, Table 42). Also compared to other fixed diameters (methods 6–11), girth diameter yielded the smallest average RMSE when non-convexity of cross-sections was ignored (Fig. 61, Table 43). Most importantly, however, the RMSEs produced by girth diameter varied clearly the least between the trees (Figs. 60 and 61), which makes this method best suited, among all the diameter selection methods considered, to single tree volume estimation and to bias correction.

With fixed diameters (methods 6–11), RMSE equalled the absolute value of bias, and hence the RMSE distribution deviated from the bias distribution only if the method yielded both negative and positive biases (Fig. 61 vs. Fig. 58). Measuring D_{min} and its perpendicular (methods 8 and 9) performed best on average when non-convexity of the cross-sections was taken into account (Table 43, Fig. 61 A and B), whereas measuring girth did best on average when non-convexity was disregarded (Table 43, Fig. 61 C and D). As to the effects of the independent vs. dependent diameter selection and the convexity assumption, no general patterns were to be found but the effect varied by the diameter selection method.

8.4.2 Cubic-Spline-Interpolated Stem Curve

With the non-parametric stem curves based on diameters at seven or more heights in a stem, the distinction between the different diameter selection methods in terms of within-tree bias was expected to become more pronounced than with the volume equation that involved only two diameters. Similarly, the difference between dependent and independent selection

Table 42. Summarised distributions of the relative within-tree RMSEs of the volume estimators based on the re-estimated Laasasenaho volume equations and girth diameter or independently or dependently selected random diameters with the uniform direction distribution, among the trees where both the 1.3 m and 6 m discs were available (n=50).

Relative RMSE	Statistic	Diameter selection method j										
		Independent selection						Dependent selection				
		0	1	2	3	4	5	1	2	3	4	5
$E[(\hat{V}_{Lj}-\tilde{V}_L)^2]^{1/2}/\tilde{V}_L$ (%)	Mean	1.19	3.07	1.58	1.56	2.34	2.33	3.22	1.56	1.54	2.45	2.44
	Std. dev.	0.27	0.99	0.44	0.44	0.68	0.68	1.11	0.46	0.47	0.75	0.75
	Min.	0.61	1.32	0.84	0.82	1.12	1.15	1.29	0.83	0.80	1.15	1.14
	Median	1.16	3.00	1.57	1.55	2.32	2.31	3.08	1.55	1.51	2.37	2.36
	Max.	1.79	5.65	2.78	2.76	4.12	4.10	5.61	2.81	2.80	4.10	4.09
$E[(\hat{V}_{CLj}-\tilde{V}_{CL})^2]^{1/2}/\tilde{V}_{CL}$ (%)	Mean	0.63	2.86	1.20	1.19	2.08	2.07	3.01	1.17	1.16	2.18	2.18
	Std. dev.	0.19	1.03	0.43	0.44	0.72	0.73	1.17	0.47	0.47	0.82	0.82
	Min.	0.34	0.94	0.59	0.55	0.70	0.69	0.91	0.53	0.51	0.69	0.68
	Median	0.58	2.72	1.12	1.12	1.99	2.00	2.88	1.12	1.12	2.09	2.10
	Max.	1.09	5.47	2.41	2.40	3.90	3.90	5.48	2.45	2.44	3.93	3.93

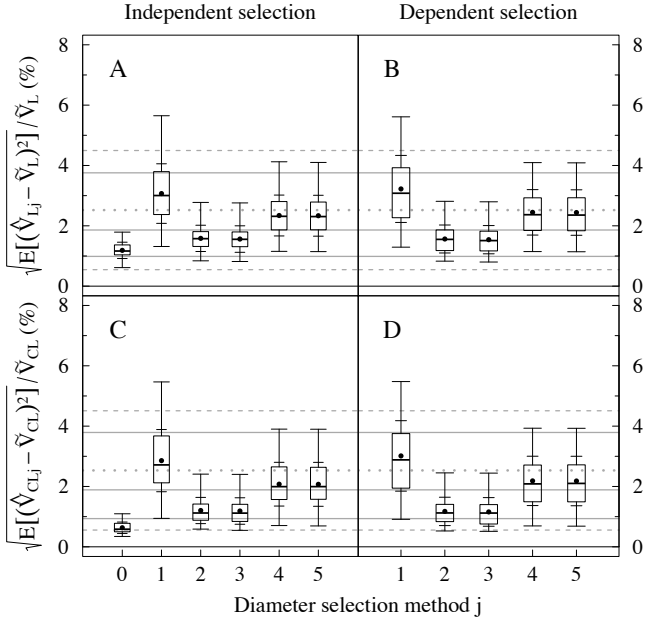

Fig. 60. Summarised distributions of the relative within-tree RMSEs of the volume estimators based on the re-estimated Laasasenaho volume equation and girth (diameter selection method 0) or random diameters (diameter selection methods 1–5) in the set of the stems for which both 1.3 m and 6 m discs were available (n=50). The equation was estimated without (A, B) or with (C, D) the assumption of convex cross-sections, and the diameters were selected independently (A, C) or dependently (B, D) within a stem. For comparison, the distribution summary of the absolute values of the relative model errors (relative residuals) in the data are given: 1st quartile, median and 3rd quartile (continuous grey line), mean (dotted grey line), and mean ± standard deviation (dashed grey line). (For the explanation of the boxplot, refer to the caption of Fig. 57.)

Table 43. Summarised distributions of the relative within-tree RMSEs of the volume estimators based on the re-estimated Laasasenaho volume equations and independently or dependently selected fixed diameters, among the trees where both 1.3 m and 6 m discs were available (n=50). For comparison, the results of the estimator based on girth diameter (diameter selection method 0) are also given.

Relative RMSE	Statistic	Diameter selection method j								
		Independent selection								
		0	6	7	8	9	10	11	min	max
$E[(\hat{V}_{Lj}-\tilde{V}_L)^2]^{1/2}/\tilde{V}_L$ (%)	Mean	1.19	1.09	1.02	0.69	0.69	2.48	2.42	4.56	6.67
	Std. dev.	0.27	0.47	0.46	0.54	0.56	0.98	0.99	1.72	1.67
	Min.	0.61	0.08	0.09	0.02	0.00	0.21	0.13	1.54	2.69
	Median	1.16	1.22	1.14	0.65	0.61	2.47	2.43	4.38	6.60
	Max.	1.79	2.02	1.91	2.03	2.12	4.81	4.75	9.34	10.37
$E[(\hat{V}_{CLj}-\tilde{V}_{CL})^2]^{1/2}/\tilde{V}_{CL}$ (%)	Mean	0.63	0.66	0.61	0.97	1.00	1.94	1.89	5.08	6.09
	Std. dev.	0.19	0.41	0.42	0.70	0.73	0.89	0.89	1.69	1.68
	Min.	0.34	0.00	0.05	0.08	0.00	0.08	0.13	2.15	2.05
	Median	0.58	0.63	0.58	0.78	0.81	1.88	1.83	4.99	6.03
	Max.	1.09	1.89	2.08	2.52	2.61	4.02	3.97	9.86	9.84
		Dependent selection								
		6	7	8	9	10	11	min	max	
$E[(\hat{V}_{Lj}-\tilde{V}_L)^2]^{1/2}/\tilde{V}_L$ (%)	Mean	1.20	1.14	0.66	0.64	2.23	2.19	3.62	5.80	
	Std. dev.	0.70	0.71	0.55	0.57	1.00	1.00	2.10	1.96	
	Min.	0.05	0.05	0.05	0.00	0.26	0.18	0.35	2.12	
	Median	1.22	1.10	0.50	0.49	2.15	2.11	3.36	5.85	
	Max.	3.15	3.09	2.19	2.35	4.81	4.76	9.31	10.26	
$E[(\hat{V}_{CLj}-\tilde{V}_{CL})^2]^{1/2}/\tilde{V}_{CL}$ (%)	Mean	0.78	0.74	0.74	0.75	1.70	1.65	4.12	5.23	
	Std. dev.	0.62	0.63	0.69	0.71	0.91	0.91	2.09	1.96	
	Min.	0.00	0.00	0.05	0.00	0.09	0.11	0.92	1.45	
	Median	0.65	0.57	0.51	0.52	1.48	1.45	3.86	5.37	
	Max.	2.48	2.42	2.75	2.91	4.05	4.04	9.83	9.73	

of diameters within a stem was hypothesised to become more pronounced than with the volume equation, particularly with the diameter selection methods involving fixed diameters.

Unlike with the volume equation and the general volume estimator, the effect of assuming cross-section convexity now emerged only via the reference volume with respect to which the within-tree biases were determined and by which they and the within-tree variances were proportioned (as the diameters of a non-convex cross-section coincide with those of the convex closure, the stem curves, and hence the volume estimates, are the same whether the cross-sections are assumed convex or not). As the reference volumes, we employed the best estimates obtained with this stem curve method, namely the estimated true stem volume ($\tilde{V}$) and the estimated convex stem volume ($\tilde{V}_C$) computed from the true area diameters and the convex area diameters, respectively.

As with the volume equation, the volume estimation error could be regarded as the sum of the error attributable to diameter selection and the error contained in the reference volume. The error in the reference volume was due to unobserved variation in stem tapering between the fixed observation heights; however, this error could not be quantified, as the true volumes of the stems were unknown and no more precise volume estimates were

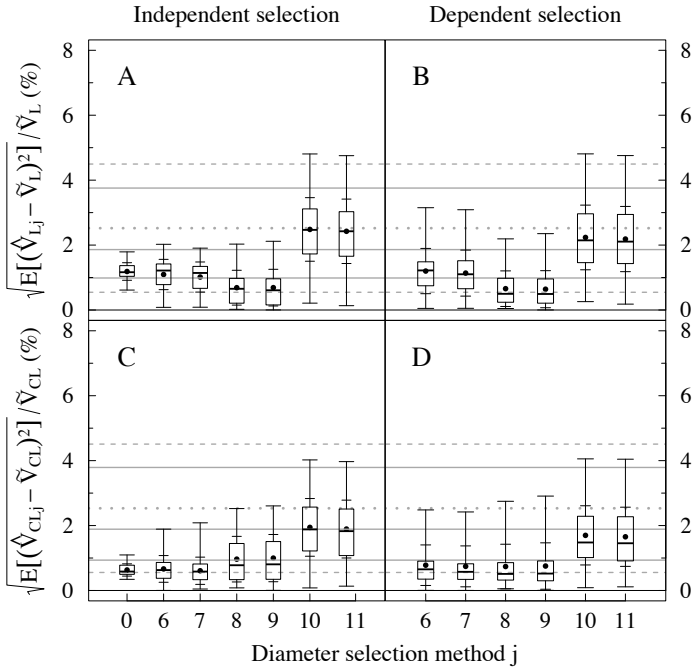

Fig. 61. Summarised distributions of the relative within-tree RMSEs of the volume estimators based on the re-estimated Laasasenaho volume equation and fixed diameters (diameter selection methods 6–11) in the set of the stems for which both 1.3 m and 6 m discs were available (n=50); for comparison, results obtained with girth (diameter selection method 0) are also given. The equation was estimated without (A, B) or with (C, D) the assumption of convex cross-sections, and the diameters were selected independently (A, C) or dependently (B, D) within a stem. For comparison, the distribution summary of the absolute values of the relative model errors (relative residuals) in the data are given: 1st quartile, median and 3rd quartile (continuous grey line), mean (dotted grey line), and mean ± standard deviation (dashed grey line). (For the explanation of the boxplot, refer to the caption of Fig. 57.)

available. Consequently, the relative within-tree biases and variances produced by the different diameter selection methods could only be compared with each other and with those obtained with the volume equation, but no notion about their magnitude with respect to the "model error" of the stem curve method could be gained.

Biases

As with the volume equation, independent and dependent selection of random diameters (diameter selection methods 1–5) yielded practically similar relative within-tree biases (the differences in the between-trees averages and standard deviations were less than three hundredths of a percentage unit). *For these methods, then, only the results from dependent selection suffice to be presented here.*

Using girth diameter (method 0) or random diameters yielded on average slightly larger relative within-tree biases with the cubic-spline-interpolated stem curve than with the

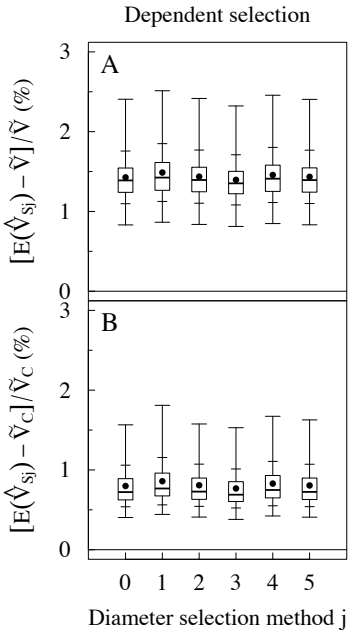

Fig. 62. Summarised distributions of the relative within-tree biases of the volume estimators based on the cubic-spline-interpolated stem curves obtained from girth (diameter selection method 0) or random diameters (diameter selection methods 1–5) among the trees where 7 or more discs were available (n=79). The reference volume was estimated without (A) or with (B) the assumption of convex cross-sections, and the diameters were selected dependently within a stem with breast height diameter determining the common diameter direction (independent selection gave practically similar results). (For the explanation of the boxplot, refer to the caption of Fig. 57.)

Table 44. Summarised distributions of the relative within-tree biases of the volume estimators based on the cubic-spline-interpolated stem curves and girth or dependently selected random diameters (measurement direction determined at breast height for all the observation heights), among the trees where 7 or more discs were available (n=79). The biases were determined with respect to estimated true volume $\tilde{V}$ or estimated convex volume $\tilde{V}_C$. Selecting random diameters independently at all the observation heights produced practically similar results.

Relative bias	Statistic	Diameter selection method j, Dependent selection					
		0	1	2	3	4	5
$[E(\hat{V}_{Sj})-\tilde{V}]/\tilde{V}$ (%)	Mean	1.43	1.49	1.43	1.40	1.46	1.43
	Std. dev.	0.33	0.36	0.33	0.31	0.35	0.33
	Min.	0.83	0.86	0.84	0.81	0.85	0.83
	Median	1.39	1.42	1.39	1.35	1.41	1.39
	Max.	2.41	2.51	2.42	2.32	2.46	2.40
$[E(\hat{V}_{Sj})-\tilde{V}_C]/\tilde{V}_C$ (%)	Mean	0.80	0.86	0.81	0.77	0.83	0.81
	Std. dev.	0.26	0.30	0.26	0.24	0.28	0.27
	Min.	0.40	0.44	0.41	0.38	0.42	0.41
	Median	0.72	0.77	0.73	0.69	0.75	0.72
	Max.	1.57	1.81	1.58	1.52	1.67	1.63

volume equation (means of 1.5% vs. 1.2% without the convexity assumption, and 0.8% vs. 0.6% with the convexity assumption); also the variation between the stems, considered in terms of range (especially maximum values) and standard deviation, became larger, but half the stems were still concentrated within 0.4 percentage units from each other, as the length of the inter-quartile range remained more or less the same (Table 44, Fig. 62; cf. Table 39, Fig. 57). In other words, the systematic overestimating error attributable to

random diameter selection or to usage of girth diameter appeared to accrue slightly with the increasing number of diameters involved in volume estimation. Yet the differences between the different diameter selection methods remained unimportantly small, even if they now slightly more perceptibly reflected the area estimation theory (Table 44, Fig. 62) — the geometric mean producing smaller biases than the arithmetic one (method 3 vs. 2, 5 vs. 4), a randomly selected second diameter resulting in larger biases than a crosswise calipered one (method 4 vs. 2, 5 vs. 3) due to the observed negative correlation between perpendicular diameters within cross-sections (see Section 8.2.1), and the geometric mean of perpendicular diameters performing better than girth (method 3 vs. 0) owing to the same negative correlation. Assuming the cross-sections convex decreased the average biases by the similar 0.6 percentage units as with the volume equation, but diminished the between-trees variation of the biases proportionately less than with the volume equation (Fig. 62 B vs. A, Table 44; cf. Fig. 57 B vs. A, Table 39); this weaker effect was an expected consequence of the fact that with this stem curve method the convexity assumption affected only the reference volume and not the actual volume estimates.

Independent selection of fixed diameters (methods 6–11) also resulted in biases that were on average 0.3–0.5 percentage units larger than with the volume equation (except D_{min} and its perpendicular (methods 8 and 9) which yielded as small average biases as with the volume

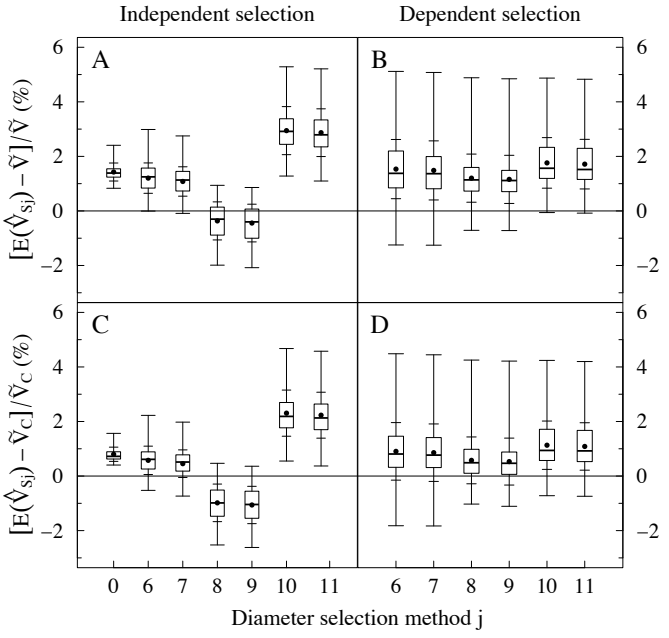

Fig. 63. Summarised distributions of the relative within-tree biases of the volume estimators based on the cubic-spline-interpolated stem curves obtained from fixed diameters (diameter selection methods 6–11) among the trees where 7 or more discs were available (n=79); for comparison, results obtained with girth (diameter selection method 0) are also given. The reference volume was estimated without (A, B) or with (C, D) the assumption of convex cross-sections, and the diameters were selected independently (A, C) or dependently (B, D) within a stem. (For the explanation of the boxplot, refer to the caption of Fig. 57.)

Table 45. Summarised distributions of the relative within-tree biases of the volume estimators based on the cubic-spline-interpolated stem curves and independently (measurement directions determined independently for all the observation heights) or dependently (measurement direction determined at breast height for all the observation heights) selected fixed diameters, among the trees where 7 or more discs were available (n=79). For comparison, the results of the estimator based on girth diameter (diameter selection method 0) are also given.

Relative bias	Statistic	Diameter selection method j								
		Independent selection								
		0	6	7	8	9	10	11	min	max
$[E(\hat{V}_{Sj})–\tilde{V}]/\tilde{V}$ (%)	Mean	1.43	1.20	1.08	–0.37	–0.44	2.94	2.87	–5.04	7.71
	Std. dev.	0.33	0.56	0.54	0.70	0.69	0.88	0.87	1.52	1.94
	Min.	0.83	0.00	–0.09	–1.99	–2.08	1.28	1.10	–0.26	4.67
	Median	1.39	1.25	1.13	–0.30	–0.40	2.92	2.79	–4.84	7.13
	Max.	2.41	2.99	2.75	0.94	0.86	5.29	5.21	–2.01	14.16
$[E(\hat{V}_{Sj})–\tilde{V}_C]/\tilde{V}_C$ (%)	Mean	0.80	0.58	0.45	–0.98	–1.06	2.31	2.23	–5.62	7.04
	Std. dev.	0.26	0.52	0.51	0.69	0.68	0.85	0.84	1.52	1.89
	Min.	0.40	–0.53	–0.73	–2.53	–2.62	0.55	0.37	–9.81	3.96
	Median	0.72	0.61	0.51	–0.99	–1.04	2.19	2.13	–5.47	6.40
	Max.	1.57	2.22	1.98	0.47	0.36	4.67	4.58	–2.62	13.44
		Dependent selection								
		6	7	8	9	10	11	min	max	
$[E(\hat{V}_{Sj})–\tilde{V}]/\tilde{V}$ (%)	Mean	1.53	1.49	1.20	1.16	1.76	1.72	–0.18	3.38	
	Std. dev.	1.09	1.08	0.88	0.88	0.93	0.91	2.51	2.48	
	Min.	–1.25	–1.26	–0.71	–0.72	–0.06	–0.08	–7.32	–1.23	
	Median	1.38	1.37	1.14	1.12	1.56	1.52	0.17	3.13	
	Max.	5.12	5.08	4.88	4.85	4.87	4.83	5.67	11.11	
$[E(\hat{V}_{Sj})–\tilde{V}_C]/\tilde{V}_C$ (%)	Mean	0.90	0.86	0.58	0.53	1.13	1.09	–0.80	2.74	
	Std. dev.	1.06	1.05	0.86	0.86	0.89	0.87	2.47	2.46	
	Min.	–1.82	–1.83	–1.03	–1.11	–0.72	–0.74	–7.99	–1.94	
	Median	0.81	0.77	0.49	0.47	0.94	0.92	0.41	2.51	
	Max.	4.48	4.45	4.25	4.21	4.24	4.20	4.98	10.26	

equation); yet the biases varied less between trees, in terms of range and standard deviation (Fig. 63 A and C, Table 45; cf. Fig. 58 A and C, Table 40). The interrelationships between the selection methods were fairly similar to those obtained with the volume equation, and also the effect of ignoring cross-section non-convexity parallelled that observed with the volume equation, shifting the bias distributions downwards by some 0.5–0.6 percentage units but not really influencing the variability (Fig. 63 A vs. C, Table 45).

Dependent selection of fixed diameters (methods 6–11), in turn, resulted in mutually strikingly similar bias distributions, quite unlike with the volume equation: all the methods produced positive between-trees means within one percentage unit of each other, as well as fairly similar between-trees standard deviations; interestingly, also the maximum values were uniformly large with all the methods (Fig. 63 B and D). This can be seen to follow from the larger number of diameters involved in the stem curve, as the influence of the dependent selection attenuating the extremity of D_{min} and D_{max} is then emphasised (recall that no regularity was found in the directions of D_{min} and D_{max} with respect to height; see Section 8.2.1). Interestingly, measuring all the diameters parallel to D_{min} at breast height (method min with dependent selection) resulted, if also in a large between-trees variability,

in the least average bias among all the diameter selection methods when no cross-section convexity was assumed (Table 45). The convexity assumption decreased the average biases uniformly by 0.6 percentage units, whereas the between-trees variation remained approximately the same (Fig. 63 D vs. B, Table 45).

The effect of stem size on relative within-tree bias obtained with girth or random diameters (methods 0 and 1–5; independent and dependent selection) was weaker than that found with the volume equation: the correlations between the estimated true stem volumes and the biases were around –0.4, and the biases in pulpwood-size stems were on average 1.3-fold compared to those in the sawlog-size stems. The effect was considerably attenuated by the convexity assumption. With fixed diameters (methods 6–11), no association between stem size and within-tree bias was found.

Unlike with the volume equation, the geographical location of the growing site appeared to influence the between-stems variation of the within-tree biases obtained with girth or random diameters (methods 0 and 1–5; independent and dependent selection): the more north the site was located, the more variable biases did the methods produce. The larger variability in stem tapering observed in Lapland (Laasasenaho 1982) and mentioned with volume equation biases does not make a plausible explanation, since the seven or more diameter observations along the stem, from which cubic-spline-interpolated stem curves were constructed, can be thought to give adequate information on tapering. Rather, the larger variability in the within-tree biases may reflect the larger variability in cross-section non-circularity in the trees in Northern Finland: the treewise averages of CV_D, D_{min}/D_{max}, b_e/a_e and isoperimetric deficit showed clearly larger variation toward the north when plotted against the cluster co-ordinate in N–S direction. (The treewise averages of the indices showed also statistically significant linear trend with respect to the cluster co-ordinate, but the slopes were so small that the effect was practically negligible; also, the correlations between the indices and the cluster co-ordinate were small. Consequently we can say that the trees were not practically more non-circular on average in Northern Finland than in Southern Finland. On the other hand, a systematically larger amount of non-circularity would cause not only a larger variation in biases but also a higher mean level of them, which was not observed.)

In the subset of the 50 stems investigated with the volume equation, the relative within-tree biases produced by the stem curve method were on average 0.1–0.2 percentage units closer to zero than in the set of all the 79 stems. This suggests that the differences in the within-tree biases between the two volume estimation methods could in reality be smaller than the results above indicate.

Variances

The convexity assumption, turning up solely in the reference volume, *did not practically influence the relative within-tree variances of the volume estimates obtained with the cubic-spline-interpolated stem curves. Hence only the results attained without the convexity assumption are presented below.*

Random diameters (methods 1–5) yielded on average smaller and less variable sampling errors (within-tree standard deviations) with the stem curve method than with the volume equation, particularly when diameters were selected independently at the separate heights (Fig. 64, Table 46; cf. Fig. 59, Table 41). This was not surprising, as a larger number of diameters observed along a stem is likely to result in more precise volume estimates. The increase in precision was weaker with dependent diameter selection, especially with the methods involving non-crosswise diameters (methods 1, 4, 5); this is probably because dependent selection entailed positive within-tree correlation between the diameters at

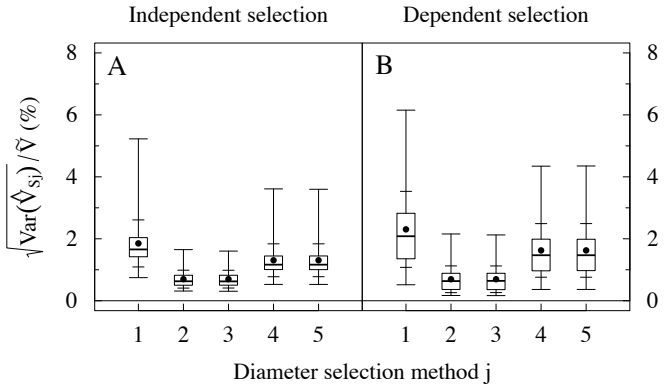

Fig. 64. Summarised distributions of the relative within-tree standard deviations of the volume estimators based on the cubic-spline-interpolated stem curves obtained from random diameters (diameter selection methods 1–5) among the trees where 7 or more discs were available (n=79). The reference volume was estimated without the assumption of convex cross-sections (assuming convexity gave practically similar results), and the diameters were selected independently (A) or dependently (B) within a stem. (For the explanation of the boxplot, refer to the caption of Fig. 57.)

Table 46. Summarised distributions of the relative within-tree standard deviations of the volume estimators based on the cubic-spline-interpolated stem curves and independently or dependently selected random diameters, among the trees where 7 or more discs were available (n=79). The standard deviations were proportioned with estimated true volume $\tilde{V}$; proportioning with estimated convex volume $\tilde{V}_C$ yielded practically similar results.

Relative std. dev.	Statistic	Diameter selection method j									
		Independent selection					Dependent selection				
		1	2	3	4	5	1	2	3	4	5
$\mathrm{Var}(\hat{V}_{Sj})^{1/2}/\tilde{V}$ (%)	Mean	1.85	0.70	0.70	1.31	1.31	2.30	0.69	0.69	1.62	1.63
	Std. dev.	0.76	0.29	0.29	0.53	0.53	1.23	0.43	0.43	0.87	0.87
	Min.	0.75	0.31	0.31	0.53	0.53	0.52	0.17	0.17	0.36	0.37
	Median	1.66	0.63	0.62	1.17	1.17	2.08	0.63	0.64	1.47	1.47
	Max.	5.23	1.65	1.60	3.61	3.60	6.15	2.16	2.12	4.34	4.35

separate heights, which then augmented volume estimator variance compared to independent selection, more with the stem curve than with the volume equation as there were more dependent diameters involved. With perpendicular diameters (methods 2, 3), this effect of dependent selection was then attenuated by the negative within-cross-section correlation of perpendicular diameters. The differences in the magnitude notwithstanding, the overall patterns of the sampling errors closely resembled those obtained with the volume equation: perpendicular diameters (methods 2, 3) gave the best precision, and the average gain from measuring the second diameter perpendicularly instead of taking it in a random direction (methods 2, 3 vs. 4, 5) was larger than that from taking two random diameters instead of only one (methods 4, 5 vs. 1) (Table 46, Fig. 64).

Tree size had no noticeable effect on the sampling errors. Geographical location of growing site, in turn, seemed to have an influence, even if to a lesser extent than on the biases and only with independently selected random diameters (methods 1–5): the sampling errors became the more variable the farther north the site was located. Like the more variable biases, the more variable sampling errors accord with the larger variability in non-circularity (larger variability in within-cross-section diameter variation) observed in Northern Finland (see the discussion on the biases above). (Clearly, systematically larger amount of non-circularity, i.e., systematically larger variation in diameter within cross-sections, which was not observed in our data, would induce not only larger variation in sampling errors but also a generally higher level of them, which was not observed either.)

In the subset of the 50 stems investigated with the volume equation, the within-tree standard deviations were on average 0.05–0.1 percentage units smaller than in the set of all the 79 stems, with all the diameter selection methods except with those involving both D_{min} and D_{max} (methods 6, 7). Thus the differences in the sampling errors between the spline-interpolated stem curve and the volume equation might actually be slightly larger than the results above suggest.

RMSEs

With the diameter selection methods involving random diameters (methods 1–5), the within-tree RMSEs largely reflected the behaviour of the within-tree sampling errors discussed above. With perpendicular diameters (methods 2, 3), the RMSE distributions became fairly similar to those produced by the volume equation (Table 47, Fig. 65; cf. Table 42, Fig. 60), as the slightly smaller sampling error component compensated for the slightly larger bias component; whether the diameters were selected independently or dependently did not matter, as the dependence in diameter selection had no practical impact on either of the components. With one or two random diameters (methods1, 4, 5), however, the dependence in diameter selection did count through the differences in sampling errors: With independently selected diameters, RMSEs decreased on average by 0.3–0.6 percentage units compared to those obtained by the volume equation, and also their between-trees variation

Table 47. Summarised distributions of the relative within-tree RMSEs of the volume estimators based on the cubic-spline-interpolated stem curves and girth diameter or independently or dependently selected random diameters, among the trees where 7 or more discs were available (n=79).

Relative RMSE	Statistic	Diameter selection method j										
		Independent selection						Dependent selection				
		0	1	2	3	4	5	1	2	3	4	5
$E[(\hat{V}_{Sj}-\tilde{V})^2]^{1/2}/\tilde{V}$ (%)	Mean	1.43	2.41	1.61	1.58	1.99	1.97	2.81	1.63	1.59	2.25	2.23
	Std. dev.	0.33	0.80	0.39	0.38	0.58	0.57	1.12	0.43	0.41	0.76	0.76
	Min.	0.83	1.36	0.98	0.94	1.25	1.24	1.19	0.92	0.89	1.12	1.11
	Median	1.39	2.21	1.51	1.49	1.83	1.81	2.68	1.54	1.51	2.10	2.10
	Max.	2.41	5.95	2.79	2.65	4.39	4.33	6.59	2.88	2.81	4.90	4.86
$E[(\hat{V}_{Sj}-\tilde{V}_C)^2]^{1/2}/\tilde{V}_C$ (%)	Mean	0.80	2.05	1.08	1.05	1.56	1.54	2.48	1.10	1.07	1.85	1.84
	Std. dev.	0.26	0.80	0.36	0.34	0.58	0.57	1.19	0.42	0.41	0.83	0.82
	Min.	0.40	0.90	0.57	0.55	0.73	0.72	0.75	0.47	0.44	0.65	0.64
	Median	0.72	1.84	0.97	0.95	1.40	1.39	2.35	1.01	0.98	1.74	1.73
	Max.	1.57	5.64	2.30	2.17	4.04	3.99	6.31	2.54	2.47	4.56	4.53

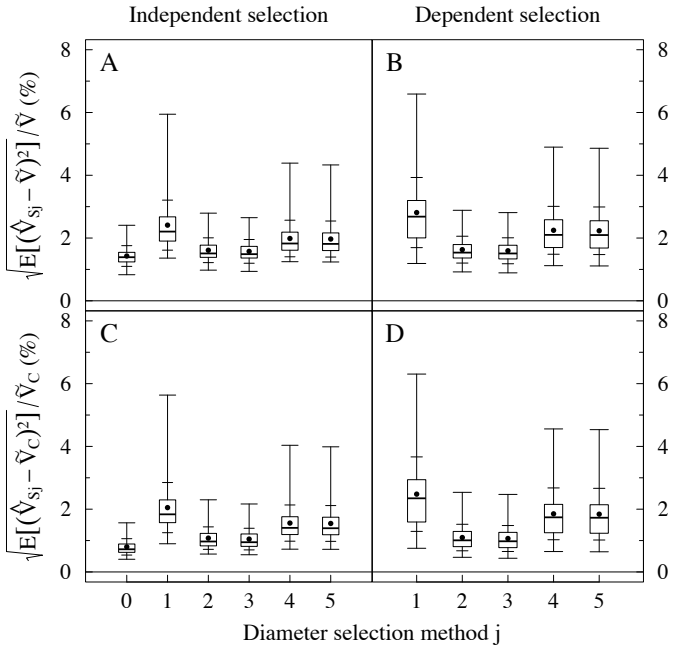

Fig. 65. Summarised distributions of the relative within-tree RMSEs of the volume estimators based on the cubic-spline-interpolated stem curves obtained from girth (diameter selection method 0) or random diameters (diameter selection methods 1–5) among the trees where 7 or more discs were available (n=79). The reference volume was estimated without (A, B) or with (C, D) the assumption of convex cross-sections, and the diameters were selected independently (A, C) or dependently (B, D) within a stem. (For the explanation of the boxplot, refer to the caption of Fig. 57.)

diminished clearly; the changes were especially pronounced with one random diameter (method 1) (Table 47, Fig. 65 A and C; cf. Table 42, Fig. 60 A and C). With dependently selected diameters, in turn, the RMSE distributions remained closer to those given by the volume equation (Table 47, Fig. 65 B and D; cf. Table 42, Fig. 60 B and D); in other words, dependent selection, as compared to independent selection, impaired the volume estimator performance more with the cubic-spline-interpolated stem curve than with the volume equation. Also the convexity assumption had a slightly larger influence on RMSEs with the cubic-spline-interpolated stem curve than with the volume equation: disregarding cross-section non-convexity shifted the RMSE distributions 0.4–0.5 percentage units closer to zero, but left the shape of the distributions practically unchanged (Table 47, Fig. 65 C vs. A and D vs. B; cf. Table 42, Fig. 60 C vs. A and D vs. B).

In comparison with the methods involving random diameters, the girth diameter (method 0) was not so strikingly superior now as with the volume equation: the difference in the average RMSE between the best method involving random diameters (methods 2, 3) and the girth diameter method was only half of that observed with the volume equation, and also the diminution in the between-trees variation of RMSEs was less pronounced (Table 47, Fig. 65; cf. Table 42, Fig. 60).

Among the diameter selection methods involving fixed diameters (methods 0, 6–11), however, the girth method exhibited clearly the smallest between-trees variation in RMSE,

Table 48. Summarised distributions of the relative within-tree RMSEs of the volume estimators based on the cubic-spline-interpolated stem curves and independently or dependently selected fixed diameters, among the trees where 7 or more discs were available (n=79). For comparison, the results of the estimator based on girth diameter (diameter selection method 0) are also given.

Relative RMSE	Statistic	Diameter selection method j								
		Independent selection								
		0	6	7	8	9	10	11	min	max
$E[(\hat{V}_{Sj}-\tilde{V})^2]^{1/2}/\tilde{V}$ (%)	Mean	1.43	1.20	1.08	0.63	0.65	2.94	2.87	5.04	7.71
	Std. dev.	0.33	0.56	0.53	0.47	0.49	0.88	0.87	1.52	1.94
	Min.	0.83	0.00	0.01	0.01	0.02	1.28	1.10	2.01	4.67
	Median	1.39	1.25	1.13	0.50	0.52	2.92	2.79	4.84	7.13
	Max.	2.41	2.99	2.75	1.99	2.08	5.29	5.21	9.26	14.16
$E[(\hat{V}_{Sj}-\tilde{V}_C)^2]^{1/2}/\tilde{V}_C$ (%)	Mean	0.80	0.65	0.56	1.02	1.09	2.31	2.23	5.62	7.04
	Std. dev.	0.26	0.43	0.38	0.63	0.64	0.85	0.84	1.52	1.89
	Min.	0.40	0.01	0.02	0.05	0.11	0.55	0.37	2.62	3.96
	Median	0.72	0.61	0.56	0.99	1.04	2.19	2.13	5.47	6.40
	Max.	1.57	2.22	1.98	2.53	2.62	4.67	4.58	9.81	13.44
		Dependent selection								
		6	7	8	9	10	11	min	max	
$E[(\hat{V}_{Sj}-\tilde{V})^2]^{1/2}/\tilde{V}$ (%)	Mean	1.59	1.55	1.25	1.21	1.76	1.72	1.98	3.48	
	Std. dev.	0.99	0.99	0.82	0.81	0.92	0.91	1.54	2.34	
	Min.	0.04	0.06	0.01	0.01	0.06	0.08	0.12	0.02	
	Median	1.38	1.37	1.14	1.11	1.56	1.52	1.70	3.13	
	Max.	5.12	5.08	4.88	4.84	4.87	4.83	7.32	11.11	
$E[(\hat{V}_{Sj}-\tilde{V}_C)^2]^{1/2}/\tilde{V}_C$ (%)	Mean	1.11	1.08	0.78	0.75	1.17	1.13	2.00	2.97	
	Std. dev.	0.83	0.82	0.68	0.67	0.83	0.81	1.65	2.18	
	Min.	0.05	0.02	0.05	0.02	0.06	0.04	0.10	0.14	
	Median	0.87	0.78	0.62	0.57	0.94	0.92	1.67	2.51	
	Max.	4.48	4.45	4.25	4.21	4.24	4.20	7.99	10.26	

although the independently or dependently selected D_{min} and its perpendicular (methods 8, 9) without convexity assumption, or the independently selected D_{min} and D_{max} (methods 6, 7), outperformed it in terms of average RMSE (Table 48, Fig. 66). When diameters were selected independently within a stem, the interrelationships between the methods were in general quite similar to those observed with the volume equation, and also the convexity assumption had a fairly similar effect (Table 48, Fig. 66 A and C; cf. Table 43, Fig. 61 A and C). When diameters were selected dependently, the RMSE distributions of the different methods became much more identical than with the volume equation, just as was the case also with the within-tree biases (Fig. 66 B and D, Fig. 63 B and D; cf. Fig. 61 B and D).

8.4.3 General Volume Estimator

With the general volume estimators of this study, based on area estimation processes involving diameters and circle area formula, independent selection of random diameters with the uniform direction distribution at observation heights was not meaningful to consider: while the biases and variances of each stochastic area estimation process would not have deviated from those obtained with dependent diameter selection, the zero covariances between the

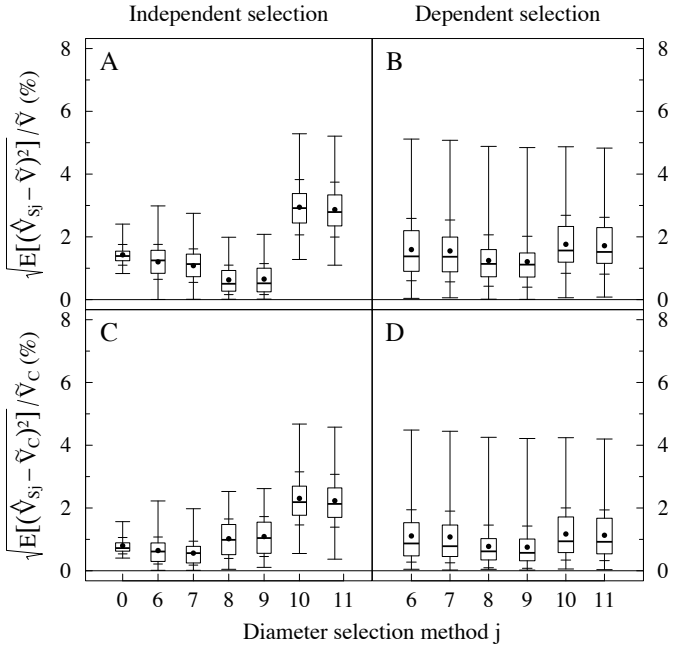

Fig. 66. Summarised distributions of the relative within-tree RMSEs of the volume estimators based on the cubic-spline-interpolated stem curves obtained from fixed diameters (diameter selection methods 6–11) among the trees where 7 or more discs were available (n=79); for comparison, results obtained with girth (diameter selection method 0) are also given. The reference volume was estimated without (A, B) or with (C, D) the assumption of convex cross-sections, and the diameters were selected independently (A, C) or dependently (B, D) within a stem. (For the explanation of the boxplot, refer to the caption of Fig. 57.)

area estimators at the observation heights would not have provided information for covariance function estimation (see the discussion in Section 7.3.4 and Section 5.2). Accordingly, we present in the following results only for dependently selected random diameters and both dependently and independently selected fixed diameters.

We were particularly interested in how, with each diameter selection method, the within-tree biases and sampling errors (variances) estimated with the general volume estimator compared with those estimated with the cubic-spline-interpolated stem curve. In both the volume estimation methods, the within-tree bias and variance in a stem were obtained by integrating the mean and covariance functions of the area estimation (error) process: In the general volume estimator, these functions were estimated by linear interpolation between the estimated area estimator biases or covariances at the observation heights along a stem (see Section 7.3.4). In the stem curve method, the functions were obtained as the pointwise means or covariances of a number of cubic-spline-interpolated stem curves (or, in the case of the mean, stem curve differences to true area diameter stem curve) based on a large sample of diameters measured at the observation heights (see Section 5.3, Eqs. 131 and 132). The differences between the methods would probably mainly derive from the differences of the interpolation methods, as at the observation heights the values of the functions (the estimated area estimator biases vs. the sample means of the area estimation errors, and the

estimated area estimator covariances vs. the sample covariances of the area estimates) were presumably quite close to each other with each diameter selection method. Note that with the general volume estimator, we only dealt with the stem segments between the lowermost and the uppermost observation heights and thus ignored the butt parts (between the stump height and the lowermost observation height) involving most uncertainty; this might affect the comparison to the stem curve method where the whole stems (from the stump height to the top of the tree) were considered.

The convexity assumption did not manifest itself in the actual general volume estimators considered here, as the area estimation processes based on diameters and circle area formula were the same be the cross-sections assumed convex or not. The assumption did, however, affect the area estimation error processes, where the area error was determined with respected to either true or convex area; the mean functions of these error processes were estimated from the area estimation biases taken with respect to true or convex area (for the stem segment between the lowermost and the uppermost observation heights), and the definite integrals of the mean functions then yielded estimates of the within-tree volume biases with respect to (partial) true stem volume or to (partial) convex stem volume. In addition, the convexity assumption influenced the reference volume by which the within-tree biases and standard deviations were proportioned; as the reference volumes, we used the estimated partial true stem volume ($\tilde{V}$) and the estimated partial convex stem volume ($\tilde{V}_C$), computed for the stem segment between the lowermost and the uppermost observation heights with the cubic-spline-interpolated stem curves obtained from the true area diameters and the convex area diameters, respectively.

In the subset of the 50 stems where the Laasasenaho volume equation was examined, the average within-tree biases were 0.1–0.2 percentage units nearer zero and the average within-tree standard deviations 0.05–0.1 percentage units smaller than in the set of all the 79 stems, with all the diameter selection methods except those based on both D_{min} and D_{max} (methods 6, 7), just as we previously found to be the case with the stem curve method. Consequently, the differences between the volume equation and the general volume estimator are probably less pronounced in terms of the within-tree biases and more pronounced in terms of the within-tree variances than the results below indicate.

Biases

With all the diameter selection methods, the results on the within-tree biases were strikingly similar to those obtained with the cubic-spline-interpolated stem curves (Tables 49 and 50, Figs. 67 and 68; cf. Tables 44 and 45, Figs. 62 and 63). This implies that the simple linear interpolation between the estimated expectations of an area estimator at 7–10 observation heights could approximate the mean function of the area estimation process in quite a similar way as the pointwise mean of a large number of more sophisticatedly interpolated stem curves based on diameters measured at the same observation heights.

The association between the within-tree biases and the stem size was practically identical to that observed with the stem curve method, the sawlog-size stems showing smaller average biases and smaller between-trees variation than the pulpwood-size stems when girth or dependently selected random diameters (methods 0, 1–5) were used, and no size effect emerging when fixed diameters (methods 6–11) were employed. Also the growing site location seemed to affect the within-tree biases in the same way as with the stem curve method, the between-trees variation of the biases produced by girth or dependently selected random diameters (methods 0, 1–5) increasing when going towards the north.

Table 49. Summarised distributions of the relative within-tree biases of the general volume estimators based on girth or dependently selected random diameters (measurement direction determined at breast height for all the observation heights), among the trees where 7 or more discs were available (n=79). The biases were (in theory) determined with respect to true volume V or convex volume V_C and proportioned with estimated true volume $\tilde{V}$ or estimated convex volume $\tilde{V}_C$.

Relative bias	Statistic	Diameter selection method j Dependent selection					
		0	1	2	3	4	5
$E(\hat{V}_{Gj}–V)/\tilde{V}$ (%)	Mean	1.45	1.50	1.46	1.42	1.48	1.45
	Std. dev.	0.33	0.35	0.33	0.32	0.34	0.33
	Min.	0.82	0.84	0.83	0.81	0.83	0.82
	Median	1.41	1.45	1.42	1.38	1.43	1.41
	Max.	2.45	2.63	2.46	2.36	2.51	2.45
$E(\hat{V}_{Gj}–V_C)/\tilde{V}_C$ (%)	Mean	0.82	0.87	0.83	0.79	0.84	0.82
	Std. dev.	0.25	0.28	0.26	0.24	0.26	0.25
	Min.	0.40	0.43	0.41	0.38	0.42	0.40
	Median	0.74	0.79	0.75	0.71	0.77	0.74
	Max.	1.57	1.80	1.58	1.49	1.68	1.57

Table 50. Summarised distributions of the relative within-tree biases of the general volume estimators based on independently (measurement directions determined independently for all the observation heights) or dependently (measurement direction determined at breast height for all the observation heights) selected fixed diameters, among the trees where 7 or more discs were available (n=79). For comparison, the results of the estimator based on girth diameter (diameter selection method 0) are also given.

Relative bias	Statistic	Diameter selection method j Independent selection								
		0	6	7	8	9	10	11	min	max
$[E(\hat{V}_{Gj})–V]/\tilde{V}$ (%)	Mean	1.45	1.18	1.05	–0.39	–0.47	2.99	2.91	–5.14	7.75
	Std. dev.	0.33	0.50	0.49	0.66	0.65	0.82	0.82	1.52	1.79
	Min.	0.82	0.12	0.03	–1.77	–1.79	1.50	1.43	–9.61	4.73
	Median	1.41	1.19	1.10	–0.30	–0.36	2.98	2.91	–4.92	7.46
	Max.	2.45	2.89	2.63	0.94	0.86	5.42	5.36	–2.09	14.47
$[E(\hat{V}_{Gj})–V_C]/\tilde{V}_C$ (%)	Mean	0.82	0.55	0.42	–1.01	–1.09	2.34	2.27	–5.73	7.07
	Std. dev.	0.25	0.46	0.45	0.65	0.65	0.78	0.78	1.53	1.73
	Min.	0.40	–0.41	–0.52	–2.34	–2.42	1.02	0.92	–10.35	4.02
	Median	0.74	0.57	0.45	–0.99	–1.04	2.28	2.17	–5.56	6.76
	Max.	1.57	2.14	1.85	0.46	0.39	4.52	4.46	–2.71	13.55
			Dependent selection							
			6	7	8	9	10	11	min	max
$[E(\hat{V}_{Gj})–V]/\tilde{V}$ (%)	Mean		1.49	1.44	1.16	1.11	1.81	1.77	–0.43	3.53
	Std. dev.		1.04	1.03	0.83	0.82	0.88	0.87	2.37	2.30
	Min.		–0.85	–0.93	–0.62	–0.63	–0.12	–0.15	–7.22	–1.18
	Median		1.41	1.38	1.12	1.00	1.64	1.61	–0.27	3.37
	Max.		4.79	4.74	4.59	4.55	4.54	4.50	4.70	12.33
$[E(\hat{V}_{Gj})–V_C]/\tilde{V}_C$ (%)	Mean		0.86	0.81	0.53	0.48	1.18	1.13	–1.05	2.88
	Std. dev.		1.00	1.00	0.79	0.79	0.84	0.83	2.33	2.29
	Min.		–1.45	–1.53	–0.94	–0.95	–0.65	–0.67	–7.97	–1.90
	Median		0.82	0.78	0.47	0.42	1.01	0.99	–0.89	2.66
	Max.		4.14	4.10	3.94	3.90	3.90	3.85	4.02	11.42

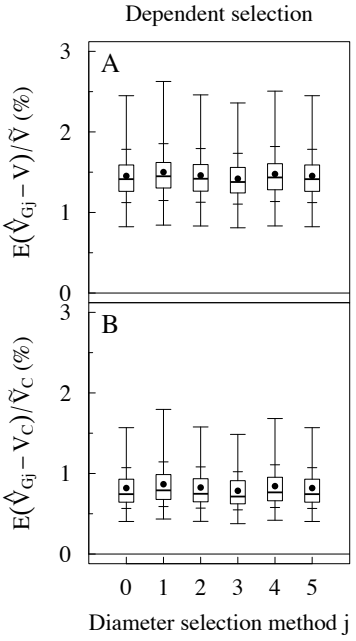

Fig. 67. Summarised distributions of the relative within-tree biases of the general volume estimators based on girth (diameter selection method 0) or random diameters (diameter selection methods 1–5) among the trees where 7 or more discs were available (n=79). The estimators were constructed without (A) or with (B) the assumption of convex cross-sections, and the diameters were selected dependently within a stem with breast height diameter determining the common diameter direction. (For the explanation of the boxplot, refer to the caption of Fig. 57.)

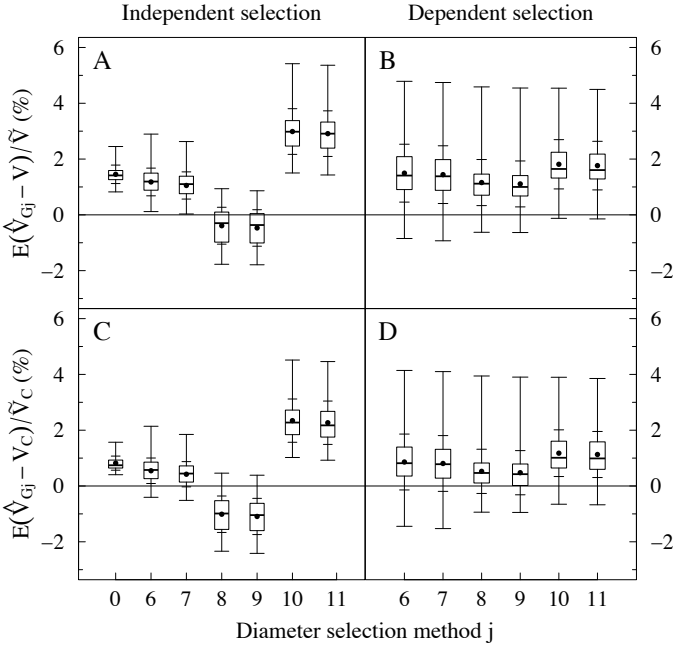

Fig. 68. Summarised distributions of the relative within-tree biases of the general volume estimators based on fixed diameters (diameter selection methods 6–11) among the trees where 7 or more discs were available (n=79); for comparison, results obtained with girth (diameter selection method 0) are also given. The estimators were constructed without (A, B) or with (C, D) the assumption of convex cross-sections, and the diameters were selected independently (A, C) or dependently (B, D) within a stem. (For the explanation of the boxplot, refer to the caption of Fig. 57.)

Variances

As with the stem curve method, *the convexity assumption* came up only in the reference volume and *did not practically affect the within-tree variances of the general volume estimators*. *Consequently, we here present only the result obtained without the convexity assumption*.

Also the within-tree sampling errors (within-tree standard deviations) practically coincided with those obtained in the stem curve method (Table 51, Fig. 69 A; cf. Table 46 dependent selection, Fig. 64 B). In other words, as an approximation of the covariance function of an area estimation process involving dependently selected random diameters, a simple linear interpolation of the within-tree covariances of the area estimator at all the combinations of 7–10 observation heights appeared to correspond well to the function composed of the pointwise covariances of a large number of the cubic-spline-interpolated stem curves based on diameters measured at those observation heights.

In terms of within-tree sampling errors, using (dependently selected) perpendicular diameters (methods 2, 3) appeared to yield more favourable correlation structure for the area estimation process, resulting in sampling errors that lay on average proportionally farther from the theoretical maximum, than employing one or two random diameters (methods 1, 4, 5): if the elements of the area estimation process were assumed fully correlated, the average within-tree standard deviations increased 2.3-fold with perpendicular diameters and 1.8-fold with one or two random diameters (Table 51, Fig. 69 B vs. A). The between-trees variation of the theoretical maximums of the within-tree sampling errors did not deviate much from that of the observed sampling errors, and the distributions were slightly widened only with perpendicular diameters.

The within-tree sampling errors or their theoretical maximum values exhibited no dependence on stem size, which again parallelled the results obtained with dependently selected random diameters in the stem curve approach. Similarly, no effect of the growing site location on the sampling errors was found (the increased variability in the sampling

Table 51. Summarised distributions of the observed relative within-tree standard deviations of the general volume estimators and the theoretical maximums of these standard deviations (obtained by assuming area estimators at different heights to be fully correlated, i.e., $\rho_{\hat{A}j}(h, k)=1$ for all h and k in [0, H]), based on dependently selected random diameters, among the trees where 7 or more discs were available (n=79). The standard deviations were proportioned with estimated true volume $\tilde{V}$; proportioning with estimated convex volume $\tilde{V}_C$ yielded practically similar results.

Relative std. dev.	Statistic	Diameter selection method j, Dependent selection				
		1	2	3	4	5
$Var(\hat{V}_{Gj})^{1/2}/\tilde{V}$ (%)	Mean	2.25	0.66	0.66	1.59	1.58
	Std. dev.	1.17	0.39	0.39	0.83	0.83
	Min.	0.56	0.15	0.14	0.43	0.45
	Median	2.07	0.58	0.59	1.47	1.48
	Max.	6.95	1.88	1.88	4.92	4.94
$Var[\hat{V}_{Gj} \mid \rho_{\hat{A}j}(h, k)=1]^{1/2}/\tilde{V}$ (%)	Mean	4.07	1.53	1.52	2.87	2.85
	Std. dev.	1.16	0.45	0.45	0.82	0.82
	Min.	2.03	0.77	0.76	1.43	1.42
	Median	3.87	1.43	1.44	2.73	2.71
	Max.	8.65	2.88	2.92	6.11	6.11

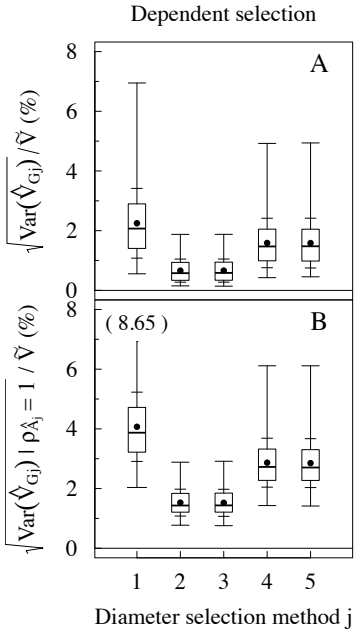

Fig. 69. Summarised distributions of the relative within-tree standard deviations of the general volume estimators based on random diameters (diameter selection methods 1–5), with the observed correlation (A) or an assumed full correlation ($\rho_{\hat{A}j}(h, k)=1$ for all h and k in [0, H]; B) between the area estimators at different heights among the trees where 7 or more discs were available (n=79). The standard deviations were proportioned with estimated true volume (proportioning with estimated convex volume gave practically similar results), and the diameters were selected dependently within a stem. (For the explanation of the boxplot, refer to the caption of Fig. 57.)

errors toward the north that was observed with the stem curve method only pertained to *independently* selected random diameters).

RMSEs

Naturally, considering the bias and sampling error results above, the distributions of the within-tree RMSEs produced by the general volume estimator were almost identical to those obtained with the cubic-spline-interpolated stem curve with all the diameter selection methods (Tables 52 and 53, Figs. 70 and 71; cf. Table 47 dependent selection, Table 48, Fig. 65 B and D, Fig. 66). With dependently selected one or two random diameters (methods 1, 4, 5), the maximum RMSEs were discernibly larger than those observed in the stem curve method. With dependent selection of fixed diameters (methods 6–11), a larger mean RMSE always implied a larger between-trees variation compared to the stem curve approach, whereas with independent selection a larger mean could also entail a smaller between-trees variation.

8.5 Estimation of Stand Totals in Bitterlich Sampling

In the theoretical part of this study (Section 4.1.2), we found that estimating the inclusion probabilities of trees by assuming non-circular breast height cross-sections circular results in errors that may cause bias in stand total estimators, and that these errors in the inclusion probabilities consist of the following two tree-specific components: (i) deviation of the true basal area factor of the tree $\kappa(\alpha)=A_C/|\mathbf{M}(\alpha)|$ (the ratio between the convex area A_C of the breast height cross-section and the inclusion area $|\mathbf{M}(\alpha)|$) from that of a circle $\sin^2(\alpha/2)$, and (ii) deviation of the area estimate $\hat{A}_j=\pi D_j^2/4$, based on diameter D_j selected by some method j in the breast height cross-section, from the convex area A_C. In the expression of

Table 52. Summarised distributions of the relative within-tree RMSEs of the general volume estimators based on girth or dependently selected random diameters, among the trees where 7 or more discs were available (n=79).

Relative RMSE	Statistic	Diameter selection method j					
		Dependent selection					
		0	1	2	3	4	5
$E[(\hat{V}_{Gj}-V)^2]^{1/2}/\tilde{V}$ (%)	Mean	1.45	2.77	1.63	1.60	2.23	2.22
	Std. dev.	0.33	1.05	0.40	0.39	0.72	0.72
	Min.	0.82	1.28	0.91	0.88	1.22	1.23
	Median	1.41	2.62	1.54	1.53	2.07	2.07
	Max.	1.59	7.43	2.68	2.60	5.53	5.49
$E[(\hat{V}_{Gj}-V_C)^2]^{1/2}/\tilde{V}_C$ (%)	Mean	0.82	2.43	1.09	1.06	1.83	1.81
	Std. dev.	0.25	1.12	0.38	0.37	0.78	0.78
	Min.	0.40	0.83	0.46	0.43	0.74	0.76
	Median	0.74	2.23	1.01	0.98	1.72	1.70
	Max.	1.57	7.12	2.23	2.21	5.17	5.15

Table 53. Summarised distributions of the relative within-tree RMSEs of the general volume estimators based on independently or dependently selected fixed diameters, among the trees where 7 or more discs were available (n=79). For comparison, also the results of the estimator based on girth diameter (diameter selection method 0) are given.

Relative RMSE	Statistic	Diameter selection method j								
		Independent selection								
		0	6	7	8	9	10	11	min	max
$E[(\hat{V}_{Gj}-V)^2]^{1/2}/\tilde{V}$ (%)	Mean	1.45	1.18	1.05	0.61	0.64	2.99	2.91	5.14	7.75
	Std. dev.	0.33	0.50	0.49	0.46	0.48	0.82	0.82	1.52	1.79
	Min.	0.82	0.12	0.03	0.00	0.02	1.50	1.43	2.09	4.73
	Median	1.41	1.19	1.10	0.45	0.47	2.98	2.91	4.92	7.46
	Max.	1.59	2.89	2.63	1.77	1.79	5.42	5.36	9.61	14.47
$E[(\hat{V}_{Gj}-V_C)^2]^{1/2}/\tilde{V}_C$ (%)	Mean	0.82	0.59	0.50	1.04	1.11	2.34	2.27	5.73	7.07
	Std. dev.	0.25	0.39	0.36	0.61	0.62	0.78	0.78	1.53	1.73
	Min.	0.40	0.04	0.01	0.01	0.04	1.02	0.92	2.71	4.02
	Median	0.74	0.57	0.46	0.99	1.04	2.28	2.17	5.56	6.76
	Max.	1.57	2.14	1.85	2.34	2.42	4.52	4.46	10.35	13.55
		Dependent selection								
			6	7	8	9	10	11	min	max
$E[(\hat{V}_{Gj}-V)^2]^{1/2}/\tilde{V}$ (%)	Mean		1.55	1.51	1.19	1.14	1.82	1.77	1.89	3.58
	Std. dev.		0.94	0.94	0.78	0.77	0.88	0.86	1.47	2.23
	Min.		0.01	0.03	0.01	0.01	0.06	0.03	0.02	0.03
	Median		1.41	1.38	1.12	1.00	1.64	1.61	1.84	3.37
	Max.		4.79	4.74	4.59	4.55	4.54	4.50	7.22	12.33
$E[(\hat{V}_{Gj}-V_C)^2]^{1/2}/\tilde{V}_C$ (%)	Mean		1.06	1.03	0.71	0.68	1.22	1.17	2.02	3.03
	Std. dev.		0.78	0.77	0.63	0.62	0.78	0.76	1.55	2.09
	Min.		0.00	0.01	0.03	0.00	0.01	0.03	0.02	0.12
	Median		0.93	0.85	0.59	0.58	1.01	0.99	1.75	2.66
	Max.		4.14	4.10	3.94	3.90	3.90	3.85	7.97	11.42

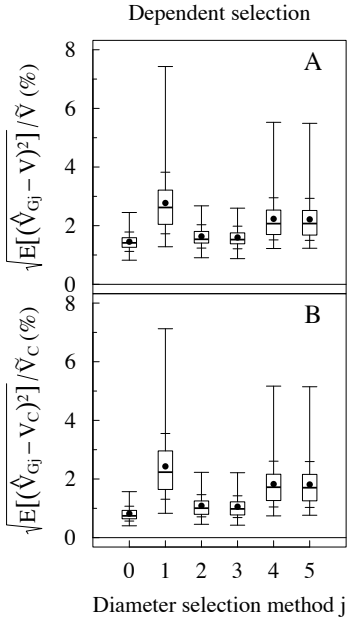

Fig. 70. Summarised distributions of the relative within-tree RMSEs of the general volume estimators based on girth (diameter selection method 0) or random diameters (diameter selection methods 1–5) among the trees where 7 or more discs were available (n=79). The volume estimators were constructed without (A) or with (B) the assumption of convex cross-sections, and the diameters were selected dependently within a stem. (For the explanation of the boxplot, refer to the caption of Fig. 57.)

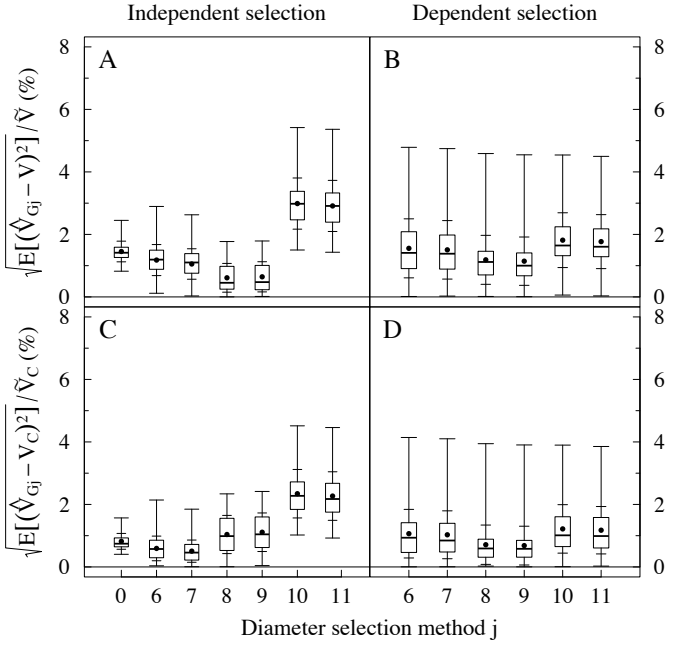

Fig. 71. Summarised distributions of the relative within-tree RMSEs of the general volume estimators based on fixed diameters (diameter selection methods 6–11) among the trees where 7 or more discs were available (n=79); for comparison, results obtained with girth (diameter selection method 0) are also given. The volume estimators were constructed without (A, B) or with (C, D) the assumption of convex cross-sections, and the diameters were selected independently (A, C) or dependently (B, D) within a stem. (For the explanation of the boxplot, refer to the caption of Fig. 57.)

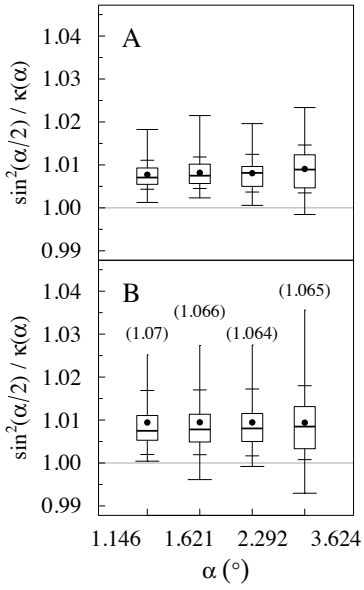

Fig. 72. Summarised distributions of $\sin^2(\alpha/2)/\kappa(\alpha)$, showing deviation of the true basal area factor $\kappa(\alpha)$ of a cross-section from that of a circle $\sin^2(\alpha/2)$, with viewing angle α values of 1.146°, 1.621°, 2.292° and 3.624° (corresponding, with circular cross-sections, to the basal area factor values of 1, 2, 4, and 10 m^2/ha, respectively) in the set of the breast height cross-sections (A; n=80) and in the set of all the cross-sections (B; n=709). The latter case (B) is a "thinking experiment": what if all the cross-sections of the data were breast height cross-sections?

the bias of a stand total (Eq. 69 in Section 4.1.2), these error components appear as tree-specific multipliers $\sin^2(\alpha/2)/\kappa(\alpha)\cdot A_C/(\pi D_j^2/4)$ of the treewise values of the characteristic for which we want to compute the stand total; a multiplier value larger than one implies that the tree contributes to the bias of the stand total with an overestimating input, whereas a value smaller than one indicates an underestimating input.

The error components were computed for all the breast height cross-sections and, as a "thinking experiment", also for all the other cross-sections of the data (imaging them as breast height cross-sections), with the viewing angle α values of 1.146°, 1.621°, 2.292° and 3.624° (corresponding, with circular cross-sections, to the basal area factor values of 1, 2, 4, and 10 m^2/ha, respectively), and with the 22 diameter selection methods (Section 7.2) that were earlier applied in cross-section area estimation and stem volume estimation. With the diameter selection methods involving randomness (methods 1–5, 1ξ–5ξ, 1ξ90, 4ξ90 and 5ξ90), the expectation of the error $E[\sin^2(\alpha/2)/\kappa(\alpha)\cdot A_C/(\pi D_j^2/4)]=\sin^2(\alpha/2)/\kappa(\alpha)\cdot A_C\cdot E[1/(\pi D_j^2/4)]$ over the diameter direction distribution was computed.

Approximating the true basal area factor with that of a circle appeared to produce exiguous errors, implicating overestimating bias smaller than 1% on average and not larger than 2.3% at maximum in the set of the breast height cross-sections (Fig. 72 A). In the set of all the cross-sections, the average errors were of the same magnitude, whereas the maximum values were clearly larger, implicating overestimating bias of up to 7.0% (Fig. 72 B). According to theory, the basal area factor approximation cannot inflict underestimating bias (i.e., $\sin^2(\alpha/2)/\kappa(\alpha)$ cannot assume a value smaller than one; see Eq. 71 in Section 4.1.2). The few unfeasible values emerging in our data (one breast height cross-section with α=3.624°, and two to four cross-sections in the whole data with α=1.621°, α=2.292° and α=3.624°) probably resulted from the low resolution in the scanning of the photographs (see Chapter 6): besides very circular in shape, the problematic cross-sections were small in size (usually taken at the height of 70% or 85%) with an unnaturally rough boundary in the scanned image, as the pixel size was "large" relative to the disc size. Examples of the cross-sections with unfeasible error values are given in Fig. 73 and of the cross-sections with the maximum error values in Fig. 74.

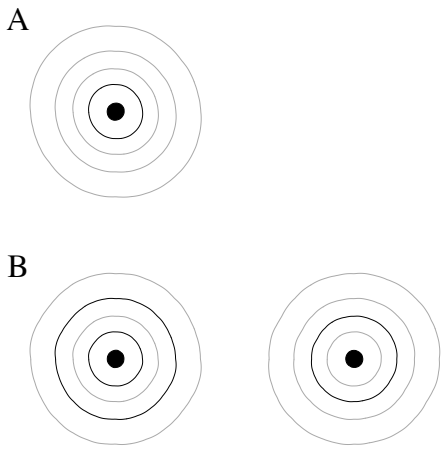

Fig. 73. The only breast height cross-section where $\sin^2(\alpha/2)/\kappa(\alpha)$ assumed an unfeasible value below one (A) and the two cross-sections in the set of all the discs where $\sin^2(\alpha/2)/\kappa(\alpha)$ assumed the smallest unfeasible below-one values (B). For each cross-section, the inclusion regions with viewing angles α=1.146° (outermost), α=1.621°, α=2.292° and α=3.624° (innermost) are shown; the inclusion regions yielding the below-one or the smallest below-one value of $\sin^2(\alpha/2)/\kappa(\alpha)$ are delineated with black line. The cross-section co-ordinates were dilated with factor 10 in relation to the inclusion region co-ordinates to facilitate perception.

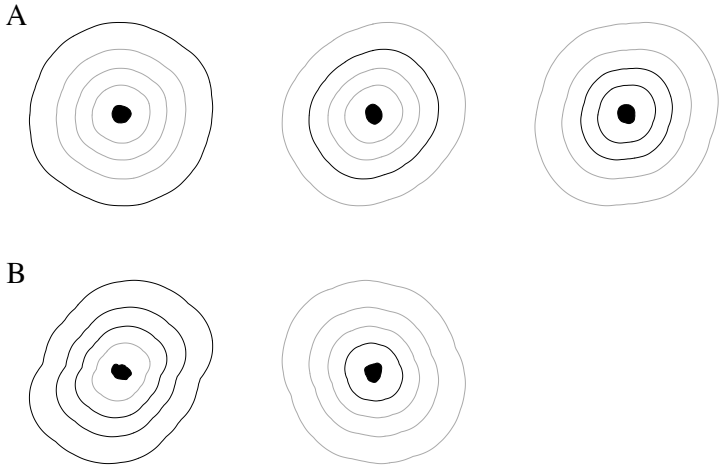

Fig. 74. Cross-sections where $\sin^2(\alpha/2)/\kappa(\alpha)$ assumed its maximum values in the set of the breast height discs (A) and in the set of all the discs (B). For each cross-section, the inclusion regions with viewing angles α=1.146° (outermost), α=1.621°, α=2.292° and α=3.624° (innermost) are shown; the inclusion regions yielding the maximum values of $\sin^2(\alpha/2)/\kappa(\alpha)$ are delineated with black line. The cross-section co-ordinates were dilated with factor 10 in relation to the inclusion region co-ordinates to facilitate perception.

Matérn's theoretical result that, with a viewing angle of the magnitude 1°, Bitterlich sampling gives practically the same bias in the relative basal area of a stand as we would get by calipering every stem in a randomly chosen direction, could be empirically confirmed: with the smallest viewing angle 1.146°, the scatterplot of $\sin^2(\alpha/2)/\kappa(\alpha)-1$ against $[E(\hat{A}_1)-A_C]/A_C$ (the relative within-cross-section bias of the area estimator involving one random diameter) showed a strong one-to-one relationship between these characteristics in individual cross-sections (and almost identical distributions), both in the set of the breast height cross-sections and in the set of all the cross-sections (to see the rationale of this consideration, combine Eqs. 81 and 85 in Section 4.1.3: $A_C \cdot \sin^2(\alpha/2)/\kappa(\alpha) \approx E(\hat{A}_1) \Leftrightarrow \sin^2(\alpha/2)/\kappa(\alpha)-1 \approx [E(\hat{A}_1)-A_C]/A_C$). With the larger viewing angles the similarity declined, being much less manifest already with the viewing angle 1.621°.

Quite strikingly, with the smallest viewing angle 1.146°, $\sin^2(\alpha/2)/\kappa(\alpha)$ correlated almost perfectly with relative isoperimetric deficit $(\hat{A}_0-A_C)/A_C=\hat{A}_0/A_C-1$ in the set of all the cross-sections and very strongly in the set of the breast height cross-sections (Table 54). (Naturally, $\sin^2(\alpha/2)/\kappa(\alpha)$ also correlated strongly negatively with girth-ellipse ratio b_e/a_e, because both b_e/a_e and $(\hat{A}_0-A_C)/A_C$ are transformations of the convex perimeter C and area A_C and therefore strongly negatively correlated; see Section 8.2.1). A scatterplot of $\sin^2(\alpha/2)/\kappa(\alpha)$ against $\hat{A}_0/A_C$ showed the slope to be 1, which implies that with small α, $\sin^2(\alpha/2)/\kappa(\alpha)=\sin^2(\alpha/2)|\mathbf{M}(\alpha)|/A_C$ is very close to $\hat{A}_0/A_C$, that is, $\sin^2(\alpha/2)|\mathbf{M}(\alpha)|$ is very close to $\hat{A}_0$. The explanation is given by the limiting value of $\sin^2(\alpha/2)|\mathbf{M}(\alpha)|$: Matérn (1956, p. 24) writes that by "geometrical consideration" $\sin^2(\alpha/2)|\mathbf{M}(\alpha)|$ tends to $E(\hat{A}_1)$ as α tends to 0; a check with α=0.001° on artificial example shapes (Fig. 10 in Section 4.1.2), another orbiform (Matérn 1956, Fig. 3 c) and ellipses of axis ratios 0.5–0.9 corroborated the result. Now, with α=1.146° $\sin^2(\alpha/2)|\mathbf{M}(\alpha)|$ is close to $E(\hat{A}_1)=\pi\mu_D^2/4+\pi\sigma_D^2/4$, which again was earlier found to be close to $\hat{A}_0=\pi\mu_D^2/4$ in most of the cross-sections (see Section 8.3.2).

Table 54. Correlation of $\sin^2(\alpha/2)/\kappa(\alpha)$ with shape indices (diameter coefficient of variation CV_D, ratio between the extreme diameters D_{min}/D_{max}, girth-area ellipse ratio b_e/a_e, absolute difference between the directions of the extreme diameters $|\theta_{Dmin}-\theta_{Dmax}|$, correlation between perpendicular diameters $\rho_D(\pi/2)$), with relative convex deficit $(A_C-A)/A_C$ and isoperimetric deficit $(\hat{A}_0-A_C)/A_C$, as well as with mean diameter μ_D in the breast height cross-sections (n=80) and in all the cross-sections of the data (n=709). The ratio $\sin^2(\alpha/2)/\kappa(\alpha)$ was computed with the viewing angle α values of 1.146°, 1.621°, 2.292° and 3.624° (corresponding, with circular cross-sections, to the basal area factor values of 1, 2, 4, and 10 m^2/ha, respectively).

Viewing angle α	CV_D	D_{min}/D_{max}	b_e/a_e	$\lvert\theta_{Dmax}-\theta_{Dmin}\rvert$	$\rho_D(\pi/2)$	$(A_C-A)/A_C$	$(\hat{A}_0-A_C)/A_C$	μ_D	
Breast height cross-sections									
1.146°	0.61	–0.66	–0.91	–0.16	–0.09	0.22	0.92	0.15	$\sin^2(\alpha/2)/\kappa(\alpha)$
1.621°	0.55	–0.60	–0.87	–0.17	0.00	0.18	0.87	0.17	
2.292°	0.57	–0.60	–0.76	–0.18	–0.06	0.02	0.77	0.21	
3.624°	0.39	–0.46	–0.73	–0.20	–0.02	0.26	0.73	0.12	
All cross-sections									
1.146°	0.76	–0.78	–0.94	–0.07	0.00	0.47	0.98	0.15	$\sin^2(\alpha/2)/\kappa(\alpha)$
1.621°	0.74	–0.76	–0.94	–0.08	0.00	0.46	0.96	0.15	
2.292°	0.72	–0.75	–0.89	–0.08	–0.03	0.44	0.92	0.14	
3.624°	0.65	–0.67	–0.80	–0.08	–0.02	0.35	0.83	0.14	

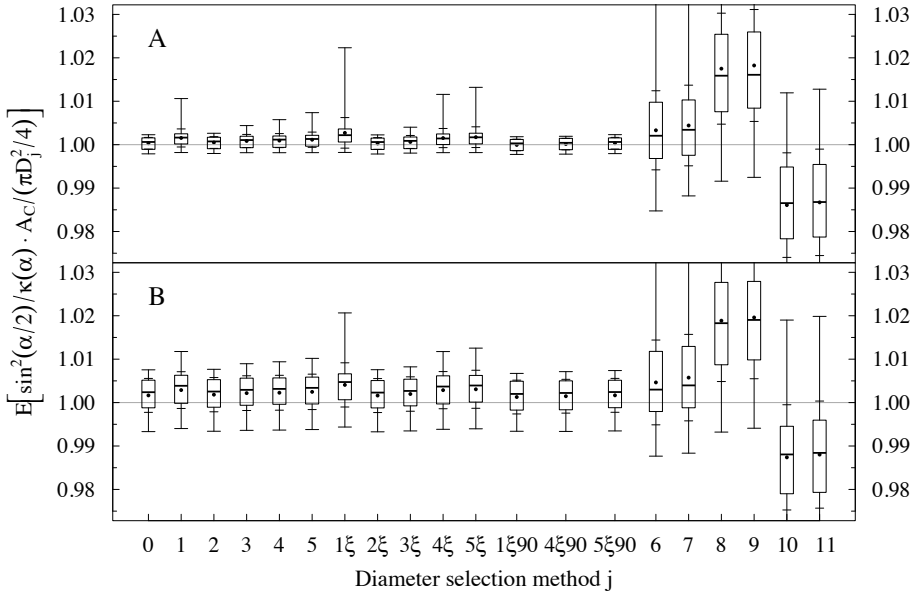

Fig. 75. Summarised distributions of the combined treewise effects of the non-circular breast height cross-sections (n=80) on the bias in stand total estimators in Bitterlich sampling, with 22 diameter selection methods (see Section 7.2) and with viewing angle α values of 1.146° (A) and 3.624° (B) (corresponding, with circular cross-sections, to the basal area factor values of 1 and 10 m^2/ha, respectively).

The decline of the correlations with the increasing viewing angle (Table 54) follows in a natural way from the behaviour of $\sin^2(\alpha/2)/\kappa(\alpha)$: as α tends to π, the inclusion region $\mathbf{M}(\alpha)$ tends to the convex closure of the cross-section (see the discussion in Section 4.1.2, and Matérn 1956, p. 24) and, thus, $\sin^2(\alpha/2)/\kappa(\alpha)=\sin^2(\alpha/2)|\mathbf{M}(\alpha)|/A_C$ tends to $\sin^2(\pi/2)A_C/A_C=1$ (which as a scalar is then uncorrelated with any variable). The path of $\sin^2(\alpha/2)/\kappa(\alpha)$ to this end value varies quite much according to shape (refer e.g. to Figs. 13 and 14 in Section 4.2.1), which for its part also explains the somewhat larger variation of $\sin^2(\alpha/2)/\kappa(\alpha)$ observed with the largest viewing angle 3.624° compared to the other viewing angles (Fig. 72).

The systematic overestimation of convex area that girth diameter (diameter selection method 0) and random or Bitterlich diameters (methods 1–5, 1ξ–5ξ, 1ξ90, 4ξ90, 5ξ 90) yield with the circle area formula seemed to neutralise effectively the error due to basal area factor approximation in the breast height cross-sections: bias implicated by the combined error due to diameter selection and basal area factor approximation was on average close to zero with the viewing angle 1.146° and less than 0.4% overestimation with the viewing angle 3.624° (Fig. 75). (Note that the diameter selection effect is slightly weaker than a straightforward insertion of the area estimator bias, shown in the set of all the cross-sections e.g. in Fig. 44 A, in the error expression would imply, because $E(1/D_j^2)\geq 1/E(D_j^2)$ with random or Bitterlich diameters.) The larger the viewing angle, the more variable the combined errors appeared to be and the larger part of the trees seemed to contribute to bias with an overestimating rather than underestimating input. Measuring only one random diameter (method 1), or Bitterlich diameter parallel to plot radius (method 1ξ), or both (methods 4ξ and 5ξ) yielded larger maximum errors than the other methods, yet implicating overestimating bias not larger than 2.2%.

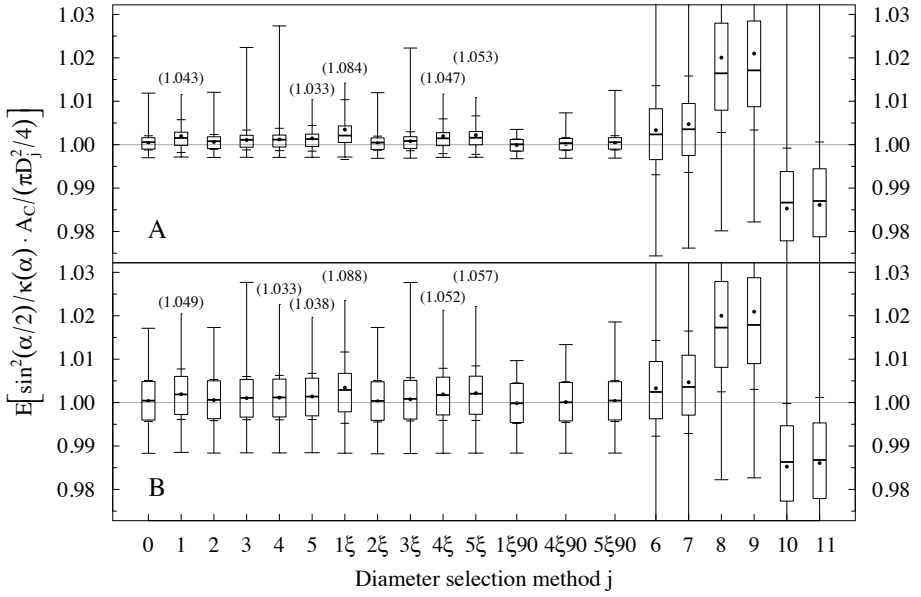

Fig. 76. Summarised distributions of the combined treewise effect of non-circular breast height cross-section on the bias in stand total estimators in Bitterlich sampling, with 22 diameter selection methods (see Section 7.2) and with viewing angle α values of 1.146° (A) and 3.624° (B) (corresponding, with circular cross-sections, to the basal area factor values of 1 and 10 m^2/ha, respectively) in the set of all the cross-sections (n=709). This is a "thinking experiment": what if all the cross-sections of the data were breast height cross-sections?

In the set of all the cross-sections, the averages of the combined errors were of the same magnitude as in the set of the breast height cross-sections, and with the viewing angle 3.624° even indicating bias closer to zero (Fig. 76). The maximum values, however, were clearly larger, implicating overestimating bias of up to 8.4% with viewing angle 1.146° and up to 8.8% with viewing angle 3.624°; the largest maximum values were produced by the same methods (1, 1ξ, 4ξ and 5ξ) as in the set of the breast height cross-sections. Interestingly, measuring Bitterlich diameter perpendicular to plot radius (method 1ξ90) or taking the arithmetic mean of Bitterlich diameters (method 4ξ90) appeared slightly more advisable than using girth diameter (method 0), as judged from the error distributions in the set of all the cross-sections.

9 Summary and Conclusions

This study explores how non-circularity of tree stem cross-sections affects cross-section area estimation, stem volume estimation and Bitterlich sampling under the circularity assumption. The primary purpose of the work was to provide theoretical tools for quantifying these non-circularity effects. The secondary purpose was to demonstrate the magnitude of the effects with reasonable data on Scots pine.

In the theoretical part of the work, we developed methods for quantifying (i) the errors that the within-cross-section variation in diameter causes to cross-section area estimates given by the circle area formula and 22 different diameter selection methods, (ii) the errors that the within-cross-section variation in diameter induces in stem volume estimates given by the Laasasenaho (1982) volume equation, a cubic-spline-interpolated stem curve and a generalised volume estimator together with the 22 diameter selection methods, and (iii) the errors that non-circular shape of breast height cross-sections and the 22 diameter selection methods inflict on stand total estimates in Bitterlich sampling. The 22 diameter selection methods, listed in Section 7.2, involved diameters measured with tape or caliper and differed from each other in terms of the choice of the measurement direction, the number of diameters to be measured and the type of mean (geometric, arithmetic) applied to the measured diameters. In the empirical part of the work, based on the digital images of 709 cross-sections taken at 6–10 heights in 81 Scots pine stems from different parts of Finland, we first investigated the variation in the shape of the cross-sections; thereafter we demonstrated how the systematic and sampling errors of the area, volume and stand total estimators presented in the theoretical part can be computed in practice and what magnitude they are in a this kind of small Scots pine data set.

The empirical results should be taken with a pinch of salt, due to certain defects of the data. First, taking and imaging discs at several heights in trees is laborious, and therefore our data set, although relatively large compared to the data sets found in literature, is still rather small for drawing general conclusions. More importantly, however, our non-probabilistic sampling of trees, resulting in an uneven spatial distribution of trees over Finland and in a two-modal size distribution with severe under-representation of log-size trees, hampers generalisation to any meaningful Scots pine population. This subjectivity in the data gathering was accepted because the idea was to illustrate the magnitude of the theoretical effects rather than estimate some actual quantities of a defined population. Finally, to avoid potential difficulties in the image interpretation, the discs were debarked before photographing, and thus the results pertain to stem wood without bark, which is contrary to the usual practice in forest mensuration.

We strove for isolating the effect of non-circularity from other sources of variation or error. To eliminate measurement errors in particular, we computed the cross-section measurements on digital images instead of taking them with common instruments on the discs. Yet in practical forest mensuration, measurement errors are virtually impossible to evade or even to quantify; moreover, modelling them appears also difficult, as the factors affecting the measurement situation can be rather complex and involve a good deal of psychology (Matérn 1990). For the only empirical results found in literature on the combined effect of non-circularity and measurement errors, see the study by Gregoire et al. (1990).

In the following, we summarise the main results of this work on (i) variation in cross-section shape, (ii) estimation of cross-section area, (iii) estimation of stem volume and (iv) estimation of stand totals with Bitterlich sampling, and attempt to come up with practical conclusions that could be useful in actual forest mensuration work.

Variation in Cross-Section Shape

Non-convexity is a potentially important source of systematic overestimation in area and volume estimation of standing trees, as it cannot be observed with caliper or girth tape measurements. In the 709 debarked stem cross-sections of this study, however, the amount of non-convexity was exiguous: the relative difference between the convex and true area was less than 1% in 87% of the cross-sections and not more than 2.9% in maximum. This may follow from the predominance of small pulpwood-size trees in the data: Matérn (1990) reported somewhat larger non-convexity in his 45 debarked cross-sections taken from log-size Scots pine stems. According to his results, bark is also likely to increase non-convexity, particularly in the lower parts of Scots pine stems.

Judging from the six scalar and three functional shape indices computed for the cross-sections in the data, ellipse did not depict cross-section shape better than circle. In fact, rather than from actual shape observations, the persistently reiterated idea of ellipse as a more realistic shape model may originate from area estimation results (see the discussion below). Further, on the basis of shape the indices, the cross-sections were found to be more non-circular in the butt of the stems than in the middle and upper parts. As a curiosity, a useful result presented by Matérn (1990) could be corroborated: also in our data, diameter coefficient of variation CV_D within a cross-section correlated almost fully negatively with the ratio of the minimum and the maximum diameter D_{min}/D_{max}, and thus D_{min}/D_{max}, which is relatively simple to measure, may very well be used to predict linearly CV_D, which is far less tractable, with $CV_D = 36 - 0.36 \cdot D_{min}/D_{max}$ (both the characteristics are expressed in percentage units).

A clearly systematic directional pattern in diameter was observed in the cross-sections in the butt of the stems: the diameters taken between the SW–NE and S–N directions were on average the largest in the cross-sections and would result in overestimates of the convex area of the magnitude 3.6–5.7% when substituted in the circle area formula, whereas the diameters taken between the NW–SE and W–E directions were on average the smallest and would yield underestimates of the magnitude 0–1.6%. A plausible explanation might be given by the south-westerly winds prevailing in Finland, combined with the relatively flat topography of the country: the torsional moment caused by the wind stress results in asymmetric growth, possibly through formation of reaction wood, that strengthens the stem in the directions of the moment.

Estimation of Cross-Section Area

The estimators of cross-section area or stem volume were assessed by the systematic error (the bias, i.e., the expectation of error with respect to true value) and the sampling error (the variance or standard deviation around the expected value) that infinitely many repeated diameter selections, with the particular selection method, would yield within a cross-section or within a tree stem. It is important to notice that the systematic error is the expectation of the error over repeated diameter selections within a cross-section or within several cross-sections in a tree, not an error being realised in each individual diameter selection. With fixed diameters involving no random choice of measurement direction, such as the diameter derived from girth or the maximum and the minimum diameter, the sampling error is naturally zero (as repeated diameter selections always result in the same diameter) and the systematic error simply equals the area or volume estimation error.

In the theoretical consideration of cross-section area estimation, citing and elaborating Matérn's (1956) theoretical results, we saw that the commonly used diameter selection

methods — diameter derived from girth (*girth diameter*, giving the expectation of diameter over all possible measurement directions), diameter calipered in a random direction, mean of this diameter and its perpendicular, and mean of two diameters calipered in random directions — together with the circle area formula systematically overestimate convex area, irrespective of the cross-section shape. The magnitude of the overestimating bias was shown by Matérn to have a lower bound that depends on diameter variance within the cross-section (the larger the variance the larger the least possible overestimation). In our data of 709 Scots pine cross-sections, the overestimation bias was found to be virtually similar for all these diameter selection methods: the average within-cross-section biases were about 0.9% with respect to convex area and about 1.6% with respect to true area, that is, of the same meagre magnitude as the amount of non-convexity, and with fairly little variation between the discs. In other words, measuring girth or a second diameter at each height, either in a random direction or crosswise, did not bring any benefit, in terms of systematic error, compared to taking only one diameter in a random direction.

In terms of sampling error, however, these diameter selection methods were found to differ from each other considerably. The girth diameter method was naturally superior as it involves no uncertainty of this kind. The methods involving random diameters, in turn, produced substantial sampling errors: with one random diameter the average sampling error was four times, with the mean of two random diameters three times, and with the mean of one random diameter and its perpendicular one and a half times the average systematic error. In other words, the benefit of taking the second diameter crosswise instead of measuring it in a random direction was greater than that gained by measuring two random diameters instead of only one. Taking the second diameter perpendicular to the first one rather than in a random direction seemed advisable also in the sense that it considerably attenuated the sampling error variation between the cross-sections. Because of the large sampling errors related to the use of random diameters, the advantageousness of using fixed diameters, especially the girth diameter, in single-tree estimation became fairly obvious in our data. Noteworthily, it appears that for estimating sampling errors we may well use the simple approximate formulae instead of the complex analytic ones (both derived in the theoretical part), as in the data the variance approximations resulted virtually in the same values as the analytic variances.

In the theoretical consideration of Bitterlich sampling, we found that if the breast height cross-section of a tree is non-circular, the diameter taken parallel or perpendicular to plot radius direction in Bitterlich sampling does not correspond to a diameter calipered in a random direction (diameter with the uniform direction distribution). A way of computing the treewise direction distributions of these *Bitterlich diameters* was presented, based on the geometrical probability of the viewing point location in the inclusion region of a tree. In practice, however, the deviations of these direction distributions from the uniform distribution proved to be unimportantly small: in our data, within the studied viewing angle range of 1.146°–3.624° (corresponding, with circular cross-sections, to the basal area factor range of 1–10 m^2/ha), Bitterlich diameters resulted in similar systematic and sampling errors in area estimation as random diameters. The deviation of Bitterlich diameters from random diameters could be made visible by confining the examination on the breast height cross-sections only: in all the breast height cross-sections, measuring Bitterlich diameter perpendicular to plot radius resulted in larger bias than taking diameter in a (uniform) random direction; likewise, in 90% of the breast height cross-sections, measuring Bitterlich diameter parallel to plot radius resulted in smaller bias than taking the diameter in a (uniform) random direction; in all the breast height cross-sections, measuring Bitterlich diameter perpendicular to plot radius resulted in larger bias than taking it parallel to plot radius; however, as said above, the differences between the methods were negligibly small.

Unlike the diameter selection methods involving the girth diameter or random diameters, those involving the minimum and/or the maximum diameter could also systematically underestimate convex area. Among all the diameter selection methods considered, the mean of the extreme diameters or the mean of the minimum diameter and its perpendicular produced the systematic errors closest to zero on average in our data, but the errors varied exceedingly between the trees, which makes these methods less suited for individual tree estimation. Moreover, these diameter methods may be less feasible in practice, as measuring the minimum and/or the maximum diameter without error in the field is likely to take a longer time than measuring the girth or a random diameter.

The geometric mean of (unequal) diameters always yields smaller area estimates in the circle area formula than the arithmetic mean, simply because the geometric mean is always smaller than the arithmetic mean. In the case of random diameters, which we saw to result in systematic overestimation of convex area, it is hence advantageous to use the geometric mean instead of the arithmetic one. This may have created the fallacy of the elliptical shape of tree cross-sections reiterated in literature, since the use of the geometric mean of perpendicular diameters in the circle area formula corresponds to computing the area of an ellipse and hence implies a seeming assumption of elliptical shape. In our data, however, employing the geometric mean did not yield noticeably better area estimation results (systematic errors closer to zero, smaller sampling errors) than using the arithmetic mean.

Matérn's (1990) empirical results on area estimation in Scots pine both under and over bark suggest that bark would considerably decrease shape irregularities and thus reduce and stabilise the systematic and sampling errors obtained with the common diameter selection methods, especially in the butt of stems. Due to the small size of his data set, however, these results remain somewhat uncertain.

Above it was emphasised that with the systematic error we here mean the within-cross-section bias, that is, the expectation of area estimation errors over (infinitely many) repeated diameter selections within a cross-section. The mean of these within-cross-section biases across cross-sections (trees) is a good criterion for choosing the diameter selection method for estimation of both stand basal area and individual cross-section area. Obviously, performing diameter selection only once in a number of cross-sections (trees) and computing the mean of the resulting area estimation errors does not necessarily yield a similar estimate of mean bias, but sometimes quite contrasting values, especially if the number of cross-sections (trees) is small. This is because the area estimation error resulting from one diameter selection may estimate very poorly the expectation of the errors over (infinitely many) repeated diameter selections within a cross-section. Thus the diameter selection methods involving random (or Bitterlich) diameters, which we saw to yield overestimating within-cross-section bias irrespective of cross-section shape, may well produce negative area estimation errors with individual diameter selections, as a result of which also the mean of these errors over trees may be negative.

As a conclusion of the effect of non-circularity on cross-section area estimation, we would recommend using girth diameter in the circle area formula both for individual tree and stand total estimation, because this method involves no sampling error and produced in our data generally small overestimating systematic errors, with clearly the least between-cross-sections variation in these errors among all the 22 diameter selection methods considered. Due to this small between-cross-sections variation, the estimator based on girth diameter would lend itself to modelling for bias correction. Measuring girth diameter is advisable also for growth estimation between two time points, as it gives the growth in mean diameter over all the measurement directions and thus takes "automatically" into account the potentially asymmetric growth in non-circular cross-sections.

Estimation of Stem Volume

In the theoretical consideration of stem volume estimation, we first dealt with the Laasasenaho (1982) volume equation, commonly used in Finland for predicting the stem volume of standing trees. The model is linear with respect to its parameters and involves tree height and diameters at the heights of 1.3 m and 6 m as the explanatory variables. For this volume estimation method together with those of the 22 diameter selection methods that involved random diameters, we derived expressions, as functions of diameter moments and tree height, of the systematic and sampling errors (the within-tree biases and variances) over all possible diameter selections within a tree. The diameter selection methods were applied both dependently and independently at the two observation heights within a stem: in the former, the diameter direction was selected at breast height, and the diameter at the upper height was then measured in the same direction; in the latter, the diameter directions were selected at each height independently of each other. The effect of diameter selection was separated from the model error (error inherent in the model, caused by variation in stem tapering and present even if the cross-sections at the heights of 1.3 m and 6 m were circular and their diameters were known without error) by defining the systematic errors with respect to the best estimate obtainable by the equation and not with respect to the estimated true volume (obtained by a more precise stem curve method). The expressions of the systematic and sampling errors became so intricate that no similar theoretical results as in area estimation, establishing systematic overestimation or underestimation by a diameter selection method, could be derived. A similar approach to quantify the diameter selection effect, however, can be taken with any linear volume equation, assuming the parameters known and the possibly involved tree height measured without error.

As the other volume estimation method, we considered a non-parametric stem curve interpolated with cubic splines between diameters observed at 8–11 heights in a stem, quite commonly used in Finland to estimate the stem volume of felled sample trees for research purposes. For this method, we presented a simple Monte Carlo integration way of estimating the systematic and sampling errors within a tree using a number of repeated volume estimations (realisations of the volume estimator) with the 22 diameter selection methods. Also here the diameter selection methods were applied both dependently and independently at the separate observation heights within a stem.

Finally, as a theoretical play, we investigated a theoretical way of estimating the errors of a general volume estimator, defined as a definite integral of an area estimation function that gives the estimate of cross-section area at all heights in the stem. We found that the systematic and sampling errors of such a volume estimator can be obtained by integrating the bias and covariance functions of the area estimation process corresponding to the area estimation function. In practice, we did not explicitly define an area estimation function corresponding to each of the 22 diameter selection methods in each tree, but considered the area estimation processes where the area estimator at each height was the circle area formula with one the 22 diameter selection methods; for each of these processes, we had discrete observations of estimated bias at 7–10 observation heights and of estimated covariance at all the 49–100 height combinations in each tree. From these observations, we constructed the bias and covariance functions by simple linear interpolation.

In our data of 50 stems for the Laasasenaho volume equation (the disc at the height of 6 m was available only in 50 trees) and 79 stems for the cubic-spline-interpolated stem curve, we found that the commonly used diameter selection methods (girth diameter, diameter calipered in a random direction, mean of this diameter and its perpendicular, mean of two diameters calipered in random directions) yielded very similar systematic overestimation of stem volume within a tree: with all the methods, the mean relative within-tree bias

attributable to diameter selection of was about 1.2% with the Laasasenaho volume equation and about 1.5% with the cubic-spline-interpolated stem curve. The systematic errors in volume estimation were hence of the same magnitude as in area estimation. Whether all the diameters in a stem were taken in the same direction (dependent selection, the prevailing practice) or whether the diameter measurement directions were chosen independently at each height (independent selection, a more laborious alternative) had no practical influence on the systematic errors. Ignoring non-convexity, which cannot be observed with the common measurement equipment from outside, reduced the systematic errors considerably, 0.5–0.6 percentage units with both the volume estimation methods. The differences between the results obtained with the geometric vs. the arithmetic mean of diameters were unimportantly small.

In terms of the sampling error attributable to diameter selection, these diameter selection methods were found to differ from each other substantially, just as in area estimation, although with slightly smaller magnitude of errors. The girth diameter method involving no sampling variation was naturally pre-eminent. Among the other methods, perpendicular diameters yielded clearly the smallest sampling errors, the mean relative within-tree standard deviation of the volume estimation errors being 1.0% with the Laasasenaho volume equation and 0.7% with the cubic-spline-interpolated stem curve, whereas one and two random diameters yielded approximately triple and double that variation, respectively. Independent selection of diameters seemed to result in slightly smaller and less variable sampling errors than dependent selection, particularly with the spline-interpolated stem curve involving more diameters than the volume equation; the gain from independent selection was so modest, however, that it does not compensate for the necessarily increasing time usage in taking the measurements.

The consideration of the combined effect of the systematic and sampling errors reveals the advantageousness of the use of girth diameter: in terms of within-tree RMSE, the girth diameter method, lacking the within-tree sampling error, was clearly superior to the methods involving random diameters. This superiority became less pronounced when a larger number of diameters was involved in the volume estimation, as the sampling error component related to the use of random errors then decreased more than the bias component increased; hence, with the cubic-spline-interpolated stem curve, the difference between the use of girth and perpendicular random diameters was not as substantial as with the volume equation.

In our data, within the studied viewing angle range of 1.146°–3.624° (corresponding, with circular cross-sections, to the basal area factor range of 1–10 m^2/ha), Bitterlich diameters produced practically similar systematic and sampling errors as random diameters, no matter which volume estimation method was used. As discovered already in area estimation, however, if only one diameter can be measured, it would be advisable to take it parallel to plot radius in Bitterlich sampling, because the expected value of this diameter is always smaller than that of the diameter perpendicular to plot radius and often also smaller than that of a random diameter (with the uniform direction distribution).

Using the minimum and/or the maximum diameters and their perpendiculars resulted in clearly more variable systematic volume errors, with also underestimating values, than the girth diameter or random diameters. Some of these diameter selection methods (mean of the minimum diameter and its perpendicular, mean of the minimum and the maximum diameters) performed very well on average, producing only little additional bias on top of the model error. Yet it would be somewhat risky to recommend these methods even for the estimation of the sum of stem volumes in a stand, as they involve rather large uncertainty (large between-trees variation in within-tree biases).

With the Laasasenaho volume equation, it was possible to compare the diameter selection effect (the combination of the systematic error and the sampling error of a diameter selection

method within a tree) to the model error (the error inherent in the model due to variation in stem tapering). With all the methods considered, this diameter selection effect appeared much smaller than the model error. Also, the model error was found to be unassociated with the diameter selection effect; in other words, large model error and a poor performance of any diameter selection method, or vice versa, did not systematically coincide in our trees.

From the theoretical play with the general volume estimator we learnt that the bias and covariance functions of an area estimation process within a stem can be meaningfully estimated in the rather crude way of linear interpolation between the estimated biases and covariances of the area estimator at several heights along the stem: the integration of such bias and covariance functions resulted in very similar within-tree volume biases and sampling errors as were obtained by repeated constructions and integrations of cubic-spline-interpolated stem curves from diameters at the same heights.

As a conclusion of the effect of diameter selection on stem volume estimation, we would recommend to use the girth diameter for both individual tree and stand estimation, with both the Laasasenaho volume equation and the cubic-spline-interpolated stem curve. This is because this method involves no sampling error and yielded in our data generally small overestimating systematic errors, with the least between-trees variation of these errors among all the 22 diameter selection methods considered. Of the methods involving random diameters, the geometric mean of one random diameter and its perpendicular (or, diameters parallel and perpendicular to plot radius in Bitterlich sampling) could also be used for the prediction of individual trees with the spline-interpolated stem curve method.

Estimation of Stand Totals with Bitterlich Sampling

In the theoretical consideration of the estimation of stand totals from a Bitterlich sample, we found that non-circularity inflicts errors in the estimation of the inclusion probabilities of the trees. These probabilities are used in stand total estimators as the inverse weights of the treewise characteristics and estimated by assuming that the breast height cross-sections of the trees are circular, using the breast height diameters of the trees as the input variables. The errors induced by non-circularity in the inclusion probability estimates may cause bias in stand total estimators. They consist of the following two tree-specific components: (i) deviation of the true basal area factor of the tree from that of a circle, and (ii) deviation of the area estimate given by the circle area formula and the breast height diameter, selected by some method, from the convex area. The first component only depends on the shape of the breast height cross-section and is thus independent of the diameter selection method.

In the 80 breast height cross-sections of our data, the error components were found to counteract each other effectively, when the commonly used diameter selection methods (girth diameter, diameter calipered in a random direction, mean of this diameter and its perpendicular, mean of two diameters calipered in random directions) were employed: the bias implicated by the combined error was on average close to zero with the viewing angle 1.146° (corresponding, with circular cross-sections, to the basal area factor of 1 m^2/ha) and less than 0.4% overestimation with the viewing angle 3.624° (the basal area factor of 10 m^2/ha). The larger the viewing angle, the more variable the combined errors appeared to be and the larger part of the trees seemed to contribute to bias with an overestimating rather than underestimating input. The differences between these diameter selection methods were small, however, and with none of them the overestimating bias became larger than 2.2%.

In the theoretical part on Bitterlich sampling, we also worked out the result already presented by Matérn (1956) that the simple estimator of the relative basal area of a stand, that is, the number of trees selected in Bitterlich sampling times the basal area factor under

the circularity assumption, overestimates the true relative basal area, be the breast height cross-sections of whatever non-circular shape. In our data, we were then able to corroborate Matérn's (1956) theoretical approximation that with the viewing angle of the magnitude of 1° (corresponding, with circular cross-sections, to the basal area factor of about 1 m^2/ha), the bias in relative basal area is about the same as we would get by calipering every stem in the stand in one randomly chosen direction; with larger viewing angles, the result did not hold any more.

In conclusion, it appears that although inflicting overestimating bias in theory, non-circularity is not necessarily much to worry about in Bitterlich sampling of young Scots pine stands in practice, except when estimating relative basal area with the simple counting method. As Matérn (1984) wrote: "In practice there are of course more serious risks of bias or errors beyond control. They have to do with conditions of visibility, the correct height in which to look at the stem and the possible subjective errors in deciding whether a boundary case (when the stem subtends an angle near [the viewing angle] α) shall be included or not." On the basis of theoretical example shapes, it appears that "boundary cases" can be reasonably checked with the usual method of measuring the diameter perpendicular to plot radius and computing the critical distance with the circular cross-section formula.

The overall conclusion of this study is that the systematic effects of non-circularity of tree cross-sections deserve attention in the estimation of cross-section area and stem volume as well as in Bitterlich sampling. The small magnitude of errors that we found in our data consisting mostly of pulpwood-size stems cannot be generalised to Scots pine stems of larger size or to other tree species. And, as already pointed out in the introductory chapter of this study, even if the systematic errors were small in magnitude, compared to measurement errors (e.g. Päivinen et al. 1992), for instance, they may cumulate into substantial errors in large area inventories. Finally, in the research context, the effects of non-circularity may appear as confounding factors, which we wish to eliminate in order to clarify our analyses and consolidate our results.

Future Work

We chose Scots pine as the species to be investigated because of its commonness and economic importance in Finland. Among the Finnish tree species, however, it is probably the most regular in shape, and thus the errors quantified in the data of this study can be thought to make a sort of "lower bound" of errors over tree species. A natural line of future work would then be to repeat the analyses of this study on other, potentially more irregular species, in Finland particularly on Norway spruce and silver birch.

Another straightforward line of future work, possible to carry out already with the data of this study, would be to combine the errors in the inclusion probabilities in Bitterlich sampling with the errors in stem volume estimates, both depending on the diameter selection method, to assess the bias caused by non-circularity on the stand volume estimate. This could of course be done also for any other treewise characteristic of interest for which data are available.

For forest inventory purposes, empirical models for bias correction in cross-section area and stem volume could be constructed, with the girth diameter as the diameter selection method. In these models with the within-cross-section or within-tree bias as the response variable, the explanatory variables should represent the factors influencing the process of non-circularity formation, such as site conditions (prevailing winds, sloping topography, potential snow load in canopy), management history of the stand and competition between the trees (growing space affecting crown size and symmetry), and tree age (indicating how

long the tree has been exposed to non-circularity formation). Gathering data appropriate for this kind of modelling, however, seems rather laborious and demanding.

Modelling cross-section shape appears challenging, as obviously it is not possible to depict it precisely enough with combinations of geometrical figures. Estimating the boundaries of convex closures on the basis of radii information, classifying these closed curves by principal components analysis (see. e.g. Ramsay and Silverman 1997), and associating the resulting classes of curves with environmental factors could be one approach. Mechanistic modelling could make another, perhaps a bit fantastic, approach: one could start by modelling physically the structure that a stem needs to develop to resist the torsional moment caused by wind, leaning position, or crown mass imbalance; modelling the crown development, however, is much more intricate as it requires knowledge of all the growing conditions of the tree, including spatial pattern of competing trees, distribution of light, and availability of water and nutrients for the tree.

References

Banks, C.C. 1973. The strength of trees. Journal of the Institute of Wood Science 6(2): 44–50.

Barrett, J.P. 1964. Correction for edge effect bias in point-sampling. Forest Science 10(1): 52–55.

Biging, G.S. & Wensel, L.C. 1984. A photographic technique for use with stem analysis. Forest Science 30(3): 715–729.

— & Wensel, L.C. 1988. The effect of eccentricity on the estimation of basal area and basal area increment of coniferous trees. Forest Science 34(3): 621–633.

Bitterlich, W. 1948a. Die Winkelzählprobe. Allgemeine Forst- und Holzwirtschaftliche Zeitung 59(1/2): 4–5.

— 1948b. Ein neues Messverfahren zur Aufname stehender Holzmassen. Österreichs Forst- und Holzwirtschaft 3(6): 89–90.

— 1984. The relascope idea: relative measurements in forestry. Commonwealth Agricultural Bureaux, Slough. 242 s.

Bøhmer, J.G. 1935. Furuens flattrykning og tømmerinnhold. [In Norwegian]. Tidsskrift for skogbruk 43(12): 342–352.

Borowski, M. 1961. Dokładność oznaczania powierzchni przekroju poprzecznego strzał sosny. [In Polish]. Zusammenfassung: Genauigkeit der Ermittlung der Querschnittfläche von Kiefernschaften. Folia Forestalia Polonica, Seria A, Zeszyt 6: 149–197.

Bouillet, J.P. & Houllier, F. 1994. Influence des éclaircies sur la forme de la section droite du tronc de Pinus kesiya dans la région du Mangoro (Madagascar). Annales de Sciences Forestières 51: 267–281.

Bucht, S. 1981. Effekten av några olika gallringmönster på beståndsutvecklingen i tallskog. [In Swedish]. Summary: The influence of some different thinning patterns on the development of Scots pine stands. Sveriges lantbruksuniversitet, Institutionen av skogskötsel, Rapport 4. 276 p.

Burdon, R.D. 1975. Compression wood in Pinus radiata clones on four different sites. New Zealand Journal of Forestry Science 5: 152–164.

Casella, G. & Berger, R.L. 1990. Statistical inference. Brooks/Cole, Pacific Grove, California. 650 p.

Cassel, C.M., Särndal, C.E. & Wretman, J.H. 1977. Foundations of inference in survey sampling. Wiley & Sons, New York. 192 p.

Chacko, V. J. 1961. A study of the shape of cross section of stems and the accuracy of caliper measurement. Indian Forester 87(12): 758–762.

Coxeter, H.S.M. 1969. Introduction to geometry. 2nd edition. John Wiley & Sons, Toronto. 469 p.

Delord, J.M. 1979. Les modalités de réalisation des mésures dendrometriques, et leur incidence sur le calcul d'accroissement en volume. Paper presented at the meeting of IUFRO groups 4.01.02 and 4.02.03 in Vienna, September 1979. 46 p.

Dillon, W.R. & Goldstein, M. 1984. Multivariate analysis: methods and applications. John Wiley & Sons, New York. 587 p.

Drake, E., Johansson, J., Johansson, L.G. & Liljeblad, Å. 1988. Furustammarnas yttre och inre geometri, inmätta inom projektet 'Kvalitetssimulering av sågtimmer'. [In Swedish]. Summary: External and internal geometry of Scots pine stems mapped in the project 'Quality Simulation of Saw Logs'. Träteknik Centrum, Rapport 8811069. 185 p.

Dryden, I.L. & Mardia, K.V. 1998. Statistical shape analysis. John Wiley & Sons, Chichester. 347 p.

Edwards, C.H. Jr. & Penney, D.E. 1994. Calculus with analytic geometry. 4th edition. Prentice Hall, Englewood Cliffs. 956 p.

Eriksson, M. 1995. Design-based approaches to horizontal-point-sampling. Forest Science 41(4): 890–907.

Exner, H.E. 1987. Shape – a key problem in quantifying microstructures. Acta Stereologica 6/III: 1023–1028.

Fox, J. 1984. Linear statistical models and related methods with applications to social research. John Wiley & Sons, New York. 449 p.

Glasbey, C.A. & Horgan, G.W. 1995. Image analysis for the biological sciences. John Wiley & Sons, Chichester. 218 p.

Georgopoulos, A. & Gofas, A. 1966. Symbole eis ten ereynan tes morfes tes egapsias diatomes kormon deykes kai tes akribeias metreseos tes kykdikes epifaneias ayton. Deutera anakoinosis. [In Greek]. Summary: Contribution to the investigation of the cross-section shape and to the precision of the basal area measurement of poplar trees. Second communication. Epeteris tes Geoponikes kai Dasologikes Scholes, Aristoteleion Panepistemion Thessalonike. p. 317–372.

Grace, J. 1977. Plant response to wind. Academic Press, London. 204 p.

GRASS User's Reference Manual 1993. Grass 4.1 (Spring 1993). U.S. Army Corps of Engineers, Construction Engineering Research Laboratories (CERL), Champaign, Illinois. 1170 p.

Gregoire, T.G. & Valentine, H.T. 1995. A sampling strategy to estimate the area and perimeter of irregularly shaped planar regions. Forest Science 41(3): 470–476.

— & Valentine, H.T. 2008. Sampling strategies for natural resources and the environment. Chapman & Hall/CRC, Boca Raton, Florida. 474 p.

— & Williams, M. 1992. Identifying and evaluating the components of non-measurement error in the application of standard volume equations. The Statistician 41: 509–518.

— , Zedaker, S.M. & Nicholas, N.S. 1990. Modeling relative error in stem basal area estimates. Canadian Journal of Forest Research 20: 496–502.

— , Schabenberger, O. & Kong, F. 2000. Prediction variance from an integrated regression equation: a forestry application. Biometrics 56: 414–419.

Grosenbaugh, L.R. 1958. Point sampling and line-sampling; probability theory, geometric implications, synthesis. USDA Forest Service, Southern Forest Experiment Station, Occasional Paper 160. 34 p.

Guide to standard Mathematica packages 1993. Version 2.2. 3rd edition. Wolfram Research Inc., Champaign, Illinois. 459 p.

Hadwiger, H. 1957. Vorlesungen über Inhalt, Oberfläche und Isoperimetrie. Grundlehren der matematischen Wissenschaften 93. Springer-Verlag, Berlin. 312 p.

Haga, T. & Maezawa, K. 1959. Bias due to edge effect in using the Bitterlich method. Forest Science 5: 370–376.

Hardy, G., Littlewood, J.E. & Pólya, G. 1988. Inequalities. 2nd edition. Cambridge University Press, Cambridge. 324 p.

Harris, J.M. 1977. Shrinkage and density of radiata pine compression wood in relation to its anatomy and mode of formation. New Zealand Journal of Forestry Science 7: 91–106.

Hazewinkel, M. (ed.) 1992. Encyclopaedia of mathematics. Vol. 8. Kluwer, Dordrecht. 540 p.

Heikkilä, T. 1913. Koealojen kaulaamisesta ja puiden poikkileikkauspinnan soikeudesta. [In Finnish]. Tapio 6(11): 324–331.

Hobolth, A. & Jensen, E.B.V. 1999. Modelling stochastic changes in curve shape, with an application to cancer diagnostics. University of Aarhus, Department of Mathematical Sciences, Laboratory for Computational Stochastics, Research Report 5. 29 p.

Holgate, P. 1967. The angle-count method. Biometrika 54(3, 4): 615–623.

Horvitz, D.G. & Thompson, D.J. 1952. A generalization of sampling without replacement from a finite universe. Journal of the American Statistical Association 47: 663–685.

Isomäki, A. 1986. Linjakäytävien vaikutus reunapuiden kehitykseen. [In Finnish]. Summary: Effect of line corridors on the development of edge trees. Folia Forestalia 678. 30 p.

Jackson, J.E. 1991. A user's guide to principal components. John Wiley & Sons, New York. 569 p.

Jolliffe, I.T. 1986. Pricipal component analysis. Springer-Verlag, New York. 269 p.

Jonsson, L. 1992. Registrering av årsringsutveckling med bildanalys. [In Swedish]. Sveriges lantbruksuniversitet, Institutionen för virkeslära, Rapport 228. 28 + 7 p.

Kärkkäinen, M. 1974. Keskusmuotoluvun perusteita tukkien ja kuitupuun mittauksessa. [In Finnish]. Summary: Foundations of middle form factor in the measurement of logs and pulpwood. Silva Fennica 8(1): 47–88.
— 1975a. Koivu- ja haapatukkien poikkipinta-alan mittaaminen. [In Finnish]. Summary: Measurement of the cross-sectional area of birch and aspen logs. Silva Fennica 9(3): 212–232.
— 1975b. Pohjoissuomalaisten mäntytukkien soikeus. [In Finnish]. Summary: Ovalness of pine logs in northern Finland. Silva Fennica 9(4): 251–258.
— 1976. Lisähavaintoja haapatukkien poikkipinta-alan mittaamisesta. [In Finnish]. Summary: Auxiliary observations on the measurement of the cross-sectional area of aspen logs. Silva Fennica 10(4): 257–265.
— 1984. Puutavaran mittauksen perusteet. [In Finnish]. Helsingin yliopisto, Helsinki. 252 p.
— 2003. Puutieteen perusteet. [In Finnish]. Metsälehti, Helsinki. 451 p.
Kellogg, R.M. & Barber, F.J. 1981. Stem eccentricity in coastal western hemlock. Canadian Journal of Forest Research 11: 714–718.
Kelly, P.J. & Weiss, M.L. 1979. Geometry and convexity: a study in mathematical methods. John Wiley & Sons, New York. 261 p.
Kendall, M. & Stuart, A. 1979. The advanced theory of statistics. Vol. 2. Inference and relationship. 4th edition. Charles Griffin & Company Limited, London. 748 p.
Kennel, R. 1959. Die Genauigkeit von Kluppung und Umfangsmessung nach einem Vergleichsversuch. Forstwissenschaftliches Centralblatt 78(7/8): 243–251.
— 1964. Erfarungen mit der Umfangsmessung. Forstwissenschaftliches Centralblatt 83(9/10): 314–320.
Kinashi, K. 1954. Forest inventory by sampling methods. Bulletin of the Kyushi University Forests 23. 153 p.
Kuusela, K. & Salminen, S. 1980. Ahvenanmaan maakunnan ja maan yhdeksän eteläisimmän piirimetsälautakunnan alueen metsävarat 1977–1979. [In Finnish]. Summary: Forest resources in the province of Ahvenanmaa and the nine southernmost Forestry Board districts in Finland 1977–1979. Folia Forestalia 446. 90 p.
— , Mattila, E. & Salminen, S. 1986. Metsävarat piirimetsälautakunnittain Pohjois-Suomessa 1982–1984. [In Finnish]. Summary: Forest resources in North Finland by Forestry Board districts, 1982 to 1984. Folia Forestalia 655. 86 p.
Laasasenaho, J. 1982. Taper curve and volume functions for pine, spruce and birch. Communicationes Instituti Forestalis Fenniae 108. 74 p.
Lahtinen, A. 1988. On the construction of monotony preserving taper curves. Acta Forestalia Fennica 203. 34 p.
— 1993. On the construction of shape preserving taper curves. Silva Fennica 27(1): 29–45.
— & Laasasenaho, J. 1979. On the construction of taper curves by using spline functions. Communicationes Instituti Forestalis Fenniae 95(8). 63 p.
Lappi, J. 1986. Mixed linear models for analyzing and predicting stem form variation of Scots pine. Communicationes Instituti Forestalis Fenniae 134. 69 p.
Lindgren, B.W. 1976. Statistical theory. 3rd edition. Mcmillan Publishing Co., Inc., New York. 614 p.
Loetsch, F., Zöhrer, F. & Haller, K.E. 1973. Forest inventory. Vol. 2. BLV Verlagsgesellschaft, München. 496 p.
Mäkinen, H. 1998. Effect of thinning and natural variation in bole roundness in Scots pine (Pinus sylvestris L.). Forest Ecology and Management 107: 231–239.
— , Nöjd, P. & Isomäki, A. 2002. Radial, height and volume increment variation in Picea abies (L.) Karst. stands with varying thinning densities. Scandinavian Journal of Forest Research 17: 304–316.
Matérn, B. 1956. On the geometry of the cross-section of a stem. Meddelanden från Statens Skogsforskningsinstitut 46(11): 1–28.

— 1972. The precision of basal area estimates. Forest Science 18(2): 123–125.
— 1984. Four lectures on forest biometry. Sveriges lantbruksuniversitet, Institutionen för biometri och skogsindelning, Avdelningen för skoglig biometri, Rapport 23. 139 p.
— 1990. On the shape of the cross-section of a tree stem. An empirical study of the geometry of mensurational methods. Swedish University of Agricultural Sciences, Department of Biometry and Forest Management, Section of Forest Biometry, Report 28. 47 p.
Müller, G. 1957. Untersuchungen über die Querschnittsformen der Baumschäfte. 1. Mitteilung. Über die Einfluss exentrischer Querschnittsformen der Waldbäume auf die Genauigkeit der Querflächenbestimmung mittels Umfangmessung. Forstwissenschaftliches Centralblatt 76(1/2): 34–54.
— 1958a. Untersuchungen über die Querschnittsformen der Baumschäfte. 2. Mitteilung. Forstwissenschaftliches Centralblatt 77(1/2): 41–59.
— 1958b. Untersuchungen über die Querschnittsformen der Baumschäfte. 3. Mitteilung. Forstwissenschaftliches Centralblatt 77(11/12): 374–381.
Oderwald, R.G. 1981. Comparison of point and plot sampling basal area estimates. Forest Science 27(1): 42–48.
Ojansuu, R. 1993. Prediction of Scots pine increment using a multivariate variance component model. Acta Forestalia Fennica 239. 72 p.
Okstad, T. 1983. Måling av diameter på skurtømmer. [In Norwegian]. Summary: Diameter measurement of sawlogs. Norwegian Forest Research Institute, Research Paper 6/83.
Overton, W.S. & Stehman, S.V. 1995. The Horvitz-Thompson theorem as a unifying perspective for probability sampling: with examples from natural resource sampling. The American Statistician 49(3): 261–268.
Päivinen, R., Nousiainen, M. & Korhonen, K.T. 1992. Puutunnusten mittaamisen luotettavuus. [In Finnish]. Summary: Accuracy of certain tree measurements. Folia Forestalia 787. 18 p.
Parzen, E. 1962. Stochastic processes. Holden-Day, San Francisco. 324 p.
Pawsey, C.K. 1966. Lean and eccentricity in Pinus radiata (D. Don) in the southeast of South Australia. Australian Forest Research 2(3): 22–35.
Pedrotti, F.L. & Pedrotti, L.S. 1987. Introduction to optics. Prentice-Hall, Englewood Cliffs, New Jersey. 551 p.
Penttinen, A. 1988. A random field approach to Bitterlich sampling. Annales Academiae Scientiarum Fennicae, Series A. I. Mathematica 13: 259–268.
Perkal, J. 1948. Determination of the volume of trees. Comptes rendus de la Société des Sciences et des Lettres de Wroclaw, Vol. 3, Communication 7. 14 p.
Pulkkinen, M. 1996. Männyn rungon epäpyöreyden vaikutus poikkileikkausala- ja tilavuusestimaatteihin. [In Finnish]. Abstract: Effect of cross-sectional non-circularity on basal area and stem volume estimates in Scots pine. Thesis for M.Sc. (For.) degree, Faculty of Forestry, University of Joensuu. 96+10 p.
Ramsay, J.O. & Silverman, B.W. 1997. Functional data analysis. Springer-Verlag, New York. 310 p.
Rao, M.M. 1979. Stochastic processes and integration. Sijthoff & Noordhoff International Publishers, Alphen aan den Rijn. 456 p.
Renvall, A. 1923. Beobachtungen über die Exzentrizität des lappländischen Kiefernstammes. Acta Forestalia Fennica 26(3): 1–14.
Robert, C.P. & Casella, G. 2000. Monte Carlo statistical methods. Corrected second printing. Springer-Verlag, New York. 507 p.
Robertson, A. 1986. Estimating mean wind flow in hilly terrain from tamarack (Larix laricina (Du Roi) K. Koch) deformation. International Journal of Biometeorology 30(4): 333–349.
— 1990. Directionality of compression wood in balsam fir wave forest trees. Canadian Journal of Forest Research 20: 1143–1148.
— 1991. Centroid of wood density, bole eccentricity, and tree-ring width in relation to vector winds in wave forests. Canadian Journal of Forest Research 21: 73–82.

Rockafellar, R.T. 1970. Convex analysis. 2nd edition. Princeton University Press, Princeton. 451 p.
Ryan, P.J. 1986. Euclidean and non-Euclidean geometry. An analytical approach. CUP, New York. 215 p.
Saint-André, L. 1998. Modélisation tridimensionnelle des profils de largeur de cerne dans un billon d'Épicea commun (Picea abies Karst.) compte tenu de la mesure de son enveloppe externe et des caractéristiques dendrométriques usuelles de l'arbre d'origine. Thèse présentée pour l'obtention du grade de Docteur de l'ENGREF, Option Sciences Forestières et du Bois. INRA, Centre de Recherches de Nancy, Équipe de Recherches sur la Qualité des Bois 1998 / 3, Décembre. 215 p.
— & Leban, J.-M. 2000. An elliptical model for tree ring shape in transverse section. Methodology and case study on Norway spruce. Holz als Roh- und Werkstoff 58: 368–374.
Santaló, L.A. 1976. Integral geometry and geometric probability. Encyclopedia of mathematics and its applications, Vol. 1. Addison-Wesley, Reading, Massachusetts. 404 p.
Särndal, C.E., Swensson, B. & Wretman, J. 1992. Model assisted survey sampling. Springer-Verlag, New York. 694 p.
Schmid, P. 1969. Stichproben am Waldrand. Mitteilungen der schweizerischen Anstalt für das forstliche Versuchswesen 45(3): 235–303.
Schreuder, H.T., Gregoire, T.G. & Wood, G.B. 1993. Sampling methods for multiresource forest inventory. John Wiley & Sons, New York. 446 p.
Skatter, S. & Høibø, O.A. 1998. Cross-sectional shape models of Scots pine (Pinus silvestris) and Norway spruce (Picea abies). Holz als Roh- und Werkstoff 56: 187-191.
Solbraa, T. 1939. Bast og andre faktorer som influerer på tømmermålingsresultatet. [In Norwegian]. Tidsskrift for Skogbruk 47: 74–79,120–134.
Sterba, H. 1980. Stem curves – a review of the literature. Forest Products Abstracts 4(4): 69–73.
Stoyan, D. & Stoyan, H. 1994. Fractals, random shapes and point fields: methods of geometrical statistics. John Wiley & Sons, Chichester. 389 p.
— , Kendall, W.S. & Mecke, J. 1986. Stochastic geometry and its applications. John Wiley & Sons, Chichester. 345 p.
Sukwong, S., Frayer, W.G. & Mogren, E.W. 1971. Generalized comparisons of the precision of fixed-radius and variable-radius plots for basal-area estimates. Forest Science 17: 263–271.
Thies, W.G. & Harvey, R.D. Jr. 1979. A photographic method for measuring tree defect. Canadian Journal of Forest Research 9(4): 541–543.
Tiercy, G. 1920. Sur les courbes orbiformes: leurs utilisation en mécanique. Tôhoku Mathematical Journal 18: 90–115.
Tiihonen, P. 1961. Tutkimuksia männnyn kapenemistaulukoiden laatimiseksi. [In Finnish]. Referat: Untersuchungen über die Aufstellung der Ausbauchungstafeln für Kiefer. Communicationes Instituti Forestalis Fenniae 53(1): 1–120.
Tirén, L. 1929. Über Grundflächenberechnung und ihre Genauigkeit. Resume: Om grundbyteberäkning och dess noggranhet. Meddelanden från Statens Skogsförsöksanstalt 25: 229–304.
Tomppo, E., Varjo, J., Korhonen, K., Ahola, A., Ihalainen, A., Heikkinen, J., Hirvelä, H., Mikkelä, H., Mikkola, E., Salminen, S. & Tuomainen, T. 1997. Country report for Finland. In: Study on European forestry information and communication systems. European Commission, Reports on forestry inventory and survey systems 1: 145–226.
Valtakunnallisen puututkimuksen (VAPU) ja kasvunvaihtelututkimuksen maastotyöohjeet 1991. [In Finnish]. Metsäntutkimuslaitos, Joensuun tutkimusasema, Joensuu. 9 p.
Vries, P.G. de 1986. Sampling theory for forest inventory. A teach-yourself course. Springer-Verlag, Heidelberg. 399 p.
Webster, R. 1994. Convexity. Oxford University Press, Oxford. 444 p.
Williamson, R.L. 1975. Out-of-roundness in Douglas-fir stems. Forest Science 21(4): 365–370.

Total of 119 references

Appendix A. Support Function of Closed Convex Set or Curve in Plane

The following précis is mostly adapted from Santaló (1976); for more details, see for example Rockafellar (1970), Stoyan et al. (1986), Stoyan and Stoyan (1994), and Webster (1994).

Any straight line in the plane is uniquely determined by its distance $p \in [0, \infty)$ from the origin O and by the angle $\theta \in [0, 2\pi)$ of its normal with the positive x-axis. As is easily seen by using suitably chosen right-angled triangles (Fig. A1), such a line intersects x-axis in the point $(p/\cos\theta, 0)$ and y-axis in the point $(0, p/\sin\theta)$, and thus has the slope $k = -\cos\theta/\sin\theta$ and the following equation termed the Hesse normal form (Stoyan and Stoyan 1994):

$$y = -\frac{\cos\theta}{\sin\theta}x + \frac{p}{\sin\theta} \;\Leftrightarrow\; x\cos\theta + y\sin\theta - p = 0 \,. \tag{A1}$$

If we let the distance p vary with the angle $\theta \in [0, 2\pi)$, we obtain a family of lines

$$F(x, y, \theta) = x\cos\theta + y\sin\theta - p(\theta) = 0 \,, \tag{A2}$$

all the members of which are tangents of a common closed curve, the *envelope* of this family of lines (Fig. A2). In general, the envelope of a family of curves is defined as the curve every point of which is a point of contact with a member curve of the family (Santaló 1976). The points of the envelope are the projections onto the xy-plane of those points on the surface $F(x, y, \theta)=0$ for which the tangent plane is parallel to the θ-axis; thus the parametric representation for the co-ordinates of the envelope is obtained by solving x and y (i.e., by eliminating θ) from the pair of equations

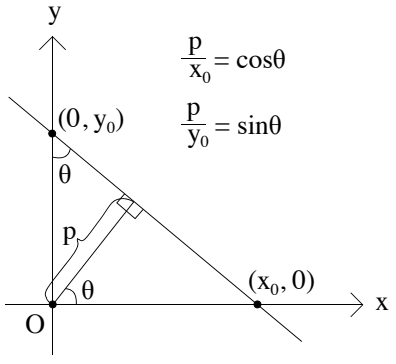

Fig. A1. Parameterisation of a line by its distance p from the origin O and by the angle θ of its normal with the x-axis, and determination of the points $(x_0, 0)$ and $(0, y_0)$ where the line intersects the co-ordinate axes.

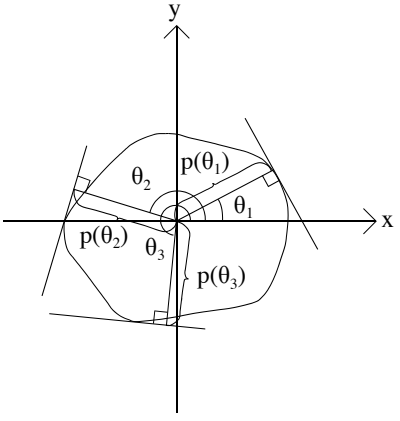

Fig. A2. The boundary of a convex set as the envelope of a family of lines parameterised by the angles $\theta \in [0, 2\pi)$ of their normals with respect to the x-axis and by their distances $p(\theta)$ from the origin. The distance function $p:[0, 2\pi) \to (0, \infty)$ is termed the support function of the set and the tangent lines are referred to as the support lines of the set.

$$\begin{cases} F(x, y, \theta) = 0 \\ \dfrac{\partial F(x, y, \theta)}{\partial \theta} = 0 \end{cases} \Leftrightarrow \begin{cases} x\cos\theta + y\sin\theta - p(\theta) = 0 \\ -x\sin\theta + y\cos\theta - p'(\theta) = 0 \end{cases}, \tag{A3}$$

which results in

$$\begin{cases} x = x(\theta) = p(\theta)\cos\theta - p'(\theta)\sin\theta \\ y = y(\theta) = p(\theta)\sin\theta + p'(\theta)\cos\theta \end{cases} \tag{A4}$$

(Santaló 1976).

If the envelope is a closed convex curve and hence forms the boundary of a convex set containing the origin O as its interior point, the distance function $p:[0, 2\pi)\rightarrow(0, \infty)$ is termed the *support function* of the set with reference to O, and the tangent lines determined by θ and $p(\theta)$ (Eq. A2) are referred to as the *support lines* of the set (Fig. A2). Note that although we have here restricted our consideration to the interval $[0, 2\pi)$, p is actually a periodic function with the domain $\cup_{n\in\mathbb{Z}}[n2\pi, (n+1)2\pi)=\mathbb{R}$.

A convex set is uniquely determined by its support function, which implies that different convex sets have different support functions (see Rockafellar 1970, or Webster 1994, for the proofs). A periodic, twice differentiable and nonnegative function p is the support function of a convex set if and only if

$$p(\theta) + p''(\theta) > 0 \tag{A5}$$

for all θ (Santaló 1976).

From the boundary co-ordinates derived above (Eq. A4), we can calculate the perimeter and the area of the convex set by employing the very standard results available for parametric representations of curves (see e.g. Coxeter 1969, and Edwards and Penney 1994). For this, we need the first derivatives of the co-ordinates with respect to the parameter θ:

$$\begin{cases} x'(\theta) = -\sin\theta\left[p(\theta) + p''(\theta)\right] \\ y'(\theta) = \cos\theta\left[p(\theta) + p''(\theta)\right]. \end{cases} \tag{A6}$$

Now for the perimeter C we obtain

$$\begin{aligned} C &= \int_0^{2\pi} \sqrt{[x'(\theta)]^2 + [y'(\theta)]^2}\, d\theta \\ &= \int_0^{2\pi} \sqrt{\left[p(\theta) + p''(\theta)\right]^2 (\sin^2\theta + \cos^2\theta)}\, d\theta \\ &= \int_0^{2\pi} \left|p(\theta) + p''(\theta)\right| d\theta \\ &= \int_0^{2\pi} \left[p(\theta) + p''(\theta)\right] d\theta \\ &= \int_0^{2\pi} p(\theta)\, d\theta + \Big/_0^{2\pi} p'(\theta) \\ &= \int_0^{2\pi} p(\theta)\, d\theta + p'(2\pi) - p'(0) \\ &= \int_0^{2\pi} p(\theta)\, d\theta\,, \end{aligned} \tag{A7}$$

where the absolute value in the third row becomes redundant because of the condition of Eq. A5, and the definite integral of $p'(\theta)$ in the fifth row vanishes because $p'(0)=p'(2\pi)$ by the periodicity of p. The area A_C, in turn, becomes

$$\begin{aligned} A_C &= \frac{1}{2}\int_0^{2\pi} \left[x(\theta)y'(\theta) - y(\theta)x'(\theta)\right] d\theta \\ &= \frac{1}{2}\int_0^{2\pi} \Big\{ \left[p(\theta)\cos\theta - p'(\theta)\sin\theta\right]\left[p(\theta)\cos\theta + p''(\theta)\cos\theta\right] \\ &\quad + \left[p(\theta)\sin\theta + p'(\theta)\cos\theta\right]\left[p(\theta)\sin\theta + p''(\theta)\sin\theta\right] \Big\} d\theta \\ &= \frac{1}{2}\int_0^{2\pi} \left[p(\theta)^2(\sin^2\theta + \cos^2\theta) + p(\theta)p''(\theta)(\sin^2\theta + \cos^2\theta)\right] d\theta \\ &= \frac{1}{2}\int_0^{2\pi} \left[p(\theta)^2 + p(\theta)p''(\theta)\right] d\theta\,, \end{aligned} \tag{A8}$$

which can be further elaborated by integration by parts and by recalling that $p(0)=p(2\pi)$ and $p'(0)=p'(2\pi)$:

$$
\begin{aligned}
A_C &= \frac{1}{2}\int_0^{2\pi}\left[p(\theta)^2 + p(\theta)p''(\theta)\right]d\theta \\
&= \frac{1}{2}\int_0^{2\pi} p(\theta)^2 d\theta + \frac{1}{2}\left[\Big/_0^{2\pi} p(\theta)p'(\theta) - \int_0^{2\pi} p'(\theta)^2 d\theta\right] \\
&= \frac{1}{2}\int_0^{2\pi}\left[p(\theta)^2 - p'(\theta)^2\right]d\theta + \frac{1}{2}\left[p(2\pi)p'(2\pi) - p(0)p'(0)\right] \\
&= \frac{1}{2}\int_0^{2\pi}\left[p(\theta)^2 - p'(\theta)^2\right]d\theta \,.
\end{aligned}
\tag{A9}
$$

Appendix B. Horvitz-Thompson Theorem

This précis is collated from Overton and Stehman (1995), Cassel et al. (1977), Särndal et al. (1992), and Schreuder et al. (1993), the original reference being the paper of Horvitz and Thompson (1952).

Let **I** denote a finite population of distinct and identifiable units — the trees within an area in the Bitterlich sampling case — and let **S** denote the set of all possible samples taken from **I** under the chosen sampling design. Further, let the sampling design be determined by a probability function $P:\mathbf{S}\rightarrow[0, 1]$, assigning to each sample $\mathbf{s}\in\mathbf{S}$ the probability $P(\mathbf{s})$ of selecting that sample and satisfying $\Sigma_{\mathbf{s}\in\mathbf{S}} P(\mathbf{s}) = 1$. The sampling is a said to be probability sampling, if $P(\mathbf{s})$ is known for all $\mathbf{s}\in\mathbf{S}$ and if every unit $i\in\mathbf{I}$ has a non-zero probability of being included into a sample.

The first order inclusion probability $\pi_i = \Pr\{i\in\mathbf{s}\} = \Sigma_{\mathbf{s}\in\mathbf{S}:\, i\in\mathbf{s}} P(\mathbf{s})$ for the unit $i\in\mathbf{I}$ is the probability that the unit i will be included in a sample taken from the population **I** by using the sampling design P. The second order inclusion probability $\pi_{ij} = \Pr\{i\in\mathbf{s}, j\in\mathbf{s}\} = \Sigma_{\mathbf{s}\in\mathbf{S}:\, i,\, j\in\mathbf{s}} P(\mathbf{s})$ for sample units i and j, in turn, is the probability that units i and j are both included in a sample. The inclusion probabilities are determined by the sampling design P and can thus be specified without reference to the variable that we wish to estimate.

The Horvitz-Thompson theorem deals with estimating a population total $Y = \Sigma_{i\in\mathbf{I}} Y_i$ from the measurements taken from the population units included in a probability sample **s**. Given that sampling is carried out without replacement, the theorem may be stated as follows: The Horvitz-Thompson estimator of Y

$$\hat{Y}_{HT}(\mathbf{s}) = \sum_{i\in\mathbf{s}} \frac{Y_i}{\pi_i} \tag{B1}$$

is unbiased with respect to the sampling design P and has variance

$$\mathrm{Var}[\hat{Y}_{HT}(\mathbf{s})] = \sum_{i\in\mathbf{I}} Y_i^2 \left(\frac{1}{\pi_i} - 1\right) + \sum_{i\in\mathbf{I}} \sum_{\substack{j\in\mathbf{I} \\ j\neq i}} Y_i Y_j \left(\frac{\pi_{ij}}{\pi_i \pi_j} - 1\right) \tag{B2}$$

In order to corroborate the theorem, we need to introduce a random variable $\delta_i(\mathbf{s})$ indicating whether the unit i is included in the sample **s**:

$$\delta_i(\mathbf{s}) = \begin{cases} 1, & i\in\mathbf{s} \\ 0, & i\notin\mathbf{s}\,, \end{cases} \tag{B3}$$

in which randomness — as in $\hat{Y}_{HT}(\mathbf{s})$ — stems from the selection of the sample **s** according to the sampling design P. The expectation of this indicator with respect to the sampling design equals the inclusion probability of the unit i:

$$E[\delta_i(\mathbf{s})] = 1\cdot\Pr\{i\in\mathbf{s}\} + 0\cdot\Pr\{i\notin\mathbf{s}\} = \Pr\{i\in\mathbf{s}\} = \pi_i\,. \tag{B4}$$

Now we see the unbiasedness of $\hat{Y}_{HT}(\mathbf{s})$ in a straightforward manner:

$$
\begin{aligned}
\mathrm{E}[\hat{\mathrm{Y}}_{\mathrm{HT}}(\mathbf{s})] &= \mathrm{E}\left(\sum_{\mathrm{i}\in\mathbf{s}} \frac{\mathrm{Y}_\mathrm{i}}{\pi_\mathrm{i}} \right) \\
&= \mathrm{E}\left[\sum_{\mathrm{i}\in\mathbf{I}} \delta_\mathrm{i}(\mathbf{s}) \frac{\mathrm{Y}_\mathrm{i}}{\pi_\mathrm{i}} \right] \\
&= \sum_{\mathrm{i}\in\mathbf{I}} \mathrm{E}[\delta_\mathrm{i}(\mathbf{s})] \frac{\mathrm{Y}_\mathrm{i}}{\pi_\mathrm{i}} \\
&= \sum_{\mathrm{i}\in\mathbf{I}} \pi_\mathrm{i} \frac{\mathrm{Y}_\mathrm{i}}{\pi_\mathrm{i}} \\
&= \sum_{\mathrm{i}\in\mathbf{I}} \mathrm{Y}_\mathrm{i} \\
&= \mathrm{Y} \, .
\end{aligned}
\tag{B5}
$$

In order to derive the variance of $\hat{\mathrm{Y}}_{\mathrm{HT}}(\mathbf{s})$, we need note that

$$
\mathrm{Var}[\delta_\mathrm{i}(\mathbf{s})] = \mathrm{E}[\delta_\mathrm{i}(\mathbf{s})^2] - \left\{ \mathrm{E}[\delta_\mathrm{i}(\mathbf{s})] \right\}^2 = 1^2 \cdot \Pr\{\mathrm{i}\in\mathbf{s}\} + 0^2 \cdot \Pr\{\mathrm{i}\notin\mathbf{s}\} - \pi_\mathrm{i}^2 = \pi_\mathrm{i} - \pi_\mathrm{i}^2 = \pi_\mathrm{i}(1-\pi_\mathrm{i}) \, ,
\tag{B6}
$$

and that

$$
\begin{aligned}
\mathrm{Cov}[\delta_\mathrm{i}(\mathbf{s}), \delta_\mathrm{j}(\mathbf{s})] &= \mathrm{E}[\delta_\mathrm{i}(\mathbf{s})\delta_\mathrm{j}(\mathbf{s})] - \mathrm{E}[\delta_\mathrm{i}(\mathbf{s})]\mathrm{E}[\delta_\mathrm{j}(\mathbf{s})] \\
&= 1\cdot 1\cdot \Pr\{\mathrm{i}\in\mathbf{s},\, \mathrm{j}\in\mathbf{s}\} + 1\cdot 0\cdot \Pr\{\mathrm{i}\in\mathbf{s},\, \mathrm{j}\notin\mathbf{s}\} + 0\cdot 1\cdot \Pr\{\mathrm{i}\notin\mathbf{s},\, \mathrm{j}\in\mathbf{s}\} \\
&\quad + 0\cdot 0\cdot \Pr\{\mathrm{i}\notin\mathbf{s},\, \mathrm{j}\notin\mathbf{s}\} - \pi_\mathrm{i}\pi_\mathrm{j} \\
&= \Pr\{\mathrm{i}\in\mathbf{s},\, \mathrm{j}\in\mathbf{s}\} - \pi_\mathrm{i}\pi_\mathrm{j} \\
&= \pi_{\mathrm{ij}} - \pi_\mathrm{i}\pi_\mathrm{j} \, .
\end{aligned}
\tag{B7}
$$

Now

$$
\begin{aligned}
\mathrm{Var}[\hat{\mathrm{Y}}_{\mathrm{HT}}(\mathbf{s})] &= \mathrm{Var}\left(\sum_{\mathrm{i}\in\mathbf{s}} \frac{\mathrm{Y}_\mathrm{i}}{\pi_\mathrm{i}} \right) \\
&= \mathrm{Var}\left[\sum_{\mathrm{i}\in\mathbf{I}} \delta_\mathrm{i}(\mathbf{s}) \frac{\mathrm{Y}_\mathrm{i}}{\pi_\mathrm{i}} \right] \\
&= \sum_{\mathrm{i}\in\mathbf{I}} \mathrm{Var}[\delta_\mathrm{i}(\mathbf{s})] \frac{\mathrm{Y}_\mathrm{i}^2}{\pi_\mathrm{i}^2} + \sum_{\mathrm{i}\in\mathbf{I}} \sum_{\substack{\mathrm{j}\in\mathbf{I} \\ \mathrm{j}\neq\mathrm{i}}} \mathrm{Cov}[\delta_\mathrm{i}(\mathbf{s}), \delta_\mathrm{j}(\mathbf{s})] \frac{\mathrm{Y}_\mathrm{i}}{\pi_\mathrm{i}} \frac{\mathrm{Y}_\mathrm{j}}{\pi_\mathrm{j}} \\
&= \sum_{\mathrm{i}\in\mathbf{I}} \pi_\mathrm{i}(1-\pi_\mathrm{i}) \frac{\mathrm{Y}_\mathrm{i}^2}{\pi_\mathrm{i}^2} + \sum_{\mathrm{i}\in\mathbf{I}} \sum_{\substack{\mathrm{j}\in\mathbf{I} \\ \mathrm{j}\neq\mathrm{i}}} (\pi_{\mathrm{ij}} - \pi_\mathrm{i}\pi_\mathrm{j}) \frac{\mathrm{Y}_\mathrm{i}}{\pi_\mathrm{i}} \frac{\mathrm{Y}_\mathrm{j}}{\pi_\mathrm{j}} \\
&= \sum_{\mathrm{i}\in\mathbf{I}} \mathrm{Y}_\mathrm{i}^2 \left(\frac{1}{\pi_\mathrm{i}} - 1 \right) + \sum_{\mathrm{i}\in\mathbf{I}} \sum_{\substack{\mathrm{j}\in\mathbf{I} \\ \mathrm{j}\neq\mathrm{i}}} \mathrm{Y}_\mathrm{i}\mathrm{Y}_\mathrm{j} \left(\frac{\pi_{\mathrm{ij}}}{\pi_\mathrm{i}\pi_\mathrm{j}} - 1 \right) .
\end{aligned}
\tag{B8}
$$

One unbiased estimator of this variance for sample **s** is given by

$$\hat{\mathrm{Var}}[\hat{Y}_{HT}(\mathbf{s})] = \sum_{i\in\mathbf{s}} \frac{Y_i^2}{\pi_i}\left(\frac{1}{\pi_i}-1\right) + \sum_{i\in\mathbf{s}}\sum_{\substack{j\in\mathbf{s}\\ j\neq i}} \frac{Y_i Y_j}{\pi_{ij}}\left(\frac{\pi_{ij}}{\pi_i\pi_j}-1\right), \quad \text{(B9)}$$

which requires that all the second order inclusion probabilities be non-zero. In fact, $\mathrm{Var}(\hat{Y}_{HT})$ can be unbiasedly estimated if and only if $\pi_{ij}>0$ for all $i\neq j$.

Appendix C. Expressing Boundary Co-ordinates, Radii and Total Area of Inclusion Region of Tree in Bitterlich Sampling in Terms of Support Function of Breast Height Cross-Section

We consider selecting a tree by Bitterlich sampling with $\alpha \in (0, \pi)$ as the viewing angle. We assume the ground level to be horizontal, the observation level to be at breast height and parallel to the ground level, and the viewing point to be uniformly randomly located in the region.

We start by finding the mathematical expressions for the boundary co-ordinates and area of the inclusion region of a tree, that is, the region from which the tree is seen in an angle greater or equal to α. We set the planar co-ordinate system parallel to the ground level so that the origin is in the centre of gravity of the breast height cross-section of the tree (or in the pith of the cross-section), and denote by $p(\cdot)$ the support function of the convex closure of the breast height cross-section. By the definition of the support function (see Chapter 2 and Appendix A), the family of straight lines

$$x\cos\theta + y\sin\theta - p(\theta) = 0 \,, \tag{C1}$$

$\theta \in [0, 2\pi)$, comprises all the tangents of the convex closure of the cross-section; these lines have distance $p(\theta)$ from the origin and direction perpendicular to the angle θ (Fig. C1). From this set of tangents, we want to single out those pairs that intersect each other at angle α; obviously, the pairs of lines with directions perpendicular to θ and $\theta+\pi-\alpha$ meet this condition (Fig. C1; Matérn 1956, p. 23). The equations of these lines are expressed as

$$\begin{cases} x\cos\theta + y\sin\theta - p(\theta) = 0 \\ x\cos(\theta+\pi-\alpha) + y\sin(\theta+\pi-\alpha) - p(\theta+\pi-\alpha) = 0 \,, \end{cases} \tag{C2}$$

which is equivalent to

$$\begin{cases} x\cos\theta + y\sin\theta - p(\theta) = 0 \\ x\cos(\theta-\alpha) + y\sin(\theta-\alpha) + p(\theta+\pi-\alpha) = 0 \,, \end{cases} \tag{C3}$$

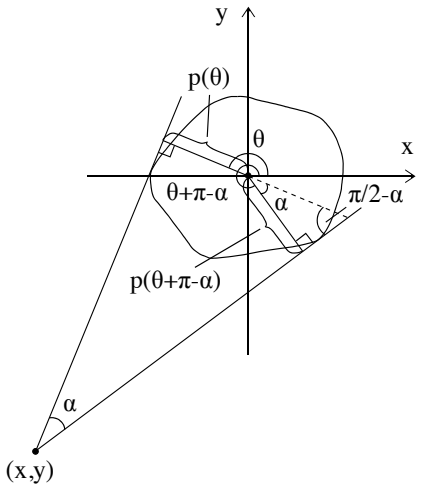

Fig. C1. Two tangents of the convex closure of a cross-section intersecting at angle α: the intersection point is (x, y); the direction angles of the perpendiculars of the tangents are θ and $\theta+\pi-\alpha$; and the distances of the tangents from the origin are $p(\theta)$ and $p(\theta+\pi-\alpha)$, where $p(\cdot)$ is the support function of the convex closure.

since $\cos(\theta+\pi)=-\cos\theta$ and $\sin(\theta+\pi)=-\sin\theta$. By solving this pair of equations, a parametric presentation for the curve of the intersection points is easily obtained: From the first equation we solve x

$$x = \frac{1}{\cos\theta}\left[p(\theta) - y\sin\theta\right], \tag{C4}$$

and substitute this in the second equation

$$\frac{1}{\cos\theta}\left[p(\theta) - y\sin\theta\right]\cos(\theta-\alpha) + y\sin(\theta-\alpha) + p(\theta+\pi-\alpha) = 0, \tag{C5}$$

from which we obtain y

$$\begin{aligned} y &= \frac{p(\theta)\cos(\theta-\alpha) + p(\theta+\pi-\alpha)\cos\theta}{\sin\theta\cos(\theta-\alpha) - \sin(\theta-\alpha)\cos\theta} \\ &= \frac{1}{\sin\alpha}\left[p(\theta)\cos(\theta-\alpha) + p(\theta+\pi-\alpha)\cos\theta\right], \end{aligned} \tag{C6}$$

since $\cos(-\theta)=\cos\theta$ and $\sin(-\theta)=-\sin\theta$ for all θ and

$$\begin{aligned} \sin\theta\cos(\theta-\alpha) - \sin(\theta-\alpha)\cos\theta &= \sin\theta\cos(\alpha-\theta) + \sin(\alpha-\theta)\cos\theta \\ &= \sin[\theta+(\alpha-\theta)] \\ &= \sin(\alpha). \end{aligned} \tag{C7}$$

With this y, we then we turn back to the "solved" x:

$$\begin{aligned} x &= \frac{1}{\cos\theta}\left[p(\theta) - y\sin\theta\right] \\ &= \frac{p(\theta)}{\cos\theta} - \frac{\sin\theta}{\sin\alpha\cos\theta}\left[p(\theta)\cos(\theta-\alpha) + p(\theta+\pi-\alpha)\cos\theta\right] \\ &= -\frac{1}{\sin\alpha}\left[p(\theta)\sin(\theta-\alpha) + p(\theta+\pi-\alpha)\sin\theta\right], \end{aligned} \tag{C8}$$

where the last form is obtained by expanding $\sin\alpha$ into $\sin\theta\cos(\theta-\alpha)-\sin(\theta-\alpha)\cos\theta$ and then back. We have hence ended up in the following intersection points:

$$\begin{cases} x = x(\theta;\alpha) = -\frac{1}{\sin\alpha}\left[p(\theta)\sin(\theta-\alpha) + p(\theta+\pi-\alpha)\sin\theta\right] \\ y = y(\theta;\alpha) = \frac{1}{\sin\alpha}\left[p(\theta)\cos(\theta-\alpha) + p(\theta+\pi-\alpha)\cos\theta\right] \end{cases} \tag{C9}$$

(Matérn 1956, p. 23), which constitute the boundary of the inclusion region $\mathbf{M}(\alpha)$.

From the boundary co-ordinates a parametric representation for the length of the radius of the inclusion region, that is, for the distance from the inclusion region boundary to the

pith of the breast height cross-section of the tree, is straightforward to derive:

$$\begin{aligned} r(\theta;\alpha) &= \sqrt{x(\theta;\alpha)^2 + y(\theta;\alpha)^2} \\ &= \left(\frac{1}{\sin^2\alpha}\right)^{\frac{1}{2}} \Big\{ p(\theta)^2\Big[\sin^2(\theta-\alpha) + \cos^2(\theta-\alpha)\Big] + p(\theta+\pi-\alpha)^2(\sin^2\theta+\cos^2\theta) \\ &\quad + 2p(\theta)p(\theta+\pi-\alpha)\Big[\cos(\theta-\alpha)\cos\theta + \sin(\theta-\alpha)\sin\theta\Big]\Big\}^{\frac{1}{2}} \\ &= \frac{1}{\sin\alpha}\sqrt{p(\theta)^2 + p(\theta+\pi-\alpha)^2 + 2p(\theta)p(\theta+\pi-\alpha)\cos\alpha}\ , \end{aligned} \tag{C10}$$

since $\sin\alpha>0$ for all $\alpha\in(0, \pi)$, $\sin^2\theta+\cos^2\theta=1$ for all θ and $\cos(\theta-\alpha)\cos\theta+\sin(\theta-\alpha)\sin\theta=\cos[\theta-(\theta-\alpha)]=\cos\alpha$. Note that the direction of this radius is not θ but $\theta+\cos^{-1}[p(\theta)/r(\theta;\alpha)]$ (Fig. C2).

In order to calculate the area of the inclusion region, we need to differentiate $x(\theta;\alpha)$ and $y(\theta;\alpha)$ with respect to θ:

$$\begin{cases} x'(\theta;\alpha) = -\dfrac{1}{\sin\alpha}\Big[p'(\theta)\sin(\theta-\alpha) + p(\theta)\cos(\theta-\alpha) + p'(\theta+\pi-\alpha)\sin\theta + p(\theta+\pi-\alpha)\cos\theta\Big] \\ y'(\theta;\alpha) = \dfrac{1}{\sin\alpha}\Big[p'(\theta)\cos(\theta-\alpha) - p(\theta)\sin(\theta-\alpha) + p'(\theta+\pi-\alpha)\cos\theta - p(\theta+\pi-\alpha)\sin\theta\Big], \end{cases} \tag{C11}$$

By these, and by recalling that $\sin^2\theta+\cos^2\theta=1$, we then attain the following expression for the area of $\mathbf{M}(\alpha)$ (Coxeter 1969, Edwards and Penney 1994):

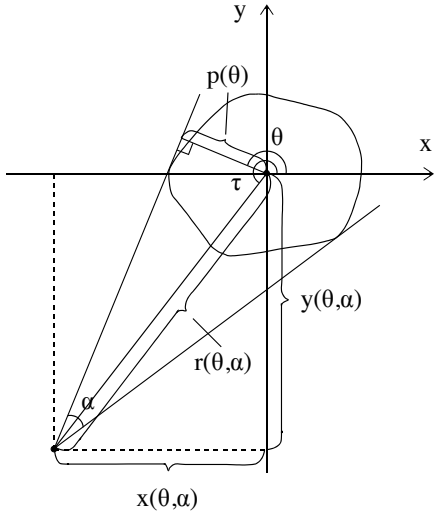

Fig. C2. Determination of the direction τ of the inclusion region radius $r(\theta;\alpha)$: $\cos(\tau-\theta)=p(\theta)/r(\theta;\alpha)$.

$$
\begin{aligned}
|\mathbf{M}(\alpha)| &= \frac{1}{2}\int_0^{2\pi}\left[x(\theta;\alpha)y'(\theta;\alpha) - y(\theta;\alpha)x'(\theta;\alpha)\right]d\theta \\
&= \frac{1}{2\sin^2\alpha}\left\{\int_0^{2\pi} p(\theta)^2 d\theta + \int_0^{2\pi} p(\theta+\pi-\alpha)^2 d\theta + 2\cos\alpha\int_0^{2\pi} p(\theta)p(\theta+\pi-\alpha)d\theta\right. \\
&\quad \left. + \sin\alpha\left[\int_0^{2\pi} p(\theta)p'(\theta+\pi-\alpha)d\theta - \int_0^{2\pi} p'(\theta)p(\theta+\pi-\alpha)d\theta\right]\right\}. \qquad \text{(C12)}
\end{aligned}
$$

This expression can indeed be considerably reduced: By the periodicity of $p(\cdot)$, which implies that the definite integral over the whole period does not depend on the starting point of the integration, we get

$$
\int_0^{2\pi} p(\theta)^2 d\theta + \int_0^{2\pi} p(\theta+\pi-\alpha)^2 d\theta = 2\int_0^{2\pi} p(\theta)^2 d\theta\,. \qquad \text{(C13)}
$$

Further, by adding and subtracting the term $\int p(\theta)p'(\theta+\pi-\alpha)d\theta$, by applying integration by parts "backwards", and by again making use of the periodicity of $p(\cdot)$, by which $p(\theta+2n\pi)=p(\theta)$ for all $n\in\mathbb{N}$, we get

$$
\begin{aligned}
&\int_0^{2\pi} p(\theta)p'(\theta+\pi-\alpha)d\theta - \int_0^{2\pi} p'(\theta)p(\theta+\pi-\alpha)d\theta \\
&= 2\int_0^{2\pi} p(\theta)p'(\theta+\pi-\alpha)d\theta - \left[\int_0^{2\pi} p(\theta)p'(\theta+\pi-\alpha)d\theta + \int_0^{2\pi} p'(\theta)p(\theta+\pi-\alpha)d\theta\right] \\
&= 2\int_0^{2\pi} p(\theta)p'(\theta+\pi-\alpha)d\theta - \Big/_0^{2\pi} p(\theta)p(\theta+\pi-\alpha) \qquad \text{(C14)} \\
&= 2\int_0^{2\pi} p(\theta)p'(\theta+\pi-\alpha)d\theta - \left[p(2\pi)p(3\pi-\alpha) - p(0)p(\pi-\alpha)\right] \\
&= 2\int_0^{2\pi} p(\theta)p'(\theta+\pi-\alpha)d\theta\,.
\end{aligned}
$$

The area of the inclusion region hence becomes

$$
|\mathbf{M}(\alpha)| = \frac{1}{\sin^2\alpha}\int_0^{2\pi}\left[p(\theta)^2 + p(\theta)p(\theta+\pi-\alpha)\cos\alpha + p(\theta)p'(\theta+\pi-\alpha)\sin\alpha\right]d\theta \qquad \text{(C15)}
$$

(cf. Matérn 1956, p. 23).

Appendix D. Expressing Probability Distribution of Bitterlich Diameter Direction in Terms of Support Function of Breast Height Cross-Section of Tree

We consider selecting a tree by Bitterlich sampling with α as the viewing angle and measuring its breast height diameter in the plot radius direction, that is, parallel to the line segment from the viewing point to the (assumed) centre of gravity, or pith, of the breast height cross-section of the tree. We assume the ground level to be horizontal, the observation level to be at breast height and parallel to the ground level, and the viewing point to be uniformly randomly located in the region of interest. We set the planar co-ordinate system on the observation level in the way that the origin lies in the centre of gravity, or pith, of the breast height cross-section of the tree and denote by $p(\cdot)$ the support function, defined with respect to the origin, of the convex closure of the cross-section.

As described in Section 4.2.1, the probability that the direction ξ of the diameter measured parallel to plot radius in Bitterlich sampling is between arbitrarily chosen directions t_1 and t_2, $t_1<t_2$, equals the probability that the plot radius direction τ lies either between t_1 and t_2 or between $t_1+\pi$ and $t_2+\pi$ (Fig. 19). These are probabilities that the viewing point is located in the sectors of the inclusion region $\mathbf{M}(\alpha)$ edged by the rays emanating from the tree pith in either directions t_1 or t_2 or directions $t_1+\pi$ or $t_2+\pi$ (Fig. 19). The probabilities can be expressed as simple ratios of the sector areas to the inclusion region area $|\mathbf{M}(\alpha)|$:

$$\begin{aligned}\Pr\{t_1 \le \xi \le t_2; \alpha\} &= \Pr\{t_1 \le \tau \le t_2; \alpha\} + \Pr\{t_1+\pi \le \tau \le t_2+\pi; \alpha\} \\ &= \frac{|\mathbf{M}(\alpha)_{t_1}^{t_2}|}{|\mathbf{M}(\alpha)|} + \frac{|\mathbf{M}(\alpha)_{t_1+\pi}^{t_2+\pi}|}{|\mathbf{M}(\alpha)|} .\end{aligned} \tag{D1}$$

As shown in Appendix C (Eqs. C12 and C15), $|\mathbf{M}(\alpha)|$ is obtained by integration from the parametric representation of the boundary co-ordinates of $\mathbf{M}(\alpha)$ involving the support function $p(\cdot)$ of the convex closure of the cross-section:

$$\begin{aligned}|\mathbf{M}(\alpha)| &= \frac{1}{2}\int_0^{2\pi}\left[x(\theta;\alpha)y'(\theta;\alpha) - y(\theta;\alpha)x'(\theta;\alpha)\right]d\theta \\ &= \frac{1}{\sin^2\alpha}\int_0^{2\pi} g(\theta;\alpha)d\theta ,\end{aligned} \tag{D2}$$

where

$$g(\theta;\alpha) = p(\theta)^2 + p(\theta)p(\theta+\pi-\alpha)\cos\alpha + p(\theta)p'(\theta+\pi-\alpha)\sin\alpha . \tag{D3}$$

However, the area of the *sector* of $\mathbf{M}(\alpha)$ is *not* attained by simply changing the integration limits $(0, 2\pi)$ above to (t_1, t_2) (or to $(t_1+\pi, t_2+\pi)$) . This is because θ in the parametric representation of the boundary point co-ordinates $(x(\theta; \alpha), y(\theta; \alpha))$ does not indicate the direction of the boundary point (i.e., the direction of the radius of the inclusion region). Instead, θ is the angle that the perpendicular of the leftward tangent of the cross-section drawn from the boundary point forms with the positive x-axis (Fig. C2 in Appendix C). Therefore, we need to transform the integration limits (t_1, t_2) into $(\theta(t_1; \alpha), \theta(t_2; \alpha))$, where $\theta(t; \alpha)$ is a function of t and α obtained by solving θ from

$$\begin{aligned}\cos(t-\theta) &= \frac{p(\theta)}{r(\theta)} \\ &= \frac{p(\theta)}{\frac{1}{\sin\alpha}\sqrt{p(\theta)^2 + p(\theta+\pi-\alpha)^2 + 2p(\theta)p(\theta+\pi-\alpha)\cos\alpha}}\,,\end{aligned} \tag{D4}$$

where $r(\theta)$ is the distance between the boundary point and the tree pith (i.e., the radius of the inclusion region in direction t; Fig. C2 in Appendix C). The area of the sector then becomes

$$\begin{aligned}|\mathbf{M}(\alpha)_{t_1}^{t_2}| &= \frac{1}{2}\int_{\theta(t_1;\alpha)}^{\theta(t_2;\alpha)} \left[x(\theta;\alpha)y'(\theta;\alpha) - y(\theta;\alpha)x'(\theta;\alpha)\right]d\theta \\ &= \frac{1}{\sin^2\alpha}\int_{\theta(t_1;\alpha)}^{\theta(t_2;\alpha)} g(\theta;\alpha)\,d\theta\,.\end{aligned} \tag{D5}$$

With geometrical consideration (Fig. D1), we see that for the integration limit transformation it holds that $\theta(t+\pi;\alpha)=\theta(t;\alpha)+\pi$ for all t. Accordingly, the area of the sector between the directions $t_1+\pi$ and $t_2+\pi$ is given by

$$\begin{aligned}|\mathbf{M}(\alpha)_{t_1+\pi}^{t_2+\pi}| &= \frac{1}{\sin^2\alpha}\int_{\theta(t_1+\pi;\alpha)}^{\theta(t_2+\pi;\alpha)} g(\theta;\alpha)\,d\theta \\ &= \frac{1}{\sin^2\alpha}\int_{\theta(t_1;\alpha)+\pi}^{\theta(t_2;\alpha)+\pi} g(\theta;\alpha)\,d\theta \\ &= \frac{1}{\sin^2\alpha}\int_{\theta(t_1;\alpha)}^{\theta(t_2;\alpha)} g(\theta+\pi;\alpha)\,d\theta\,.\end{aligned} \tag{D6}$$

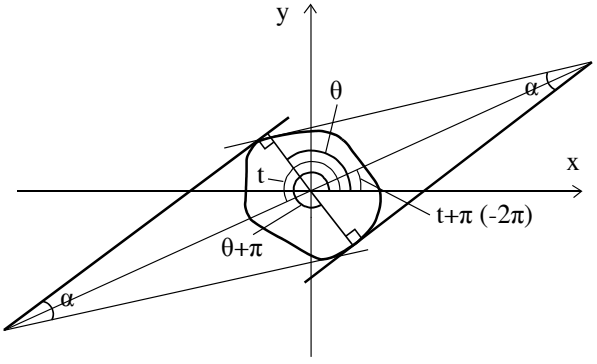

Fig. D1. Illustration of the relation between the direction t of the inclusion region radius and the angle θ of the perpendicular of the leftward cross-section tangent that makes up the left edge of the viewing sector (cf. Figs. C1 and C2 in Appendix C). Obviously, the angle that corresponds to the radius direction t+π is θ+π. In other words, if t is transformed into θ(t; α)=θ, then t+π is transformed into θ(t+π; α)=θ+π=θ(t; α)+π.

Due to the periodicity of $p(\cdot)$, by which $p(\theta+2n\pi)=p(\theta)$ and $p'(\theta+2n\pi)=p'(\theta)$ for all $n\in\mathbb{N}$,

$$\begin{aligned} g(\theta+\pi;\alpha) &= p(\theta+\pi)^2 + p(\theta+\pi)p(\theta+2\pi-\alpha)\cos\alpha + p(\theta+\pi)p'(\theta+2\pi-\alpha)\sin\alpha \\ &= p(\theta+\pi)^2 + p(\theta+\pi)p(\theta-\alpha)\cos\alpha + p(\theta+\pi)p'(\theta-\alpha)\sin\alpha \,. \end{aligned} \tag{D7}$$

Now the probability that the direction ξ of the diameter measured parallel to plot radius is between t_1 and t_2 becomes

$$\begin{aligned} \Pr\{t_1 \le \xi \le t_2;\alpha\} &= \frac{|\mathbf{M}(\alpha)_{t_1}^{t_2}|}{|\mathbf{M}(\alpha)|} + \frac{|\mathbf{M}(\alpha)_{t_1+\pi}^{t_2+\pi}|}{|\mathbf{M}(\alpha)|} \\ &= \frac{\frac{1}{\sin^2\alpha}\int_{\theta(t_1;\alpha)}^{\theta(t_2;\alpha)} \left[g(\theta;\alpha)+g(\theta+\pi;\alpha)\right]d\theta}{\frac{1}{\sin^2\alpha}\int_0^{2\pi} g(\theta;\alpha)\,d\theta} \\ &= C(\alpha)\int_{\theta(t_1;\alpha)}^{\theta(t_2;\alpha)} \left[g(\theta;\alpha)+g(\theta+\pi;\alpha)\right]d\theta \,, \end{aligned} \tag{D8}$$

where

$$\begin{aligned} C(\alpha) &= \left[\int_0^{2\pi} g(\theta;\alpha)\,d\theta\right]^{-1} \\ &= \left\{\int_0^{2\pi}\left[p(\theta)^2 + p(\theta)p(\theta+\pi-\alpha)\cos\alpha + p(\theta)p'(\theta+\pi-\alpha)\sin\alpha\right]d\theta\right\}^{-1} \end{aligned} \tag{D9}$$

is the scaling factor independent of t_1 and t_2. From this probability (Eq. D8), the cumulative distribution function $F_\xi(\cdot\,;\alpha)$ of $\xi\in[0,\pi)$ is obtained by setting $t_1=0$ and $t_2=t$, $t\in[0,\pi)$:

$$\begin{aligned} F_\xi(t;\alpha) &= \Pr\{\xi \le t;\alpha\} \\ &= C(\alpha)\int_{\theta(0;\alpha)}^{\theta(t;\alpha)} \left[g(\theta;\alpha)+g(\theta+\pi;\alpha)\right]d\theta \\ &= C(\alpha)\int_{\theta(0;\alpha)}^{\theta(t;\alpha)} \Big\{p(\theta)^2 + p(\theta+\pi)^2 + \cos\alpha\left[p(\theta)p(\theta+\pi-\alpha) + p(\theta+\pi)p(\theta-\alpha)\right] \\ &\quad + \sin\alpha\left[p(\theta)p'(\theta+\pi-\alpha) + p(\theta+\pi)p'(\theta-\alpha)\right]\Big\}d\theta \,. \end{aligned} \tag{D10}$$

As the direction transformation function $\theta(u;\alpha)$ is continuously differentiable within the domain $u\in[0,\pi)$ (which is evident again by geometrical consideration), the definite integral above can be expressed as follows with the original directions as the integration limits:

$$\int_{\theta(0;\alpha)}^{\theta(t;\alpha)} \left[g(\theta;\alpha) + g(\theta+\pi;\alpha) \right] d\theta = \int_0^t \left\{ g[\theta(u;\alpha);\alpha] + g[\theta(u;\alpha)+\pi;\alpha] \right\} \theta'(u;\alpha)\, du \quad , \text{(D11)}$$

where $\theta'(u;\alpha)$ is the derivative of $\theta(u;\alpha)$ with respect to u. Evidently, the resulting distribution function

$$F_\xi(t;\alpha) = C(\alpha) \int_0^t \left\{ g[\theta(u;\alpha);\alpha] + g[\theta(u;\alpha)+\pi;\alpha] \right\} \theta'(u;\alpha)\, du \quad \text{(D12)}$$

is the integral function of the probability density function

$$\begin{aligned} f_\xi(t;\alpha) &= F'_\xi(t;\alpha) \\ &= C(\alpha) \left\{ g[\theta(t;\alpha);\alpha] + g[\theta(t;\alpha)+\pi;\alpha] \right\} \theta'(t;\alpha) \\ &= C(\alpha) \left\{ p[\theta(t;\alpha)]^2 + p[\theta(t;\alpha)+\pi]^2 \right. \\ &\quad + \cos\alpha \left\{ p[\theta(t;\alpha)] p[\theta(t;\alpha)+\pi-\alpha] + p[\theta(t;\alpha)+\pi] p[\theta(t;\alpha)-\alpha] \right\} \\ &\quad \left. + \sin\alpha \left\{ p[\theta(t;\alpha)] p'[\theta(t;\alpha)+\pi-\alpha] + p[\theta(t;\alpha)+\pi] p'[\theta(t;\alpha)-\alpha] \right\} \right\} \cdot \\ &\quad \theta'(t;\alpha) \,. \end{aligned} \quad \text{(D13)}$$

As an example, let us consider the case where the breast height cross-section of a tree is a circle with radius R. In this case, $p(\theta)=R$ and $p'(\theta)=0$ for all $\theta \in [0, \pi)$, and hence

$$\begin{aligned} g(\theta;\alpha) + g(\theta+\pi;\alpha) &= R^2 + R^2\cos\alpha + R^2 + R^2\cos\alpha \\ &= 2R^2(1+\cos\alpha) \end{aligned} \quad \text{(D14)}$$

(see Eqs. D3 and D7), which is invariant of θ. Further, the scaling coefficient becomes

$$C(\alpha) = \left[\int_0^{2\pi} (R^2 + R^2\cos\alpha)\, d\theta \right]^{-1} = \frac{1}{2\pi R^2(1+\cos\alpha)} \,. \quad \text{(D15)}$$

(see Eq. D9). The radius of the inclusion region is given by

$$\begin{aligned} r(\theta;\alpha) &= \frac{1}{\sin\alpha} \sqrt{R^2 + R^2 + 2R^2\cos\alpha} \\ &= \frac{R\sqrt{2(1+\cos\alpha)}}{\sin\alpha} \end{aligned} \quad \text{(D16)}$$

(see Eq. D4), and thus the direction mapping becomes

$$\begin{aligned} \cos(u-\theta) &= \frac{p(\theta)}{r(\theta;\alpha)} = \frac{R}{\frac{R\sqrt{2(1+\cos\alpha)}}{\sin\alpha}} = \frac{\sin\alpha}{\sqrt{2(1+\cos\alpha)}} \\ \Leftrightarrow \quad \theta &= \theta(u;\alpha) = u - \cos^{-1}\left[\frac{\sin\alpha}{\sqrt{2(1+\cos\alpha)}} \right], \end{aligned} \quad \text{(D17)}$$

for which $\theta'(u; \alpha)=1$ for all u. Now, combining these results, we obtain the density of the direction of the diameter taken parallel to the plot radius:

$$\begin{aligned} f_{\xi}(t;\alpha) &= C(\alpha)\left[g(\theta;\alpha)+g(\theta+\pi;\alpha)\right]\theta'(t;\alpha) \\ &= \frac{1}{2\pi R^2(1+\cos\alpha)}\cdot 2R^2(1+\cos\alpha)\cdot 1 \\ &= \frac{1}{\pi}, \end{aligned} \tag{D18}$$

which is the density function of the uniform distribution over $[0, \pi)$. This is exactly what it should be: if the cross-section is circular, also the inclusion region is circular, all the directions are equally likely to become the plot radius direction, and hence all the diameters (which happen to be equal in this case) are equally likely to be measured.

Appendix E. Within-Tree Expectations of Volume Predictions by Laasasenaho Volume Equation with Diameter Selection Methods 1–5, 1ξ–5ξ, 1ξ90, 4ξ90 and 5ξ90

For the empirical part of this study, we aspire to express the within-tree expectations (Eq. 114 in Section 5.1)

$$\begin{aligned} E[\hat{V}_L(\boldsymbol{\theta})] &= c_1 E[D(\boldsymbol{\theta},1.3)^2] + c_2 E[D(\boldsymbol{\theta},1.3)^3] \\ &\quad + c_3 E[D(\boldsymbol{\theta},1.3)D(\boldsymbol{\theta},6)] + c_4 E[D(\boldsymbol{\theta},6)^2], \end{aligned} \tag{E1}$$

where the breast height diameter $D(\boldsymbol{\theta}, 1.3)$ and upper diameter $D(\boldsymbol{\theta}, 6)$ are obtained by one of the diameter selection methods 1–5, 1ξ–5ξ, 1ξ90, 4ξ90 and 5ξ90 (see Sections 3.3.2 and 4.2.2), in terms of diameter moments that are taken over one-dimensional direction distributions. Those moments are straightforward to estimate from the 180 diameters computed for each cross-section in the empirical part of this study (refer to Chapters 6 and 7).

Dependent selection, where the breast height diameter and upper diameter are measured in the same direction chosen at breast height, is considered with all the diameter selection methods. Independent selection, where the diameter directions are selected at the two heights independently, is considered only with the methods 1–5; this is because independent selection is practically unfeasible with Bitterlich sampling.

Diameter Selection Methods 1–5: Diameters with Uniform Direction Distribution

Dependent selection is presented in a) and independent selection in b).

1. a) $D(\boldsymbol{\theta}, 1.3)=D(\theta, 1.3)$ and $D(\boldsymbol{\theta}, 6)=D(\theta, 6)$, $\theta \sim \text{Unif}(0, \pi)$:

$$\begin{aligned} E[\hat{V}_{L1}(\boldsymbol{\theta})] &= c_1 E[D(\theta, 1.3)^2] + c_2 E[D(\theta, 1.3)^3] \\ &\quad + c_3 E[D(\theta, 1.3)D(\theta, 6)] + c_4 E[D(\theta, 6)^2] \end{aligned} \tag{E2}$$

1. b) $D(\boldsymbol{\theta}, 1.3)=D(\theta_1, 1.3)$ and $D(\boldsymbol{\theta}, 6)=D(\theta_2, 6)$, $\theta_1, \theta_2 \sim \text{Unif}(0, \pi)$ i.i.d.:

$$\begin{aligned} E[\hat{V}_{L1}(\boldsymbol{\theta})] &= c_1 E[D(\theta_1, 1.3)^2] + c_2 E[D(\theta_1, 1.3)^3] \\ &\quad + c_3 E[D(\theta_1, 1.3)] E[D(\theta_2, 6)] + c_4 E[D(\theta_2, 6)^2] \end{aligned} \tag{E3}$$

2. a) $D(\boldsymbol{\theta}, 1.3)=[D(\theta, 1.3)+D(\theta+\pi/2, 1.3)]/2$ and $D(\boldsymbol{\theta}, 6)=[D(\theta, 6)+D(\theta+\pi/2, 6)]/2$, $\theta \sim \text{Unif}(0, \pi)$:

$$\begin{aligned} E[\hat{V}_{L2}(\boldsymbol{\theta})] &= \frac{c_1}{2}\left\{ E[D(\theta, 1.3)^2] + E[D(\theta, 1.3)D(\theta+\pi/2, 1.3)] \right\} \\ &\quad + \frac{c_2}{4}\left\{ E[D(\theta, 1.3)^3] + 3E[D(\theta, 1.3)^2 D(\theta+\pi/2, 1.3)] \right\} \\ &\quad + \frac{c_3}{2}\left\{ E[D(\theta, 1.3)D(\theta, 6)] + E[D(\theta, 1.3)D(\theta+\pi/2, 6)] \right\} \\ &\quad + \frac{c_4}{2}\left\{ E[D(\theta, 6)^2] + E[D(\theta, 6)D(\theta+\pi/2, 6)] \right\} \end{aligned} \tag{E4}$$

2. b) $D(\boldsymbol{\theta}, 1.3)=[D(\theta_1, 1.3)+D(\theta_1+\pi/2, 1.3)]/2$ and $D(\boldsymbol{\theta}, 6)=[D(\theta_2, 6)+D(\theta_2+\pi/2, 6)]/2$, $\theta_1, \theta_2 \sim \text{Unif}(0, \pi)$ i.i.d.:

$$\begin{aligned} E[\hat{V}_{L2}(\boldsymbol{\theta})] &= \frac{c_1}{2}\Big\{ E[D(\theta_1, 1.3)^2] + E[D(\theta_1, 1.3)D(\theta_1 + \pi/2, 1.3)] \Big\} \\ &+ \frac{c_2}{4}\Big\{ E[D(\theta_1, 1.3)^3] + 3E[D(\theta_1, 1.3)^2 D(\theta_1 + \pi/2, 1.3)] \Big\} \\ &+ c_3 E[D(\theta_1, 1.3)]E[D(\theta_2, 6)] \\ &+ \frac{c_4}{2}\Big\{ E[D(\theta_2, 6)^2] + E[D(\theta_2, 6)D(\theta_2 + \pi/2, 6)] \Big\} \end{aligned} \tag{E5}$$

3. a) $D(\boldsymbol{\theta}, 1.3)=[D(\theta, 1.3)D(\theta+\pi/2, 1.3)]^{1/2}$ and $D(\boldsymbol{\theta}, 6)=[D(\theta, 6)D(\theta+\pi/2, 6)]^{1/2}$, $\theta \sim \text{Unif}(0, \pi)$:

$$\begin{aligned} E[\hat{V}_{L3}(\boldsymbol{\theta})] &= c_1 E[D(\theta, 1.3)D(\theta + \pi/2, 1.3)] \\ &+ c_2 E\Big\{ [D(\theta, 1.3)D(\theta + \pi/2, 1.3)]^{3/2} \Big\} \\ &+ c_3 E\Big\{ [D(\theta, 1.3)D(\theta + \pi/2, 1.3)D(\theta, 6)D(\theta + \pi/2, 6)]^{1/2} \Big\} \\ &+ c_4 E[D(\theta, 6)D(\theta + \pi/2, 6)] \end{aligned} \tag{E6}$$

3. b) $D(\boldsymbol{\theta}, 1.3)=[D(\theta_1, 1.3)D(\theta_1+\pi/2, 1.3)]^{1/2}$ and $D(\boldsymbol{\theta}, 6)=[D(\theta_2, 6)D(\theta_2+\pi/2, 6)]^{1/2}$, $\theta_1, \theta_2 \sim \text{Unif}(0, \pi)$ i.i.d.:

$$\begin{aligned} E[\hat{V}_{L3}(\boldsymbol{\theta})] &= c_1 E[D(\theta_1, 1.3)D(\theta_1 + \pi/2, 1.3)] \\ &+ c_2 E\Big\{ [D(\theta_1, 1.3)D(\theta_1 + \pi/2, 1.3)]^{3/2} \Big\} \\ &+ c_3 E\Big\{ [D(\theta_1, 1.3)D(\theta_1 + \pi/2, 1.3)]^{1/2} \Big\} E\Big\{ [D(\theta_2, 6)D(\theta_2 + \pi/2, 6)]^{1/2} \Big\} \\ &+ c_4 E[D(\theta_2, 6)D(\theta_2 + \pi/2, 6)] \end{aligned} \tag{E7}$$

4. a) $D(\boldsymbol{\theta}, 1.3)=[D(\theta_1, 1.3)+D(\theta_2, 1.3)]/2$ and $D(\boldsymbol{\theta}, 6)=[D(\theta_1, 6)+D(\theta_2, 6)]/2$, $\theta_1, \theta_2 \sim \text{Unif}(0, \pi)$ i.i.d.:

$$\begin{aligned} E[\hat{V}_{L4}(\boldsymbol{\theta})] &= \frac{c_1}{2}\Big\{ E[D(\theta_1, 1.3)^2] + E[D(\theta_1, 1.3)]^2 \Big\} \\ &+ \frac{c_2}{4}\Big\{ E[D(\theta_1, 1.3)^3] + 3E[D(\theta_1, 1.3)]E[D(\theta_2, 1.3)^2] \Big\} \\ &+ \frac{c_3}{2}\Big\{ E[D(\theta_1, 1.3)D(\theta_1, 6)] + E[D(\theta_1, 1.3)]E[D(\theta_2, 6)] \Big\} \\ &+ \frac{c_4}{2}\Big\{ E[D(\theta_1, 6)^2] + E[D(\theta_1, 6)]^2 \Big\} \end{aligned} \tag{E8}$$

4. b) $D(\boldsymbol{\theta}, 1.3)=[D(\theta_1, 1.3)+D(\theta_2, 1.3)]/2$ and $D(\boldsymbol{\theta}, 6)=[D(\theta_3, 6)+D(\theta_4, 6)]/2$, $\theta_1, \theta_2, \theta_3, \theta_4 \sim \text{Unif}(0, \pi)$ i.i.d.:

$$\begin{aligned} E[\hat{V}_{L4}(\boldsymbol{\theta})] &= \frac{c_1}{2}\left\{ E[D(\theta_1, 1.3)^2] + E[D(\theta_1, 1.3)]^2 \right\} \\ &+ \frac{c_2}{4}\left\{ E[D(\theta_1, 1.3)^3] + 3E[D(\theta_1, 1.3)]E[D(\theta_2, 1.3)^2] \right\} \\ &+ c_3 E[D(\theta_1, 1.3)]E[D(\theta_3, 6)] \\ &+ \frac{c_4}{2}\left\{ E[D(\theta_3, 6)^2] + E[D(\theta_3, 6)]^2 \right\} \end{aligned} \quad \text{(E9)}$$

5. a) $D(\boldsymbol{\theta}, 1.3)=[D(\theta_1, 1.3)D(\theta_2, 1.3)]^{1/2}$ and $D(\boldsymbol{\theta}, 6)=[D(\theta_1, 6)D(\theta_2, 6)]^{1/2}$, $\theta_1, \theta_2 \sim \text{Unif}(0, \pi)$ i.i.d.:

$$\begin{aligned} E[\hat{V}_{L5}(\boldsymbol{\theta})] &= c_1 E[D(\theta_1, 1.3)]^2 \\ &+ c_2 E\left\{ [D(\theta_1, 1.3)]^{3/2} \right\}^2 \\ &+ c_3 E\left\{ [D(\theta_1, 1.3)D(\theta_1, 6)]^{1/2} \right\}^2 \\ &+ c_4 E[D(\theta_1, 6)]^2 \end{aligned} \quad \text{(E10)}$$

5. b) $D(\boldsymbol{\theta}, 1.3)=[D(\theta_1, 1.3)D(\theta_2, 1.3)]^{1/2}$ and $D(\boldsymbol{\theta}, 6)=[D(\theta_3, 6)D(\theta_4, 6)]^{1/2}$, $\theta_1, \theta_2, \theta_3, \theta_4 \sim \text{Unif}(0, \pi)$ i.i.d.:

$$\begin{aligned} E[\hat{V}_{L5}(\boldsymbol{\theta})] &= c_1 E[D(\theta_1, 1.3)]^2 \\ &+ c_2 E\left\{ [D(\theta_1, 1.3)]^{3/2} \right\}^2 \\ &+ c_3 E\left\{ [D(\theta_1, 1.3)]^{1/2} \right\}^2 E\left\{ [D(\theta_3, 6)]^{1/2} \right\}^2 \\ &+ c_4 E[D(\theta_3, 6)]^2 \end{aligned} \quad \text{(E11)}$$

Diameter Selection Methods 1ξ–5ξ: Diameters Parallel To Plot Radius in Bitterlich Sampling

The non-uniform distribution $F_\xi(\xi; \alpha)$ of the diameter direction ξ parallel to plot radius in Bitterlich sampling, with viewing angle α, is determined at breast height. For brevity, α is omitted in the diameter moment denotations (i.e., e.g. $E[D(\xi, 1.3); \alpha]$ is denoted with $E[D(\xi, 1.3)]$), although it essentially determines the distribution $F_\xi(\xi; \alpha)$ over which the moments are taken.

1ξ. $D(\boldsymbol{\theta}, 1.3)=D(\xi, 1.3)$ and $D(\boldsymbol{\theta}, 6)=D(\xi, 6)$, $\xi \sim F_\xi(\xi; \alpha)$:

$$\begin{aligned} E[\hat{V}_{L1\xi}(\boldsymbol{\theta})] &= c_1 E[D(\xi, 1.3)^2] + c_2 E[D(\xi, 1.3)^3] \\ &+ c_3 E[D(\xi, 1.3)D(\xi, 6)] + c_4 E[D(\xi, 6)^2] \end{aligned} \quad \text{(E12)}$$

2ξ. $D(\boldsymbol{\theta}, 1.3)=[D(\xi, 1.3)+D(\xi+\pi/2, 1.3)]/2$ and $D(\boldsymbol{\theta}, 6)=[D(\xi, 6)+D(\xi+\pi/2, 6)]/2$, $\xi \sim F_\xi(\xi; \alpha)$:

$$\begin{aligned}
E[\hat{V}_{L2\xi}(\boldsymbol{\theta})] &= \frac{c_1}{4}\Big\{ E[D(\xi,1.3)^2] + E[D(\xi+\pi/2,1.3)^2] + 2E[D(\xi,1.3)D(\xi+\pi/2,1.3)] \Big\} \\
&+ \frac{c_2}{8}\Big\{ E[D(\xi,1.3)^3] + E[D(\xi+\pi/2,1.3)^3] + 3E[D(\xi,1.3)^2 D(\xi+\pi/2,1.3)] \\
&\quad + 3E[D(\xi,1.3)D(\xi+\pi/2,1.3)^2] \Big\} \\
&+ \frac{c_3}{4}\Big\{ E[D(\xi,1.3)D(\xi,6)] + E[D(\xi,1.3)D(\xi+\pi/2,6)] \\
&\quad + E[D(\xi+\pi/2,1.3)D(\xi,6)] + E[D(\xi+\pi/2,1.3)D(\xi+\pi/2,6)] \Big\} \\
&+ \frac{c_4}{4}\Big\{ E[D(\xi,6)^2] + E[D(\xi+\pi/2,6)^2] + 2E[D(\xi,6)D(\xi+\pi/2,6)] \Big\}
\end{aligned} \tag{E13}$$

3ξ. $D(\boldsymbol{\theta}, 1.3)=[D(\xi, 1.3)D(\xi+\pi/2, 1.3)]^{1/2}$ and $D(\boldsymbol{\theta}, 6)=[D(\xi, 6)D(\xi+\pi/2, 6)]^{1/2}$, $\xi \sim F_\xi(\xi; \alpha)$:

$$\begin{aligned}
E[\hat{V}_{L3\xi}(\boldsymbol{\theta})] &= c_1 E[D(\xi,1.3)D(\xi+\pi/2,1.3)] \\
&+ c_2 E\Big\{ [D(\xi,1.3)D(\xi+\pi/2,1.3)]^{3/2} \Big\} \\
&+ c_3 E\Big\{ [D(\xi,1.3)D(\xi+\pi/2,1.3)D(\xi,6)D(\xi+\pi/2,6)]^{1/2} \Big\} \\
&+ c_4 E[D(\xi,6)D(\xi+\pi/2,6)]
\end{aligned} \tag{E14}$$

4ξ. $D(\boldsymbol{\theta}, 1.3)=[D(\xi, 1.3)+D(\theta, 1.3)]/2$ and $D(\boldsymbol{\theta}, 6)=[D(\xi, 6)+D(\theta, 6)]/2$, $\xi \sim F_\xi(\xi; \alpha)$, $\theta \sim \text{Unif}(0, \pi)$, ξ and θ independent:

$$\begin{aligned}
E[\hat{V}_{L4\xi}(\boldsymbol{\theta})] &= \frac{c_1}{4}\Big\{ E[D(\xi,1.3)^2] + E[D(\theta,1.3)^2] + 2E[D(\xi,1.3)]E[D(\theta,1.3)] \Big\} \\
&+ \frac{c_2}{8}\Big\{ E[D(\xi,1.3)^3] + E[D(\theta,1.3)^3] + 3E[D(\xi,1.3)]E[D(\theta,1.3)^2] \\
&\quad + 3E[D(\xi,1.3)^2]E[D(\theta,1.3)] \Big\} \\
&+ \frac{c_3}{4}\Big\{ E[D(\xi,1.3)D(\xi,6)] + E[D(\theta,1.3)D(\theta,6)] + E[D(\xi,1.3)]E[D(\theta,6)] \\
&\quad + E[D(\theta,1.3)]E[D(\xi,6)] \Big\} \\
&+ \frac{c_4}{4}\Big\{ E[D(\xi,6)^2] + E[D(\theta,6)^2] + E[D(\xi,6)]E[D(\theta,6)] \Big\}
\end{aligned} \tag{E15}$$

5ξ. $D(\boldsymbol{\theta},1.3)=[D(\xi,1.3)D(\theta,1.3)]^{1/2}$ and $D(\boldsymbol{\theta},6)=[D(\xi,6)D(\theta,6)]^{1/2}$, $\xi\sim F_{\xi}(\xi;\alpha)$, $\theta\sim\text{Unif}(0,\pi)$, ξ and θ independent:

$$\begin{aligned}E[\hat{V}_{L5\xi}(\boldsymbol{\theta})] &= c_1E[D(\xi,1.3)]E[D(\theta,1.3)]\\ &+ c_2E\left\{[D(\xi,1.3)]^{3/2}\right\}E\left\{[D(\theta,1.3)]^{3/2}\right\}\\ &+ c_3E\left\{[D(\xi,1.3)D(\xi,6)]^{1/2}\right\}E\left\{[D(\theta,1.3)D(\theta,6)]^{1/2}\right\}\\ &+ c_4E[D(\xi,6)]E[D(\theta,6)]\end{aligned} \quad \text{(E16)}$$

Diameter Selection Methods 1ξ90, 4ξ90 and 5ξ90: Diameters Perpendicular to Plot Radius in Bitterlich Sampling

1ξ90. $D(\boldsymbol{\theta},1.3)=D(\xi+\pi/2,1.3)$ and $D(\boldsymbol{\theta},6)=D(\xi+\pi/2,6)$, $\xi\sim F_{\xi}(\xi;\alpha)$: to obtain $E[\hat{V}_{L1\xi90}(\boldsymbol{\theta})]$, substitute $D(\xi+\pi/2,1.3)$ for $D(\xi,1.3)$ and $D(\xi+\pi/2,6)$ for $D(\xi,6)$ in Eq. E12.

4ξ90. $D(\boldsymbol{\theta},1.3)=[D(\xi+\pi/2,1.3)+D(\theta,1.3)]/2$ and $D(\boldsymbol{\theta},6)=[D(\xi+\pi/2,6)+D(\theta,6)]/2$, $\xi\sim F_{\xi}(\xi;\alpha)$, $\theta\sim\text{Unif}(0,\pi)$, ξ and θ independent: to obtain $E[\hat{V}_{L4\xi90}(\boldsymbol{\theta})]$, substitute $D(\xi+\pi/2,1.3)$ for $D(\xi,1.3)$ and $D(\xi+\pi/2,6)$ for $D(\xi,6)$ in Eq. E15.

5ξ90. $D(\boldsymbol{\theta},1.3)=[D(\xi+\pi/2,1.3)D(\theta,1.3)]^{1/2}$ and $D(\boldsymbol{\theta},6)=[D(\xi+\pi/2,6)D(\theta,6)]^{1/2}$, $\xi\sim F_{\xi}(\xi;\alpha)$, $\theta\sim\text{Unif}(0,\pi)$, ξ and θ independent: to obtain $E[\hat{V}_{L5\xi90}(\boldsymbol{\theta})]$, substitute $D(\xi+\pi/2,1.3)$ for $D(\xi,1.3)$ and $D(\xi+\pi/2,6)$ for $D(\xi,6)$ in Eq. E16.

Appendix F. Within-Tree Variances of Volume Predictions by Laasasenaho Volume Equation with Diameter Selection Methods 1–5, 1ξ–5ξ, 1ξ90, 4ξ90 and 5ξ90

For the empirical part of this study, we want to express the within-tree variances (Eq. 115 in Section 5.1)

$$\begin{aligned}\mathrm{Var}[\hat{V}_L(\boldsymbol{\theta})] &= \mathrm{E}[\hat{V}_L(\boldsymbol{\theta})^2] - \left\{ \mathrm{E}[\hat{V}_L(\boldsymbol{\theta})] \right\}^2 \\ &= c_2^2\mathrm{E}[D(\boldsymbol{\theta},1.3)^6] + 2c_1c_2\mathrm{E}[D(\boldsymbol{\theta},1.3)^5] + c_1^2\mathrm{E}[D(\boldsymbol{\theta},1.3)^4] \\ &\quad + 2c_2c_3\mathrm{E}[D(\boldsymbol{\theta},1.3)^4 D(\boldsymbol{\theta},6)] + 2c_2c_4\mathrm{E}[D(\boldsymbol{\theta},1.3)^3 D(\boldsymbol{\theta},6)^2] \\ &\quad + 2c_1c_3\mathrm{E}[D(\boldsymbol{\theta},1.3)^3 D(\boldsymbol{\theta},6)] + (c_3^2 + 2c_1c_4)\mathrm{E}[D(\boldsymbol{\theta},1.3)^2 D(\boldsymbol{\theta},6)^2] \\ &\quad + 2c_3c_4\mathrm{E}[D(\boldsymbol{\theta},1.3)D(\boldsymbol{\theta},6)^3] + c_4^2\mathrm{E}[D(\boldsymbol{\theta},6)^4] \\ &\quad - \left\{ \mathrm{E}[\hat{V}_L(\boldsymbol{\theta})] \right\}^2 ,\end{aligned} \tag{F1}$$

where $D(\boldsymbol{\theta},1.3)$ and $D(\boldsymbol{\theta},6)$ are obtained by one of the diameter selection methods 1–5, 1ξ–5ξ, 1ξ90, 4ξ90 and 5ξ90 (see Sections 3.2.2 and 4.2.2), in terms of diameter moments taken over one-dimensional direction distributions. As the expectations $\mathrm{E}[\hat{V}_L(\boldsymbol{\theta})]$ were dealt with in Appendix E, the task is reduced to finding the expressions for $\mathrm{E}[\hat{V}_L(\boldsymbol{\theta})^2]$.

As in Appendix E, the diameter selection methods 1–5 are applied both dependently and independently, whereas with the methods 1ξ–5ξ, 1ξ90, 4ξ90 and 5ξ90 only dependent selection is considered.

Diameter Selection Methods 1–5: Diameters with Uniform Direction Distribution

Dependent selection is presented in a) and independent selection in b).

1. a) $D(\boldsymbol{\theta},1.3)=D(\theta,1.3)$ and $D(\boldsymbol{\theta},6)=D(\theta,6)$, $\theta\sim\mathrm{Unif}(0,\pi)$:

$$\begin{aligned}\mathrm{E}[\hat{V}_{L1}(\boldsymbol{\theta})^2] &= c_2^2\mathrm{E}[D(\theta,1.3)^6] + 2c_1c_2\mathrm{E}[D(\theta,1.3)^5] + c_1^2\mathrm{E}[D(\theta,1.3)^4] \\ &\quad + 2c_2c_3\mathrm{E}[D(\theta,1.3)^4 D(\theta,6)] + 2c_2c_4\mathrm{E}[D(\theta,1.3)^3 D(\theta,6)^2] \\ &\quad + 2c_1c_3\mathrm{E}[D(\theta,1.3)^3 D(\theta,6)] + (c_3^2 + 2c_1c_4)\mathrm{E}[D(\theta,1.3)^2 D(\theta,6)^2] \\ &\quad + 2c_3c_4\mathrm{E}[D(\theta,1.3)D(\theta,6)^3] + c_4^2\mathrm{E}[D(\theta,6)^4]\end{aligned} \tag{F2}$$

1. b) $D(\boldsymbol{\theta},1.3)=D(\theta_1,1.3)$ and $D(\boldsymbol{\theta},6)=D(\theta_2,6)$, θ_1, $\theta_2\sim\mathrm{Unif}(0,\pi)$ i.i.d.:

$$\begin{aligned}\mathrm{E}[\hat{V}_{L1}(\boldsymbol{\theta})^2] &= c_2^2\mathrm{E}[D(\theta_1,1.3)^6] + 2c_1c_2\mathrm{E}[D(\theta_1,1.3)^5] + c_1^2\mathrm{E}[D(\theta_1,1.3)^4] \\ &\quad + 2c_2c_3\mathrm{E}[D(\theta_1,1.3)^4]\mathrm{E}[D(\theta_2,6)] + 2c_2c_4\mathrm{E}[D(\theta_1,1.3)^3]\mathrm{E}[D(\theta_2,6)^2] \\ &\quad + 2c_1c_3\mathrm{E}[D(\theta_1,1.3)^3]\mathrm{E}[D(\theta_2,6)] + (c_3^2 + 2c_1c_4)\mathrm{E}[D(\theta_1,1.3)^2]\mathrm{E}[D(\theta_2,6)^2] \\ &\quad + 2c_3c_4\mathrm{E}[D(\theta_1,1.3)]\mathrm{E}[D(\theta_2,6)^3] + c_4^2\mathrm{E}[D(\theta_2,6)^4]\end{aligned} \tag{F3}$$

2. a) $D(\boldsymbol{\theta},1.3)=[D(\theta,1.3)+D(\theta+\pi/2,1.3)]/2$ and $D(\boldsymbol{\theta},6)=[D(\theta,6)+D(\theta+\pi/2,6)]/2$, $\theta\sim\text{Unif}(0,\pi)$:

$$
\begin{aligned}
E[\hat{V}_{L2}(\boldsymbol{\theta})^2] = {} & \frac{c_2^2}{64}E\left\{[D(\theta,1.3)+D(\theta+\pi/2,1.3)]^6\right\} \\
& + \frac{c_1c_2}{16}E\left\{[D(\theta,1.3)+D(\theta+\pi/2,1.3)]^5\right\} \\
& + \frac{c_1^2}{16}E\left\{[D(\theta,1.3)+D(\theta+\pi/2,1.3)]^4\right\} \\
& + \frac{c_2c_3}{16}E\left\{[D(\theta,1.3)+D(\theta+\pi/2,1.3)]^4[D(\theta,6)+D(\theta+\pi/2,6)]\right\} \\
& + \frac{c_2c_4}{16}E\left\{[D(\theta,1.3)+D(\theta+\pi/2,1.3)]^3[D(\theta,6)+D(\theta+\pi/2,6)]^2\right\} \qquad \text{(F4)} \\
& + \frac{c_1c_3}{8}E\left\{[D(\theta,1.3)+D(\theta+\pi/2,1.3)]^3[D(\theta,6)+D(\theta+\pi/2,6)]\right\} \\
& + \frac{c_3^2+2c_1c_4}{16}E\left\{[D(\theta,1.3)+D(\theta+\pi/2,1.3)]^2[D(\theta,6)+D(\theta+\pi/2,6)]^2\right\} \\
& + \frac{c_3c_4}{8}E\left\{[D(\theta,1.3)+D(\theta+\pi/2,1.3)][D(\theta,6)+D(\theta+\pi/2,6)]^3\right\} \\
& + \frac{c_4^2}{16}E\left\{[D(\theta,6)+D(\theta+\pi/2,6)]^4\right\}
\end{aligned}
$$

2. b) $D(\boldsymbol{\theta},1.3)=[D(\theta_1,1.3)+D(\theta_1+\pi/2,1.3)]/2$ and $D(\boldsymbol{\theta},6)=[D(\theta_2,6)+D(\theta_2+\pi/2,6)]/2$, $\theta_1, \theta_2\sim\text{Unif}(0,\pi)$ i.i.d.:

$$
\begin{aligned}
E[\hat{V}_{L2}(\boldsymbol{\theta})^2] = {} & \frac{c_2^2}{64}E\left\{[D(\theta_1,1.3)+D(\theta_1+\pi/2,1.3)]^6\right\} \\
& + \frac{c_1c_2}{16}E\left\{[D(\theta_1,1.3)+D(\theta_1+\pi/2,1.3)]^5\right\} \\
& + \frac{c_1^2}{16}E\left\{[D(\theta_1,1.3)+D(\theta_1+\pi/2,1.3)]^4\right\} \\
& + \frac{c_2c_3}{8}E\left\{[D(\theta_1,1.3)+D(\theta_1+\pi/2,1.3)]^4\right\}E[D(\theta_2,6)] \\
& + \frac{c_2c_4}{16}E\left\{[D(\theta_1,1.3)+D(\theta_1+\pi/2,1.3)]^3\right\}E\left\{[D(\theta_2,6)+D(\theta_2+\pi/2,6)]^2\right\} \\
& + \frac{c_1c_3}{4}E\left\{[D(\theta_1,1.3)+D(\theta_1+\pi/2,1.3)]^3\right\}E[D(\theta_2,6)] \\
& + \frac{c_3^2+2c_1c_4}{16}E\left\{[D(\theta_1,1.3)+D(\theta_1+\pi/2,1.3)]^2\right\}E\left\{[D(\theta_2,6)+D(\theta_2+\pi/2,6)]^2\right\} \\
& + \frac{c_3c_4}{4}E[D(\theta_1,1.3)]E\left\{[D(\theta_2,6)+D(\theta_2+\pi/2,6)]^3\right\} \\
& + \frac{c_4^2}{16}E\left\{[D(\theta_2,6)+D(\theta_2+\pi/2,6)]^4\right\}
\end{aligned}
\qquad \text{(F5)}
$$

3. a) $D(\boldsymbol{\theta}, 1.3)=[D(\theta, 1.3)D(\theta+\pi/2, 1.3)]^{1/2}$ and $D(\boldsymbol{\theta}, 6)=[D(\theta, 6)D(\theta+\pi/2, 6)]^{1/2}$, $\theta \sim \text{Unif}(0, \pi)$:

$$
\begin{aligned}
E[\hat{V}_{L3}(\boldsymbol{\theta})^2] &= c_2^2 E[D(\theta, 1.3)^3 D(\theta+\pi/2, 1.3)^3] \\
&+ 2c_1c_2 E[D(\theta, 1.3)^{5/2} D(\theta+\pi/2, 1.3)^{5/2}] \\
&+ c_1^2 E[D(\theta, 1.3)^2 D(\theta+\pi/2, 1.3)^2] \\
&+ 2c_2c_3 E[D(\theta, 1.3)^2 D(\theta+\pi/2, 1.3)^2 D(\theta, 6)^{1/2} D(\theta+\pi/2, 6)^{1/2}] \\
&+ 2c_2c_4 E[D(\theta, 1.3)^{3/2} D(\theta+\pi/2, 1.3)^{3/2} D(\theta, 6) D(\theta+\pi/2, 6)] \\
&+ 2c_1c_3 E[D(\theta, 1.3)^{3/2} D(\theta+\pi/2, 1.3)^{3/2} D(\theta, 6)^{1/2} D(\theta+\pi/2, 6)^{1/2}] \\
&+ (c_3^2 + 2c_1c_4) E[D(\theta, 1.3) D(\theta+\pi/2, 1.3) D(\theta, 6) D(\theta+\pi/2, 6)] \\
&+ 2c_3c_4 E[D(\theta, 1.3)^{1/2} D(\theta+\pi/2, 1.3)^{1/2} D(\theta, 6)^{3/2} D(\theta+\pi/2, 6)^{3/2}] \\
&+ c_4^2 E[D(\theta, 6)^2 D(\theta+\pi/2, 6)^2]
\end{aligned}
\tag{F6}
$$

3. b) $D(\boldsymbol{\theta}, 1.3)=[D(\theta_1, 1.3)D(\theta_1+\pi/2, 1.3)]^{1/2}$ and $D(\boldsymbol{\theta}, 6)=[D(\theta_2, 6)D(\theta_2+\pi/2, 6)]^{1/2}$, $\theta_1, \theta_2 \sim \text{Unif}(0, \pi)$ i.i.d.:

$$
\begin{aligned}
E[\hat{V}_{L3}(\boldsymbol{\theta})^2] &= c_2^2 E[D(\theta_1, 1.3)^3 D(\theta_1+\pi/2, 1.3)^3] \\
&+ 2c_1c_2 E[D(\theta_1, 1.3)^{5/2} D(\theta_1+\pi/2, 1.3)^{5/2}] \\
&+ c_1^2 E[D(\theta_1, 1.3)^2 D(\theta_1+\pi/2, 1.3)^2] \\
&+ 2c_2c_3 E[D(\theta_1, 1.3)^2 D(\theta_1+\pi/2, 1.3)^2] E[D(\theta_2, 6)^{1/2} D(\theta_2+\pi/2, 6)^{1/2}] \\
&+ 2c_2c_4 E[D(\theta_1, 1.3)^{3/2} D(\theta_1+\pi/2, 1.3)^{3/2}] E[D(\theta_2, 6) D(\theta_2+\pi/2, 6)] \\
&+ 2c_1c_3 E[D(\theta_1, 1.3)^{3/2} D(\theta_1+\pi/2, 1.3)^{3/2}] E[D(\theta_2, 6)^{1/2} D(\theta_2+\pi/2, 6)^{1/2}] \\
&+ (c_3^2 + 2c_1c_4) E[D(\theta_1, 1.3) D(\theta_1+\pi/2, 1.3)] E[D(\theta_2, 6) D(\theta_2+\pi/2, 6)] \\
&+ 2c_3c_4 E[D(\theta_1, 1.3)^{1/2} D(\theta_1+\pi/2, 1.3)^{1/2}] E[D(\theta_2, 6)^{3/2} D(\theta_2+\pi/2, 6)^{3/2}] \\
&+ c_4^2 E[D(\theta_2, 6)^2 D(\theta_2+\pi/2, 6)^2]
\end{aligned}
\tag{F7}
$$

4. a) $D(\boldsymbol{\theta}, 1.3)=[D(\theta_1, 1.3)+D(\theta_2, 1.3)]/2$ and $D(\boldsymbol{\theta}, 6)=[D(\theta_1, 6)+D(\theta_2, 6)]/2$, $\theta_1, \theta_2 \sim \text{Unif}(0, \pi)$ i.i.d.:

$$
\begin{aligned}
E[\hat{V}_{L4}(\boldsymbol{\theta})^2] \;=\; & \frac{c_2^2}{32}\Big\{ E[D(\theta_1, 1.3)^6] + 6E[D(\theta_1, 1.3)^5]E[D(\theta_2, 1.3)] \\
& + 15E[D(\theta_1, 1.3)^4]E[D(\theta_2, 1.3)^2] + 10\Big\{E[D(\theta_1, 1.3)^3]\Big\}^2 \Big\} \\
& + \frac{c_1 c_2}{8}\Big\{ E[D(\theta_1, 1.3)^5] + 5E[D(\theta_1, 1.3)^4]E[D(\theta_2, 1.3)] \\
& + 10E[D(\theta_1, 1.3)^3]E[D(\theta_2, 1.3)^2] \Big\} \\
& + \frac{c_1^2}{8}\Big\{ E[D(\theta_1, 1.3)^4] + 4E[D(\theta_1, 1.3)^3]E[D(\theta_2, 1.3)] + 3\Big\{E[D(\theta_1, 1.3)^2]\Big\}^2 \Big\} \\
& + \frac{c_2 c_3}{8}\Big\{ E[D(\theta_1, 1.3)^4 D(\theta_1, 6)] + E[D(\theta_1, 1.3)^4]E[D(\theta_2, 6)] \\
& + 4E[D(\theta_1, 1.3)^3 D(\theta_1, 6)]E[D(\theta_2, 1.3)] + 6E[D(\theta_1, 1.3)^2 D(\theta_1, 6)]E[D(\theta_2, 1.3)^2] \\
& + 4E[D(\theta_1, 1.3)D(\theta_1, 6)]E[D(\theta_2, 1.3)^3] \Big\} \\
& + \frac{c_2 c_4}{8}\Big\{ E[D(\theta_1, 1.3)^3 D(\theta_1, 6)^2] + E[D(\theta_1, 1.3)^3]E[D(\theta_2, 6)^2] \\
& + 2E[D(\theta_1, 1.3)^3 D(\theta_1, 6)]E[D(\theta_2, 6)] \\
& + 3E[D(\theta_1, 1.3)^2 D(\theta_1, 6)^2]E[D(\theta_2, 1.3)] \\
& + 6E[D(\theta_1, 1.3)^2 D(\theta_1, 6)]E[D(\theta_2, 1.3)D(\theta_2, 6)] \\
& + 3E[D(\theta_1, 1.3)D(\theta_1, 6)^2]E[D(\theta_2, 1.3)^2] \Big\} \\
& + \frac{c_1 c_3}{4}\Big\{ E[D(\theta_1, 1.3)^3 D(\theta_1, 6)] + E[D(\theta_1, 1.3)^3]E[D(\theta_2, 6)] \\
& + 3E[D(\theta_1, 1.3)^2 D(\theta_1, 6)]E[D(\theta_2, 1.3)] + 3E[D(\theta_1, 1.3)D(\theta_1, 6)]E[D(\theta_2, 1.3)^2] \Big\} \\
& + \frac{c_3^2 + 2c_1 c_4}{8}\Big\{ E[D(\theta_1, 1.3)^2 D(\theta_1, 6)^2] + E[D(\theta_1, 1.3)^2]E[D(\theta_2, 6)^2] \\
& + 2E[D(\theta_1, 1.3)^2 D(\theta_1, 6)]E[D(\theta_2, 6)] + 2E[D(\theta_1, 1.3)D(\theta_1, 6)^2]E[D(\theta_2, 1.3)] \\
& + 2\Big\{E[D(\theta_1, 1.3)D(\theta_1, 6)]\Big\}^2 \Big\} \\
& + \frac{c_3 c_4}{4}\Big\{ E[D(\theta_1, 1.3)D(\theta_1, 6)^3] + E[D(\theta_1, 1.3)]E[D(\theta_2, 6)^3] \\
& + 3E[D(\theta_1, 1.3)D(\theta_1, 6)^2]E[D(\theta_2, 6)] + 3E[D(\theta_1, 1.3)D(\theta_1, 6)]E[D(\theta_2, 6)^2] \Big\} \\
& + \frac{c_4^2}{8}\Big\{ E[D(\theta_1, 6)^4] + 4E[D(\theta_1, 6)^3]E[D(\theta_2, 6)] + 3\Big\{ E[D(\theta_1, 6)^2] \Big\}^2 \Big\}
\end{aligned}
\tag{F8}
$$

4. b) $D(\boldsymbol{\theta}, 1.3)=[D(\theta_1, 1.3)+D(\theta_2, 1.3)]/2$ and $D(\boldsymbol{\theta}, 6)=[D(\theta_3, 6)+D(\theta_4, 6)]/2$, $\theta_1, \theta_2, \theta_3, \theta_4 \sim \text{Unif}(0, \pi)$ i.i.d.:

$$
\begin{aligned}
E[\hat{V}_{L4}(\boldsymbol{\theta})^2] \;=\; & \frac{c_2^2}{32}\Big\{ E[D(\theta_1,1.3)^6] + 6E[D(\theta_1,1.3)^5]E[D(\theta_2,1.3)] \\
& + 15E[D(\theta_1,1.3)^4]E[D(\theta_2,1.3)^2] + 10\Big\{ E[D(\theta_1,1.3)^3]\Big\}^2 \Big\} \\
& + \frac{c_1c_2}{8}\Big\{ E[D(\theta_1,1.3)^5] + 5E[D(\theta_1,1.3)^4]E[D(\theta_2,1.3)] \\
& + 10E[D(\theta_1,1.3)^3]E[D(\theta_2,1.3)^2]\Big\} \\
& + \frac{c_1^2}{8}\Big\{ E[D(\theta_1,1.3)^4] + 4E[D(\theta_1,1.3)^3]E[D(\theta_2,1.3)] + 3\Big\{ E[D(\theta_1,1.3)^2]\Big\}^2 \Big\} \\
& + \frac{c_2c_3}{4}\Big\{ E[D(\theta_1,1.3)^4]E[D(\theta_3,6)] + 4E[D(\theta_1,1.3)^3]E[D(\theta_2,1.3)]E[D(\theta_3,6)] \\
& + 3\Big\{ E[D(\theta_1,1.3)^2]\Big\}^2 E[D(\theta_3,6)]\Big\} \\
& + \frac{c_2c_4}{4}\Big\{ E[D(\theta_1,1.3)^3]E[D(\theta_3,6)^2] + 3E[D(\theta_1,1.3)^2]E[D(\theta_2,1.3)]E[D(\theta_3,6)^2] \\
& + E[D(\theta_1,1.3)^3]\Big\{E[D(\theta_3,6)]\Big\}^2 + 3E[D(\theta_1,1.3)^2]E[D(\theta_2,1.3)]\Big\{ E[D(\theta_3,6)]\Big\}^2 \Big\} \\
& + \frac{c_1c_3}{2}\Big\{ E[D(\theta_1,1.3)^3]E[D(\theta_3,6)] + 3E[D(\theta_1,1.3)^2]E[D(\theta_2,1.3)]E[D(\theta_3,6)]\Big\} \\
& + \frac{c_3^2+2c_1c_4}{4}\Big\{ E[D(\theta_1,1.3)^2]E[D(\theta_3,6)^2] + \Big\{ E[D(\theta_1,1.3)]\Big\}^2 E[D(\theta_3,6)^2] \\
& + E[D(\theta_1,1.3)^2]\Big\{ E[D(\theta_3,6)]\Big\}^2 + \Big\{ E[D(\theta_1,1.3)]\Big\}^2\Big\{ E[D(\theta_3,6)]\Big\}^2 \Big\} \\
& + \frac{c_3c_4}{2}\Big\{ E[D(\theta_1,1.3)]E]D(\theta_3,6)^3] + 3E[D(\theta_1,1.3)]E[D(\theta_3,6)^2]E[D(\theta_4,6)]\Big\} \\
& + \frac{c_4^2}{8}\Big\{ E[D(\theta_3,6)^4] + 4E[D(\theta_3,6)^3]E[D(\theta_4,6)] + 3\Big\{ E[D(\theta_3,6)^2]\Big\}^2 \Big\}
\end{aligned}
\tag{F9}
$$

5. a) $D(\boldsymbol{\theta},1.3)=[D(\theta_1,1.3)D(\theta_2,1.3)]^{1/2}$ and $D(\boldsymbol{\theta},6)=[D(\theta_1,6)D(\theta_2,6)]^{1/2}$, θ_1, θ_2~Unif$(0,\pi)$ i.i.d.:

$$\begin{aligned}
E[\hat{V}_{L5}(\boldsymbol{\theta})^2] &= c_2^2\left\{E[D(\theta_1,1.3)^3]\right\}^2 \\
&+ 2c_1c_2\left\{E[D(\theta_1,1.3)^{5/2}]\right\}^2 \\
&+ c_1^2\left\{E[D(\theta_1,1.3)^2]\right\}^2 \\
&+ 2c_2c_3\left\{E[D(\theta_1,1.3)^2D(\theta_1,6)^{1/2}]\right\}^2 \\
&+ 2c_2c_4\left\{E[D(\theta_1,1.3)^{3/2}D(\theta_1,6)]\right\}^2 \\
&+ 2c_1c_3\left\{E[D(\theta_1,1.3)^{3/2}D(\theta_1,6)^{1/2}]\right\}^2 \\
&+ (c_3^2+2c_1c_4)\left\{E[D(\theta_1,1.3)D(\theta_1,6)]\right\}^2 \\
&+ 2c_3c_4\left\{E[D(\theta_1,1.3)^{1/2}D(\theta_1,6)^{3/2}]\right\}^2 \\
&+ c_4^2\left\{E[D(\theta_1,6)^2]\right\}^2
\end{aligned} \tag{F10}$$

5. b) $D(\boldsymbol{\theta},1.3)=[D(\theta_1,1.3)D(\theta_2,1.3)]^{1/2}$ and $D(\boldsymbol{\theta},6)=[D(\theta_3,6)D(\theta_4,6)]^{1/2}$, θ_1, θ_2, θ_3, θ_4~Unif$(0,\pi)$ i.i.d.:

$$\begin{aligned}
E[\hat{V}_{L5}(\boldsymbol{\theta})^2] &= c_2^2\left\{E[D(\theta_1,1.3)^3]\right\}^2 \\
&+ 2c_1c_2\left\{E[D(\theta_1,1.3)^{5/2}]\right\}^2 \\
&+ c_1^2\left\{E[D(\theta_1,1.3)^2]\right\}^2 \\
&+ 2c_2c_3\left\{E[D(\theta_1,1.3)^2]\right\}^2\left\{E[D(\theta_3,6)^{1/2}]\right\}^2 \\
&+ 2c_2c_4\left\{E[D(\theta_1,1.3)^{3/2}]\right\}^2\left\{E[D(\theta_3,6)]\right\}^2 \\
&+ 2c_1c_3\left\{E[D(\theta_1,1.3)^{3/2}]\right\}^2\left\{E[D(\theta_3,6)^{1/2}]\right\}^2 \\
&+ (c_3^2+2c_1c_4)\left\{E[D(\theta_1,1.3)]\right\}^2\left\{E[D(\theta_3,6)]\right\}^2 \\
&+ 2c_3c_4\left\{E[D(\theta_1,1.3)^{1/2}]\right\}^2\left\{E[D(\theta_3,6)^{3/2}]\right\}^2 \\
&+ c_4^2\left\{E[D(\theta_3,6)^2]\right\}^2
\end{aligned} \tag{F11}$$

Diameter Selection Methods 1ξ–5ξ: Diameters Parallel to Plot Radius in Bitterlich Sampling

The non-uniform distribution $F_\xi(\xi; \alpha)$ of the diameter direction ξ parallel to plot radius in Bitterlich sampling, with viewing angle α, is determined at breast height. For brevity, α is omitted in the diameter moment denotations, although it essentially determines the distribution $F_\xi(\xi; \alpha)$ over which the moments are taken.

1ξ. $D(\boldsymbol{\theta}, 1.3)=D(\xi, 1.3)$ and $D(\boldsymbol{\theta}, 6)=D(\xi, 6)$, $\xi \sim F_\xi(\xi; \alpha)$:

$$\begin{aligned} E[\hat{V}_{L1\xi}(\boldsymbol{\theta})^2] &= c_2^2 E[D(\xi,1.3)^6] + 2c_1c_2 E[D(\xi,1.3)^5] + c_1^2 E[D(\xi,1.3)^4] \\ &+ 2c_2c_3 E[D(\xi,1.3)^4 D(\xi,6)] + 2c_2c_4 E[D(\xi,1.3)^3 D(\xi,6)^2] \\ &+ 2c_1c_3 E[D(\xi,1.3)^3 D(\xi,6)] + (c_3^2 + 2c_1c_4) E[D(\xi,1.3)^2 D(\xi,6)^2] \\ &+ 2c_3c_4 E[D(\xi,1.3) D(\xi,6)^3] + c_4^2 E[D(\xi,6)^4] \end{aligned} \tag{F12}$$

2ξ. $D(\boldsymbol{\theta}, 1.3)=[D(\xi, 1.3)+D(\xi+\pi/2, 1.3)]/2$ and $D(\boldsymbol{\theta}, 6)=[D(\xi, 6)+D(\xi+\pi/2, 6)]/2$, $\xi \sim F_\xi(\xi; \alpha)$:

$$\begin{aligned} E[\hat{V}_{L2\xi}(\boldsymbol{\theta})^2] &= \frac{c_2^2}{64} E\left\{ [D(\xi,1.3) + D(\xi+\pi/2,1.3)]^6 \right\} \\ &+ \frac{c_1c_2}{16} E\left\{ [D(\xi,1.3) + D(\xi+\pi/2,1.3)]^5 \right\} \\ &+ \frac{c_1^2}{16} E\left\{ [D(\xi,1.3) + D(\xi+\pi/2,1.3)]^4 \right\} \\ &+ \frac{c_2c_3}{16} E\left\{ [D(\xi,1.3) + D(\xi+\pi/2,1.3)]^4 [D(\xi,6) + D(\xi+\pi/2,6)] \right\} \\ &+ \frac{c_2c_4}{16} E\left\{ [D(\xi,1.3) + D(\xi+\pi/2,1.3)]^3 [D(\xi,6) + D(\xi+\pi/2,6)]^2 \right\} \\ &+ \frac{c_1c_3}{8} E\left\{ [D(\xi,1.3) + D(\xi+\pi/2,1.3)]^3 [D(\xi,6) + D(\xi+\pi/2,6)] \right\} \\ &+ \frac{c_3^2 + 2c_1c_4}{16} E\left\{ [D(\xi,1.3) + D(\xi+\pi/2,1.3)]^2 [D(\xi,6) + D(\xi+\pi/2,6)]^2 \right\} \\ &+ \frac{c_3c_4}{8} E\left\{ [D(\xi,1.3) + D(\xi+\pi/2,1.3)] [D(\xi,6) + D(\xi+\pi/2,6)]^3 \right\} \\ &+ \frac{c_4^2}{16} E\left\{ [D(\xi,6) + D(\xi+\pi/2,6)]^4 \right\} \end{aligned} \tag{F13}$$

3ξ. $D(\boldsymbol{\theta},1.3)=[D(\xi,1.3)D(\xi+\pi/2,1.3)]^{1/2}$ and $D(\boldsymbol{\theta},6)=[D(\xi,6)D(\xi+\pi/2,6)]^{1/2}$, $\xi\sim F_\xi(\xi;\alpha)$:

$$
\begin{aligned}
E[\hat{V}_{L3\xi}(\boldsymbol{\theta})^2] \;=\; & c_2^2E[D(\xi,1.3)^3D(\xi+\pi/2,1.3)^3] \\
& + 2c_1c_2E[D(\xi,1.3)^{5/2}D(\xi+\pi/2,1.3)^{5/2}] \\
& + c_1^2E[D(\xi,1.3)^2D(\xi+\pi/2,1.3)^2] \\
& + 2c_2c_3E[D(\xi,1.3)^2D(\xi+\pi/2,1.3)^2D(\theta,6)^{1/2}D(\xi+\pi/2,6)^{1/2}] \\
& + 2c_2c_4E[D(\xi,1.3)^{3/2}D(\xi+\pi/2,1.3)^{3/2}D(\xi,6)D(\xi+\pi/2,6)] \\
& + 2c_1c_3E[D(\xi,1.3)^{3/2}D(\xi+\pi/2,1.3)^{3/2}D(\xi,6)^{1/2}D(\xi+\pi/2,6)^{1/2}] \\
& + (c_3^2+2c_1c_4)E[D(\xi,1.3)D(\xi+\pi/2,1.3)D(\xi,6)D(\xi+\pi/2,6)] \\
& + 2c_3c_4E[D(\xi,1.3)^{1/2}D(\xi+\pi/2,1.3)^{1/2}D(\xi,6)^{3/2}D(\xi+\pi/2,6)^{3/2}] \\
& + c_4^2E[D(\xi,6)^2D(\xi+\pi/2,6)^2]
\end{aligned}
\qquad \text{(F14)}
$$

4ξ. $D(\boldsymbol{\theta},1.3)=[D(\xi,1.3)+D(\theta,1.3)]/2$ and $D(\boldsymbol{\theta},6)=[D(\xi,6)+D(\theta,6)]/2$, $\xi\sim F_\xi(\xi;\alpha)$, $\theta\sim\text{Unif}(0,\pi)$, ξ and θ independent:

$$
\begin{aligned}
E[\hat{V}_{L4\xi}(\boldsymbol{\theta})^2] \;=\; & \frac{c_2^2}{64}\Big\{ E[D(\xi,1.3)^6]+E[D(\theta,1.3)^6] \\
& + 6E[D(\xi,1.3)^5]E[D(\theta,1.3)] + 6E[D(\xi,1.3)]E[D(\theta,1.3)^5] \\
& + 15E[D(\xi,1.3)^4]E[D(\theta,1.3)^2] + 15E[D(\xi,1.3)^2]E[D(\theta,1.3)^4] \\
& + 20E[D(\xi,1.3)^3]E[D(\theta,1.3)^3]\Big\} \\
& + \frac{c_1c_2}{16}\Big\{ E[D(\xi,1.3)^5]+E[D(\theta,1.3)^5] \\
& + 5E[D(\xi,1.3)^4]E[D(\theta,1.3)] + 5E[D(\xi,1.3)]E[D(\theta,1.3)^4] \\
& + 10E[D(\xi,1.3)^3]E[D(\theta,1.3)^2] + 10E[D(\xi,1.3)^2]E[D(\theta,1.3)^3]\Big\} \\
& + \frac{c_1^2}{16}\Big\{ E[D(\xi,1.3)^4]+E[D(\theta,1.3)^4] \\
& + 4E[D(\xi,1.3)^3]E[D(\theta,1.3)] + 4E[D(\xi,1.3)]E[D(\theta,1.3)^3] \\
& + 6E[D(\xi,1.3)^2]E[D(\theta,1.3)^2]\Big\} \\
& + \frac{c_2c_3}{16}\Big\{ E[D(\xi,1.3)^4D(\xi,6)]+E[D(\theta,1.3)^4D(\theta,6)] \\
& + E[D(\xi,1.3)^4]E[D(\theta,6)] + E[D(\theta,1.3)^4]E[D(\xi,6)] \\
& + 4E[D(\xi,1.3)^3D(\xi,6)]E[D(\theta,1.3)] + 4E[D(\xi,1.3)^3]E[D(\theta,1.3)D(\theta,6)] \\
& + 4E[D(\xi,1.3)D(\xi,6)]E[D(\theta,1.3)^3] + 4E[D(\xi,1.3)]E[D(\theta,1.3)^3D(\theta,6)] \\
& + 6E[D(\xi,1.3)^2D(\xi,6)]E[D(\theta,1.3)^2] + 6E[D(\xi,1.3)^2]E[D(\theta,1.3)^2D(\theta,6)]\Big\}
\end{aligned}
$$

$$
\begin{aligned}
&+\frac{c_2c_4}{16}\Big\{ E[D(\xi,1.3)^3D(\xi,6)^2]+E[D(\theta,1.3)^3D(\theta,6)^2] \\
&+E[D(\xi,1.3)^3]E[D(\theta,6)^2]+E[D(\theta,1.3)^3]E[D(\xi,6)^2] \\
&+2E[D(\xi,1.3)^3D(\xi,6)]E[D(\theta,6)]+2E[D(\theta,1.3)^3D(\theta,6)]E[D(\xi,6)] \\
&+3E[D(\xi,1.3)^2D(\xi,6)^2]E[D(\theta,1.3)]+3E[D(\theta,1.3)^2D(\theta,6)^2]E[D(\xi,1.3)] \\
&+6E[D(\xi,1.3)^2D(\xi,6)]E[D(\theta,1.3)D(\theta,6)] \\
&+6E[D(\theta,1.3)^2D(\theta,6)]E[D(\xi,1.3)D(\xi,6)] \\
&+3E[D(\xi,1.3)D(\xi,6)^2]E[D(\theta,1.3)^2]+3E[D(\theta,1.3)D(\theta,6)^2]E[D(\xi,1.3)^2]\Big\} \\
&+\frac{c_1c_3}{8}\Big\{ E[D(\xi,1.3)^3D(\xi,6)]+E[D(\theta,1.3)^3D(\theta,6)] \\
&+E[D(\xi,1.3)^3]E[D(\theta,6)]+E[D(\theta,1.3)^3]E[D(\xi,6)] \\
&+3E[D(\xi,1.3)^2D(\xi,6)]E[D(\theta,1.3)]+3E[D(\theta,1.3)^2D(\theta,6)]E[D(\xi,1.3)] \\
&+3E[D(\xi,1.3)D(\xi,6)]E[D(\theta,1.3)^2]+3E[D(\theta,1.3)D(\theta,6)]E[D(\xi,1.3)^2]\Big\} \\
&+\frac{c_3^2+2c_1c_4}{16}\Big\{ E[D(\xi,1.3)^2D(\xi,6)^2]+E[D(\theta,1.3)^2D(\theta,6)^2] \\
&+E[D(\xi,1.3)^2]E[D(\theta,6)^2]+E[D(\theta,1.3)^2]E[D(\xi,6)^2] \\
&+2E[D(\xi,1.3)^2D(\xi,6)]E[D(\theta,6)]+2E[D(\theta,1.3)^2D(\theta,6)]E[D(\xi,6)] \\
&+2E[D(\xi,1.3)D(\xi,6)^2]E[D(\theta,1.3)]+2E[D(\theta,1.3)D(\theta,6)^2]E[D(\xi,1.3)] \\
&+4E[D(\xi,1.3)D(\xi,6)]E[D(\theta,1.3)D(\theta,6)]\Big\} \\
&+\frac{c_3c_4}{8}\Big\{ E[D(\xi,1.3)D(\xi,6)^3]+E[D(\theta,1.3)D(\theta,6)^3] \\
&+E[D(\xi,1.3)]E[D(\theta,6)^3]+E[D(\theta,1.3)]E[D(\xi,6)^3] \\
&+3E[D(\xi,1.3)D(\xi,6)^2]E[D(\theta,6)]+3E[D(\theta,1.3)D(\theta,6)^2]E[D(\xi,6)] \\
&+3E[D(\xi,1.3)D(\xi,6)]E[D(\theta,6)^2]+3E[D(\theta,1.3)D(\theta,6)]E[D(\xi,6)^2]\Big\} \\
&+\frac{c_4^2}{16}\Big\{ E[D(\xi,6)^4]+E[D(\theta,6)^4] \\
&+4E[D(\xi,6)^3]E[D(\theta,6)]+4E[D(\theta,6)^3]E[D(\xi,6)] \\
&+6E[D(\xi,6)^2]E[D(\theta,6)^2]\Big\}
\end{aligned}
\tag{F15}
$$

5ξ. $D(\boldsymbol{\theta}, 1.3)=[D(\xi, 1.3)D(\theta, 1.3)]^{1/2}$ and $D(\boldsymbol{\theta}, 6)=[D(\xi, 6)D(\theta, 6)]^{1/2}$, $\xi \sim F_{\xi}(\xi; \alpha)$, $\theta \sim \text{Unif}(0, \pi)$, ξ and θ independent:

$$\begin{aligned}
E[\hat{V}_{L5\xi}(\boldsymbol{\theta})^2] = {} & c_2^2 E[D(\xi, 1.3)^3]E[D(\theta, 1.3)^3] \\
& + 2c_1c_2 E[D(\xi, 1.3)^{5/2}]E[D(\theta, 1.3)^{5/2}] \\
& + c_1^2 E[D(\xi, 1.3)^2]E[D(\theta, 1.3)^2] \\
& + 2c_2c_3 E[D(\xi, 1.3)^2 D(\xi, 6)^{1/2}]E[D(\theta, 1.3)^2 D(\theta, 6)^{1/2}] \\
& + 2c_2c_4 E[D(\xi, 1.3)^{3/2} D(\xi, 6)]E[D(\theta, 1.3)^{3/2} D(\theta, 6)] \\
& + 2c_1c_3 E[D(\xi, 1.3)^{3/2} D(\xi, 6)^{1/2}]E[D(\theta, 1.3)^{3/2} D(\theta, 6)^{1/2}] \\
& + (c_3^2 + 2c_1c_4)E[D(\xi, 1.3)D(\xi, 6)]E[D(\theta, 1.3)D(\theta, 6)] \\
& + 2c_3c_4 E[D(\xi, 1.3)^{1/2} D(\xi, 6)^{3/2}]E[D(\theta, 1.3)^{1/2} D(\theta, 6)^{3/2}] \\
& + c_4^2 E[D(\xi, 6)^2]E[D(\theta, 6)^2]
\end{aligned} \tag{F16}$$

Diameter Selection Methods 1ξ90, 4ξ90 and 5ξ90: Diameters Perpendicular to Plot Radius in Bitterlich Sampling

1ξ90. $D(\boldsymbol{\theta}, 1.3)=D(\xi+\pi/2, 1.3)$ and $D(\boldsymbol{\theta}, 6)=D(\xi+\pi/2, 6)$, $\xi \sim F_{\xi}(\xi; \alpha)$: to obtain $E[\hat{V}_{L1\xi 90}(\boldsymbol{\theta})^2]$, substitute $D(\xi+\pi/2, 1.3)$ for $D(\xi, 1.3)$ and $D(\xi+\pi/2, 6)$ for $D(\xi, 6)$ in Eq. F12.

4ξ90. $D(\boldsymbol{\theta}, 1.3)=[D(\xi+\pi/2, 1.3)+D(\theta, 1.3)]/2$ and $D(\boldsymbol{\theta}, 6)=[D(\xi+\pi/2, 6)+D(\theta, 6)]/2$, $\xi \sim F_{\xi}(\xi; \alpha)$, $\theta \sim \text{Unif}(0, \pi)$, ξ and θ independent: to obtain $E[\hat{V}_{L4\xi 90}(\boldsymbol{\theta})^2]$, substitute $D(\xi+\pi/2, 1.3)$ for $D(\xi, 1.3)$ and $D(\xi+\pi/2, 6)$ for $D(\xi, 6)$ in Eq. F15.

5ξ90. $D(\boldsymbol{\theta}, 1.3)=[D(\xi+\pi/2, 1.3)D(\theta, 1.3)]^{1/2}$ and $D(\boldsymbol{\theta}, 6)=[D(\xi+\pi/2, 6)D(\theta, 6)]^{1/2}$, $\xi \sim F_{\xi}(\xi; \alpha)$, $\theta \sim \text{Unif}(0, \pi)$, ξ and θ independent: to obtain $E[\hat{V}_{L5\xi 90}(\boldsymbol{\theta})^2]$, substitute $D(\xi+\pi/2, 1.3)$ for $D(\xi, 1.3)$ and $D(\xi+\pi/2, 6)$ for $D(\xi, 6)$ in Eq. F16.

Appendix G. Computation of Diameters, Breadths and Radii from Vector Image of Cross-Section

In scanning, the photographs of the cross-sections were rotated in the way that the mark indicating the plot radius direction was always located on the left side of the image. In the vector image, the origin of the co-ordinate system was then placed in the lower left corner of the image and the y-axis and x-axis were set to run parallel to the left and lower side of the image, respectively (Fig. 26 C in Chapter 6).

The computation of the diameters, breadths and radii of a cross-section was based on (i) the co-ordinates of the contour points of the cross-section and its convex closure (vector images), (ii) the co-ordinates of the centres of gravity of the cross-section, its convex closure and the mark indicating the plot radius direction, and (iii) the plot radius direction (the direction from the plot centre to the assumed tree pith that can be thought to correspond to the centre of gravity of the cross-section) with respect to N–S direction as measured in the field. As a preprocessing for the breadth and radius computation, the "gaps" in the contour point co-ordinate lists were filled by linear interpolation so that a transition from one pixel to the next one was horizontally and vertically not longer than one pixel edge length.

The diameters, breadths and radii of a cross-section and its convex closure were computed using elementary analytical Euclidean geometry in $\mathbb{R}^2$ (see e.g. Ryan 1982). The *diameter* of a cross-section (or equivalently of its convex closure) *in plot radius direction* was defined here as the distance between two parallel tangents perpendicular to the ray emanating from the plot centre (at the plane of the tree cross-section) to the centre of gravity of the cross-section (Fig. G1). To compute this, the direction angle ξ of the plot radius with respect to the x-axis of the image was first determined as

$$\xi = \tan^{-1}\left(\frac{y_{cg} - y_{pr}}{x_{cg} - x_{pr}}\right), \tag{G1}$$

where (x_{cg}, y_{cg}) and (x_{pr}, y_{pr}) are the centres of gravity of the cross-section and the mark indicating the plot radius direction, respectively (Fig. G1). The slope of any straight line

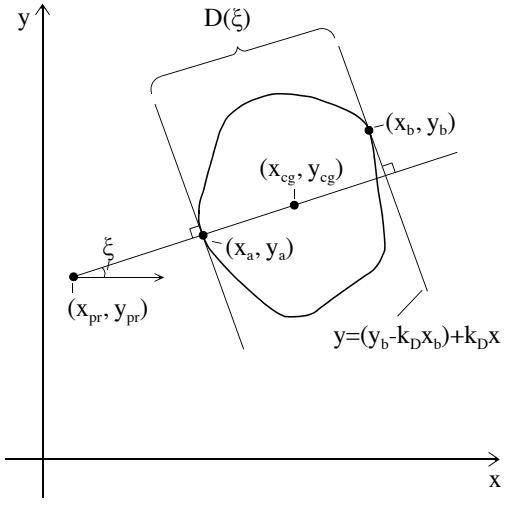

Fig. G1. Computing the diameter $D(\xi)$ of a cross-section in plot radius direction: (x_{pr}, y_{pr}) is the point indicating the plot radius direction, (x_{cg}, y_{cg}) is the centre of gravity of the cross-section, ξ is the direction of plot radius with respect to the x-axis, (x_a, y_a) and (x_b, y_b) are the points in which the tangents perpendicular to ξ touch the contour of the cross-section, and $y=(y_b-k_Dx_b)+k_Dx$ is the equation of the one of those tangents that passes through (x_b, y_b).

parallel to the plot radius was now tanξ, and since the product of the slopes of two perpendicular lines is always –1, the slope of the tangents perpendicular to plot radius became

$$k_D = -\frac{1}{\tan(\xi)} . \quad \text{(G2)}$$

The two points (x_a, y_a) and (x_b, y_b) in which the two tangents with the slope k_D touched the contour of the cross-section (Fig. G1) were found among all the contour points (x, y) as those that yielded the minimum and the maximum value for the intercept k_0 a when substituted in the tangent line equation $y=k_0+k_Dx$. The diameter D(ξ) was then computed as the distance between the point (x_a, y_a) and the tangent $y=(y_b–k_Dx_b)+k_Dx$ passing through (x_b, y_b):

$$D(\xi) = \frac{|k_D x_a - y_a + (y_b - k_D x_b)|}{\sqrt{k_D^2 + 1}} . \quad \text{(G3)}$$

The diameter perpendicular to plot radius was obtained by using the angle ξ+π/2 in computing k_D, (x_a, y_a), (x_b, y_b), and finally D(ξ+π/2).

This procedure was then applied to compute the *180 systematic diameters* in a cross-section, defined to start from the N–S direction and be taken at rotation intervals of π/180. For this, the direction angle β of the N–S line with respect to the x-axis in the image was required. By field measurements, the direction angle ψ of the plot radius (from the plot centre to the assumed tree pith) was known with respect to the N–S direction; as a compass bearing, ψ increased clockwise (i.e., in N ψ=0, in E ψ=π/2, in S ψ=π, and in W ψ=3π/2). In order to compute β from ψ, two steps were taken. First, ψ was transformed into the direction angle

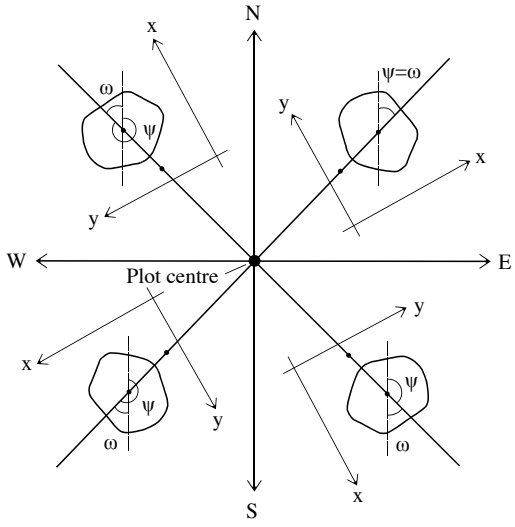

Fig. G2. Determination of the direction angle ω of the N–S line with respect to the plot radius (the line between the plot centre and the centre of gravity of the tree cross-section), by using the compass bearing ψ of the tree taken from the plot centre. The co-ordinate axes imitate those of the vector images.

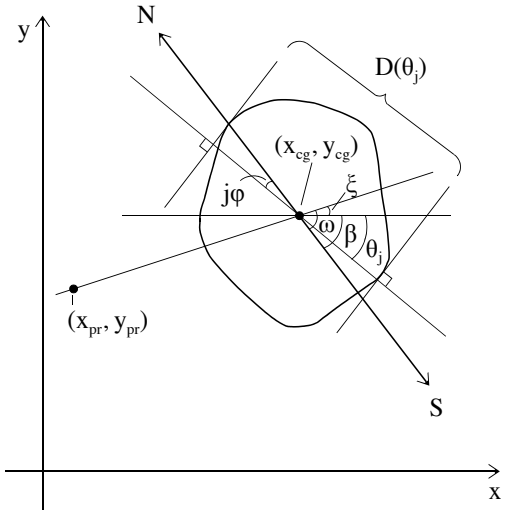

Fig. G3. Determination of the diameters $D(\theta_j)$ at systematic rotation angles $\theta_j=\beta+j\varphi$ with respect to the N–S direction: (x_{cg}, y_{cg}) is the centre of gravity of the cross-section and (x_{pr}, y_{pr}) is the point indicating the plot radius direction, ω denotes the direction angle of the N–S line with respect to the plot radius, ξ denotes the direction angle of the plot radius with respect to the x-axis in the image, and β denotes the direction angle of the N–S line with respect to the x-axis in the image. In this study, $\varphi=\pi/180$ and $j=1, ..., 179$. (Note that in this figure, ω, β, and θ_j are negative.)

$\omega \in [-\pi/2, \pi/2]$ of the N–S line with respect to the plot radius direction; the transformation depended on which quadrant of compass circle the tree was located (Fig. G2):

$$\omega = \begin{cases} \psi, & 0 \le \psi < \dfrac{\pi}{2} \\ \psi - \pi, & \dfrac{\pi}{2} \le \psi < \dfrac{3\pi}{2} \\ \psi - 2\pi, & \dfrac{3\pi}{2} \le \psi < 2\pi \ . \end{cases} \tag{G4}$$

Second, ω was combined with the direction angle ξ of the plot radius determined with respect to the x-axis in the image (Eq. G1) to obtain the direction angle β of the N–S line with respect to the x-axis of the image (Fig. G3):

$$\beta = \begin{cases} \omega + \xi + \pi, & \omega + \xi < -\dfrac{\pi}{2} \\ \omega + \xi, & -\dfrac{\pi}{2} \le \omega + \xi \le \dfrac{\pi}{2} \\ \omega + \xi - \pi, & \omega + \xi > \dfrac{\pi}{2} \ . \end{cases} \tag{G5}$$

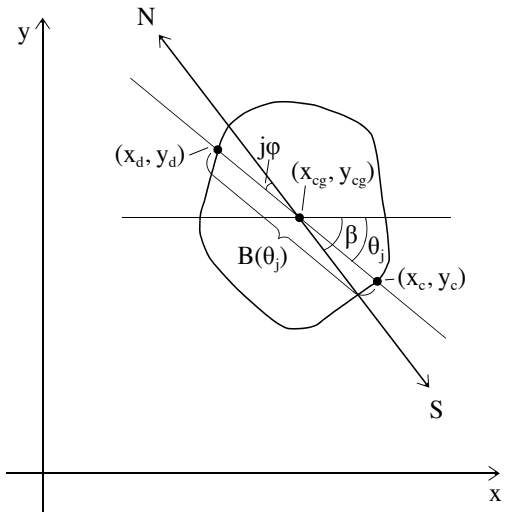

Fig. G4. Determination of the breadths $B(\theta_j)$ at systematic rotation angles $\theta_j=\beta+j\varphi$ with respect to the N–S direction: (x_{cg}, y_{cg}) is the centre of gravity of the cross-section, β denotes the direction angle of the N–S line passing through (x_{cg}, y_{cg}), and (x_c, y_c) and (x_d, y_d) are the points where the line with direction angle θ_j and passing through (x_{cg}, y_{cg}) intersects the contour of the cross-section. In this study, $\varphi=\pi/180$ and j=1, ..., 179.

Now the angles of the 180 systematic diameters with the rotation angle interval φ and with the N–S direction as the reference direction were obtained as (Fig. G3)

$$\theta_j = \beta + j\varphi \,, \tag{G6}$$

where j=0, 1, ..., 179, and $\varphi=\pi/180$. The diameters were then computed by the procedure described above: for each θ_j, the slope

$$k_{Dj} = -\frac{1}{\tan(\theta_j)} \tag{G7}$$

of the tangents perpendicular to θ_j was determined, the points of contact of the two parallel tangents with the cross-section contour found, and the diameter computed as the distance between one of these points and the tangent passing through the other.

In the computation of the breadths and radii, the above 180 systematic angles (Eq. G6) were used. The *breadth* of a cross-section in direction θ_j was here defined as the distance between the points in which the straight line passing in direction θ_j through the centre of gravity (x_{cg}, y_{cg}) of the cross-section intersected the contour of the cross-section (Fig. G4). The slope of this breadth line was

$$k_{Bj} = \tan(\theta_j) \,, \tag{G8}$$

and since it was to go through (x_{cg}, y_{cg}), its equation could be expressed as $y=(y_{cg}–k_{Bj}\,x_{cg})+k_{Bj}\,x$. Next, the points (x_c, y_c) and (x_d, y_d) most closely satisfying the breadth line equation were

found among the discrete contour points, and the breadth was then obtained as the distance between these points:

$$B(\theta_j) = \sqrt{(x_c - x_d)^2 + (y_c - y_d)^2} \ . \tag{G9}$$

A total of 180 breadths were computed for both the cross-section and its convex closure.

The *radius* of a cross-section in direction θ_j was here defined as the distance from the centre of gravity (x_{cg}, y_{cg}) to the point where the ray emanating from (x_{cg}, y_{cg}) in direction θ_j intersected the contour of the cross-section. From each pair of points (x_c, y_c) and (x_d, y_d) determined above for both the cross-section and its convex closure, a pair of radii in directions θ_j and $\theta_j+\pi$ were obtained as

$$R(\theta_j) = \sqrt{(x_c - x_{cg})^2 + (y_c - y_{cg})^2} \tag{G10}$$

and

$$R(\theta_j + \pi) = \sqrt{(x_d - x_{cg})^2 + (y_d - y_{cg})^2} \ , \tag{G11}$$

making a total of 360 radii for both the cross-section and its convex closure.

Appendix H. Computation of Contour Co-ordinates, Sector Areas and Total Area of Inclusion Region in Bitterlich Sampling from Vector Image of Cross-Section

In each cross-section vector image, the co-ordinate system was set and the direction angle β of the N–S line determined with respect to the image x-axis in the way explained in Appendix G. For each cross-section, the inclusion region contour, sector areas and total area were computed using the following four viewing angle values: 1.146°, 1.621°, 2.292° and 3.624° (corresponding, with circular cross-sections, to the basal area factor values of 1, 2, 4, and 10 m^2/ha, respectively).

In Bitterlich sampling with viewing angle α, the contour of the inclusion region is composed of the intersection points of the cross-section tangents (the convex closure tangents) intersecting each other at angle α. If υ is the direction angle of *the right-hand-side tangent* (when viewed at the intersection point) with respect to the x-axis, the direction angle of the left-hand-side tangent becomes υ+α (Fig. H1), and the slopes of the tangent equations are then tanυ and tan(α+υ), respectively. The intercepts of the tangent equations naturally vary along with the slopes. If the tangent equations are

$$\begin{cases} y = a + x\tan\upsilon \\ y = b + x\tan(\upsilon+\alpha)\,, \end{cases} \tag{H1}$$

their intersection point becomes

$$\begin{cases} x = \dfrac{b-a}{\tan\upsilon - \tan(\upsilon+\alpha)} \\ y = a + (b-a)\dfrac{\tan\upsilon}{\tan\upsilon - \tan(\upsilon+\alpha)}\,. \end{cases} \tag{H2}$$

In this study, each inclusion region was determined by computing 3600 contour points (tangent intersection points): The direction angle of the right-hand-side tangent was set to

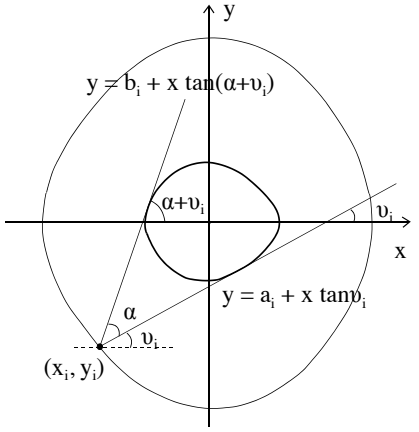

Fig. H1. In Bitterlich sampling with viewing angle α, the contour of the inclusion region consists of the points at which cross-section tangents intersect each other at angle α. If the direction angle of the right-hand-side tangent is υ_i, the direction angle of the left-hand-side tangent becomes $\alpha+\upsilon_i$. The slopes ($\tan\upsilon_i$ and $\tan(\alpha+\upsilon_i)$) and the intercepts (a_i and b_i) of the tangent equations depend on the value of υ_i (and α); by varying υ_i, we get a set of contour points (x_i, y_i).

increase systematically, starting from the N–S direction (direction angle β, see Appendix G), as

$$\upsilon_i = \beta + i\varphi \,, \tag{H3}$$

where i=0, 1, ..., 3599, and φ=π/1800. The intercept a_i of each right-hand-side tangent $y=a_i+x\tan\upsilon_i$ was determined by computing $y-x\tan\upsilon_i$ with all the cross-section contour points (x, y) and by taking either the minimum or the maximum value (depending on the quadrant in which υ_i was residing). The intercept b_i of each left-hand-side tangent $y=b_i+x\tan(\upsilon_i+\alpha)$ was determined in a similar manner. Finally, the co-ordinates of the inclusion region contour points (x_i, y_i) were obtained by substituting υ_i, a_i, $\upsilon_i+\alpha$ and b_i in Eq. H2.

From the inclusion region contour points (x_i, y_i), the corresponding inclusion region radii were determined as the line segments to the centre of gravity (x_{cg}, y_{cg}) of the cross-section. The directions of these radii were obtained as

$$\theta_i = \tan^{-1}\left(\frac{y_{cg}-y_i}{x_{cg}-x_i}\right), \tag{H4}$$

and the lengths as

$$r(\theta_i) = \sqrt{(x_{cg}-x_i)^2 + (y_{cg}-y_i)^2} \,, \tag{H5}$$

i=0, 1, ..., 3599. Clearly, the angles between the radii varied, that is, the radii were not located at regular angular intervals starting from the N–S direction.

In order to estimate the direction distributions of the Bitterlich diameters (the diameters parallel or perpendicular to plot radius direction in Bitterlich sampling), we needed the areas of the contiguous inclusion region sectors around the 360 systematic cross-section radius directions $\tau_j=\beta+j\varphi$, j=0, 1, ..., 359, φ=π/180, starting from the N–S direction β. The sides of the sectors were formed by the inclusion region radii with directions $\tau_j-\varphi/2$ and $\tau_j+\varphi/2$ (Fig. H2). As none of the 3600 previously determined radii necessarily coincided with the sector side radii, their lengths had to be estimated separately. The points where the sector sides intersected the inclusion region contour (the end points of the sector side radii) were determined with linear interpolation between the end points of the two nearest inclusion region radii among the 3600 previously determined ones (Fig. H2). Let $r(\theta_1)$ and $r(\theta_2)$ denote the lengths of the radii (with directions θ_1 and θ_2) that are closest to the right-hand side of the sector, the length of which we denote by $r(\tau_j-\varphi/2)$. The corresponding contour points closest to the sector side end point $(x, y)=(r(\tau_j-\varphi/2)\cos(\tau_j-\varphi/2), r(\tau_j-\varphi/2)\sin(\tau_j-\varphi/2))$ are then $(x_1, y_1)=(r(\theta_1)\cos\theta_1, r(\theta_1)\sin\theta_1)$ and $(x_2, y_2)=(r(\theta_2)\cos\theta_2, r(\theta_2)\sin\theta_2)$. By linear interpolation, the y co-ordinate of the sector side end point becomes (Fig. H2 B)

$$\begin{aligned} y &= y_1 + \frac{y_2-y_1}{x_2-x_1}(x-x_1) \;\Leftrightarrow \\ r(\tau_j-\varphi/2)\sin(\tau_j-\varphi/2) &= r(\theta_1)\sin\theta_1 \\ &\quad + \frac{r(\theta_2)\sin\theta_2 - r(\theta_1)\sin\theta_1}{r(\theta_2)\cos\theta_2 - r(\theta_1)\cos\theta_1}\left[r(\tau_j-\varphi/2)\cos(\tau_j-\varphi/2) - r(\theta_1)\cos\theta_1\right], \end{aligned} \tag{H6}$$

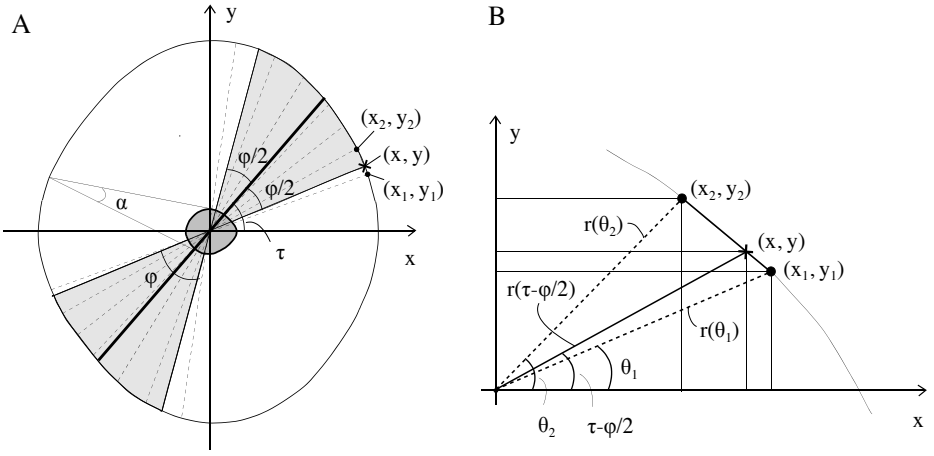

Fig. H2. Estimating, in Bitterlich sampling with viewing angle α, the area of the inclusion region sectors around the directions τ and τ+π and of angular width φ, by using the 3600 radii computed before to determine the inclusion region (dashed lines, in reality with angular interval π/1800, i.e., much closer to each other than in this illustration; note that the inclusion region contour consists of the line segments between the end points of these radii) (A): the area of the sector is estimated by summing up the areas of the contiguous triangles with the known radii as their the sides. As none of the known radii necessarily coincides with the sector sides in directions τ-φ/2 and τ+φ/2 (or τ+π-φ/2 and τ+π+φ/2), the sector sides are determined by means of the nearest known radii (B): the point (x, y) where the sector side with direction τ-φ/2 and length r(τ-φ/2) intersects the inclusion region contour is obtained with linear interpolation between (x_1, y_1) and (x_2, y_2), the end points of the closest radii with directions θ_1 and θ_2 and lengths $r(\theta_1)$ and $r(\theta_2)$.

from which the sector side length is solved as

$$r(\tau_j - \varphi/2) = \frac{r(\theta_1)(\sin\theta_1 - k\cos\theta_1)}{\sin(\tau_j - \varphi/2) - k\cos(\tau_j - \varphi/2)}, \quad \text{(H7)}$$

where

$$k = \frac{r(\theta_2)\sin\theta_2 - r(\theta_1)\sin\theta_1}{r(\theta_2)\cos\theta_2 - r(\theta_1)\cos\theta_1}. \quad \text{(H8)}$$

The length $r(\tau_j+\varphi/2)$ of the left-hand side of the sector was determined in a similar manner. The sector area was estimated as the sum of the areas of the narrow contiguous triangles formed by the previously determined radii or sector sides (Fig. H2). If the side lengths of a triangle are $r(\theta_{i-1})$ and $r(\theta_i)$ with the angle $|\theta_i - \theta_{i-1}|$ between them, the area is given by

$$A_i = \frac{1}{2} r(\theta_{i-1}) r(\theta_i) \sin|\theta_i - \theta_{i-1}|. \quad \text{(H9)}$$

The total inclusion area was estimated as the sum of the 360 sector areas.

The direction distributions of the Bitterlich diameters were estimated in a discretised form, with point probabilities associated to the 180 systematic diameter directions $\xi_j=\beta+j\varphi$, $j=0, 1, ..., 179$, $\varphi=\pi/180$, starting from the N–S direction β. For each direction ξ_j, the probability mass was estimated as the summed area of the two sectors of angular width φ around the directions τ_j and $\tau_{j+180}=\tau_j+\pi$ divided by the total inclusion area.

Appendix I. Computation of Scale in Vector Image of Cross-Section

Although two fixed distances between the camera lens and the plane under the disc were applied (632 mm for the discs with the diameter up to 15 cm, and 982 mm for the discs larger than that), the camera was focused separately on each disc due to the variation in disc thickness, and therefore also the scale had to be computed separately for each disc.

The determination of the scale — defined as the proportion of the disc dimensions in reality to those in the photograph (raster image) — was complicated by two faults in the photographing and printing procedure: First, when taking the photographs, the ruler was placed on the same plane as the disc bottom, as a result of which it ended up about 3 cm (disc thickness) farther from the camera lens than the disc surface. Hence, we could not attain the scale straightforwardly by measuring in pixels the length of a 10-cm piece of the ruler in the photograph but had to resort to the lens equation and the disc thickness measurements. Second, due to some misunderstanding between the author and the technician who developed and printed the photographs, the sizing in the print-making phase was not accurate but the negative was occasionally slightly cropped (i.e., the 10 cm × 15 cm sized print did not cover the whole 24 mm × 36 mm sized negative, but some part of the edges were left out), whereupon the cross-section in the photograph became larger than it should have been. Hence, we could not compute the scale straightforwardly by means of the lens equation and the disc thickness measurements either but had to reverse the two independent sizing operations that had taken place in the photograph-making procedure (Fig. I1): the shrinking from the real disc to the film negative (1), and the enlarging from the film negative to the photograph print (2).

The determination of the scale between the real disc and the film negative was based on the *lens equation* of basic optics; as the camera was focused not on the ruler but on the disc surface, we applied the equation to the disc. Let f denote the focal distance of the lens system of the camera, a be the distance of the disc surface from (the middle plane of) the lens, and b stand for the distance between the image produced on the film negative and the lens (Fig. I2). For an accurate image it holds that

$$\frac{1}{f} = \frac{1}{a} + \frac{1}{b} \;\Leftrightarrow\; b = \frac{af}{a-f} \tag{I1}$$

(Pedrotti and Pedrotti 1987). Let r and n then denote the dimensions of the disc in reality and in the film negative, respectively. From the equiform triangles of Fig. I2, their proportion (the inverse of the *line magnification*) is found to be

$$\frac{r}{n} = \frac{a}{b}\,. \tag{I2}$$

Combined with the lens equation (Eq. I1), the scale hence becomes

$$\frac{r}{n} = \frac{a}{b} = \frac{a-f}{f}\,. \tag{I3}$$

In this study, the focal distance f of the camera was 50 mm. The distance between the lens and the plane on which the disc was lying was either 632 mm or 982 mm depending on the size of the disc; from this, the distance a between the camera lens and the upper surface of the disc was obtained by subtracting the disc thickness. As the disc thickness we used the mean of the thickness measurements made on each disc in four points at the edge (at

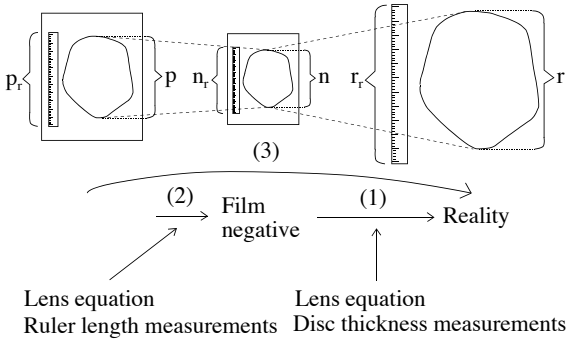

Fig. I1. The independent components (1) and (2) of the scale computation (3); p, n and r denote the dimensions of the cross-section in reality, in the film negative, and in the photograph, respectively; p_r, n_r and r_r stand for those of the ruler.

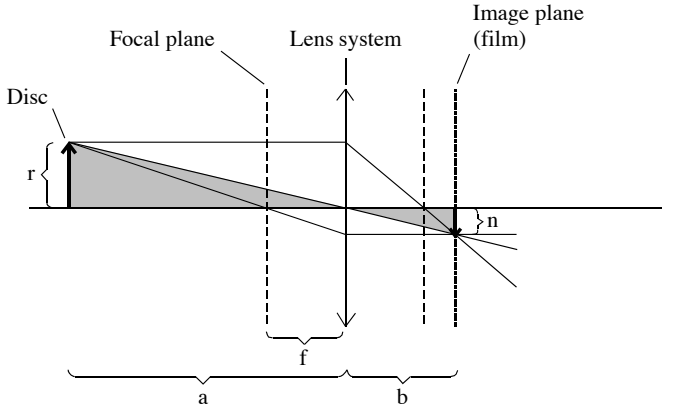

Fig. I2. The simplified principle of the image formation in a camera; f is the focal distance of the lens system, r and n are the dimensions of the object in reality and in the image (film), respectively, and a and b are the distances of the middle plane of the lens system from the object and the image, respectively.

regular rotation angle intervals of $\pi/2$ radians and starting from the plot radius direction); radial displacement calculations showed that the observed within-disc variation in thickness had no noteworthy effect on the scale.

The determination of the scale between the film negative and the photograph was based on the ruler length measurement in the photograph. As the ruler was located farther from the camera lens system than the disc surface on which the camera was focused, the accurate image of the ruler was formed in front of the film (Fig. I3):

$$\frac{1}{f} = \frac{1}{a_r} + \frac{1}{b_r} \;\Leftrightarrow\; b_r = \frac{a_r f}{a_r - f} < b\,, \tag{I4}$$

where a_r and b_r are the distances of the ruler and its accurate image from (the middle plane of) the lens system, respectively. The image of the ruler formed on the film (on the

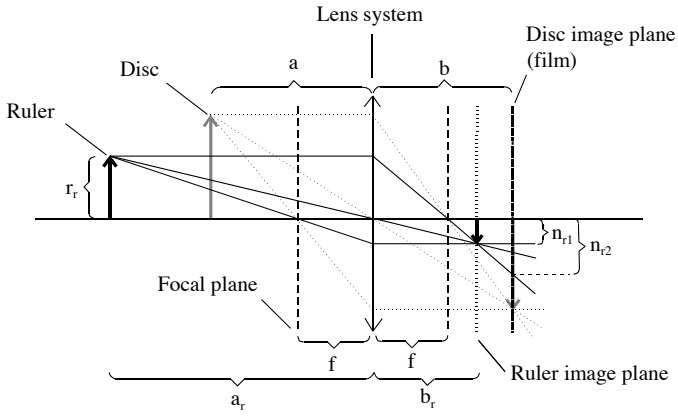

Fig. I3. The formation of the image of the ruler (located lower than the disc surface on which the camera was focused) on the disc image plane; a_r is the distance between the ruler surface and the middle plane of the lens system, b_r stands for the distance of the accurate image of the ruler from the middle plane of the lens system, and n_{r1} and n_{r2} denote the smallest and the largest images of the ruler produced on the film; other notations as in Fig. I2.

disc image plane) then became somewhat diffuse, as it in fact consisted of a multitude of images (Fig. I3). Let r_r denote the length of the ruler in reality, and n_{r1} and n_{r2} stand for the ruler length in the smallest and the largest ruler images on the film, respectively. From the equiform triangles of Fig. I3 and the lens equations (Eqs. I1 and I4) we find that

$$\frac{n_{r1}}{r_r} = \frac{b_r}{a_r} \Leftrightarrow n_{r1} = r_r \frac{f}{a_r - f}, \tag{I5}$$

and

$$\frac{n_{r2}}{r_r} = \frac{b - f}{f} \Leftrightarrow n_{r2} = r_r \frac{f}{a - f}. \tag{I6}$$

As the length measurement was taken in principle not at the utmost outer edge but in the *middle* of the border of the ruler in the photograph, we decided to employ the arithmetic mean of these extremities as the ruler length in the film negative:

$$n_r = \frac{n_{r1} + n_{r2}}{2} = r_r \frac{(a_r + a)f - 2f^2}{2(a_r - f)(a - f)}. \tag{I7}$$

The scale between the film negative and the photograph was then found to be

$$\frac{n}{p} = \frac{n_r}{p_r} = \frac{r_r}{p_r} \cdot \frac{(a_r + a)f - 2f^2}{2(a_r - f)(a - f)}, \tag{I8}$$

where p and p_r are the dimensions in pixels of the cross-section and the ruler in the photograph, respectively. As mentioned before, the length r_r of the ruler in reality was 10 cm,

the focal distance f was 50 mm, and the distance a between the disc surface and the camera lens either 632 mm or 982 mm minus the mean disc thickness; further, as the ruler thickness was 2 mm, the distance a_r between the ruler surface and the middle plane of the camera lens was either 630 mm or 980 mm depending on the size of the disc.

Finally, by combining the scale components (Eqs. I3 and I8), we attained the scale between the dimensions of the real disc r and those of the cross-section in the photograph p:

$$\frac{r}{p} = \frac{r}{n} \cdot \frac{n}{p} = \frac{a-f}{f} \cdot \frac{r_r}{p_r} \cdot \frac{(a_r+a)f-2f^2}{2(a_r-f)(a-f)} = \frac{r_r}{p_r} \cdot \frac{(a_r+a)-2f}{2(a_r-f)} \,. \tag{I9}$$

Naturally, the scale of areas was obtained as the square of this scale of lengths.

Appendix K. Examples of Association Between Some Shape Indices and Actual Shapes of Cross-Sections

In Figs. K1–K7, we display those convex closures or true cross-sections in our data that exhibited the extreme or median values of the shape indices (Sections 7.1.1 and 8.2.1) and the convex and isoperimetric deficits (Sections 7.1.2, 7.2, 8.2.2 and 8.3.1). In Fig. K8, we show the four convex closures that were assessed, on the basis of the values of the shape indices, as the most elliptic in the data (Section 8.2.1). The contours are scaled into approximately the same size. For each convex closure or cross-section, identification information (cf. Table 10 and Fig. 22 in Chapter 6) as well as the values of the indices and deficits are given in Table K1.

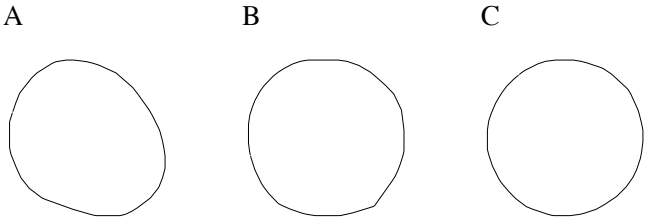

Fig. K1. Convex closures where the diameter coefficient of variation (CV_D) assumed its (A) maximum (9.94%), (B) median (1.73%) and (C) minimum (0.37%) value.

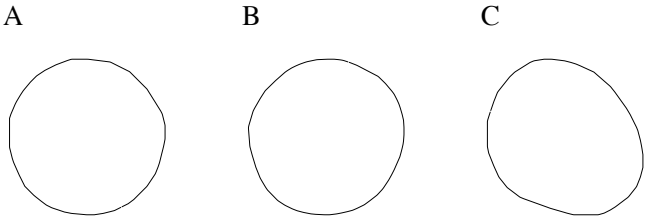

Fig. K2. Convex closures where the ratio between the minimum and the maximum diameter (D_{min}/D_{max}) assumed its (A) maximum (98.5%), (B) median (94.4%) and (C) minimum (73.4%) value.

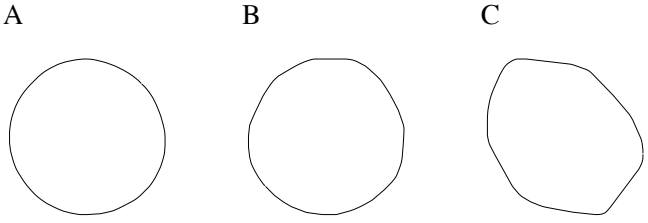

Fig. K3. Convex closures where the girth-area ellipse ratio (b_e/a_e) assumed its (A) maximum (93.4%), (B) median (87.2%) and (C) minimum (67.8%) value.

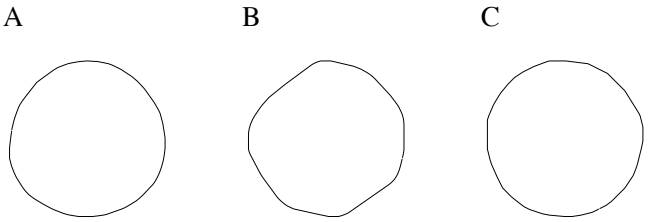

Fig. K4. Convex closures where the angle between the minimum and the maximum diameter ($|\theta_{Dmin}-\theta_{Dmax}|$) assumed its (A) maximum (90°), (B) median (68°) and (C) minimum (17°) value.

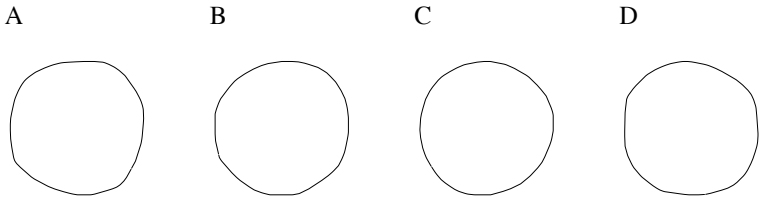

Fig. K5. Convex closures where the correlation between perpendicular diameters ($\rho_D(\pi/2)$) assumed its (A) maximum (0.78), (B) median (–0.71) and (C) minimum value (–0.99) as well as (D) the value closest to zero (0.01).

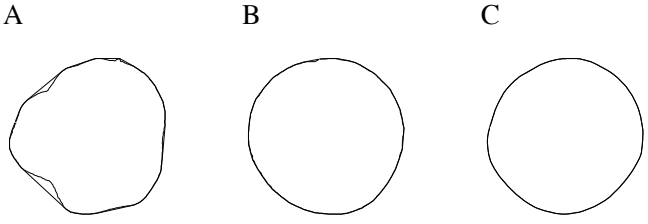

Fig. K6. Cross-sections where the convex deficit ($(A_C-A)/A_C$) assumed its (A) maximum (2.88%), (B) median (0.63%) and (C) minimum (0.25%) value; convex closures of are drawn with thin lines.

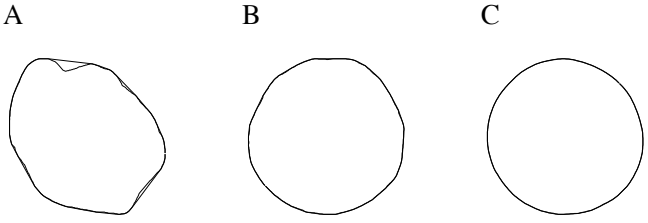

Fig. K7. Cross-sections where the isoperimetric deficit ($(\hat{A}_0-A_C)/A_C$) assumed its (A) maximum (5.78%), (B) median (0.71%) and (C) minimum (0.18%) value; convex closures are drawn with thin lines. Note that the cross-sections here are the same as those in Fig. K3.

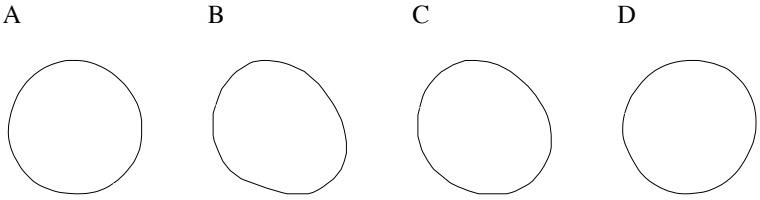

Fig. K8. Convex closures that were judged as the most elliptic ones in the data.

Table K1. Identification information, values of the five shape indices (diameter coefficient of variation CV_D, ratio between extreme diameters D_{min}/D_{max}, girth-area ellipse ratio b_e/a_e, angle between minimum diameter and maximum diameter $|\theta_{Dmin}–\theta_{Dmax}|$, correlation between perpendicular diameters $\rho_D(\pi/2)$), convex deficit $((A_C–A)/A_C)$ and isoperimetric deficit $((\hat{A}_0–A_C)/A_C)$ for the convex closures or cross-sections displayed in Figs. K1–K8.

Fig.		Plot	Tree	Obs. height	CV_D (%)	D_{min}/D_{max} (%)	b_e/a_e (%)	$\lvert\theta_{Dmin}–\theta_{Dmax}\rvert$ (°)	$\rho_D(\pi/2)$	$(A_C–A)/A_C$ (%)	$(\hat{A}_0–A_C)/A_C$ (%)
K1	A	310	8	6 m	9.94	73.4	71.3	87	–0.99	1.14	4.35
	B	303	6	85%	1.73	93.0	85.2	39	–0.12	1.07	0.97
	C	308	5	85%	0.37	98.3	91.0	30	–0.54	0.90	0.34
K2	A	317	11	85%	0.38	98.5	88.0	17	–0.26	0.90	0.61
	B	312	4	15%	1.67	94.4	89.1	81	–0.94	0.61	0.50
	C	See Fig. K1 A									
K3	A	321	14	30%	0.77	97.9	93.4	87	–0.91	0.28	0.18
	B	307	3	2.5%	0.79	97.1	87.2	72	–0.33	0.53	0.71
	C	303	12	1%	9.88	77.0	67.8	79	–0.95	2.33	5.78
K4	A	303	5	30%	2.09	94.0	88.3	90	–0.98	0.64	0.59
	B	304	1	1%	5.40	83.3	76.4	68	–0.79	1.31	2.73
	C	See Fig. K2 A									
K5	A	304	15	6 m	1.89	94.0	83.1	42	0.78	0.51	1.30
	B	311	3	70%	1.59	95.0	87.1	62	–0.71	0.67	0.71
	C	307	3	85%	1.22	95.8	89.6	89	–0.99	0.74	0.45
	D	308	13	30%	1.80	94.4	85.4	65	0.01	0.51	0.93
K6	A	303	5	2.5%	1.94	93.3	74.5	57	–0.62	2.88	3.29
	B	305	14	30%	2.72	91.9	87.7	85	–0.97	0.63	0.65
	C	318	18	7.5%	1.62	94.8	89.8	80	–0.50	0.25	0.44
K7	A	See Fig. K3 C									
	B	See Fig. K3 B									
	C	See Fig. K3 A									
K8	A	310	8	85%	7.24	81.2	78.5	83	–0.99	1.16	2.21
	B	See Fig. K1 A									
	C	318	9	6 m	3.28	90.9	88.6	81	–0.99	0.34	0.55
	D	318	18	6 m	1.78	95.1	91.3	84	–0.99	0.26	0.31